Antimalarial Drug Rescue through Safety Improvement: Design, Synthesis and Evaluation of Amodiaquine Analogues

Dennis Ongarora

Supervisor:
Prof Kelly Chibale,
Department of Chemistry, University of Cape Town.

Co-supervisor:
Dr Collen Masimirembwa,
African Institute of Biomedical Science and Technology, Harare.

Thesis Presented for the Degree of Doctor of Philosophy

in the Department of Chemistry,

University of Cape Town.

November 2013

DECLARATION

I, **Dennis Ongarora**, declare that:

(i) this thesis is my own unaided work, both in conception and execution, and that apart from the normal guidance of my supervisors, I have received no assistance apart from that acknowledged;

(ii) neither the substance nor any part of the thesis has been submitted in the past, or is being, or is to be submitted for a degree in the University of Cape Town or any other University.

Signed: _____ Date _____

DEDICATION

Ase mama na tata.

And to my wife Dorcas, my son Job and my daughter Joy.

For your unending love and sacrifice that have made this possible.

ACKNOWLEDGEMENTS

This work would not have been possible at all without the blessing of life, love, health and succor of the **α** and the **ω**, my God, to whom I give all praise and honor.

I am profoundly grateful to Professor Kelly Chibale whose supervision, guidance, patience and understanding saw me through my research expedition, and whose faith in me constantly exceeded my own self confidence. My co-supervisor Professor Collen Masimirembwa's invaluable guidance, particularly in the field of pharmacokinetics is also greatly appreciated.

My sincere gratitude goes to my colleagues and friends in the MedChem research group (glued together by the indefatigable Elaine Rutherfoord-Jones and Dr Aloysius Nchinda) and the Chemistry Department at UCT as well as the AiBST group (Harare) who hosted me in 2011. Your camaraderie prevented many a visit to a psychiatric clinic! I make special mention of Peggoty Mutai-Kemei whose academic strand has been inextricably intercalated with my own for the past 14 years. I thank Mathew Njoroge and Nicholas Njuguna for their help with LCMS analyses. I laud the important role played by the administrative and support staff in the Department of Chemistry at UCT in making our work environment safe and enjoyable.

Furthermore, I acknowledge the contribution of our collaborators at the University of California, San Francisco (Professor Philip Rosenthal) and the Swiss Tropical and Public Health Institute (Dr Sergio Whittlin). Professor Timothy Egan (UCT, Chemistry) and Professor Peter Smith (UCT, Phamacology) are acknowledged for their support in the β-hematin inhibition and cytotoxicity assays, respectively. In this regard, I thank Kathryn Wicht for kindly carrying out the β-hematin inhibition assay.

Organic Chemistry is largely dependent on spectroscopy and I proportionately wish to thank Peter Roberts and Noel Hendricks who did the NMR analysis and also trained and supported me in the use of the Varian NMR spectrometers. The ‘massive’ contribution of Gianpiero Benincasa (LRMS) and the Stellenbosch University MS Unit (HRMS) is also acknowledged.

I acknowledge, with gratitude, the Carnegie Corporation of New York, the Medical Research Council of South Africa, the National Research Foundation and the Department of Chemistry at UCT for their financial support without which I would not have had the opportunity to pursue my dreams (and overtake them!). On the same note I am grateful to the University of Nairobi for granting me a generous study leave.

My wife Dorcas, my son Job and my daughter Joy who shed tears every time they waved me off at the JKIA sacrificed immensely for me to fulfill my dreams and I will always love them and pledge to support them to achieve their dreams too. My parents Mama Bathseba Bosibori and Mzee Peter Ongarora, my brothers and sisters together with my extended family and friends have prayed for me, encouraged me and propped me up in more ways than I can list; I am deeply grateful for all this support. A big thumbs-up to Dr Moira Niehaus and Ms Mpho Sibanda who housed me in Cape Town and Harare, respectively, during my studies and were more of family to me than landladies. Lastly, I thank my church family at Mowbray SDA for their warmth, prayers and encouragement.

ABSTRACT

Malaria is a major cause of morbidity and mortality globally, resulting in over 200 million cases and 650, 000 deaths in 2010 according to the 2012 WHO Malaria Report. Furthermore, malaria endemicity is associated with poor economic growth. One of the greatest challenges facing malaria chemotherapy is the emergence of *Plasmodium* strains resistant to all known clinically used antimalarials. This underscores the need for the development of new drugs that retain efficacy against the resistant parasites.

In this study, analogue-based drug design was employed as a form of drug 'rescue' in the development of novel potential antimalarials. The main aim was to design and synthesize analogues of the 4-aminoquinoline drug amodiaquine with potentially improved safety and efficacy profiles using prior knowledge of the drug metabolism and pharmacokinetics (DMPK), toxicity and efficacy profile of the drug.

A representative set of compounds in four different series was synthesized in which the 4-aminoquinoline ring was coupled with benzothiazole, benzimidazole, benzoxazole and pyridyl rings bearing different aliphatic amines and diamines. The chemistry involved aromatic nucleophilic substitution reactions and hydrogenation of nitro aromatic compounds. Benzothiazole and benzoxazole analogues with a tertiary protonatable nitrogen were found to possess potent antiplasmodial activity against the drug resistant W2 and K1 *Plasmodium falciparum* strains. Among the most active compounds were benzothiazole analogues **3.2c** (W2 IC_{50} 12 nM, K1 IC_{50} 14 nM) and **3.2d** (W2 IC_{50} 13 nM, K1 IC_{50} 7 nM) and benzoxazole analogue **3.9b** (W2 IC_{50} 8 nM, K1 IC_{50} 22 nM).

Using electrochemistry online with electrospray ionization mass spectrometry, benzothiazole analogues were found to form glutathione adducts most readily, followed

by benzimidazole and pyridyl analogues. Benzoxazole analogues **3.9a** and **3.9b** did not form glutathione adducts. In trapping experiments with methoxylamine and KCN, all compounds with protonatable tertiary nitrogen atoms formed adducts. All the four series of compounds were potent but reversible CYP3A4 inhibitors and moderate CYP2D6 inhibitors. The benzoxazole series were selected for an expanded structure-activity relationship study based on the glutathione trapping results.

A library of benzoxazole analogues was synthesized in the last phase of the project. Consistent with our earlier findings, tertiary protonatable nitrogen containing compounds had potent antiplasmodial activity against the chloroquine sensitive NF54 strain and the drug resistant K1 strain. Compounds in which the tertiary amine was attached to the benzoxazole ring via an ethyl linker such as **3.9c** (NF54 IC_{50} 10 nM, K1 IC_{50} 24 nM), **3.9e** (NF54 IC_{50} 11 nM, K1 IC_{50} 42 nM) and **3.9f** (NF54 IC_{50} 12 nM, K1 IC_{50} 42 nM) were the most potent. A weak correlation between antiplasmodial activity and β-hematin formation inhibition was observed particularly for dialkylamino analogues. Although compounds with potent antiplasmodial activity displayed cytotoxicity against Chinese Hamster Ovary cells in the low micromolar range, they had high selectivity indexes. In general the compounds were more metabolically stable than amodiaquine in human and rat liver microsomes, the most stable compound being **3.9f** (>99% remaining after incubation for 30 minutes). In *P. berghei* infected mice, analogues **3.9b**, **3.9c** and **3.9j** suppressed parasitemia by >99% at oral doses of 4 x 50 mg/kg. Analogue **3.9b** cured all three treated mice (30 mean survival days) while analogues **3.9c** and **3.9j** cured 1/3 (27 mean survival days) and 2/3 (30 mean survival days) of treated mice, respectively. In conclusion, the benzoxazole analogues are a new class of leads for further exploration as antimalarial compounds.

LIST OF ABBREVIATIONS

WHO	World Health Organization
GMEP	Global Malaria Eradication Program
DDT	Dichlorodiphenyltrichloroethane
US	United States
HIV	Human Immunodeficiency Virus
AIDS	Acquired Immune Deficiency Syndrome
ITN	Insecticide Treated Nets
ACT	Artemisinin Combination Therapy
TRAP	Thrombospondin Related Adhesive Protein
RBC	Red Blood Cell
GPI	Glycosylphosphatidylinositol
TLR	Toll-like Receptors
ALI	Acute Lung Injury
ARDS	Acute Respiratory Distress Syndrome
DHPS	Dihydropteroate Synthetase
DHFR	Dihydrofolate Reductase
DHODH	Dihydroorotate Dehydrogenase
DNA	Deoxyribonucleic Acid
HDAC	Histone Deacetylase
NPP	New Permeability Pathway
FP	Falcipain
PM	Plasmepsin
HAP	Histo-Aspartic Protease
ROS	Reactive Oxygen Species

SOD	Superoxide Dismutase
G6PD	Glucose 6-Phosphate Dehydrogenase
pfcrt	*Plasmodium falciparum* Chloroquine Resistance Transporter
pfmdr	*Plasmodium falciparum* Multidrug Resistance
Pgh	P-glycoprotein homologue
SERCA	Sarco/Endoplasmic Reticulum Membrane Calcium ATPase
ATP	Adenosine Triphosphate
TCTP	Translationally Controled Tumor Protein
ADR	Adverse Drug Reaction
UK	United Kingdom
USD	United States Dollars
NHS	National Health Service
IDR	Idiosyncratic Drug Reactions
NAPQI	*N*-acetyl-*p*-benzoquinoneimine
ADME(T)	Absorption, Distribution, Metabolism, Excretion (Toxicity)
CYP	Cytochrome P450
NADP(H)	(Reduced) Nicotinamide Adenine Dinucleotide Phosphate
NAD(H)	(Reduced) Nicotinamide Adenine Dinucleotide
GSH	Reduced glutathione
LC	Liquid Chromatography
MS	Mass Spectroscopy
TDI	Time-dependent Inhibition
EC-ESI/MS	Electrochemical oxidation online with Electrospray Mass Spectrometry
NMR	Nuclear Magnetic Resonance
PMN	Polymorphonuclear

PABA	*Para* aminobenzoic acid
DMPK	Drug metabolism and pharmacokinetics
HSAB	Hard Soft Acid Base
THF	Tetrahydrofuran
DMSO	Dimethylsulfoxide
DCM	Dichloromethane
EtOAc	Ethyl acetate
ppm	parts per million
SAR	Structure-activity relationship
PSA	Polar surface area
SI	Selectivity index
MLM	Mouse liver microsomes
HLM	Human liver microsomes
TLC	Thin layer chromatography
DMF	Dimethylformamide

TABLE OF CONTENTS

DECLARATION i
DEDICATION ii
ACKNOWLEDGEMENTS iii
ABSTRACT v
LIST OF ABBREVIATIONS vii
TABLE OF CONTENTS x
LIST OF FIGURES xv
LIST OF TABLES xvii
PUBLICATIONS AND CONFERENCES xix
Chapter 1 1
INTRODUCTION AND LITERATURE REVIEW 1
1.1 CHAPTER OVERVIEW 1
1.2 ETIOLOGY OF MALARIA 1
1.3 EPIDEMIOLOGY 2
1.4 LIFE CYCLE 5
1.5 PATHOPHYSIOLOGY AND CLINICAL PRESENTATION 7
1.6 MALARIA CHEMOTHERAPY 10
1.6.1 Targets for antimalarial chemotherapy 10
1.6.2 Hemoglobin metabolism in *Plasmodium* 13
1.6.2.1 The fate of heme in the parasite 14
1.6.3 Classes of drugs used in malaria chemotherapy 17
1.6.3.1 Quinoline antimalarials 17
1.6.3.2 Folate antagonists 22
1.6.3.3 Artemisinin derivatives 25
1.7 ADVERSE DRUG REACTIONS/DRUG TOXICITY 29
1.7.1: The economic and health significance of ADRs 29
1.7.1.1 ADRs: The industry perspective 29
1.7.1.2 ADRs: The patient's perspective 30
1.7.2 Types of ADRs 30

1.7.2.1 Type A ADRs 30
1.7.2.2 Type B ADRs 31
1.7.2.3 Type C ADRs 31
1.7.2.4 Type D ADRs 32
1.7.2.5 Type E ADRs 333
1.7.3 Overview of drug metabolism 33
1.7.3.1 Phase I metabolism 34
1.7.3.2 Phase II metabolism 36
1.7.4 Bioactivation 37
1.7.4.1 The concept of structural alerts 37
1.7.4.2 Reactivity of reactive metabolites 39
1.7.4.3 Assessment of bioactivation 40
1.7.4.3.1 Trapping reactions 40
1.7.4.3.2 Covalent binding 41
1.7.4.3.3 Mechanism-based CYP inhibition 42
1.7.4.4 Animal models for bioactivation and the use of integrated systems 42
1.7.4.5 Electrochemical oxidation online with electrospray ionization mass spectrometry (EC-ESI/MS) 43
1.8 AMODIAQUINE 44
1.8.1 Pharmacokinetics 44
1.8.2 Toxicity 44
1.8.3 Amodiaquine analogues synthesized to circumvent toxicity 48
1.9 JUSTIFICATION 49
1.10 RESEARCH QUESTION AND SPECIFIC OBJECTIVES 50
1.10.1 Hypothesis 50
1.10.2 Specific aims 50
Chapter 2 80
DESIGN AND SYNTHESIS OF BENZOHETEROCYCLIC AND PYRIDYL AMODIAQUINE ANALOGUES 80
2.1 DESIGN 80
2.2 SYNTHESIS 82

2.2.1 Towards chemically tractable intermediates 83
2.2.1.1 Bromo intermediates 83
2.2.1.2 2-(Methylthio)-5-nitrobenzoxazole 84
2.2.2 First nucelophilic substitution step 85
2.2.3 Reduction of the nitro group 91
2.2.4 Second substitution reaction (coupling with 4,7-dichloroquinoline) 93
2.3 CHARACTERIZATION OF TARGET MOLECULES 94
2.4 CONCLUSION 102
REFERENCES 103
Chapter 3 107
REACTIVE METABOLITE STUDIES 107
3.1 INTRODUCTION 107
3.1.1 The EC/ESI-MS procedure 108
3.1.2 The CYP inhibition assay procedure 108
3.1.3 Treatment of results 109
3.2 RESULTS AND DISCUSSION 111
3.2.1 Glutathione trapping 111
3.2.2 Trapping with cyanide and methoxylamine 115
3.2.3 CYP inhibition assays 117
3.2.3.1 CYP3A4 inhibition 117
3.2.3.2 CYP2D6 inhibition 119
3.2.3.3 CYP2C9 inhibition 120
3.2.3.4 CYP1A2 inhibition 121
3.2.4 Time-dependent inhibition results 121
3.3 DISCUSSION 123
3.4 CONCLUSION 127
REFERENCES 128
CHAPTER 4 135
EVALUATION OF PHYSICOCHEMICAL PROPERTIES, METABOLIC STABILITY AND ANTIPLASMODIAL ACTIVITY OF AMODIAQUINE ANALOGUES 135
4.1 CHAPTER OVERVIEW 135

4.2 PHYSICOCHEMICAL PROPERTIES 135
4.2.1 Introduction and rationale 135
4.2.2 Results of physicochemical evaluation 138
4.3 ANTIPLASMODIAL ACTIVITY 142
4.3.1 Introduction and rationale 142
4.3.2 Antiplasmodial activity results 142
4.3.2.1 Antiplasmodial activity of the initial library of benzoheterocyclic and pyridine analogues 142
4.3.2.2Cytotoxicity and selectivity indexes of the initial library of benzoheterocyclic and pyridine analogues 145
4.3.2.3 Antiplasmodial activity of alkyl, amide, dialkylamino and cycloalkylamino analogues 146
4.3.2.4 Antiplasmodial activity of benzylamino and alkylpyridyl benzoxazole analogues 149
4.3.2.5 Antiplasmoodial activity of piperazinyl and dialkyl benzoxazole analogues 150
4.3.2.6 Antiplasmodial activity of selected intermediates 151
4.3.2.7 Cytotoxicity and selectivity indexes of benzoxazole analogues 152
4.3.2.8 Discussion of antiplasmodial activity data 154
4.4 BETA HEMATIN FORMATION INHIBITION ACTIVITY 155
4.4.1 Introduction 155
4.4.2 Results and discussion (β-hematin inhibition) 157
4.5 MICROSOMAL STABILITY STUDIES 160
4.5.1 Introduction and rationale 160
4.5.2 Procedure for microsomal stability studies 161
4.5.3 Results and discussion of microsomal stability studies 162
4.6 *IN VIVO* EFFICACY STUDIES 164
4.6.1 Introduction 164
4.6.2 Results and discussion 165
4.7 CONCLUSION 167
REFERENCES 169
Chapter 5 175

SUMMARY, CONCLUSIONS AND RECOMMENDATIONS FOR FUTURE WORK ... 175
5.1 SUMMARY AND CONCLUSIONS ... 175
5.2 RECOMMENDATIONS FOR FUTURE WORK ... 178
Chapter 6 ... 179
EXPERIMENTAL ... 179
6.1 REAGENTS AND SOLVENTS ... 179
6.2 CHROMATOGRAPHY ... 179
6.3 PHYSICAL AND SPECTROSCOPIC CHARACTERIZATION ... 180
6.4 SYNTHESIS ... 181
6.5 ANTIPLASMODIAL ACTIVITY ASSAYS ... 221
6.5.1 In vitro antiplasmodial assay against K1 and NF54 strains of P. falciparum ... 221
6.5.2 *In vitro* antiplasmodial assay against the W2 strain ... 222
6.6 *IN VIVO* ANTIMALARIAL EFFICACY STUDIES ... 222
6.7 CYTOTOXICITY ASSAYS ... 223
6.7.1 *In vitro* cytotoxicity against L6 cells ... 223
6.7.2 *In vitro* cytotoxicity against CHO cells ... 224
6.8 DETERGENT MEDIATED *B*-HEMATIN FORMATION INHIBITION ASSAY ... 225
6.9 TURBIDIMETRIC SOLUBILITY ASSAY ... 226
6.10 CYP INHIBITION ASSAY ... 227
6.11 TIME DEPENDENT CYP3A4 INHIBITION ASSAY ... 229
6.11.1 Incubation 1 (Inactivation assay) ... 229
6.11.2 Incubation 2 (Activity assay) ... 230
6.12 EC-ESI/MS TRAPPING EXPERIMENTS ... 230
6.13 METABOLIC STABILITY ASSAY ... 231
REFERENCES ... 232
APPENDIX 235

LIST OF FIGURES

Figure 1.1: Global distribution of (a) *Plasmodium falciparum* and (b) *Plasmodium vivax*.3

Figure 1.2: Life cycle of *Plasmodium* parasites. 6

Figure 1.3: The structure of Fe^{III}-protoporphyrin IX with arrows indicating torsional degrees of freedom for the vinyl and propionic acid groups. 15

Figure 1.4: Three β-hematin dimers linked by hydrogen bonds between propionic acid groups. 16

Figure 1.5: Chemical structures of quinoline antimalarials and related phenanthrene methanols..... 20

Figure 1.6: Chemical structures of folate antagonists..... 23

Figure 1.7: Chemical structures of selected artemisinin derivatives ozonides..... 27

Figure 1.8: Bioactivation of acetaminophen 32

Figure 1.9: Xenobiotic metabolism and toxicity 33

Figure 1.10: Phase 1 drug metabolizing enzymes. 35

Figure 1.11: CYP450 catalytic cycle. 36

Figure 1.12: Drug pairs where substitution of the structural alert (dotted box) has resulted in safer molecules..... 38

Figure 1.13: Metabolic routes of amodiaquine and desethylamodiaquine observed in rat and human liver microsomes and recombinant CYP1A1 and CYP1B1..... 47

Figure 1.14: Examples of analogues synthesized to prevent bioactivation to the quinone imine..... 49

Figure 2.1: General chemical structures of the four series of amodiaquine analogues . 81

Figure 2.2: Amines employed in substitution reactions. 82

Figure 2.3: General structures of amine intermediates 86

Figure 2.4: The ^{1}H NMR spectrum of **2.2d** showing an expansion of the aromatic region. 88

Figure 2.5: The aromatic region of the ^{1}H NMR spectra of **2.2d** and its reduced intermediate 93

Figure 2.6: The ^{1}H NMR spectrum of **3.9k** in CD_3OD: a=aromatic, b=aliphatic..... 96

Figure 2.7: The ^{13}C spectrum of **3.9k** in CD_3OD. 97

Figure 2.8: The aromatic region of the ^{1}H NMR spectrum of **3.9r.** 98

Figure 2.9: The ^{13}C spectrum of **3.9r**..... 99

Figure 3.1: Schematic overview of the electrochemical system [7]..... 108

Figure 3.2: Bioactivation of clozapine and detoxification by glutathione..... 109

Figure 3.3: Proposed bioactivation of the pyridyl and benzazole analogues to soft electrophiles and their conjugation with GSH. 113

Figure 3.4: Bioactivation of amsacrine 114

Figure 3.5: Bioactivation of mitoxantrone 114

Figure 3.6: Bioactivation of piperidinyl compounds 117

Figure 3.7: Results for the CYP3A4 inhibition assay. 117

Figure 3.8: Results for the CYP2D6 inhibition assay..... 119

Figure 3.9: Results for the CYP2C9 inhibition assay..... 120

Figure 3.10: Results for the CYP1A2 inhibition assay..... 121

Figure 3.11: Results for the CYP3A4 time dependent inhibition assay 122

Figure 3.12: 3D view (Marvin Sketch®) of **3.6a** with the benzimidazole ring out of plane with the quinoline ring..... 124

LIST OF TABLES

Table 1.1: New and old targets for malaria chemotherapy 11

Table 1.2: Common structural alerts, their reactive metabolites and associated toxicities 39

Table 2.1: Yields of benzothiazole analogues 89

Table 2.2: Yields of benzimidazole analogues 89

Table 2.3: Yields of pyridyl analogues 90

Table 2.4: Yields of benzoxazole analogues 90

Table 2.5: Isolated yields of benzothiazole target molecules 100

Table 2.6: Isolated yields of benzimidazole targets 100

Table 2.7: Isolated yields of pyridyl targets 101

Table 2.8: Isolated yields of benzoxazole targets 101

Table 3.1: Glutathione trapping results 111

Table 3.2: Potassium cyanide and methoxyalmine trapping experiment results 115

Table 4.1: Physicochemical properties of benzothiazole, benzimidazole and pyridine analogues 139

Table 4.2: Physicochemical properties of dialkylamino and cycloalkylamino benzoxazole analogues 140

Table 4.3: Physicochemical properties of benzylamino and alkylpyridyl benzoxazole analogues 141

Table 4.4: Physicochemical properties of piperazinyl and dialkyl benzoxazole analogues 141

Table 4.5: Antiplasmodial activity of the initial library of benzoheterocyclic and pyridine analogues 144

Table 4.6: Cytotoxicity and selectivity indexes of the initial library of benzoheterocyclic and pyridine analogues 145
Table 4.7: Antiplasmodial activity of alkyl, amide, dialkylamino and cycloalkylamino analogues..... 147
Table 4.8: Antiplasmodial activity of carbon-linked analogues 149
Table 4.9: Antiplasmodial activity of benzylamino and alkylpyridyl benzoxazole analogues..... 150
Table 4.10: Antiplasmoodial activity of piperazinyl and dialkyl benzoxazole analogues 151
Table 4.11: Activity of selected benzoxazole intermediates 152
Table 4.12: Cytotoxicity against CHO cells and selectivity indexes..... 153
Table 4.13: β-hematin inhibition activity of benzoxazole analogues..... 156
Table 4.14: Percentage of compound remaining after 30 min incubation with microsomes..... 162
Table 4.15: *In vivo* suppression of parasitemia by **3.9b**, **3.9c** and **3.9j**..... 165
Table 4.16: Effect of **3.9b**, **3.9c** and **3.9j** on mouse survival. 166
Table 6.1: HPLC conditions..... 180
Table 6.2: CYP1A2 incubation setup 227
Table 6.3: CYP3A4 incubation setup 228
Table 6.4: CYP2C9 incubation setup 228
Table 6.5: CYP2C19 incubation setup 228
Table 6.6: CYP2D6 incubation setup 229
Table 6.7: Inactivation assay setup 229
Table 6.8: Activity assay setup..... 230

PUBLICATIONS AND CONFERENCES

Publication so far arising from this thesis

Ongarora, D. S. B., Gut, J., Rosenthal, P. J., Masimirembwa, C. M., & Chibale, K. (**2012**). Benzoheterocyclic amodiaquine analogues with potent antiplasmodial activity: synthesis and pharmacological evaluation. *Bioorganic & Medicinal Chemistry Letters*, *22*(15), 5046–5050

Other publications and review

1. Dyanne L. Cruickshank, Yassir Younis, Nicholas M. Njuguna, **Dennis S. B. Ongarora**, Kelly Chibale and Mino R. Caira. Alternative solid-state forms of a potent antimalarial aminopyridine: X-ray crystallographic, thermal and solubility aspects. *CrystEngComm*, **in press**.
2. Njuguna, N. M., **Ongarora, D. S. B.**, & Chibale, K. (**2012**). Artemisinin derivatives: a patent review (2006 - present). *Expert Opinion on Therapeutic Patents*, *22*(10), 1179–1203.

Conference attendance

1. 4th Molecular Approaches to Malaria Conference (MAM 2012). February 19-23 **2012**, Lorne, Australia. (Poster presentation)
2. ASTMH 62nd Annual Meeting. November 13-17, **2013**, Marriott Wardman Park, Washington, DC, USA. (Poster presentation)

Chapter 1

INTRODUCTION AND LITERATURE REVIEW

1.1 CHAPTER OVERVIEW

This Chapter starts with a review of aspects of the etiology, epidemiology, pathophysiology and chemotherapy of malaria. Adverse drug reactions are subsequently discussed under the topics of the significance and classification of ADRs. The role of drug metabolism in the bioactivation of xenobiotics and the various methods used to assess bioactivation potential are highlighted thereafter. Literature on amodiaquine pharmacokinetics and bioactivation is reviewed followed by medicinal chemistry efforts aimed at preventing this bioactivation. Justification, the research question and specific objectives are given at the end of the chapter.

1.2 ETIOLOGY OF MALARIA

The protozoal disease malaria arises from infection by apicomplexan parasites of the genus *Plasmodium*. As of 2008, approximately 200 *Plasmodium* species from different mammalian, avian and reptile intermediate hosts had been described [1]. In humans, *Plasmodium falciparum*, *P. vivax*, *P. ovale* and *P. malariae* are the malaria parasites of clinical significance based on the severity of disease and prevalence of infection [2]. However, *P. knowlesi*, originally considered a malaria parasite of macaque monkeys, has been identified in patients in parts of Southeast Asia and is currently regarded as the fifth malaria parasite [2,3]. Based on findings from multilocus genetic analysis Surtherland and co-workers concluded that *Plasmodium ovale* actually consists of two non-recombining species, *P. ovale curtisi* and *P. ovale wallikeri* [4].

1.3 EPIDEMIOLOGY

According to the 2012 World Malaria Report, there were an estimated 219 million cases of malaria in 101 malaria endemic countries in 2011, 80 % of which were reported in Africa. In the same year, 3.17 billion people globally were at risk of malaria [5]. The number of malaria deaths was estimated to be 660,000 in 2010. Of these, 86 % were children under 5 years of age and again >90% of malaria deaths occurred in the WHO Africa region [6]. The disproportionately high mortality and morbidity associated with malaria in Africa is attributed to the differential distribution of *Plasmodium* species as well as economic development. *Plasmodium falciparum*, the most virulent species, is preponderant in tropical Africa. Two countries, Nigeria and the Democratic Republic of Congo, account for 23 % of the global *P. falciparum* burden [7]. In South America, *P. vivax* is the major species while in south-eastern Asia and Western Pacific, both *P. falciparum* and *P. vivax* are prevalent [8,9]. However, *P. vivax* has been virtually non-existent in West Africa where Duffy blood group negativity predominates [10]. Perhaps as a stark reminder of the evolutionary ability of the malaria parasite and the imperative for continuing research into approaches of eradicating malaria, reports have emerged that Duffy negativity may no longer confer immunity against *P. vivax* [11,12]. Figure 1 illustrates the global distribution of these two species. Although *P. malariae* is widely distributed around the world, its prevalence is generally low. In Africa, *P. malariae* infections are usually reported mixed with those of *P. falciparum* [13]. *Plasmodium ovale* is principally distributed, albeit at a low prevalence, in tropical Africa but has been reported in the Middle East, India and other parts of the world [14] while *P. knowlesi* is localized to South-East Asia [3].

Malaria primarily affects poor populations in tropical and subtropical regions [15]. The Nobel laureate T.H. Weller noted that "a malarious community is an impoverished community" [16]. Indeed, malaria was once widespread in temperate areas including Western Europe and the United States. Economic development and public health interventions such as the WHO sponsored Global Malaria Eradication Program (GMEP) of the 1950s have virtually eliminated the disease in these areas [15]. Unfortunately, the GMEP, which relied on chloroquine chemotherapy and vector control using DDT, did not attempt to eradicate malaria in Africa, the worst affected continent [15]. More recently, however, major advances in malaria research and public health practices, coupled with

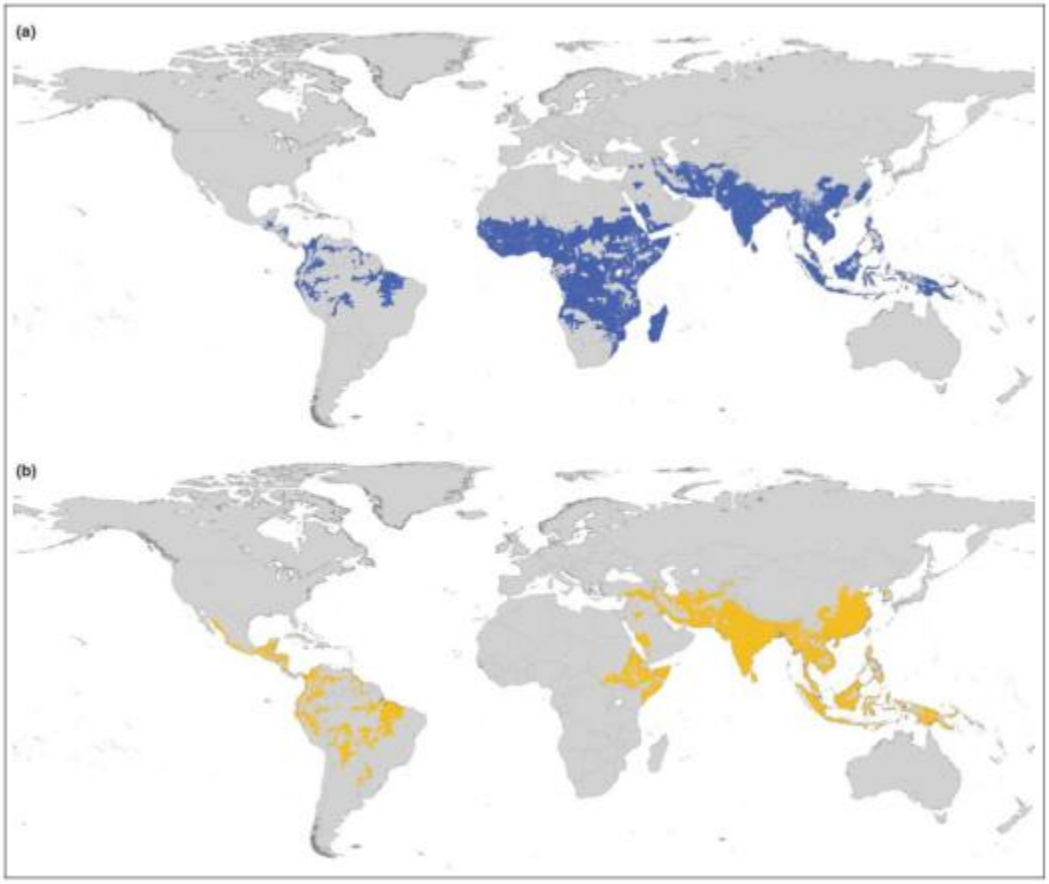

Figure 1.1: Global distribution of (a) *Plasmodium falciparum* and (b) *Plasmodium vivax*[9].

careful epidemiologic and economic analyses of malaria burden and cost effective ways to lessen it have renewed optimism for malaria control, particularly in Africa [17]. Once more, malaria control is on the political agenda of the world's leading economies with impressive funding being provided to fight the disease via the Global Fund to Fight AIDS, Tuberculosis and Malaria, The US President's Malaria Initiative, the World Bank and bilateral donors. The coordination of these global efforts is the function of the Roll Back Malaria Partnership and involves the use of preventive measures such as promoting the use of insecticide treated nets (ITNs), proper diagnostics and Artemisinin Combination Therapies (ACTs) [18]. It is worth noting that between 2005 and 2010, malaria cases decreased from 244 to 216 million while there was a reduction in global malaria mortality rates by 26 % between 2000 and 2010 [8]. Despite this welcome trend, a lot still remains to be done in containing the burden of malaria. Reports of emerging *Plasmodium* resistance to artemisinin in parts of Asia [19] are a sobering reminder against complacence.

With regard to the impact of malaria on economic development, Gallup and Sachs observed that countries that eliminated malaria experienced higher economic growth thereafter compared to their neighbors [16]. Further, they report that countries with intensive malaria grew 1.3 % less per person while a 10 % reduction in malaria incidences resulted in 0.3 % higher growth.

1.4 LIFE CYCLE

As illustrated in figure 1.2, the life cycle of malaria parasites involves two hosts: human beings and female *Anopheles* mosquitoes, which act as the definitive hosts and malaria vectors, respectively [20]. The sexual phase (sporogony) takes place in the mosquito while the asexual stage (schizogony) occurs in the human host [2]. During a blood meal, a mosquito will inject approximately 15-20 motile sporozoites into the subcutaneous tissue and sometimes directly into the bloodstream [21,22]. The sporozoites are transported in blood to the liver where they invade hepatocytes thus concealing themselves from the host's immune system. Sporozoite motility and hepatocyte invasion have been attributed to a protein referred to as thrombospondin related adhesive protein (TRAP). Within the hepatocytes, each sporozoite develops into a tissue schizont containing between 10,000 and 30,000 merozoites. The higher merozoite content is characteristic of *Plasmodium falciparum* infections. This liver stage of the disease, referred to as exoerythrocytic schizogony, lasts for between 6 days (*P*. *falciparum*) and 14 days (*P*. *malariae*) and is asymptomatic. Subsequently, mature schizonts rupture and release merozoites into the bloodstream to start the erythrocytic schizogony. [2,20–22] *P*. *vivax* and *P*. *ovale* can persist in the liver as hypnozoites for months to years and are responsible for relapse after successful treatment. This phenomenon represents a formidable barrier to malaria eradication [23].

In the erythrocytic schizogony, each merozoite invades a red blood cell (RBC) heralding the beginning of symptomatic malaria. The selective invasion of RBCs is mediated by interaction between merozoite ligands and RBC receptors. Invasion is both rapid and

efficient which is necessary for merozoite survival considering that the antigens on the merozoite surface are highly vulnerable to immune attack [24].

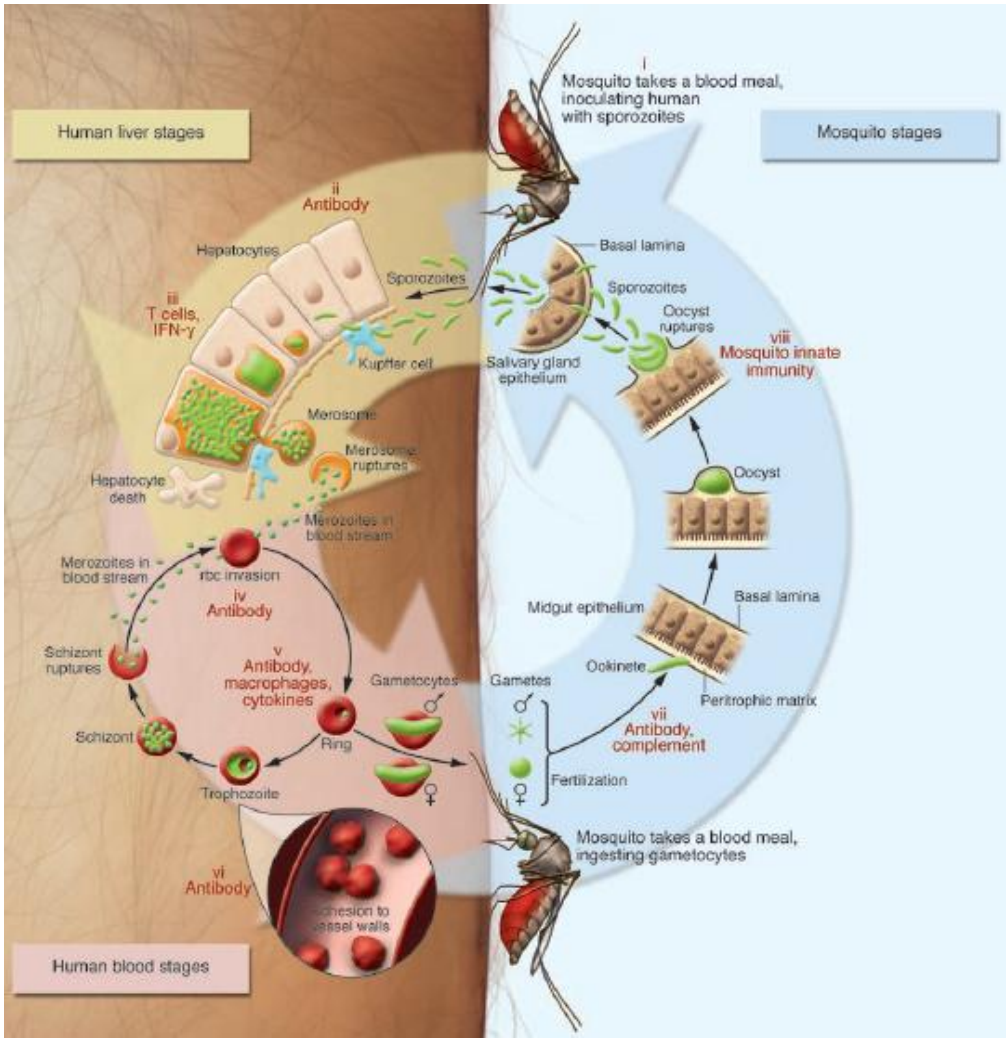

Figure 1.2: Life cycle of *Plasmodium* parasites [15].

Furthermore, some of the ligands involved in invasion are stored in micronemes and rhoptries and only secreted during invasion [21]. Once the merozoite gets in contact with the RBC, it reorients itself and a tight junction is formed between the parasite and host membrane. This tight junction then moves from the apical to the posterior end of the merozoite and eventually envelops it. In the process, the merozoite sheds its own

coating and enters the RBC wrapped in a parasitophorous vacuole that is hospitable for development [24,25].

Within the RBCs merozoites develop asexually from a ring stage via a trophozoite stage into a blood schizont containing 16-32 merozoites [26]. Upon maturation, the swollen infected erythrocyte explodes to releases fresh merozoites which will further re-infect other RBCs in repeated erythrocytic cycles greatly multiplying the number of parasites in the host [27,28]. The cycle time is 48 h for *P. falciparum*, *P. vivax* and *P. ovale* and 72 h for *P. malariae*. Some merozoites differentiate into male and female gametocytes which enter the sporogonic cycle when ingested by the *Anopheles* mosquito during a blood meal and develop into infective sporozoites [22].

1.5 PATHOPHYSIOLOGY AND CLINICAL PRESENTATION

The WHO classifies malaria as uncomplicated or severe. Uncomplicated malaria is defined as asymptomatic malaria without signs of severity or evidence of vital organ damage. It presents as a nonspecific febrile illness which may be accompanied by chills and sweats, headache, vomiting, watery diarrhea, anemia, jaundice, and splenomegally [29]. Malaria fever presents as a classical cyclical paroxysm that coincides with the rupture of blood schizonts during a synchronous asexual erythrocytic schizogony. The fever lasts for only a few hours, occurring every 48 hours (tertian) for *P. falciparum*, *P. vivax*, and *P. ovale*, and every 72 hours (quartan) for *P. malariae* [30]. Malaria fever starts at a pyrogenic threshold. *Plasmodium vivax* has a lower pyrogenic threshold and elicits a greater inflammatory response than *P. falciparum* infections of similar or greater parasite biomass. This may be attributed to higher cytokine production in vivax malaria

[31]. Two malaria toxins, heme and malaria glycosylphosphatidylinositol (GPI) are among the products released during rupture of the schizont and their interaction with host toll-like receptors (TLRs) results in stimulation of a pro-inflammatory response [30,32]. If untreated or not contained by the host immune response, uncomplicated malaria progresses to severe malaria.

Severe malaria is characterized by the presence of *P. falciparum* asexual parasitemia and the presence of one or more of the following symptoms with no other obvious cause: impaired consciousness or unrousable coma, prostration, failure to feed, multiple convulsions, deep breathing, respiratory distress (acidotic breathing), circulatory collapse or shock, systolic blood pressure <70 mm Hg in adults and <50 mm Hg in children, clinical jaundice plus evidence of other vital organ dysfunction, hemoglobinuria, abnormal spontaneous bleeding and pulmonary edema [33,34]. Malaria deaths are a result of any combination of these complications. The main manifestations of severe malaria are highlighted in the following paragraphs.

Key differences among *Plasmodium* species in the erythrocytic schizogony explain the difference in severity of malaria. *Plasmodium falciparum* infects RBCs of all ages while *P. vivax* only infects reticulocytes. Thus *P. falciparum* infection results in higher parasitemia [21] while vivax malaria parasitemias rarely exceed 2 % of circulating RBCs [31]. Significant mortality is observed when parasitemia exceeds 5 % even with appropriate parenteral antimalarial therapy. Exchange transfusion may rapidly reduce parasitemia in such cases [33]. Additionally, unlike other malaria parasites *P. falciparum* modifies the surface of infected RBCs so that gametocytes and asexual parasites can adhere to the microvascular endothelium and asexual parasites to the placenta [21]

resulting in parasite sequestration in deep tissue and microvascular obstruction. Sequestration of asexual parasites in the brain is responsible for cerebral malaria. The pathology underlying cerebral malaria may involve the initiation of an inflammatory process, endothelial activation, release of endothelial microparticles and apoptosis around the region of cytoadherence and sequestration. Cerebral malaria is a leading cause of malaria deaths in children in sub-Saharan Africa [35]. Parasite adherence to the placenta is responsible for premature deliveries, low birth weight, increased infant mortality and maternal anemia [21].

Severe anemia is common in *P. falciparum* and *P. vivax* infections and is a major hazard to pregnant women in malaria endemic areas and a leading factor in child deaths resulting from malaria. The three mechanisms postulated to explain anemia in malaria are direct destruction of RBCs as schizonts rupture, suppressed erythropoiesis which implies that not all destroyed cells are replaced and increased destruction of uninfected cells [36]. Anemia resultant from *P. vivax* infection does not correlate with the observed low parasite biomass. Studies have shown that in vivax malaria, for every infected erythrocyte destroyed, 32 uninfected erythrocytes are removed from circulation [31]. This is in contrast to the destruction of only 8 uninfected RBCs for every infected erythrocyte in falciparum malaria [37].

It has been observed that in falciparum malaria, deformability of infected and non-infected RBCs under shear stresses in arterioles and capillaries with reduced flow is reduced. This phenomenon is a predictor of mortality in severe malaria. It leads to reduced microcirculatory flow and reduced oxygen delivery to tissues and eventually to anerobic glycolysis which correlates with elevated lactate levels [38].

Respiratory distress is a common feature in severe falciparum malaria occurring in up to 25 % of adults and 40 % of children infected with the disease. Causes include severe anemia, metabolic acidosis, noncardiogenic pulmonary edema, concomitant pneumonia and fluid overload. Acute lung injury (ALI) and Acute Respiratory Distress Syndrome (ARDS) may develop in patients with severe falciparum, vivax, and knowlesi malaria, often several days after antimalarial drug treatment. The pathophysiology of ARDS centers on inflammatory-mediated increased capillary permeability or endothelial damage leading to diffuse alveolar damage [39].

Malaria and HIV/AIDS are the leading infectious diseases in Africa. Not only is there enormous geographic overlap between the two diseases but there is growing evidence of interactive pathology. HIV increases the risk of malaria infection and the development of clinical malaria [40]. A study in Malawi reported increased prevalence of malaria and higher parasitemia in HIV infected pregnant patients compared to uninfected patients. [41]. Grimwade et al. demonstrated a strong association between HIV infection and poor outcome in adults with *P. falciparum* malaria [42]. Clearly, the emergence of HIV has serious implications on any programs targeting the treatment and prevention of malaria.

1.6 MALARIA CHEMOTHERAPY

1.6.1 Targets for antimalarial chemotherapy

Antimalarial drugs target different stages of the malaria parasite life cycle. The main pathways traditionally targeted are nucleic acid and heme metabolism as well as the redox system. Increased understanding of *Plasmodium* biology as well as the development of sophisticated methods of molecular analysis including genome

sequence analysis have facilitated the discovery of numerous novel targets [43,44]. For example, elucidation of the genome sequence of Chromosome 2 of *P. falciparum* enabled researchers to identify several lipid biosynthesis genes in the parasite targeted to the apicoplast. These genes play a critical role in parasite viability and are attractive drug targets [45]. The identification and exploitation of such new targets is of particular importance in the search for molecules that circumvent existing and emerging resistance against antimalarial drugs [46]. Table 1.1 summarizes main targets for malaria chemotherapy.

Table 1.1: New and old targets for malaria chemotherapy [43,47–49]

Pathway	**Target**	**Notes**
Nucleic acid metabolism	Dihydropteroate synthetase (DHPS) inhibition	Reduced folate co-factors are essential for many reactions involving one-carbon unit transfer such as DNA and protein synthesis. *Plasmodium* possesses a *de novo* folate biosynthesis pathway unlike the host making it an excellent antimalarial target [50,51].
	Dihydrofolate reductase (DHFR) inhibition	
	Dihydroorotate dehydrogenase (DHODH) inhibition	DHODH catalyzes the rate limiting step in pyrimidine biosynthesis. Malaria parasites only rely on *de novo* pyrimidine biosynthesis making this an attractive target [52].
	Purine nucleoside phosphorylase inhibition	Malaria parasites are unable to synthesize purines *de novo* but rely on an elaborate salvage pathway which can be targeted by drugs [53].
	Adenosine deaminase inhibition	
	Hypoxanthine-guanine-xanthine phosphoribosyltransferase	

	inhibition	
Heme detoxification	Hemozoin formation inhibition	
Hemoglobin proteolysis	Falcipain and plasmepsin inhibitors	Cysteine proteases (falcipains 1, 2, 2' and 3) and aspartic proteases (plasmepsins I, II, and IV) are necessary for the cleavage of host proteins to provide the parasite with amino acids [54].
Redox system	Generation of free radicals which alkylate or hydroxylate some unidentified targets.	An efficient antioxidant system is required in intra-erythrocytic malaria parasites to counter the oxidant effects of hemoglobin digestion. The parasites lack catalase and glutathione peroxidase making them even more susceptible to oxidative stress. [55]
Apicoplast function	Protein, DNA and fatty acid biosynthesis disruption	The absence of apicoplasts in the human host underlies the selectivity of compounds targeting this organelle [56].
DNA replication	Histone deacetylase (HDAC) inhibition	HDAC regulates gene transcription and is very important for parasite survival. These enzymes are also found in humans and inhibition selectivity is a primary concern [57].
Signal transduction	Kinase inhibitors	The *Plasmodium* kinome, comprising several families of kinases that are clearly distinct from human kinases, provides a potential target for malaria chemotherapy [58,59].
Parasite membrane transport	New permeability pathway (NPP) inhibitors	NPPs are induced in infected RBCs partly to provide entry for essential nutrients [60].

1.6.2 Hemoglobin metabolism in *Plasmodium*

The metabolism of hemoglobin is necessary for the survival of the malaria parasite and is, consequently, an important antimalarial target [61]. Chloroquine, arguably the most important antimalarial drug historically, together with related quinoline antimalarial drugs, targets this important pathway. Although chloroquine resistance is now widespread, the attractiveness of hemoglobin metabolism as a drug target has in no way diminished. Indeed, it is worth noting that chloroquine resistance does not actually result from modification of this target but from alteration of a transmembrane protein on the parasite [62].

In the blood stages, the malaria parasite resides in a parasitophorous vacuole within the RBC [63]. Hemoglobin comprises 95% of the RBC cytosolic protein and is a major nutrient source for the maturing trophozoites [64,65]. *Plasmodium* degrades up to 80% of host cell hemoglobin [65,66].

Hemoglobin degradation occurs in the food vacuole, a sophisticated, acidic (pH≈5) organelle optimized for its function [67]. Host cell cytosol is taken up through a cytosome formed by invagination of the parasitophorous vacuolar membrane and parasite plasma membrane. Transport vesicles then bud off from the cytosome, migrate toward and fuse with the food vacuole. Once in the vacuole they are lysed to release the contents [64,68].

In the initial catabolism of hemoglobin, three cysteine proteases (FP-2, FP-2', FP-3) and four aspartic proteases (PM I, PM II, HAP, and PM IV) are involved. Studies have demonstrated that plasmepsins are activated by falcipains but that there exists a level of redundancy in the activity of these proteases such that autoprocessing of plasmepsins can occur if falcipain activity were blocked [54]. The products of hemoglobin metabolism

are ferrous heme and amino acids. The parasite has a limited capacity for *de novo* amino acid synthesis. Studies have confirmed that hemoglobin metabolism is sufficient to supply most of the parasite's amino acid requirements for protein synthesis and energy production [69]. However, hemoglobin is a poor source of methionine, cysteine, glutamine, and glutamate and contains no isoleucine at all. This implies that the parasite must additionally rely on an exogenous source of amino acids [65].

1.6.2.1 The fate of heme in the parasite

Ferrous heme (Fe^{II}-protoporphyrin IX) is a water-soluble substance which autocatalytically oxidizes to ferric heme (Fe^{III}-protoporphyrin IX) upon release from hemoglobin [70]. The presence of iron, the high oxygen content and the acidic pH of the food vacuole are conducive for oxygen radical formation via the Fenton and Haber-Weiss reactions. The reactive oxygen species (ROS) formed include superoxide anions (O_2^-), hydroxyl radicals and hydrogen peroxide. These are a major source of oxidative stress to the parasite and may cause protein and DNA denaturation as well as membrane disruption resulting in cell lysis and death [22,65,66]. *Plasmodium* employs various mechanisms to counter oxidative stress. Superoxide dismutase (SOD) converts superoxide radicals to hydrogen peroxide. Catalase, most likely obtained from the host in ingested cytosol, catalyzes the conversion of hydrogen peroxide to water and oxygen [65]. The parasite also employs thioredoxin and glutathione redox cycles [55]. Thus, not surprisingly, free heme at elevated concentrations is toxic to the parasite and must be efficiently detoxified.

Plasmodium lacks heme oxygenase which in humans detoxifies free heme into biliverdin [71]. Instead, the parasite primarily detoxifies heme via dimerization to an inert crystalline substance called hemozoin [62,72].

Synthetic β-hematin (Fe^{III}-protoporphyrin IX)$_2$ is chemically, spectroscopically and crystallographically identical to hemozoin [73]. The structure of Fe^{III}-protoporphyrin IX used in the structure solution of β-hematin is shown in figure 1.3 below. Dimerization occurs through Fe1-O41 links whereas the dimers are cross-linked by the formation of hydrogen bonds through O36 and O37 [73] as illustrated in figure 1.4.

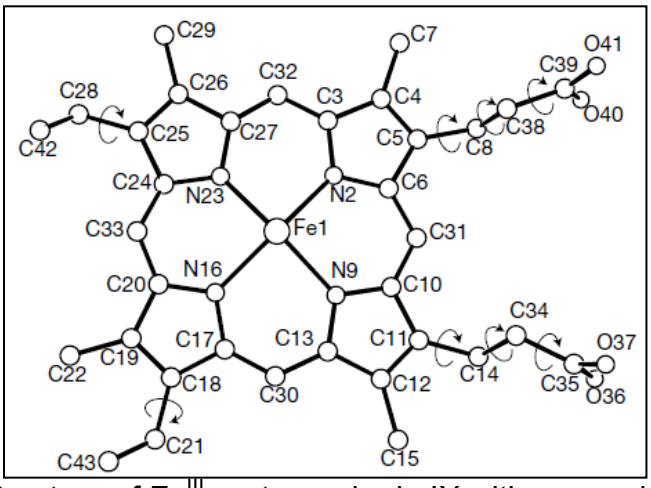

Figure 1.3: The structure of Fe^{III}-protoporphyrin IX with arrows indicating torsional degrees of freedom for the vinyl and propionic acid groups [73].

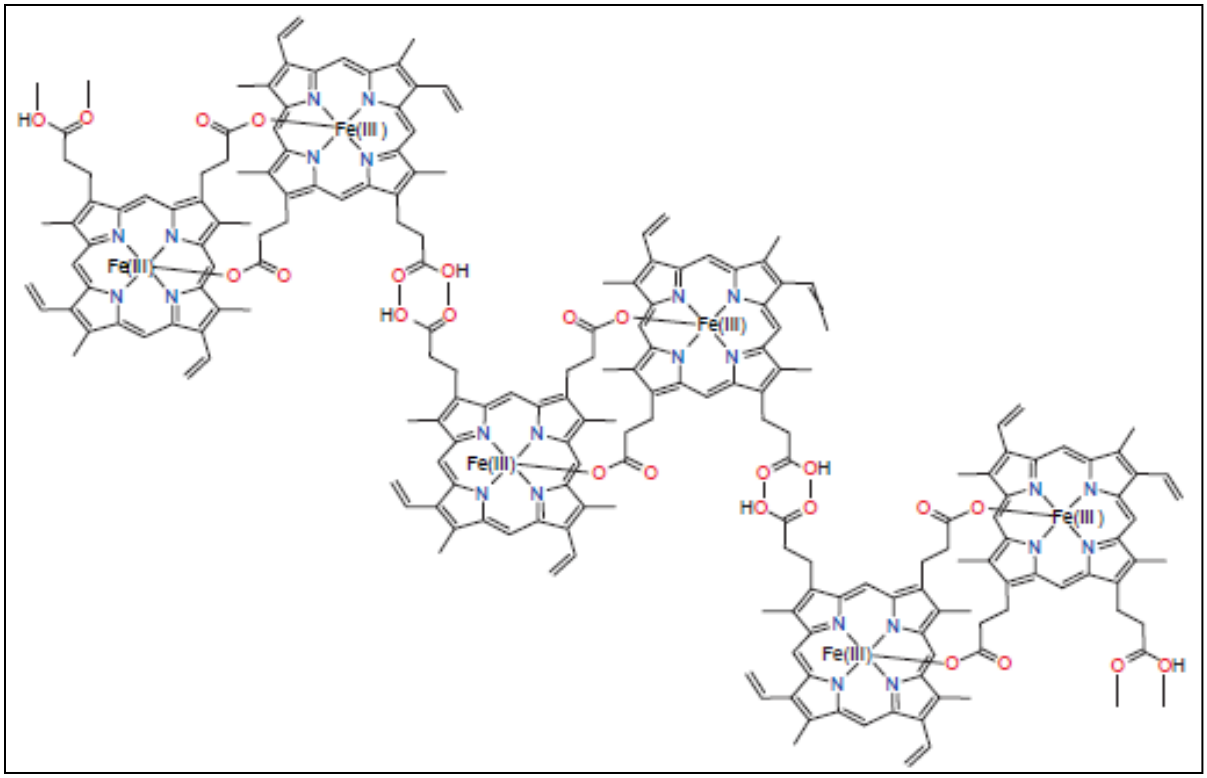

Figure 1.4: Three β-hematin dimers linked by hydrogen bonds between propionic acid groups [62].

In a recent review, Egan highlights the lack of consensus on the mechanism of hemozoin formation [74]. One of the earliest theories was the involvement of an enzyme, heme polymerase [66], but this was disputed. A second hypothesis was that hemozoin promotes β-hematin formation while yet a third school of thought was that lipids are responsible, two theories that have been experimentally demonstrated. Egan notes that although an enzymatic process may not be feasible given the almost macroscopic size of the product, a protein may act as a nucleation site for crystal growth as happens in other biomineralization processes [74]. The conclusion reached is that hemozoin formation may involve an autocatalytic process after initiation by lipids and proteins including the histidine rich protein [74]. Notwithstanding this lack of consensus, the fact that hemozoin and hematin are fixed chemical entities not susceptible to mutation and

that they are handled by a unique biochemical pathway in the malaria parasite, makes them attractive for antimalarial drug development [62].

1.6.3 Classes of drugs used in malaria chemotherapy

The eradication of malaria requires long-term efforts focused on decreasing malaria-associated fatalities through integrated, creative trans-disciplinary approach that spans basic biomedical research, public health efforts and policy implementation. It relies on both vector and parasite control strategies. Among the vector control strategies deployed widely are insecticide-treated nets and indoor residual spraying. Parasite control depends on the judicious use of available antimalarial drugs for prophylaxis as well as treatment [75]. Apart from primaquine, which acts on the pre-erythrocytic stage of malaria, all antimalarial drugs are primarily blood schizonticides. The main classes of antimalarial drugs that have been or are currently being used clinically are quinoline containing drugs, folate antagonists and artemisinin derivatives [48].

1.6.3.1 Quinoline antimalarials

Quinoline antimalarials have played an important role in the treatment of malaria. Quinine (**1**), the oldest universally known antimalarial agent, was first isolated from the bark of the cinchona tree in 1820. It continues to play an important role in the treatment of severe and complicated malaria [76]. A synthetic quinoline drug, chloroquine (**2**), was perhaps the most successful antimalarial drug known and at one time gave rise to the hope of eradicating malaria globally in the 1950s and 1960s [77].

a. The 8-aminoquinolines

The observation that methylene blue exhibited some antimalarial activity spurred the synthesis of the 8-aminoquinolines. The first synthetic antimalarial, pamaquine (**3**), synthesized in the 1920s, belongs to this class [78]. However, pamaquine was found to precipitate severe methemoglobinemia in patients with glucose 6-phosphate dehydrogenase (G6PD) deficiency [79,80] and this drove the search for safer analogues [81]. Primaquine (**4**), the less toxic primary amine analogue of pamaquine, is currently considered the drug of choice for the radical cure of malaria [82]. Apart from their activity against *Plasmodium vivax* and *P. ovale* hypnozoites, 8-aminoquinolines display rapid gametocytocidal activity [83].

b. The 4-aminoquinolines

Modifications of the ring system of pamaquine led to the development of mepacrine and the eventual synthesis of chloroquine in 1934 by scientists at Bayer laboratories [77,84]. Chloroquine became the most widely used antimalarial drug by the 1940s. The popularity of chloroquine was as a result of its efficacy and low risk of side effects when used at prescribed doses [77]. Resistance to chloroquine developed slowly but once established rapidly spread around the world limiting the use of this drug [85]. Several chloroquine analogues have been synthesized to address the problem of resistance. Amodiaquine (**5**) was once used for malaria prophylaxis but due to toxicity is currently used with artesunate in ACT for acute malaria treatment [86]. To address the shortcomings of the older 4-aminoquinolines, compounds such as ferroquine (**6**) [87], *tert*-butyl isoquine (**7**) [88] and AQ-13 (**8**) [89] have been synthesized and progressed to clinical

trials. Ferroquine is in the most advanced stage of clinical development, having recently completed phase II clinical trials. While *tert*-butyl isoquine development has been terminated, AQ-13 will be entering phase II clinical trials in Mali to study its efficacy in uncomplicated *P. falciparum* malaria (http://clinicaltrials.gov/ct2/show/NCT01614964?term=aq13).

c. Quinoline methanols and the related phenanthrene methanols.

Synthetic quinoline methanols such as mefloquine (**9**) are structural analogues of quinine which possessed excellent activity against multidrug resistant malaria parasites. Severe adverse neurological effects have eroded the clinical use of mefloquine [90]. Nonetheless, mefloquine still enjoys widespread use for malaria chemoprophylaxis among travelers and as a curative agent in the treatment of malaria infections [91]. Studies have demonstrated that the (+)-*erythro*-enantiomer may have an improved safety profile over the marketed racemic mixture [92]. The 9-phenanthrene methanols such as halofantrine (**10**) were developed by replacing the quinoline ring of the quinoline methanols with various aromatic substituents. Halofantrine use is, however, restricted due to severe cardiotoxicity. This serious side effect has not been reported with the use of the structurally related lumefantrine (**11**) [93]. Indeed, lumefantrine is combined with artemether in the first ACT recommended and prequalified by the WHO for the treatment of uncomplicated malaria [94,95]. The artemether/ lumefantrine combination, marketed as Coartem®, accounts for 75% of ACT treatments [96]. Representative chemical structures of quinoline antimalarials and phenanthrene methanols are shown in figure 1.5.

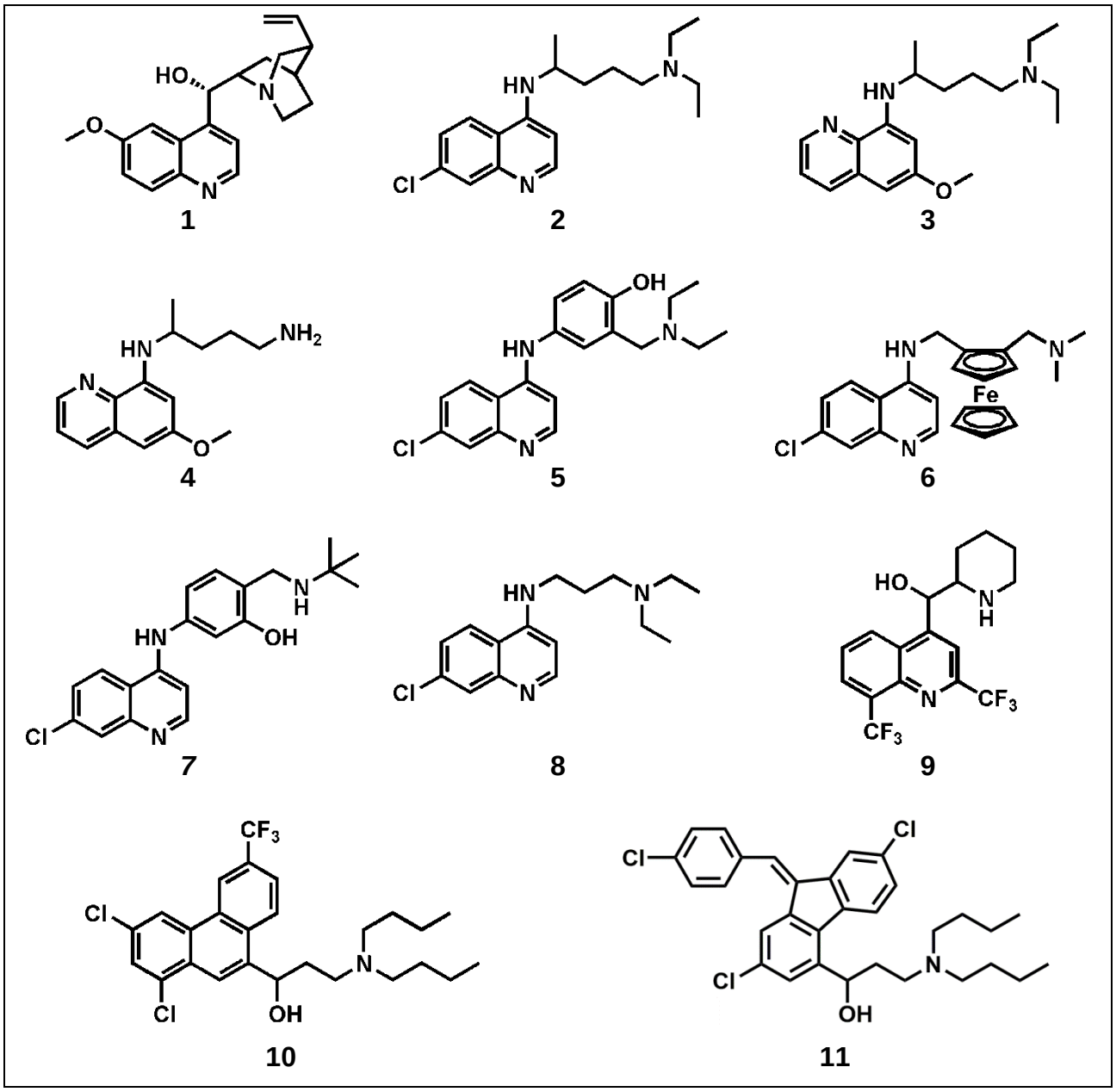

Figure 1.5: Chemical structures of quinoline antimalarials and related phenanthrene methanols

d. Mode of action of quinoline antimalarials

Quinoline antimalarials in general and the 4-aminoquinolines in particular, are believed to exert their antimalarial activity primarily by decreasing the rate of hemozoin formation [97]. This results in high concentrations of heme in the food vacuole that are ultimately fatal to the parasite. Chloroquine has been extensively studied in an attempt to

understand the mode of action of quinoline antimalarials. In the acidic food vacuole, chloroquine is 99.99 % protonated making it membrane impermeable. It, therefore, accumulates in the vacuole to very high concentrations. Chloroquine enters the food vacuole both by passive diffusion and active transportation. Studies have implicated a plasmodial Na^+/H^+ exchanger in the active importation of chloroquine into the food vacuole [77]. Chloroquine caps hemozoin molecules by π-stacking of the quinoline ring to the porphyrin of heme [92]. This prevents further heme biocrystallization resulting in its buildup to toxic concentrations. Furthermore, chloroquine forms a ferriprotoporphyrin-chloroquine complex that is highly toxic to the parasite and disrupts membrane function. The end result is cell lysis and auto-digestion of the parasite [98]. The quinoline methanols tend to associate only weakly with heme and may exert their effects by interfering with other steps in hemoglobin metabolism. The 8-aminoquinolines act by interfering with mitochondrial function. This action may be related to that of the naphthoquinones which inhibit the cytochrome bc1 complex of the mitochondrial respiratory chain and collapse the mitochondrial membrane potential [77,99].

e. Resistance to quinoline antimalarials

Resistance to quinoline antimalarials is, again, best explained using the well studied example of chloroquine. Chloroquine-resistant parasites accumulate chloroquine less efficiently in their food vacuoles than sensitive strains. Thus resistance is primarily a result of exclusion of the drug from the site of action rather than an alteration of the target [62,77]. Mutations on the *pfcrt* (*Plasmodium falciparum* chloroquine resistance transporter) gene residing on chromosome 7 have been identified in the chloroquine

resistance phenotype of various strains and are now recognized as the primary cause of chloroquine resistance [44,100]. Although the gene displays considerable polymorphism, only one amino acid change, K76T, located in the first transmemberane domain, is found consistently in all chloroquine-resistance parasites. However, it has been observed that K76T never occurs alone but with at least three other changes. In K76T, the positively charged lysine is substituted with an uncharged threonine residue. It is postulated that the positively charged K76 prevents or limits the efflux of chloroquine from the food vacuole and its substitution with an unprotonated amino acid may allow efflux to occur. Moreover, it appears that the mutant PfCRT becomes a gated channel through which charged chloroquine escapes from the food vacuole [44].

Similarities between the multidrug-resistant phenotype of tumor cells including partial resistance reversal by calcium channel antagonists led scientists to hypothesize that resistance to quinoline antimalarials may be mediated by accelerated drug efflux [48,101]. Such efflux would result from increased expression of P-glycoprotein on the food vacuole membrane. *Pfmdr*1 and 2 (*Plasmodium falciparum* multidrug resistance) genes have been identified in *Plasmodium* species. *Pfmd*r1 is located on chromosome 5 and codes for P-glycoprotein homologue-1 (Pgh-1). Several polymorphisms of this gene such as A86T have been associated with chloroquine resistance [85].

1.6.3.2 Folate antagonists

Folate antagonists used as antimalarials belong to two classes: DHPS inhibitors or class I antifolates and DHFR inhibitors also known as class II antifolates. The two classes act synergistically and are, therefore, used in combination [51].

a. DHFR inhibitors

Proguanil (**12**), chlorproguanil (**13**) and the 2,4-diaminopyrimidine pyrimethamine (**14**) are among the DHFR inhibitors that have been used as antimalarial agents. Themselves virtually inactive antimalarial prodrugs, proguanil and chlorproguanil are metabolized *in vivo* to the highly active cycloguanil (**15**) and chlorcycloguanil (**16**) (see figure 1.6).

b. DHPS inhibitors

DHPS inhibitors are sulfone or sulfonamide containing drugs. Dapsone (**17**), the oldest and most potent DHPS inhibitor, sulfadoxine (**18**), sulfaphenazole (**19**) and sulfamethoxypyrazine (**20**) (figure 1.6) have been used in various combinations with DHFR inhibitors. Combinations that have been marketed for malaria chemotherapy include sulfadoxine/pyrimethamine, sulfamethoxypyrazine/pyrimethamine and dapsone/chlorproguanil [50,51].

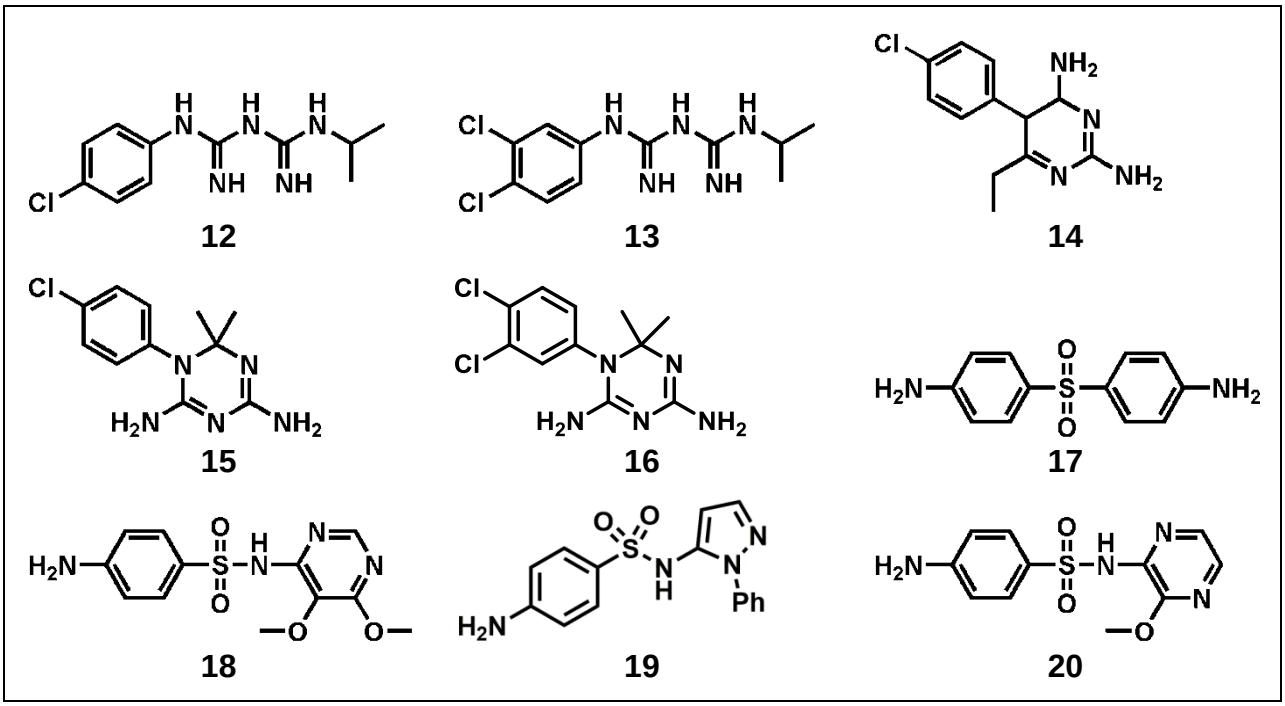

Figure 1.6: Chemical structures of folate antagonists

c. Mode of action

Folate antagonists sequentially inhibit two key enzymes involved in the *de novo* synthesis of folic acid in the malaria parasite. In so doing, they deprive the parasite of reduced folate co-factors essential for many reactions involving one-carbon unit transfer such as DNA and amino acid synthesis. This is not only an effective way of killing the parasites but it also blocks the ability of the parasite to multiply [50]. DHPS inhibitors mimic *para* aminobenzoic acid (PABA) and competitively inhibit the enzyme. In addition, these drugs condense with 2-amino-4-hydroxy-6-hydroxymethyl-7,8-dihydropteridine pyrophosphate to form sulfa-dihydropteroate (sulfa-DHP) which may disrupt folate metabolism by other mechanisms [102].

d. Resistance to folate antagonists

Resistance to folate antagonists developed rapidly upon introduction of these drugs and is associated with point mutations on DHFR and DHPS. The mutant enzymes have altered properties and interact sub-optimally with the antagonists making them less susceptible to inhibition. Gregson and Plowe have extensively reviewed the various point mutations involved in conferring resistance to folate antagonists [103]. Specificity has been observed in resistance of various DHFR mutants to different DHFR inhibitors. It has further been suggested that parasites have a limitation in mutation possibilities. Such observations have served as an impetus for the development of new folate antagonists. Additional molecular targets in the folate biosynthesis pathway are also being exploited to develop new antimalarials [50].

1.6.3.3 Artemisinin derivatives

Artemisinin (**21**) was isolated from *Artemisia annua*, long used in Chinese herbal medicine for the treatment of fever, in 1972. This followed the demonstration of potent antimalarial activity of *A. annua* extracts in 1967 by Chinese scientists [104]. Following widespread resistance to chloroquine and folate antagonists, ACT is now the first-line treatment for uncomplicated malaria [105]. Artemisinin derivatives have a rapid onset of action and rapidly clear parasitemia leading to quick resolution of symptoms. Additionally, these compounds are rapidly eliminated and are thus recommended to delay resistance mechanisms [106].

a. First generation artemisinins

Artemisinin is only marginally soluble in water or oil thus making it difficult to formulate and limiting its bioavailability. Its short *in vivo* half life (about 2 h) necessitates a weeklong treatment regimen. The first generation of semisynthetic derivatives developed to address this shortcoming include dihydroartemisinin (**22**) (which is also a metabolite of artemisinin), a compound that is twice as potent as artemisinin but that is thermally less stable and possibly neurotoxic [107]. The water-soluble artesunate (**23**) and artelinate (**24**) are administered intravenously in the treatment of severe malaria. Artemether (**25**) and arteether (**26**) are β-alkyl ethers of dihydroartemisinin with increased lipid solubility and improved pharmacokinetic and antimalarial efficacy [108]. Combinations of artemisinin derivatives in use include artesunate-amodiaquine, artesunate-mefloquine, dihydroartemisinin-piperaquine and artemether-lumefantrine [105].

b. Second generation artemisinins

Thousands of second generation artemisinin derivatives have been synthesized that preserve the trioxane's powerful antimalarial activity against both drug sensitive and resistant malaria strains while improving the pharmacokinetic and solubility characteristics and lowering the potential for neurotoxicity. These include various semisynthetic monomeric, dimeric, trimeric and tetrameric analogues of artemisinin and dihydroartemisinin, synthetic endoperoxides and hybrids of both classes peroxide antimalarials [107]. Owing to the structural complexity of artemisinin, commercial production relies on extraction and purification from *Artemisia annua* [109]. With increasing demand for artemisinin-based therapies, especially fueled by the provision of subsidized medicines to fight malaria, plant extraction may no longer remain a sustainable source [110]. Inspired by the excellent activity of the artemisinins and the need to find viable alternatives to plant extraction, chemists have developed novel purely synthetic endoperoxides that are synthetically tractable and can be produced at low cost [111].

Several trioxanes, trioxolanes and tetraoxanes have been synthesized to this end. Two ozonides from these campaigns, **OZ277 (27)** and **OZ439 (28)**, are currently undergoing clinical trials as candidate drugs for malaria treatment. **OZ439** has greater stability in blood and improved oral bioavailability relative to **OZ277** which was found to have increased chemical instability in iron-rich infected blood [92,112]. In 2012, **OZ277** was approved for the Indian market as a combination product with piperaquine phosphate (Synriam) for the treatment of malaria [207].

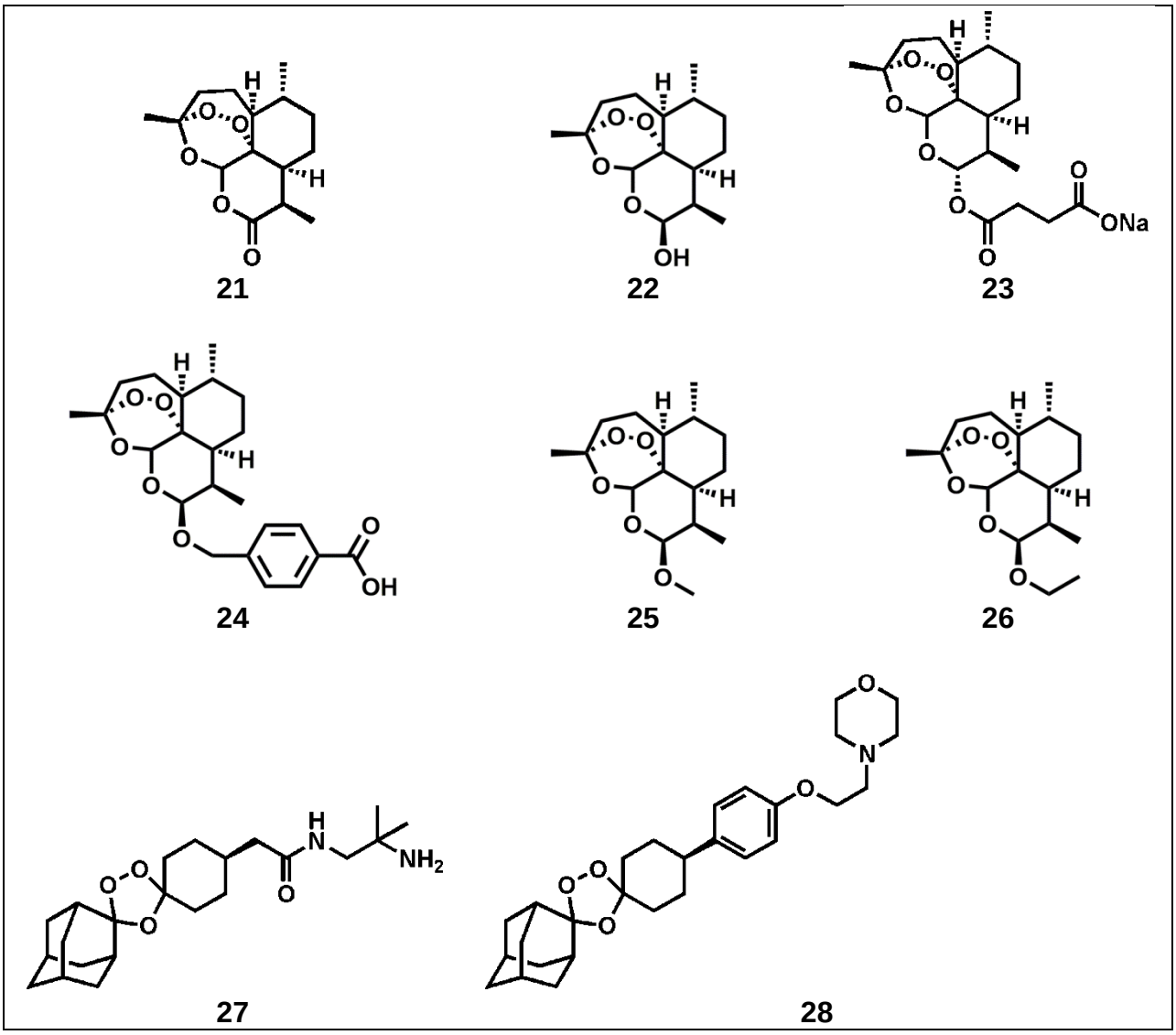

Figure 1.7: Chemical structures of selected artemisinin derivatives ozonides

c. Mode of action of artemisinin derivatives

The demonstration that the endoperoxide bridge was necessary for antimalarial activity suggested that reactive oxygen species and free radicals may be involved in artemisinin's mechanism of action [113]. The opening of the peroxide bridge to form free radicals may be activated by heme or free iron [114]. It is generally believed that reductive scission of the peroxide bridge produces an O-centered radical which undergoes

rearrangement to generate a C-centered free radical [115]. The C-centered radicals could be involved in the alkylation of several malarial proteins. Specifically, cysteine adducts of artemisinin have been reported, implicating alkylation of cysteine residues of various proteins as a possible mechanism by which this compound interferes with protein function. Indeed, artemisinin derivatives have been shown to inhibit falcipains, thus interfering with hemoglobin degradation [115]. In addition, inhibition of PfATP6, the sarco/endoplasmic reticulum membrane calcium ATPase (SERCA) by artemisinin has been demonstrated. This inhibition leads to increased cytosolic free calcium concentrations resulting in parasite death [116]. Parasite membrane damage by accumulation within neutral lipids appears to be yet another mechanism of action of the artemisinins. Thus artemisinin derivatives appear to exert their effects by acting at several targets which partly explains why they are active against multidrug resistant parasites [106].

d. Mechanism of resistance to artemisinin derivatives

The first cases of artemisinin resistance were reported in South-East Asia along the Thai-Cambodia border [19]. Among the proteins implicated in modulating *Plasmodium* susceptibility to antimalarials are PfATP6, translationally controlled tumor protein (TCTP), PfCRT and PfMDR1 [108]. Point mutations of the genes encoding these proteins may be responsible for the development of resistance against artemisinin. O'Brien et al. have aptly concluded that with precious few drugs available to replace ARTs should they fail, the importance of countering resistance cannot be underestimated [117]. This dire predicament is also a major rationale for the search for new antimalarial drugs [118].

1.7 ADVERSE DRUG REACTIONS/DRUG TOXICITY

Edwards and Aronson comprehensively and unambiguously define adverse drug reactions (ADRs) as "an appreciably harmful or unpleasant reaction, resulting from an intervention related to the use of a medicinal product, which predicts hazard from future administration and warrants prevention or specific treatment, or alteration of the dosage regimen, or withdrawal of the product" [119]. The impact of ADRs can be viewed from two perspectives: the pharmaceutical industry perspective and the clinical perspective.

1.7.1: The economic and health significance of ADRs

1.7.1.1 ADRs: The industry perspective

As far as the pharmaceutical industry is concerned, nonclinical and clinical safety has remained a major cause of drug attrition and the attendant enormous financial and time ramifications. Attrition can occur during preclinical or clinical development and at the post-approval stage, resulting in withdrawal of marketed drugs accounting for approximately one-third of all drug discontinuation [120]. Lasser et al. reported that out of the 548 new chemical entities approved for the US market between 1975 and 1999, 16 were subsequently withdrawn from the market while 45 acquired at least one black box warning as a consequence of their toxicity [121]. About 2.3 million case reports of adverse events for the cumulative number of approximately 6000 marketed drugs were entered in the US Adverse Event Reporting System database between 1969 and 2002. As a result, 75 drugs and drug products were withdrawn by the US Food and Drug Administration over this period [122].

1.7.1.2 ADRs: The patient's perspective

From the patient's perspective, adverse reactions are a significant cause of patient morbidity and mortality besides prohibiting the use of effective treatment. ADRs are a major cause of hospital admission. Pirmohamed et al. reported that 6.4 % of hospital admissions in two large UK hospitals were related to ADRs with an overall fatality of 0.15 % and a projected national annual cost to the NHS of USD 847 million [123]. In a later study it was estimated that 1 out of every 7 in-patients experiences an ADR resulting in prolonged hospitalization [124]. Elsewhere, a 2001 study in the Netherlands found that 1.83 % of all acute hospital admissions were ADR related. This was slightly below the 2.4 % to 6.4 % estimated from meta-analyses for Western countries [125]. Fatalities directly attributable to adverse drug reactions are estimated to be the fourth to sixth leading cause of death in US hospitals, exceeding deaths caused by pneumonia and diabetes [126]. Clearly, therefore, it is imperative to address the issue of drug safety as early as possible in drug development in order to save time, money and lives while at the same time contributing to safer treatment options. ADRs can be divided into five main classes [119,127].

1.7.2 Types of ADRs

1.7.2.1 Type A ADRs

Type A (Augmented) reactions can be predicted from the known pharmacology of the drug, both on-target and off-target. They are the most frequent ADRs and generally arise from an exaggeration of pharmacological effect. The difference between type A

reactions and other ADRs is that in the case of type A reactions, the identity of the pharmacological target (whether the primary or the secondary one) is established [127,128].

1.7.2.2 Type B ADRs

Also referred to as idiosyncratic drug reactions (IDRs), type B (Bizarre) reactions do not exhibit the classic dose-response relationship, cannot be predicted from the known pharmacology of a drug, are host-dependent and are rare within the range of doses used clinically [129]. These reactions generally require repeat administration of a drug to elicit a toxic response. Characteristics of type B reactions suggest the involvement of the immune system. The covalent binding of reactive metabolites (or of the parent drug in a few cases) to proteins or other macromolecules is considered the first pivotal event in type B toxicity [128]. The 'hapten hypothesis' has been put forward to link the reactive metabolites with immune-mediated IDRs. According to this hypothesis, modification of a protein may result in the immune system recognizing the protein as foreign and subsequently mounting an immune response [130]. The liver, blood cells and skin are the three prime sites of type B toxicity. Consequently, these reactions manifest as hepatotoxicity, blood dyscrasias, such as agranulocytosis, and dermatitis. In almost all cases, type B reactions are delayed and occur a week or more after exposure [129].

1.7.2.3 Type C ADRs

Type C (chemical) reactions are caused by a chemical reaction between the drug or its metabolite and macromolecules resulting in a rapidly ensuing response [127]. Similarly to type B reactions, bioactivation to reactive metabolites plays a role except for a few drugs such as alkylating antineoplastic drugs which directly form covalent bonds with proteins. Type C reactions in most cases show a dose-response relationship [128]. These

reactions can be predicted or rationalized in terms of chemical structure [131]. A well known example of a type C adverse drug reaction is the hepatotoxicity caused by high doses of acetaminophen (paracetamol). Acetaminophen is metabolized to the readily water soluble *O*-glucuronide or sulfate and excreted in urine. A small percentage of the dose undergoes bioactivation to *N*-acetyl-*p*-benzoquinoneimine (NAPQI) which, at therapeutic doses, is quenched with glutathione. Following an overdose, glutathione depletion occurs and NAPQI covalently reacts with liver proteins resulting in toxicity [132]. *N*-acetyl cysteine, which acts by restoring GSH levels, has been widely used as an antidote to acetaminophen poisoning and the associated hepatotoxicity [208].

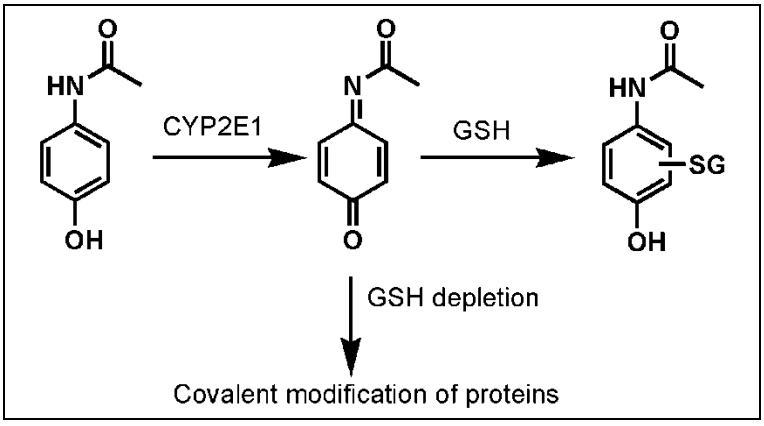

Figure 1.8: Bioactivation of acetaminophen

1.7.2.4 Type D ADRs

Type D (Delayed) reactions, exemplified by teratology and carcinogenicity, occur months or even years after exposure to the drug [119]. Carcinogenicity is associated with a dose-response relationship in which the duration of exposure is more important than the concentration or dose size. It can be caused by genotoxins, in most cases reactive metabolites, or by disruption of endocrinological processes. Thus, mechanisms for delayed toxicity tend to overlap with those of types A, B and C reactions [128].

1.7.2.5 Type E ADRs

Type E (end of treatment) reactions occur when a drug is withdrawn such as the withdrawal syndrome observed with opioid analgesics [131]. Another class of reactions that occurs commonly are type F (unexpected failure) reactions. These are dose related and are often caused by drug interactions for example with cytochrome P450 inducers which result in inadequate dosage of the coadministered drugs [119]. The figure below illustrates the role of drug bioactivation in drug toxicity.

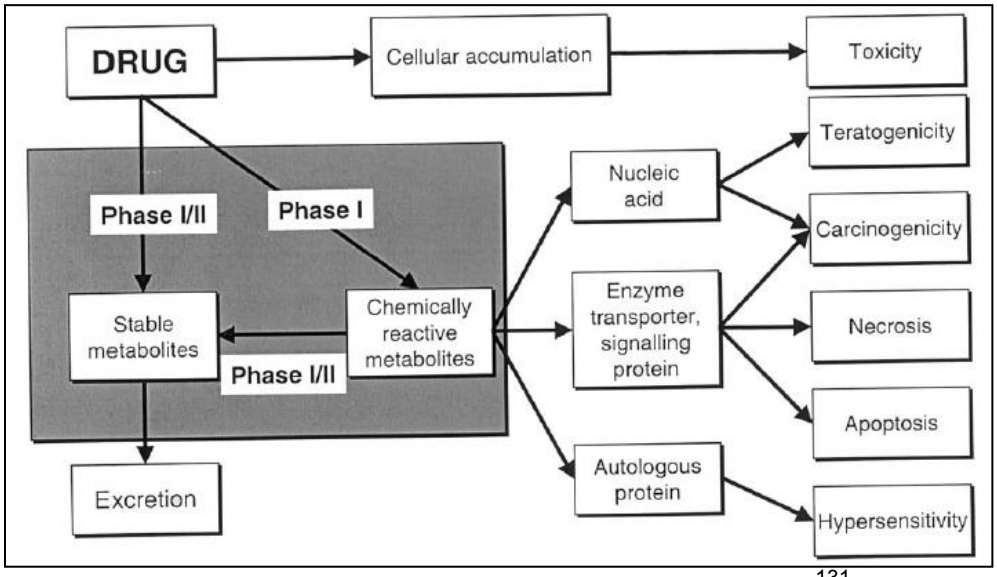

Figure 1.9: Xenobiotic metabolism and toxicity [131]

1.7.3 Overview of drug metabolism

In drug discovery and development, the optimization of pharmacokinetics properties is of paramount importance [133]. These properties include absorption, distribution, metabolism and excretion (ADME). Toxicity is commonly considered with ADME properties (hence the acronym ADMET) because of its close association with pharmacokinetics [134]. Prior to 1990, ADME properties were a leading cause of drug attrition. However, incorporating them early in drug discovery largely minimized their

contribution to attrition [135]. As Kola and Landis reported in their landmark study, after the year 2000, clinical safety and toxicology are emerging as the leading causes of drug attrition [135].

From the preceding discussion on ADRs, it is evident that drug metabolism plays a critical role in drug toxicity. However, bioactivation is a minor pathway in the overall drug metabolism. In a meta-analysis of 6767 drugs, Testa, Pedretti, and Vistoli found toxic and reactive metabolites to account for 7 % of total metabolites [136].

The primary function of drug metabolism is to make a lipophilic molecule more hydrophilic so that it can be readily conjugated and/or excreted from the body [137]. Drug metabolism has been, albeit inaccurately, traditionally divided into phase I and phase II metabolism [138].

1.7.3.1 Phase I metabolism

Phase I metabolism introduces or unmasks chemically reactive functional groups on which phase 2 reactions can occur [139]. Apart from a few exceptions, phase I metabolism generally precedes phase II metabolism. Over 75% of phase I drug metabolism is carried out by cytochrome P450 monooxygenases [140] although a more recent analysis puts this figure at about 60% [136]. Five of the 57 human P450s (1A2, 2C9, 2C19, 2D6, and 3A4) catalyze over 90% of P450 reactions. Overall, only about a quarter of the CYPs are involved in xenobiotic metabolism. Reactions catalyzed by CYP450 enzymes include epoxidation, hydroxylation, dealkylation (*N*-, *S*-, and *O*-), oxidation (*N*-, *S*- and *P*-), desulfuration, dehalogenation as well as nitro and azo reduction [141]. CYP3A4 accounts for approximately 50 % of the total metabolism by these 5 enzymes as illustrated in the figure below which also depicts the contribution of other enzymes to

phase I metabolism [140,142]. Another enzyme involved in phase I metabolism, in particular the oxygenation of heteroatom-containing compounds, is the flavin-containing monooxygenase [143].

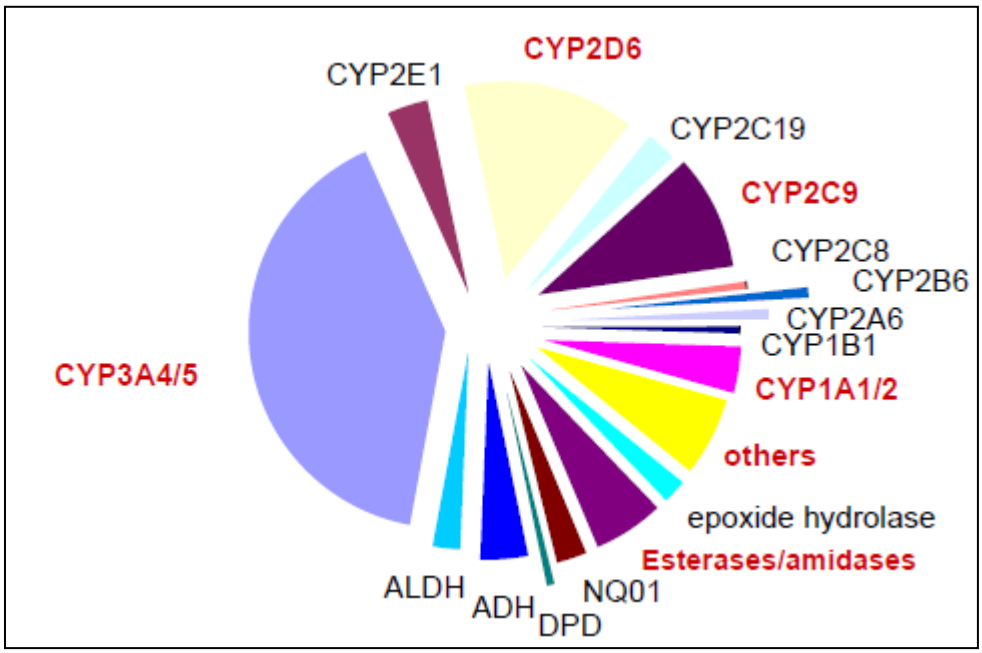

Figure 1.10: Phase 1 drug metabolizing enzymes. CYP: cytochrome P450, NQ01: NADPH:quinone oxidoreductase; DPD: dihydropyrimidine dehydrogenase; ADH: alcohol dehydrogenase; ALDH: aldehyde dehydrogenase [144].

The CYP450 catalytic cycle

The main function of CYP450 enzymes is the activation of molecular oxygen to a reactive species that can attack relatively inert chemical sites such as hydrocarbon chains and aromatic rings [145,146]. This involves the split of molecular oxygen into two atoms, one of which gets incorporated into the substrate and the other released as part of a water molecule [146]. The typical oxidation reaction (with the substrate represented by R-H) requires NADH or NADPH as a cofactor as shown below [147].

$NAD(P)H + O_2 + R\text{-}H + H^+ \rightarrow NAD(P)^+ + R\text{-}O\text{-}H + H_2O$.

The CYP450 catalytic cycle (figure 1.11) is represented as a series of distinct steps: substrate binding, reduction of ferric P450 to ferrous P450, reaction with oxygen to form a ferrous-O_2 adduct, reduction of the adduct, release of one oxygen atom as part of a water molecule, the actual oxidation of the substrate and its final release [145,148].

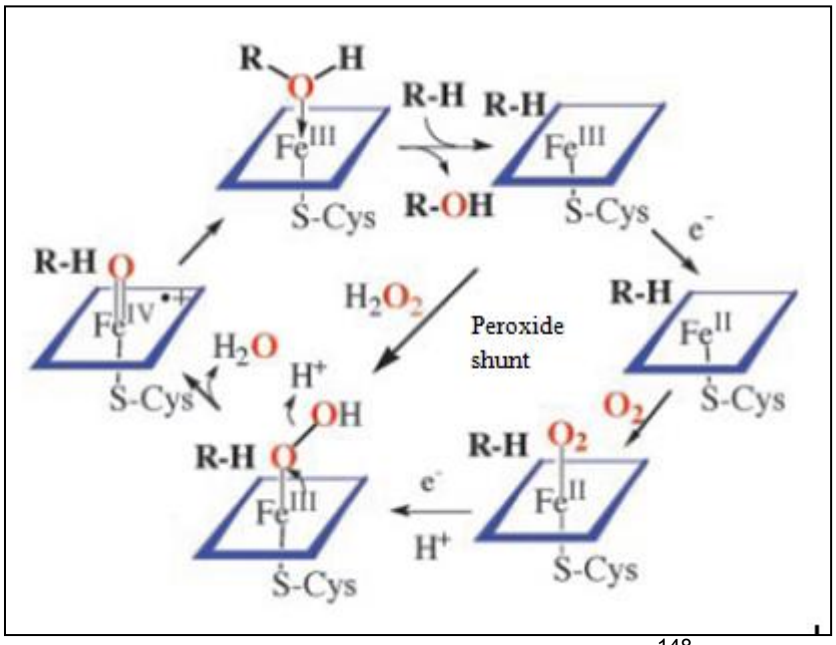

Figure 1.11: CYP450 catalytic cycle [148].

1.7.3.2 Phase II metabolism

Phase II metabolism generally involves conjugation of nucleophilic groups present in a molecule or introduced in phase I metabolism with small molecular weight organic donor molecules [149]. These conjugation reactions enhance the water solubility and hence the excretion of the resulting metabolites. Furthermore, they play a fundamental role in metabolic inactivation and detoxification though in a few cases they are involved in bioactivation [150]. The main enzymes involved include UDP-glucuronosyltransferases, sulfotransferases, *N*-acetyltransferases, glutathione-*S*-transferases and

methyltransferases such as thiopurine-*S*-methyl transferase and catechol-*O*-methyl transferase [151].

1.7.4 Bioactivation

Bioactivation is the process whereby an innocuous molecule is metabolically converted to a reactive metabolite, potentially deleterious to the cell [152]. The reactive chemical species are either electrophiles or free radicals and exert their effects by subsequently covalently reacting with tissue nucleophiles resulting in their modification or denaturation [142]. The CYP450 enzymes are the major enzymes involved in drug bioactivation. Other reactions such as glucuronidation and sulfation are, however, also involved in bioactivation as exemplified by the bioactivation of nonsteroidal anti-inflammatory drugs to acyl glucuronides [131]. Moreover, bioactivation by oxidative chemicals, particularly hypochlorous acid, released by activated neutrophils has been implicated in the development of blood dyscrasias such as amodiaquine-induced agranulocytosis [131].

The potential for reactive metabolite formation is routinely examined as part of lead optimization efforts in drug discovery [153].

1.7.4.1 The concept of structural alerts

Several substructures, referred to as structural alerts, that form chemically reactive metabolites have been identified [154]. Stepan et al. analyzed the top 200 drugs marketed in the USA in 2009 and found that 78-86 % of the drugs associated with toxicity contained at least one structural alert [153]. This confirms the assertion that most drugs

that elicit ADRs possess structural alerts and undergo bioactivation culminating in toxicity [155,156]. Several examples exist where the substitution of structural alerts with metabolically (more) benign groups in drugs exhibiting toxicity has improved the safety profile of the resulting molecules. The procainamide (**29a**)/flecainide (**29b**), metiamide (**30a**)/cimetidine (**30b**), suprofen (**31a**)/ketoprofen (**31b**) drug pairs (figure 1.12) are but a few examples [157,158].

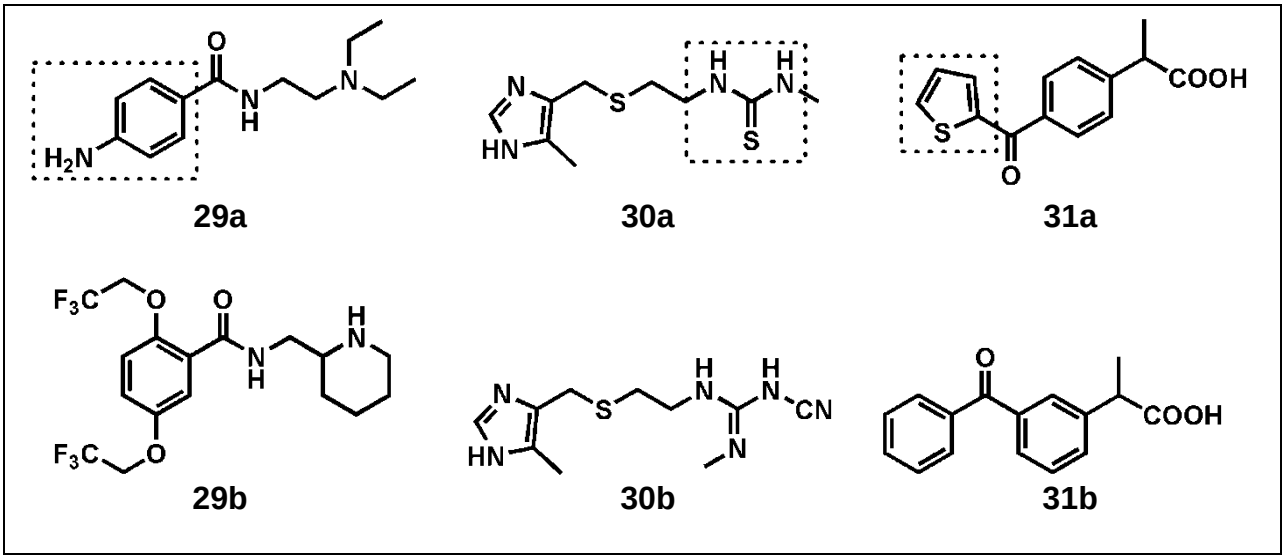

Figure 1.12: Drug pairs where substitution of the structural alert (dotted box) has resulted in safer molecules

The avoidance of structural alerts is, therefore, almost a norm in drug design. However, the challenge facing medicinal chemists is the fact that not all molecules that possess structural alerts cause ADRs and there are a number of safe drugs in the market to illustrate this point [153]. It is now recognized that factors such as dose, duration of usage, detoxification efficiency and the presence of multiple metabolism and/or elimination pathways play a role in determining whether a molecule with a structural alert will elicit toxicity [155,156,158]. A list of functional groups recognized as structural alerts and their reactive metabolites is given in Table 1.2.

Table 1.2: Common structural alerts, their reactive metabolites and associated toxicities [155,158]

Functional group	Reactive metabolite	Examples
Aromatic amines (anilines, anilides, *p*-aminophenols)	Quinone imine or nitroso	Acetaminophen (hepatotoxicity) Procainamide (lupus erythematosus)
Hydrazine, hydrazide	Diazene or diazonium ion	Isoniazid (hepatotoxicity)
Nitroarenes	Nitroso	Tolcapome (hepatotoxicity)
Fused azaheterocycles	Nitrenium ion	Clozapime (agranulocytosis)
Sulfonylureas	Isocyanate	Tolbutamide (teratogenicity)
Furans	α,β-unsaturated dicarbonyl	Furosemide (nephrotoxicity)
Thiophenes	α,β-unsaturated dicarbonyl	Ticlopidine (agranulocytosis)
Thiazoles	Thioamide, glyoxal	Sudoxicam (hepatotoxicity)
Thiazolidinediones	S-oxide, isocyanate	Troglitazone (hepatotoxicity)
α,β-unsaturated carbonyls	Intrinsic electrophilicity	Cyclophosphamide (hemorrhagic cystitis)
Aliphatic amines	Iminium ion	1-methyl-4-phenyl-1,2,3,6-tetrahydropyridine (neurotoxicity)

1.7.4.2 Reactivity of reactive metabolites

Most reactive metabolites are short-lived and unstable thus making their detection in circulating blood or plasma impossible [159,160]. This can be attributed to rapid conjugation with the endogenous anti-oxidant, glutathione (GSH), elimination via some other detoxification process such as hydrolysis or reaction with cell macromolecules resulting in toxicity [153,156,161]. As a result, the formation of reactive metabolites is often inferred from the detection of stable glutathione conjugates[156].

Electrophilic reactive metabolites are generally classified as soft or hard electrophiles [158]. A majority of reactive metabolites are soft electrophiles and include quinones,

quinone imines, quinone methides, epoxides, arene oxides and nitrenium ions [162]. Hard reactive metabolites include aldehydes and iminium ions. Generally hard electrophiles react with hard nucleophiles which are mostly nitrogen containing compounds while soft electrophiles react with soft nucleophiles, usually sulfur containing compounds [163]. Reactive metabolite formation can be assessed using three main techniques: trapping reactions, covalent protein binding and mechanism-based CYP inhibition [161,163].

1.7.4.3 Assessment of bioactivation

1.7.4.3.1 Trapping reactions

The chemical reaction of reactive metabolites with trapping agents to form stable adducts which are then characterized by liquid chromatography coupled with tandem mass spectroscopy (LC-MS/MS) and/or nuclear magnetic resonance (NMR) spectroscopy is a widely used technique for assessing reactive metabolite formation. Such trapping experiments are carried out using liver microsomes in the presence of NADPH or other co-factors to generate reactive metabolites and an appropriate trapping agent that immediately reacts with the metabolites [163].

For soft electrophiles, GSH is the trapping agent most commonly used, although other thiol containing compounds such as *N*-acetylcysteine can be used [164]. Potassium cyanide, methoxylamine, semicarbazide, *γ*-glutamylcysteinyl lysine are some of the compounds that have been employed to trap hard electrophiles [165,166]. It has been demonstrated that *γ*-glutamylcysteinyl lysine can simultaneously trap both soft and hard electrophiles thus increasing the sensitivity and reliability of reactive metabolite screening [162]. To improve on the sensitivity and specificity of trapping reactions, the

radiolabeling of GSH, semicarbazide and potassium cyanide has been successfully employed [167,168].

The use of microsomes and NADPH is predicated on the fact that bioactivation is mainly a function of phase I metabolism. It is, therefore, important to consider other bioactivation pathways for example by the addition of different co-factors and the use of different *in vitro* systems such as hepatocytes or neutrophils [164]. The use of electrochemical oxidation to mimic phase I metabolism will be discussed later on. Free radicals may be trapped using spin-trapping reagents. These include 5,5-dimethylpyrroline-*N*-oxide, *tert*-nitrosobutane, phenyl-*tert*-butylnitrone and α-(4-pyridyl-*N*-oxide)-*N*-*tert*-butylnitrone [163].

1.7.4.3.2 Covalent binding

The formation and irreversible binding of reactive metabolites to macromolecules can be detected and quantified using ^{14}C- and/or ^{3}H-labeled compounds [163]. The radiolabeled compounds are usually incubated with liver microsomes in the presence of appropriate co-factors. Freshly isolated hepatocytes may be used to assess bioactivation processesses that depend on a full complement of cellular enzymes [166]. The amount of unextractable radioactivity remaining in the protein pellet is an indication of the extent of covalent binding and is expressed in pmol /mg of protein [163]. A value of >50 pmol /mg of proteins is generally considered, but not absolutely fixed, to imply potential toxicity [159].

1.7.4.3.3 Mechanism-based CYP inhibition

In some cases, the metabolite formed by an enzyme is so reactive that it reacts directly with the enzyme active site resulting in inactivation of the enzyme [169]. Such mechanism-based inhibition is NADPH-, time- and concentration-dependent [170] and is also referred to as time-dependent inhibition (TDI). The TDI assay involves an inactivation assay where the enzyme is incubated with the inhibitor followed by an activity assay where a substrate is added to assess remaining enzyme activity using MS or fluorescence techniques [171]. Since a positive TDI hit indicates the formation of reactive metabolites, TDI is employed as an *in vitro* screening method for these metabolites [163].

1.7.4.4 Animal models for bioactivation and the use of integrated systems

It is virtually impossible to reproduce certain adverse drug reactions that occur in humans in *in vitro* systems [153]. The use of animal models is, therefore, an important tool for mechanistic studies especially of type B reactions. However, challenges of extrapolation to humans and the paucity of practical and valid animal models still remain [129]. Consequently, in the case of drug-induced hypersensitivity, the use of lymphocytes from hypersensitive patients in *ex vivo* studies represents the only relevant system to study cellular, molecular and chemical mechanisms [158]. In the pharmaceutical industry, an integrated system of risk assessment and mitigation strategies for reactive metabolites in drug development such as that described by Thompson and co-workers would be useful in decision making. This system quantifies CYP450 dependent and CYP450 independent cell toxicity, mitochondrial impairment, inhibition of the Bile Salt Export Pump as well as covalent binding of radiolabeled drug to human hepatocyte

proteins [172]. Such comprehensive testing is likely to minimize chances of false positives or false negatives usually associated with the use of a single test.

1.7.4.5 Electrochemical oxidation online with electrospray ionization mass spectrometry (EC-ESI/MS)

When using conventional *in vivo* and *in vitro* techniques, detection of reactive metabolites is hampered because the reactive species formed are immediately covalently bound to cellular macromolecules [160]. To overcome this challenge, the use of electrochemical oxidation, electrochemically assisted Fenton chemistry and synthetic metalloporphines to mimic CYP450 catalyzed oxidations has been extensively investigated [173]. Electrochemical oxidation has been found to successfully mimic benzylic hydroxylation, hydroxylation of aromatic rings containing electron-donating groups, N-dealkylation, S-oxidation, dehydrogenation and, less efficiently, N-oxidation and O-dealkylation [173]. Johansson and co-workers have demonstrated the utility of electrochemical oxidation to mimic CYP450 and liver microsome catalyzed oxidation of amodiaquine and desethylamodiaquine [174]. This finding corroborates observations by other researchers on the usefulness of electrochemistry in mimicking phase I oxidation of paracetamol, clozapine, and trimethoprim [175] and diclofenac [176]. The coupling of EC with MS means that MS/MS can be used to provide important structural information about the reactive metabolites formed. An important advantage of using electrochemical oxidation, however, is that it can be employed at a semi-preparative to preparative scale to generate reactive metabolite adducts which can be characterized by NMR thus facilitating unambiguous structural identification [177].

1.8 AMODIAQUINE

1.8.1 Pharmacokinetics

Amodiaquine is rapidly absorbed and extensively metabolized after oral administration in humans, which leads to a low plasma exposure of the parent drug [178]. Desethylamodiaquine is the main metabolite of amodiaquine. Other reported metabolites are bisdesethylamodiaquine and 2-hydroxydesethylamodiaquine [179,180]. The elimination of desethylamodiaquine is very slow unlike that of amodiaquine; giving this metabolite a long terminal half-life [181,182]. Both parent and metabolite have antimalarial activity, making amodiaquine act as a prodrug of desethylamodiaquine [179]. The main enzyme responsible for amodiaquine deethylation was shown to be CYP2C8 [183,184]. Asymmetrical permeability properties of amodiaquine in the Caco-2 absorption model system have been observed, which alludes to the possible role of active transport of the drug [185,186]. Both amodiaquine and desethylamodiaquine have been shown to be potent inhibitors of the important drug metabolising enzyme, CYP2D6 [187].

1.8.2 Toxicity

In spite of its excellent antimalarial activity, it was observed, through pharmacovigilance programs, that prophylactic use of amodiaquine caused severe side effects including hepatitis, aplastic anemia and agranulocytosis [155,188,189]. Among patients undergoing treatment with amodiaquine, the risk of each of these adverse effects is estimated to be 1 in 15,500 for hepatotoxicity, 1 in 2,100 for agranulocytosis and 1 in 30,000 for aplastic anemia [190]. Its use is, consequently, restricted to the treatment of the acute phase of malaria, during which no serious cases of toxicity have been reported [182]. In acute malaria treatment, amodiaquine is administered in combination with other antimalarial

agents such as artesunate in the artemisinin-based combination therapy currently recommended by the World Health Organization [191].

The 4-aminophenol moiety of amodiaquine has been identified as a 'structural alert' for toxicity. Bioactivation of this moiety to a reactive quinone imine metabolite has been identified as the likely cause of amodiaquine toxicity [155]. This reactive metabolite acts by covalently binding to cellular macromolecules causing drug-induced toxicity and cell damage directly or via immunological mechanisms. The detoxification of the quinone imine and other reactive intermediates involves rapid binding to a trapping agent, usually reduced glutathione (GSH) [159]. Indeed, studies in rats indicate that amodiaquine is excreted exclusively as the thioether conjugates of glutathione and cysteine [192]. High doses of the drug overwhelm the detoxification mechanisms and the depletion of GSH is recognized as one of the risk factors for amodiaquine-induced hepatotoxicity [193]. Naisbitt and co-workers showed that this protein-reactive quinone imine metabolite depleted intracellular glutathione levels when incubated with neutrophils in an activating medium [194]. Incubation of amodiaquine with stimulated polymorphonuclear leukocytes (PMN) produced the quinone imine metabolite [195]. These and several other studies point to the possible role of bioactivation in drug-induced agranulocytosis. Immune-mediated hypersensitivity reactions have also been suggested as an attendant mechanism of quinone imine toxicity [196,197]. This mechanism has been corroborated by the detection of antidrug IgG antibodies in some patients receiving amodiaquine [198].

The aldehyde metabolite has been postulated as another possible explanation for amodiaquine toxicity. Using a panel of 13 human recombinantly expressed cytochromes P450 (rP450s), CYP1A1 and CYP1B1 were shown to mediate the formation of an

unidentified metabolite, M2 [183]. These two enzymes are found in extrahepatic tissues including leukocytes. Another group of researchers found that electrochemical oxidation of amodiaquine using EC-ESI/MS generated, besides the quinone imine species, another oxidation product with the same molecular mass as M2, for which they proposed an aldehyde structure [177]. Using *in vitro* systems (CYP1A1 and CYP1B1) and electrochemical oxidation, Masimirembwa and coworkers confirmed (using retention times, accurate mass, and product ion spectra) that the second major oxidation product from the electrochemical system was identical with the major metabolite formed by CYP1A1 and CYP1B1. This metabolite, with a pseudomolecular ion at m/z 299, was the same as the unidentified metabolite M2 and was not observed in incubations with human liver microsomes [174]. Since these enzymes are involved in the bioactivation of many procarcinogens [199,200], it was of interest to establish the structure of M2 and assess its potential reactivity. The electrochemical generation of the aldehyde metabolite was repeated on a preparative scale, and NMR spectroscopy confirmed the structure of M2 as the aldehyde metabolite of amodiaquine [174]. The same study demonstrated using trapping experiments with N-acetylcysteine that the aldehyde metabolite undergoes further oxidation to an aldehyde quinone imine species [174]. The distinct distribution of ADQ metabolising enzymes may be construed to imply that the quinone imine is responsible for hepatotoxicity while the aldehyde and/or the aldehyde quinone imine may be responsible for the blood dyscrasias..

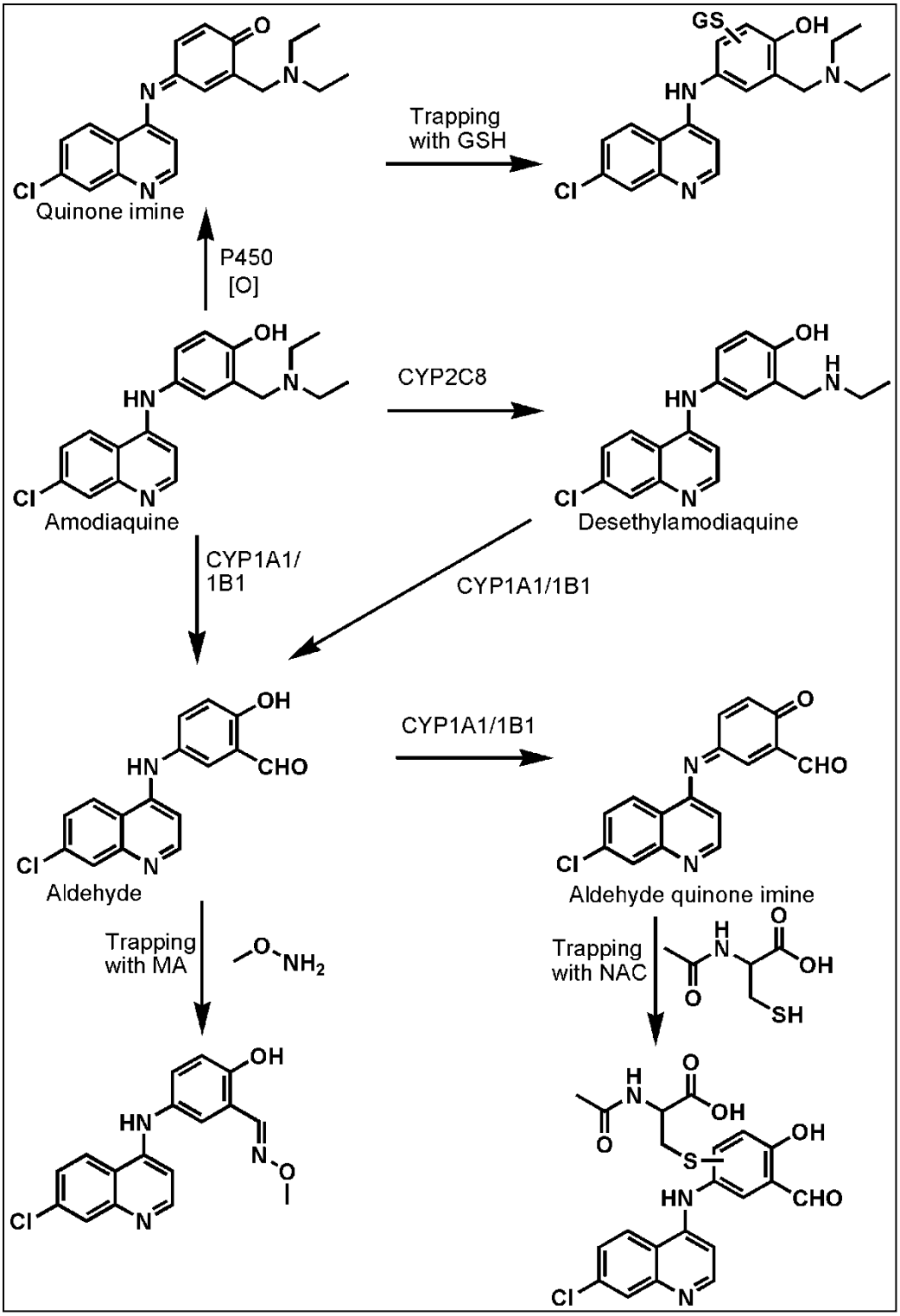

Figure 1.13: Metabolic routes of amodiaquine and desethylamodiaquine observed in rat and human liver microsomes and recombinant CYP1A1 and CYP1B1. MA is methoxamine, NAC is *N*-acetylcysteine.

1.8.3 Amodiaquine analogues synthesized to circumvent toxicity

The implication of the quinone imine metabolite of amodiaquine (**5**) in its toxicity has spurred the synthesis of many analogues to prevent its formation, with little attention paid to the aldehyde metabolite. Park et al. have demonstrated that the 4′-hydroxyl group of amodiaquine (**5**) could be replaced with a 4′-fluorine atom to produce analogue **32** with antimalarial activity in the low nanomolar range. Though less active than amodiaquine (**5**), compounds with this substitution pattern do not form the reactive quinone imine metabolite [195,201].

Interchange of the 4′-hydroxyl and the 3′ Mannich side chain function of amodiaquine (**5**) has been carried out to provide the isoquine series of analogues. These do not form the toxic quinone imine metabolite and isoquine (**33**) was shown to possess excellent antimalarial activity against both the chloroquine sensitive HB3 and chloroquine resistant K1 strains of *Plasmodium falciparum* [202]. A drawback with isoquine is the low oral bioavailability in animal models due to extensive metabolism of the *N*-diethylamino Mannich side chain as well as a narrow therapeutic index and the associated off-target pharmacology of the isoquine series. Further studies in this area have revealed that N-*tert*-butyl isoquine (**7**) has superior pharmacokinetic and pharmacodynamic profiles compared to isoquine. This compound completed preclinical evaluation with Glaxo-SmithKline pharmaceuticals and entered phase I clinical trial in April 2008 [88]. *N-tert*-butyl fluoroamodiaquine (**34**) which has moderate to excellent oral bioavailability compared to isoquine was identified as 'back-up' compound for N-*tert*-butyl isoquine [203]. The clinical development of *N-tert*-butyl isoquine has since been discontinued due to exposures insufficient to demonstrate drug safety superior to chloroquine [204].

Elsewhere, Miroshnikova and coworkers synthesized various isotebuquine analogs (**35)**. Although the antimalarial activity of the analogs was comparable to that of tebuquine, with no formation of the quinone imine, the compounds were not orally bioavailable [205].

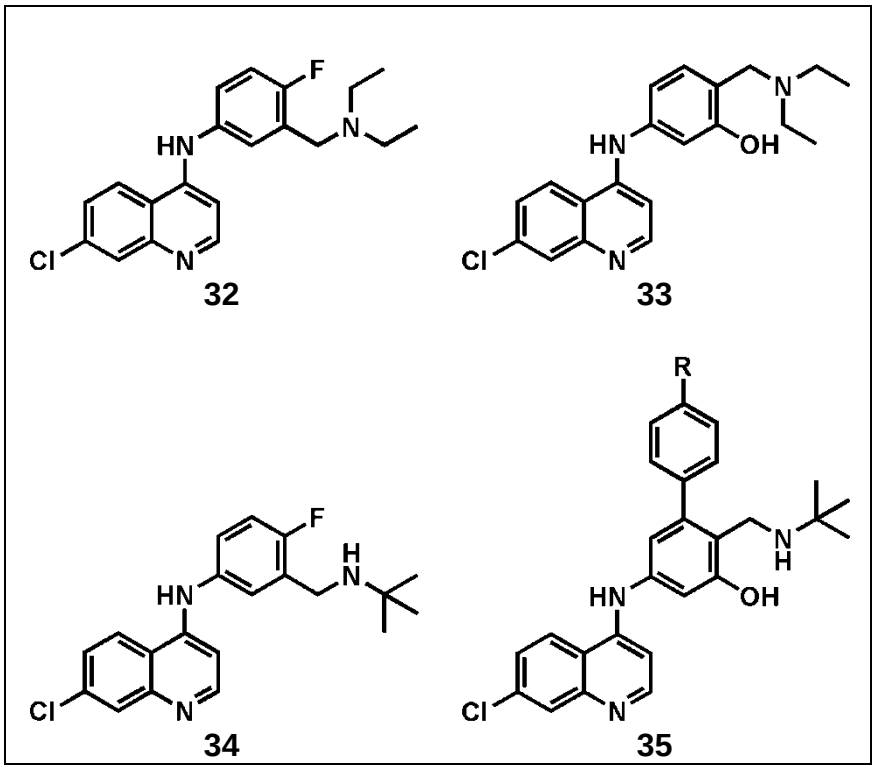

Figure 1.14: Examples of analogues synthesized to prevent bioactivation to the quinone imine

1.9 JUSTIFICATION

The 4-aminoquinoline drug amodiaquine has many favorable aspects including a high degree of efficacy against most of the highly chloroquine-resistant strains, a reasonable costing, relatively easy synthesis, and few compliance issues since it is only administered over three days [206]. These factors make amodiaquine a good lead compound for the exploration of newer antimalarials. In addition and as already mentioned, it is known that 4-aminoquinoline resistance is not related to the target but is

due to mutations affecting a membrane transporter on the food vacuole. Thus it is possible, using available knowledge on the resistance mechanism, to produce efficacious drugs that inhibit hemozoin formation. The well established role of bioactivation in amodiaquine toxicity also implies that it is possible to rationally design compounds with a potentially improved safety profile. Previous research efforts have only focused on avoiding quinone imine formation but have not resulted in compounds with an acceptable safety profile.

1.10 RESEARCH QUESTION AND SPECIFIC OBJECTIVES

1.10.1 Hypothesis

The research question is whether it will be possible to discover analogues of the 4-aminoquinoline drug amodiaquine with potentially improved safety and efficacy profiles using the present and available knowledge of the drug metabolism and pharmacokinetics (DMPK), toxicity and efficacy profile of the drug.

1.10.2 Specific aims

- To synthesize analogues of amodiaquine which potentially prevent bioactivation to the quinone imine and aldehyde metabolites which could be associated with hepatotoxicity and agranulocytosis.
- To use EC-ESI/MS and CYP inhibition studies to assess the bioactivation potential of the amodiaquine analogues synthesized.
- To use bioactivation and antiplasmodial data to select the series with the best efficacy/safety profile for further SAR expansion.

- To conduct *in vitro* metabolic stability and solubility assays on synthesized analogues.
- To conduct mechanistic studies on the synthesized analogues.
- To conduct *in vivo* efficacy studies on compounds with the most potent antiplasmodial activity and good metabolic stability.

REFERENCES

(1) Perkins, S. L.; Austin, C. C. Four new species of Plasmodium from New Guinea lizards: integrating morphology and molecules. *J. Parasitol.* **2009**, *95*, 424–33.

(2) Antinori, S.; Galimberti, L.; Milazzo, L.; Corbellino, M. Biology of human malaria plasmodia including Plasmodium knowlesi. *Mediterr. J. Hematol. Infect. Dis.* **2012**, *4*, e2012013.

(3) Cox-Singh, J.; Davis, T. M. E.; Lee, K.-S.; Shamsul, S. S. G.; Matusop, A.; Ratnam, S.; Rahman, H. A.; Conway, D. J.; Singh, B. Plasmodium knowlesi malaria in humans is widely distributed and potentially life threatening. *Clin. Infect. Dis.* **2008**, *46*, 165–71.

(4) Sutherland, C. J.; Tanomsing, N.; Nolder, D.; Oguike, M.; Jennison, C.; Pukrittayakamee, S.; Dolecek, C.; Hien, T. T.; do Rosário, V. E.; Arez, A. P.; Pinto, J.; Michon, P.; Escalante, A. A.; Nosten, F.; Burke, M.; Lee, R.; Blaze, M.; Otto, T. D.; Barnwell, J. W.; Pain, A.; Williams, J.; White, N. J.; Day, N. P. J.; Snounou, G.; Lockhart, P. J.; Chiodini, P. L.; Imwong, M.; Polley, S. D. Two nonrecombining sympatric forms of the human malaria parasite Plasmodium ovale occur globally. *J. Infect. Dis.* **2010**, *201*, 1544–50.

(5) WHO *World Malaria Report 2012*; 2012.

(6) WHO World Malaria Report 2011. **2011**, 1–3.

(7) Hay, S. I.; Okiro, E. A.; Gething, P. W.; Patil, A. P.; Tatem, A. J.; Guerra, C. A.; Snow, R. W. Estimating the global clinical burden of Plasmodium falciparum malaria in 2007. *PLoS Med.* **2010**, *7*, e1000290.

(8) Autino, B.; Noris, A.; Russo, R.; Castelli, F. Epidemiology of malaria in endemic areas. *Mediterr. J. Hematol. Infect. Dis.* **2012**, *4*, e2012060.

(9) Guerra, C. A.; Snow, R. W.; Hay, S. I. Mapping the global extent of malaria in 2005. *Trends Parasitol.* **2006**, *22*, 353–8.

(10) Carlton, J. M.; Adams, J. H.; Silva, J. C.; Bidwell, S. L.; Lorenzi, H.; Caler, E.; Crabtree, J.; Angiuoli, S. V; Merino, E. F.; Amedeo, P.; Cheng, Q.; Coulson, R. M. R.; Crabb, B. S.; Del Portillo, H. A.; Essien, K.; Feldblyum, T. V; Fernandez-Becerra, C.; Gilson, P. R.; Gueye, A. H.; Guo, X.; Kang'a, S.; Kooij, T. W. A.; Korsinczky, M.; Meyer, E. V.-S.; Nene, V.; Paulsen, I.; White, O.; Ralph, S. A.; Ren, Q.; Sargeant, T. J.; Salzberg, S. L.; Stoeckert, C. J.; Sullivan, S. A.; Yamamoto, M. M.; Hoffman, S. L.; Wortman, J. R.; Gardner, M. J.; Galinski, M. R.; Barnwell, J. W.; Fraser-Liggett, C. M. Comparative genomics of the neglected human malaria parasite Plasmodium vivax. *Nature* **2008**, *455*, 757–63.

(11) Ménard, D.; Barnadas, C.; Bouchier, C.; Henry-Halldin, C.; Gray, L. R.; Ratsimbasoa, A.; Thonier, V.; Carod, J.-F.; Domarle, O.; Colin, Y.; Bertrand, O.; Picot, J.; King, C. L.; Grimberg, B. T.; Mercereau-Puijalon, O.; Zimmerman, P. A. Plasmodium vivax clinical malaria is commonly observed in Duffy-negative Malagasy people. *Proc. Natl. Acad. Sci. U. S. A.* **2010**, *107*, 5967–71.

(12) Mendes, C.; Dias, F.; Figueiredo, J.; Mora, V. G.; Cano, J.; de Sousa, B.; do Rosário, V. E.; Benito, A.; Berzosa, P.; Arez, A. P. Duffy negative antigen is no longer a barrier to Plasmodium vivax--molecular evidences from the African West Coast (Angola and Equatorial Guinea). *PLoS Negl. Trop. Dis.* **2011**, *5*, e1192.

(13) Collins, W. E.; Jeffery, G. M. Plasmodium malariae: parasite and disease. *Clin. Microbiol. Rev.* **2007**, *20*, 579–92.

(14) Mueller, I.; Zimmerman, P. A.; Reeder, J. C. Plasmodium malariae and Plasmodium ovale--the “bashful” malaria parasites. *Trends Parasitol.* **2007**, *23*, 278–83.

(15) Greenwood, B. M.; Fidock, D. A.; Kyle, D. E.; Kappe, S. H. I.; Alonso, P. L.; Collins, F. H.; Duffy, P. E. Malaria: progress, perils, and prospects for eradication. *J. Clin. Invest.* **2008**, *118*, 1266–76.

(16) Gallup, J. L.; Sachs, J. D. The economic burden of malaria. *Am. J. Trop. Med. Hyg.* **2001**, *64*, 85–96.

(17) Breman, J. G.; Alilio, M. S.; Mills, A. Conquering the intolerable burden of malaria: what’s new, what's needed: a summary. *Am. J. Trop. Med. Hyg.* **2004**, *71*, 1–15.

(18) O’Meara, W. P.; Mangeni, J. N.; Steketee, R.; Greenwood, B. Changes in the burden of malaria in sub-Saharan Africa. *Lancet Infect. Dis.* **2010**, *10*, 545–55.

(19) Dondorp, A. M.; Yeung, S.; White, L.; Nguon, C.; Day, N. P. J.; Socheat, D.; von Seidlein, L. Artemisinin resistance: current status and scenarios for containment. *Nat. Rev. Microbiol.* **2010**, *8*, 272–80.

(20) Ménard, R. The journey of the malaria sporozoite through its hosts: two parasite proteins lead the way. *Microbes Infect.* **2000**, *2*, 633–42.

(21) Miller, L. H.; Baruch, D. I.; Marsh, K.; Doumbo, O. K. The pathogenic basis of malaria. *Nature* **2002**, *415*, 673–9.

(22) Schlitzer, M. Malaria chemotherapeutics part I: History of antimalarial drug development, currently used therapeutics, and drugs in clinical development. *ChemMedChem* **2007**, *2*, 944–86.

(23) Meister, S.; Plouffe, D. M.; Kuhen, K. L.; Bonamy, G. M. C.; Wu, T.; Barnes, S. W.; Bopp, S. E.; Borboa, R.; Bright, A. T.; Che, J.; Cohen, S.; Dharia, N. V; Gagaring, K.; Gettayacamin, M.; Gordon, P.; Groessl, T.; Kato, N.; Lee, M. C. S.; McNamara, C. W.; Fidock, D. A.; Nagle, A.; Nam, T.; Richmond, W.; Roland, J.; Rottmann, M.; Zhou, B.; Froissard, P.; Glynne, R. J.; Mazier, D.; Sattabongkot, J.; Schultz, P. G.; Tuntland, T.; Walker, J. R.; Zhou, Y.; Chatterjee, A.; Diagana, T. T.; Winzeler, E. A. Imaging of Plasmodium liver stages to drive next-generation antimalarial drug discovery. *Science* **2011**, *334*, 1372–7.

(24) Cowman, A. F.; Crabb, B. S. Invasion of red blood cells by malaria parasites. *Cell* **2006**, *124*, 755–66.

(25) Baum, J.; Maier, A. G.; Good, R. T.; Simpson, K. M.; Cowman, A. F. Invasion by P. falciparum merozoites suggests a hierarchy of molecular interactions. *PLoS Pathog.* **2005**, *1*, e37.

(26) Wickham, M. E.; Culvenor, J. G.; Cowman, A. F. Selective inhibition of a two-step egress of malaria parasites from the host erythrocyte. *J. Biol. Chem.* **2003**, *278*, 37658–63.

(27) Lew, V. L. Malaria: endless fascination with merozoite release. *Curr. Biol.* **2005**, *15*, R760–1.

(28) Bannister, L.; Mitchell, G. The ins, outs and roundabouts of malaria. *Trends Parasitol.* **2003**, *19*, 209–213.

(29) Laishram, D. D.; Sutton, P. L.; Nanda, N.; Sharma, V. L.; Sobti, R. C.; Carlton, J. M.; Joshi, H. The complexities of malaria disease manifestations with a focus on asymptomatic malaria. *Malar. J.* **2012**, *11*, 29.

(30) Oakley, M. S.; Gerald, N.; McCutchan, T. F.; Aravind, L.; Kumar, S. Clinical and molecular aspects of malaria fever. *Trends Parasitol.* **2011**, *27*, 442–9.

(31) Anstey, N. M.; Russell, B.; Yeo, T. W.; Price, R. N. The pathophysiology of vivax malaria. *Trends Parasitol.* **2009**, *25*, 220–7.

(32) Zhu, J.; Krishnegowda, G.; Li, G.; Gowda, D. C. Proinflammatory responses by glycosylphosphatidylinositols (GPIs) of Plasmodium falciparum are mainly mediated through the recognition of TLR2/TLR1. *Exp. Parasitol.* **2011**, *128*, 205–11.

(33) Trampuz, A.; Jereb, M.; Muzlovic, I.; Prabhu, R. M. Clinical review: Severe malaria. *Crit. Care* **2003**, *7*, 315–23.

(34) Castelli, F.; Tomasoni, L. R.; Matteelli, A. Advances in the treatment of malaria. *Mediterr. J. Hematol. Infect. Dis.* **2012**, *4*, e2012064.

(35) Idro, R.; Marsh, K.; John, C. C.; Newton, C. R. J. Cerebral malaria: mechanisms of brain injury and strategies for improved neurocognitive outcome. *Pediatr. Res.* **2010**, *68*, 267–74.

(36) Jakeman, G. N.; Saul, A.; Hogarth, W. L.; Collins, W. E. Anaemia of acute malaria infections in non-immune patients primarily results from destruction of uninfected erythrocytes. *Parasitology* **1999**, *119 (Pt 2*, 127–33.

(37) Collins, W. E.; Jeffery, G. M.; Roberts, J. M. A retrospective examination of anemia during infection of humans with Plasmodium vivax. *Am. J. Trop. Med. Hyg.* **2003**, *68*, 410–2.

(38) Dondorp, A. M.; Kager, P. A.; Vreeken, J.; White, N. J. Abnormal blood flow and red blood cell deformability in severe malaria. *Parasitol. Today* **2000**, *16*, 228–32.

(39) Taylor, W. R. J.; Hanson, J.; Turner, G. D. H.; White, N. J.; Dondorp, A. M. Respiratory manifestations of malaria. *Chest* **2012**, *142*, 492–505.

(40) Abu-Raddad, L. J.; Patnaik, P.; Kublin, J. G. Dual infection with HIV and malaria fuels the spread of both diseases in sub-Saharan Africa. *Science* **2006**, *314*, 1603–6.

(41) Verhoeff, F. H.; Brabin, B. J.; Hart, C. A.; Chimsuku, L.; Kazembe, P.; Broadhead, R. L. Increased prevalence of malaria in HIV-infected pregnant women and its implications for malaria control. *Trop. Med. Int. Health* **1999**, *4*, 5–12.

(42) Grimwade, K.; French, N.; Mbatha, D. D.; Zungu, D. D.; Dedicoat, M.; Gilks, C. F. HIV infection as a cofactor for severe falciparum malaria in adults living in a region of unstable malaria transmission in South Africa. *AIDS* **2004**, *18*, 547–54.

(43) Sahu, N. K.; Sahu, S.; Kohli, D. V. Novel molecular targets for antimalarial drug development. *Chem. Biol. Drug Des.* **2008**, *71*, 287–97.

(44) Hyde, J. E. Drug-resistant malaria - an insight. *FEBS J.* **2007**, *274*, 4688–98.

(45) Hoffman, S. L.; Subramanian, G. M.; Collins, F. H.; Venter, J. C. Plasmodium, human and Anopheles genomics and malaria. *Nature* **2002**, *415*, 702–9.

(46) Macreadie, I.; Ginsburg, H.; Sirawaraporn, W.; Tilley, L. Antimalarial drug development and new targets. *Parasitol. Today* **2000**, *16*, 438–44.

(47) Wells, T. N. C.; Alonso, P. L.; Gutteridge, W. E. New medicines to improve control and contribute to the eradication of malaria. *Nat. Rev. Drug Discov.* **2009**, *8*, 879–91.

(48) Olliaro, P. Mode of action and mechanisms of resistance for antimalarial drugs. *Pharmacol. Ther.* **2001**, *89*, 207–19.

(49) Grellier, P.; Depoix, D.; Schrével, J.; Florent, I. Discovery of new targets for antimalarial chemotherapy. *Parasite* **2008**, *15*, 219–25.

(50) Yuthavong, Y.; Kamchonwongpaisan, S.; Leartsakulpanich, U.; Chitnumsub, P. Folate metabolism as a source of molecular targets for antimalarials. *Future Microbiol.* **2006**, *1*, 113–25.

(51) Nzila, A. The past, present and future of antifolates in the treatment of Plasmodium falciparum infection. *J. Antimicrob. Chemother.* **2006**, *57*, 1043–54.

(52) Booker, M. L.; Bastos, C. M.; Kramer, M. L.; Barker, R. H.; Skerlj, R.; Sidhu, A. B.; Deng, X.; Celatka, C.; Cortese, J. F.; Guerrero Bravo, J. E.; Crespo Llado, K. N.; Serrano, A. E.; Angulo-Barturen, I.; Jiménez-Díaz, M. B.; Viera, S.; Garuti, H.; Wittlin, S.; Papastogiannidis, P.; Lin, J.-W.; Janse, C. J.; Khan, S. M.; Duraisingh, M.; Coleman, B.; Goldsmith, E. J.; Phillips, M. a; Munoz, B.; Wirth, D. F.; Klinger, J. D.; Wiegand, R.; Sybertz, E. Novel inhibitors of Plasmodium falciparum dihydroorotate dehydrogenase with anti-malarial activity in the mouse model. *J. Biol. Chem.* **2010**, *285*, 33054–64.

(53) Madrid, D. C.; Ting, L.-M.; Waller, K. L.; Schramm, V. L.; Kim, K. Plasmodium falciparum purine nucleoside phosphorylase is critical for viability of malaria parasites. *J. Biol. Chem.* **2008**, *283*, 35899–907.

(54) Drew, M. E.; Banerjee, R.; Uffman, E. W.; Gilbertson, S.; Rosenthal, P. J.; Goldberg, D. E. Plasmodium food vacuole plasmepsins are activated by falcipains. *J. Biol. Chem.* **2008**, *283*, 12870–6.

(55) Müller, S. Redox and antioxidant systems of the malaria parasite Plasmodium falciparum. *Mol. Microbiol.* **2004**, *53*, 1291–305.

(56) Ralph, S. A.; D'Ombrain, M. C.; McFadden, G. I. The apicoplast as an antimalarial drug target. *Drug Resist. Updat.* **2001**, *4*, 145–51.

(57) Andrews, K. T.; Tran, T. N.; Lucke, A. J.; Kahnberg, P.; Le, G. T.; Boyle, G. M.; Gardiner, D. L.; Skinner-Adams, T. S.; Fairlie, D. P. Potent antimalarial activity of histone deacetylase inhibitor analogues. *Antimicrob. Agents Chemother.* **2008**, *52*, 1454–61.

(58) Doerig, C.; Billker, O.; Haystead, T.; Sharma, P.; Tobin, A. B.; Waters, N. C. Protein kinases of malaria parasites: an update. *Trends Parasitol.* **2008**, *24*, 570–7.

(59) Doerig, C.; Meijer, L. Antimalarial drug discovery: targeting protein kinases. *Expert Opin. Ther. Targets* **2007**, *11*, 279–90.

(60) Staines, H. M.; Ellory, J. C.; Chibale, K. The new permeability pathways: targets and selective routes for the development of new antimalarial agents. *Comb. Chem. High Throughput Screen.* **2005**, *8*, 81–8.

(61) Padmanaban, G.; Rangarajan, P. N. Heme metabolism of Plasmodium is a major antimalarial target. *Biochem. Biophys. Res. Commun.* **2000**, *268*, 665–8.

(62) Egan, T. J. Haemozoin (malaria pigment): a unique crystalline drug target. *TARGETS* **2003**, *2*, 115–124.

(63) Dluzewski, A. R.; Mitchell, G. H.; Fryer, P. R.; Griffiths, S.; Wilson, R. J.; Gratzer, W. B. Origins of the parasitophorous vacuole membrane of the malaria parasite, Plasmodium falciparum, in human red blood cells. *J. Cell Sci.* **1992**, *102 (Pt 3*, 527–32.

(64) Goldberg, D. E.; Slater, A. F.; Cerami, A.; Henderson, G. B. Hemoglobin degradation in the malaria parasite Plasmodium falciparum: an ordered process in a unique organelle. *Proc. Natl. Acad. Sci. U. S. A.* **1990**, *87*, 2931–5.

(65) Francis, S. E.; Sullivan, D. J.; Goldberg, D. E. Hemoglobin metabolism in the malaria parasite Plasmodium falciparum. *Annu. Rev. Microbiol.* **1997**, *51*, 97–123.

(66) Sullivan, D. J. Theories on malarial pigment formation and quinoline action. *Int. J. Parasitol.* **2002**, *32*, 1645–53.

(67) Olliaro, P. L.; Goldberg, D. E. The plasmodium digestive vacuole: metabolic headquarters and choice drug target. *Parasitol. Today* **1995**, *11*, 294–7.

(68) Banerjee, R.; Goldberg, D. E. The Plasmodium Food Vacuole. In *Infectious Disease*; Georgiev, V. St., Ed.; Humana Press, 2001; pp. 43–63.

(69) Liu, J.; Istvan, E. S.; Gluzman, I. Y.; Gross, J.; Goldberg, D. E. Plasmodium falciparum ensures its amino acid supply with multiple acquisition pathways and redundant proteolytic enzyme systems. *Proc. Natl. Acad. Sci. U. S. A.* **2006**, *103*, 8840–5.

(70) Hawley, S. R.; Bray, P. G.; Mungthin, M.; Atkinson, J. D.; O'Neill, P. M.; Ward, S. A. Relationship between antimalarial drug activity, accumulation, and inhibition of heme polymerization in Plasmodium falciparum in vitro. *Antimicrob. Agents Chemother.* **1998**, *42*, 682–6.

(71) Lynn, A.; Chandra, S.; Malhotra, P.; Chauhan, V. S. Heme binding and polymerization by Plasmodium falciparum histidine rich protein II: influence of pH on activity and conformation. *FEBS Lett.* **1999**, *459*, 267–71.

(72) Kumar, S.; Guha, M.; Choubey, V.; Maity, P.; Bandyopadhyay, U. Antimalarial drugs inhibiting hemozoin (beta-hematin) formation: a mechanistic update. *Life Sci.* **2007**, *80*, 813–28.

(73) Pagola, S.; Stephens, P. W.; Bohle, D. S.; Kosar, A. D.; Madsen, S. K. The structure of malaria pigment beta-haematin. *Nature* **2000**, *404*, 307–10.

(74) Egan, T. J. Recent advances in understanding the mechanism of hemozoin (malaria pigment) formation. *J. Inorg. Biochem.* **2008**, *102*, 1288–99.

(75) Birkholtz, L.; Bornman, R.; Focke, W.; Mutero, C.; de Jager, C. Sustainable malaria control: transdisciplinary approaches for translational applications. *Malar. J.* **2012**, *11*, 431.

(76) Mukonzo, J. K.; Waako, P.; Ogwal-Okeng, J.; Gustafsson, L. L.; Aklillu, E. Genetic variations in ABCB1 and CYP3A5 as well as sex influence quinine disposition among Ugandans. *Ther. Drug Monit.* **2010**, *32*, 346–52.

(77) Foley, M.; Tilley, L. Quinoline antimalarials: mechanisms of action and resistance and prospects for new agents. *Pharmacol. Ther.* **1998**, *79*, 55–87.

(78) Solomon, V. R.; Lee, H. Chloroquine and its analogs: a new promise of an old drug for effective and safe cancer therapies. *Eur. J. Pharmacol.* **2009**, *625*, 220–33.

(79) Carson, P. E.; Hohl, R.; Nora, M. V; Parkhurst, G. W.; Ahmad, T.; Scanlan, S.; Frischer, H. Toxicology of the 8-aminoquinolines and genetic factors associated with their toxicity in man. *Bull. World Health Organ.* **1981**, *59*, 427–37.

(80) Howes, R. E.; Battle, K. E.; Satyagraha, A. W.; Baird, J. K.; Hay, S. I. *G6PD Deficiency: Global Distribution, Genetic Variants and Primaquine Therapy.*; Elsevier, 2013; Vol. 81, pp. 133–201.

(81) Baird, J. K. Primaquine toxicity forestalls effective therapeutic management of the endemic malarias. *Int. J. Parasitol.* **2012**, *42*, 1049–54.

(82) Baird, J. K.; Hoffman, S. L. Primaquine therapy for malaria. *Clin. Infect. Dis.* **2004**, *39*, 1336–45.

(83) Clyde, D. F. Clinical problems associated with the use of primaquine as a tissue schizontocidal and gametocytocidal drug. *Bull. World Health Organ.* **1981**, *59*, 391–5.

(84) O'Neill, P. M.; Barton, V. E.; Ward, S. A.; Chadwick, J. 4-Aminoquinolines: Chloroquine, Amodiaquine and Next-Generation Analogues. In *Treatment and Prevention of Malaria*; Staines, H. M.; Krishna, S., Eds.; Springer Basel: Basel, 2012; pp. 19–45.

(85) Farooq, U.; Mahajan, R. C. Drug resistance in malaria. *J. Vector Borne Dis.* **2004**, *41*, 45–53.

(86) Beer, N.; Ali, A. S.; Rotllant, G.; Abass, A. K.; Omari, R. S.; Al-mafazy, A. H.; Björkman, A.; Källander, K. Adherence to artesunate-amodiaquine combination therapy for uncomplicated malaria in children in Zanzibar, Tanzania. *Trop. Med. Int. Health* **2009**, *14*, 766–74.

(87) Dubar, F.; Khalife, J.; Brocard, J.; Dive, D.; Biot, C. Ferroquine, an ingenious antimalarial drug: thoughts on the mechanism of action. *Molecules* **2008**, *13*, 2900–7.

(88) O'Neill, P. M.; Park, B. K.; Shone, A. E.; Maggs, J. L.; Roberts, P.; Stocks, P. A.; Biagini, G. A.; Bray, P. G.; Gibbons, P.; Berry, N.; Winstanley, P. A.; Mukhtar, A.; Bonar-Law, R.; Hindley, S.; Bambal, R. B.; Davis, C. B.; Bates, M.; Hart, T. K.; Gresham, S. L.; Lawrence, R. M.; Brigandi, R. A.; Gomez-delas-Heras, F. M.; Gargallo, D. V; Ward, S. A. Candidate selection and preclinical evaluation of N-tert-butyl isoquine (GSK369796), an affordable and effective 4-aminoquinoline antimalarial for the 21st century. *J. Med. Chem.* **2009**, *52*, 1408–15.

(89) Sáenz, F. E.; Mutka, T.; Udenze, K.; Oduola, A. M. J.; Kyle, D. E. Novel 4-aminoquinoline analogs highly active against the blood and sexual stages of Plasmodium in vivo and in vitro. *Antimicrob. Agents Chemother.* **2012**, *56*, 4685–92.

(90) Milner, E.; McCalmont, W.; Bhonsle, J.; Caridha, D.; Cobar, J.; Gardner, S.; Gerena, L.; Goodine, D.; Lanteri, C.; Melendez, V.; Roncal, N.; Sousa, J.; Wipf, P.; Dow, G. S. Anti-malarial activity of a non-piperidine library of next-generation quinoline methanols. *Malar. J.* **2010**, *9*, 51.

(91) Toovey, S. Mefloquine neurotoxicity: a literature review. *Travel Med. Infect. Dis.* **2009**, *7*, 2–6.

(92) Burrows, J. N.; Chibale, K.; Wells, T. N. C. The state of the art in anti-malarial drug discovery and development. *Curr. Top. Med. Chem.* **2011**, *11*, 1226–54.

(93) Bouchaud, O.; Imbert, P.; Touze, J. E.; Dodoo, A. N. O.; Danis, M.; Legros, F. Fatal cardiotoxicity related to halofantrine: a review based on a worldwide safety data base. *Malar. J.* **2009**, *8*, 289.

(94) Barnes, K. I.; Durrheim, D. N.; Little, F.; Jackson, A.; Mehta, U.; Allen, E.; Dlamini, S. S.; Tsoka, J.; Bredenkamp, B.; Mthembu, D. J.; White, N. J.; Sharp, B. L. Effect of artemether-lumefantrine policy and improved vector control on malaria burden in KwaZulu-Natal, South Africa. *PLoS Med.* **2005**, *2*, e330.

(95) Kokwaro, G.; Mwai, L.; Nzila, A. Artemether/lumefantrine in the treatment of uncomplicated falciparum malaria. *Expert Opin. Pharmacother.* **2007**, *8*, 75–94.

(96) Olliaro, P.; Wells, T. N. C. The global portfolio of new antimalarial medicines under development. *Clin. Pharmacol. Ther.* **2009**, *85*, 584–95.

(97) Egan, T. J.; Ncokazi, K. K. Quinoline antimalarials decrease the rate of beta-hematin formation. *J. Inorg. Biochem.* **2005**, *99*, 1532–9.

(98) Saifi, M. A.; Beg, T.; Harrath, A. H.; Suleman, F.; Altayalan, H.; Quraishy, S. Al Antimalarial drugs: Mode of action and status of resistance. *African J. Pharm. Pharmacol.* **2013**, *7*, 148–156.

(99) Vale, N.; Moreira, R.; Gomes, P. Primaquine revisited six decades after its discovery. *Eur. J. Med. Chem.* **2009**, *44*, 937–53.

(100) Zishiri, V. K.; Joshi, M. C.; Hunter, R.; Chibale, K.; Smith, P. J.; Summers, R. L.; Martin, R. E.; Egan, T. J. Quinoline antimalarials containing a dibemethin group are active against chloroquinone-resistant Plasmodium falciparum and inhibit chloroquine transport via the P. falciparum chloroquine-resistance transporter (PfCRT). *J. Med. Chem.* **2011**, *54*, 6956–68.

(101) Martinelli, A.; Moreira, R.; Ravo, P. V. L. Malaria combination therapies: advantages and shortcomings. *Mini Rev. Med. Chem.* **2008**, *8*, 201–12.

(102) Patel, O. G.; Mberu, E. K.; Nzila, A. M.; Macreadie, I. G. Sulfa drugs strike more than once. *Trends Parasitol.* **2004**, *20*, 1–3.

(103) Gregson, A.; Plowe, C. V. Mechanisms of resistance of malaria parasites to antifolates. *Pharmacol. Rev.* **2005**, *57*, 117–45.

(104) Klayman, D. L.; Lin, A. J.; Acton, N.; Scovill, J. P.; Hoch, J. M.; Milhous, W. K.; Theoharides, A. D.; Dobek, A. S. Isolation of artemisinin (qinghaosu) from Artemisia annua growing in the United States. *J. Nat. Prod.* **1984**, *47*, 715–7.

(105) Nosten, F.; White, N. J. Artemisinin-based combination treatment of falciparum malaria. *Am. J. Trop. Med. Hyg.* **2007**, *77*, 181–92.

(106) O'Neill, P. M.; Barton, V. E.; Ward, S. A. The molecular mechanism of action of artemisinin--the debate continues. *Molecules* **2010**, *15*, 1705–21.

(107) Slack, R. D.; Jacobine, A. M.; Posner, G. H. Antimalarial peroxides: advances in drug discovery and design. *Medchemcomm* **2012**, *3*, 281.

(108) Golenser, J.; Waknine, J. H.; Krugliak, M.; Hunt, N. H.; Grau, G. E. Current perspectives on the mechanism of action of artemisinins. *Int. J. Parasitol.* **2006**, *36*, 1427–41.

(109) Seydou, M.; Gillet, J. C.; Li, X.; Wang, H.; Posner, G. H.; Grégoire, G.; Schermann, J. P.; Bowen, K. H.; Desfrançois, C. Studies of protonated and anionic artemisinin in the gas-phase by infrared multi-photon dissociation and by negative ion photoelectron spectroscopies. *Chem. Phys. Lett.* **2007**, *449*, 286–290.

(110) Van Noorden, R. Demand for malaria drug soars. *Nature* **2010**, *466*, 672–3.

(111) Wu, T.; Nagle, A. S.; Chatterjee, A. K. Road towards new antimalarials - overview of the strategies and their chemical progress. *Curr. Med. Chem.* **2011**, *18*, 853–71.

(112) Vennerstrom, J. L.; Arbe-Barnes, S.; Brun, R.; Charman, S. A.; Chiu, F. C. K.; Chollet, J.; Dong, Y.; Dorn, A.; Hunziker, D.; Matile, H.; McIntosh, K.; Padmanilayam, M.; Santo Tomas, J.; Scheurer, C.; Scorneaux, B.; Tang, Y.; Urwyler, H.; Wittlin, S.; Charman, W. N. Identification of an antimalarial synthetic trioxolane drug development candidate. *Nature* **2004**, *430*, 900–4.

(113) Meunier, B.; Robert, A. Heme as trigger and target for trioxane-containing antimalarial drugs. *Acc. Chem. Res.* **2010**, *43*, 1444–51.

(114) Meshnick, S. R. Artemisinin: mechanisms of action, resistance and toxicity. *Int. J. Parasitol.* **2002**, *32*, 1655–60.

(115) Cui, L.; Su, X.-Z. Discovery, mechanisms of action and combination therapy of artemisinin. *Expert Rev. Anti. Infect. Ther.* **2009**, *7*, 999–1013.

(116) Krishna, S.; Uhlemann, A.-C.; Haynes, R. K. Artemisinins: mechanisms of action and potential for resistance. *Drug Resist. Updat.* **2004**, *7*, 233–44.

(117) O'Brien, C.; Henrich, P. P.; Passi, N.; Fidock, D. A. Recent clinical and molecular insights into emerging artemisinin resistance in Plasmodium falciparum. *Curr. Opin. Infect. Dis.* **2011**, *24*, 570–7.

(118) Noedl, H. The need for new antimalarial drugs less prone to resistance. *Curr. Pharm. Des.* **2013**, *19*, 266–9.

(119) Edwards, I. R.; Aronson, J. K. Adverse drug reactions: definitions, diagnosis, and management. *Lancet* **2000**, *356*, 1255–9.

(120) Laverty, H. G.; Benson, C.; Cartwright, E. J.; Cross, M. J.; Garland, C.; Hammond, T.; Holloway, C.; McMahon, N.; Milligan, J.; Park, B. K.; Pirmohamed, M.; Pollard, C.; Radford, J.; Roome, N.; Sager, P.; Singh, S.; Suter, T.; Suter, W.; Trafford, A.; Volders, P. G. A.; Wallis, R.; Weaver, R.; York, M.; Valentin, J. P. How can we improve our understanding of cardiovascular safety liabilities to develop safer medicines? *Br. J. Pharmacol.* **2011**, *163*, 675–93.

(121) Lasser, K. E.; Allen, P. D.; Woolhandler, S. J.; Himmelstein, D. U.; Wolfe, S. M.; Bor, D. H. Timing of new black box warnings and withdrawals for prescription medications. *JAMA* **2002**, *287*, 2215–20.

(122) Wysowski, D. K.; Swartz, L. Adverse drug event surveillance and drug withdrawals in the United States, 1969-2002: the importance of reporting suspected reactions. *Arch. Intern. Med.* **2005**, *165*, 1363–9.

(123) Pirmohamed, M.; James, S.; Meakin, S.; Green, C.; Scott, A. K.; Walley, T. J.; Farrar, K.; Park, B. K.; Breckenridge, A. M. Adverse drug reactions as cause of admission to hospital: prospective analysis of 18 820 patients. *BMJ* **2004**, *329*, 15–9.

(124) Davies, E. C.; Green, C. F.; Taylor, S.; Williamson, P. R.; Mottram, D. R.; Pirmohamed, M. Adverse drug reactions in hospital in-patients: a prospective analysis of 3695 patient-episodes. *PLoS One* **2009**, *4*, e4439.

(125) Van der Hooft, C. S.; Sturkenboom, M. C. J. M.; van Grootheest, K.; Kingma, H. J.; Stricker, B. H. C. Adverse drug reaction-related hospitalisations: a nationwide study in The Netherlands. *Drug Saf.* **2006**, *29*, 161–8.

(126) White, T. J.; Arakelian, A.; Rho, J. P. Counting the costs of drug-related adverse events. *Pharmacoeconomics* **1999**, *15*, 445–58.

(127) Smith, D. A.; Obach, R. S.; Williams, D. P.; Park, B. K. Clearing the MIST (metabolites in safety testing) of time: The impact of duration of administration on drug metabolite toxicity. *Chem. Biol. Interact.* **2009**, *179*, 60–7.

(128) Smith, D. A.; Obach, R. S. Metabolites in safety testing (MIST): considerations of mechanisms of toxicity with dose, abundance, and duration of treatment. *Chem. Res. Toxicol.* **2009**, *22*, 267–79.

(129) Uetrecht, J. Idiosyncratic drug reactions: current understanding. *Annu. Rev. Pharmacol. Toxicol.* **2007**, *47*, 513–39.

(130) Uetrecht, J. Screening for the potential of a drug candidate to cause idiosyncratic drug reactions. *Drug Discov. Today* **2003**, *8*, 832–7.

(131) Park, B. K.; Naisbitt, D. J.; Gordon, S. F.; Kitteringham, N. R.; Pirmohamed, M. Metabolic activation in drug allergies. *Toxicology* **2001**, *158*, 11–23.

(132) Park, B. K.; Kitteringham, N. R.; Maggs, J. L.; Pirmohamed, M.; Williams, D. P. The role of metabolic activation in drug-induced hepatotoxicity. *Annu. Rev. Pharmacol. Toxicol.* **2005**, *45*, 177–202.

(133) Gombar, V. K.; Silver, I. S.; Zhao, Z. Role of ADME characteristics in drug discovery and their in silico evaluation: in silico screening of chemicals for their metabolic stability. *Curr. Top. Med. Chem.* **2003**, *3*, 1205–25.

(134) Hou, T.; Wang, J. Structure-ADME relationship: still a long way to go? *Expert Opin. Drug Metab. Toxicol.* **2008**, *4*, 759–70.

(135) Kola, I.; Landis, J. Can the pharmaceutical industry reduce attrition rates? *Nat. Rev. Drug Discov.* **2004**, *3*, 711–5.

(136) Testa, B.; Pedretti, A.; Vistoli, G. Reactions and enzymes in the metabolism of drugs and other xenobiotics. *Drug Discov. Today* **2012**, *17*, 549–60.

(137) Glue, P.; Clement, R. P. Cytochrome P450 enzymes and drug metabolism--basic concepts and methods of assessment. *Cell. Mol. Neurobiol.* **1999**, *19*, 309–23.

(138) Wilkinson, G. R. Drug metabolism and variability among patients in drug response. *N. Engl. J. Med.* **2005**, *352*, 2211–21.

(139) Gibson, G. G.; Skett, P. *Introduction to Drug Metabolism*; Third.; Nelson Thornes: Cheltenham, UK, 2001.

(140) Guengerich, F. P.; Rendic, S. Update information on drug metabolism systems--2009, part I. *Curr. Drug Metab.* **2010**, *11*, 1–3.

(141) Rose, R. L.; Hodgson, E. Metabolism of Toxicants. In *A Textbook of Modern Toxicology*; Hodgson, E., Ed.; John Wiley & Sons, Inc.: Hoboken, NJ, USA., 2004; pp. 111–148.

(142) Guengerich, F. P. Cytochrome P450s and other enzymes in drug metabolism and toxicity. *AAPS J.* **2006**, *8*, E101–11.

(143) Cashman, J. R.; Zhang, J. Human flavin-containing monooxygenases. *Annu. Rev. Pharmacol. Toxicol.* **2006**, *46*, 65–100.

(144) Evans, W. E.; Relling, M. V. Pharmacogenomics: Translating Functional Genomics into Rational Therapeutics. *Science (80-.).* **1999**, *286*, 487–491.

(145) Guengerich, F. P.; Isin, E. M. Mechanisms of Cytochrome P450 Reactions. *Acta Chim Slov* **2008**, *55*, 7–19.

(146) Danielson, P. B. The cytochrome P450 superfamily: biochemistry, evolution and drug metabolism in humans. *Curr. Drug Metab.* **2002**, *3*, 561–97.

(147) Hamdane, D.; Zhang, H.; Hollenberg, P. Oxygen activation by cytochrome P450 monooxygenase. *Photosynth. Res.* **2008**, *98*, 657–66.

(148) Groves, J. T. The bioinorganic chemistry of iron in oxygenases and supramolecular assemblies. *Proc. Natl. Acad. Sci. U. S. A.* **2003**, *100*, 3569–74.

(149) McCarver, D. G.; Hines, R. N. The ontogeny of human drug-metabolizing enzymes: phase II conjugation enzymes and regulatory mechanisms. *J. Pharmacol. Exp. Ther.* **2002**, *300*, 361–6.

(150) Chen, Y.; Tang, Y.; Guo, C.; Wang, J.; Boral, D.; Nie, D. Nuclear receptors in the multidrug resistance through the regulation of drug-metabolizing enzymes and drug transporters. *Biochem. Pharmacol.* **2012**, *83*, 1112–26.

(151) Jancova, P.; Anzenbacher, P.; Anzenbacherova, E. Phase II drug metabolizing enzymes. *Biomed. Pap. Med. Fac. Univ. Palacky. Olomouc. Czech. Repub.* **2010**, *154*, 103–16.

(152) Ioannides, C.; Lewis, D. F. V Cytochromes P450 in the bioactivation of chemicals. *Curr. Top. Med. Chem.* **2004**, *4*, 1767–88.

(153) Stepan, A. F.; Walker, D. P.; Bauman, J.; Price, D. A.; Baillie, T. A.; Kalgutkar, A. S.; Aleo, M. D. Structural alert/reactive metabolite concept as applied in medicinal chemistry to mitigate the risk of idiosyncratic drug toxicity: a perspective based on

the critical examination of trends in the top 200 drugs marketed in the United States. *Chem. Res. Toxicol.* **2011**, *24*, 1345–410.

(154) Edwards, P. J.; Sturino, C. Managing the liabilities arising from structural alerts: a safe philosophy for medicinal chemists. *Curr. Med. Chem.* **2011**, *18*, 3116–35.

(155) Kalgutkar, A. S.; Gardner, I.; Obach, R. S.; Shaffer, C. L.; Callegari, E.; Henne, K. R.; Mutlib, A. E.; Dalvie, D. K.; Lee, J. S.; Nakai, Y.; O'Donnell, J. P.; Boer, J.; Harriman, S. P. A comprehensive listing of bioactivation pathways of organic functional groups. *Curr. Drug Metab.* **2005**, *6*, 161–225.

(156) Kalgutkar, A. S.; Didiuk, M. T. Structural alerts, reactive metabolites, and protein covalent binding: how reliable are these attributes as predictors of drug toxicity? *Chem. Biodivers.* **2009**, *6*, 2115–37.

(157) Kalgutkar, A. S. Role of Bioactivation in Idiosyncratic Drug Toxicity: Structure–Toxicity Relationships. In *Advances in Bioactivation Research*; Elfarra, A., Ed.; Springer New York: New York, NY, **2008**; pp. 27–56.

(158) Park, B. K.; Boobis, A.; Clarke, S.; Goldring, C. E. P.; Jones, D.; Kenna, J. G.; Lambert, C.; Laverty, H. G.; Naisbitt, D. J.; Nelson, S.; Nicoll-Griffith, D. A.; Obach, R. S.; Routledge, P.; Smith, D. A.; Tweedie, D. J.; Vermeulen, N.; Williams, D. P.; Wilson, I. D.; Baillie, T. A. Managing the challenge of chemically reactive metabolites in drug development. *Nat. Rev. Drug Discov.* **2011**, *10*, 292–306.

(159) Attia, S. M. Deleterious Effects of Reactive Metabolites. *Oxid. Med. Cell. Longev.* **2010**, *3*, 238–253.

(160) Lohmann, W.; Karst, U. Generation and identification of reactive metabolites by electrochemistry and immobilized enzymes coupled on-line to liquid chromatography/mass spectrometry. *Anal. Chem.* **2007**, *79*, 6831–9.

(161) Lee, K. S.; Oh, S. J.; Kim, H. M.; Lee, K. H.; Kim, S. K. Assessment of reactive metabolites in drug-induced liver injury. *Arch. Pharm. Res.* **2011**, *34*, 1879–86.

(162) Yan, Z.; Maher, N.; Torres, R.; Huebert, N. Use of a trapping agent for simultaneous capturing and high-throughput screening of both “soft” and “hard” reactive metabolites. *Anal. Chem.* **2007**, *79*, 4206–14.

(163) Ma, S.; Subramanian, R. Detecting and characterizing reactive metabolites by liquid chromatography/tandem mass spectrometry. *J. Mass Spectrom.* **2006**, *41*, 1121–39.

(164) Staack, R. F.; Hopfgartner, G. New analytical strategies in studying drug metabolism. *Anal. Bioanal. Chem.* **2007**, *388*, 1365–80.

(165) Laine, J. E.; Auriola, S.; Pasanen, M.; Juvonen, R. O. D-Isomer of gly-tyr-pro-cys-pro-his-pro peptide: a novel and sensitive in vitro trapping agent to detect reactive metabolites by electrospray mass spectrometry. *Toxicol. In Vitro* **2011**, *25*, 411–25.

(166) Evans, D. C.; Watt, A. P.; Nicoll-Griffith, D. A.; Baillie, T. A. Drug-protein adducts: an industry perspective on minimizing the potential for drug bioactivation in drug discovery and development. *Chem. Res. Toxicol.* **2004**, *17*, 3–16.

(167) Rousu, T.; Pelkonen, O.; Tolonen, A. Rapid detection and characterization of reactive drug metabolites in vitro using several isotope-labeled trapping agents

and ultra-performance liquid chromatography/time-of-flight mass spectrometry. *Rapid Commun. Mass Spectrom.* **2009**, *23*, 843–55.

(168) Mutlib, A.; Lam, W.; Atherton, J.; Chen, H.; Galatsis, P.; Stolle, W. Application of stable isotope labeled glutathione and rapid scanning mass spectrometers in detecting and characterizing reactive metabolites. *Rapid Commun. Mass Spectrom.* **2005**, *19*, 3482–92.

(169) Fontana, E.; Dansette, P. M.; Poli, S. M. Cytochrome p450 enzymes mechanism based inhibitors: common sub-structures and reactivity. *Curr. Drug Metab.* **2005**, *6*, 413–54.

(170) Zhou, S.; Yung Chan, S.; Cher Goh, B.; Chan, E.; Duan, W.; Huang, M.; McLeod, H. L. Mechanism-based inhibition of cytochrome P450 3A4 by therapeutic drugs. *Clin. Pharmacokinet.* **2005**, *44*, 279–304.

(171) Thelingwani, R. S.; Zvada, S. P.; Dolgos, H.; Ungell, A. B.; Masimirembwa, C. M. In vitro and in silico identification and characterization of thiabendazole as a mechanism-based inhibitor of CYP1A2 and simulation of possible pharmacokinetic drug-drug interactions. *Drug Metab. Dispos.* **2009**, *37*, 1286–94.

(172) Thompson, R. A.; Isin, E. M.; Li, Y.; Weaver, R.; Weidolf, L.; Wilson, I.; Claesson, A.; Page, K.; Dolgos, H.; Kenna, J. G. Risk assessment and mitigation strategies for reactive metabolites in drug discovery and development. *Chem. Biol. Interact.* **2011**, *192*, 65–71.

(173) Johansson, T.; Weidolf, L.; Jurva, U. Mimicry of phase I drug metabolism--novel methods for metabolite characterization and synthesis. *Rapid Commun. Mass Spectrom.* **2007**, *21*, 2323–31.

(174) Johansson, T.; Jurva, U.; Grönberg, G.; Weidolf, L.; Masimirembwa, C. Novel metabolites of amodiaquine formed by CYP1A1 and CYP1B1: structure elucidation using electrochemistry, mass spectrometry, and NMR. *Drug Metab. Dispos.* **2009**, *37*, 571–9.

(175) Madsen, K. G.; Olsen, J.; Skonberg, C.; Hansen, S. H.; Jurva, U. Development and evaluation of an electrochemical method for studying reactive phase-I metabolites: correlation to in vitro drug metabolism. *Chem. Res. Toxicol.* **2007**, *20*, 821–31.

(176) Madsen, K. G.; Skonberg, C.; Jurva, U.; Cornett, C.; Hansen, S. H.; Johansen, T. N.; Olsen, J. Bioactivation of diclofenac in vitro and in vivo: correlation to electrochemical studies. *Chem. Res. Toxicol.* **2008**, *21*, 1107–19.

(177) Jurva, U.; Holmén, A.; Grönberg, G.; Masimirembwa, C.; Weidolf, L. Electrochemical generation of electrophilic drug metabolites: characterization of amodiaquine quinoneimine and cysteinyl conjugates by MS, IR, and NMR. *Chem. Res. Toxicol.* **2008**, *21*, 928–35.

(178) Laurent, F.; Saivin, S.; Chretien, P.; Magnaval, J. F.; Peyron, F.; Sqalli, A.; Tufenkji, A. E.; Coulais, Y.; Baba, H.; Campistron, G. Pharmacokinetic and pharmacodynamic study of amodiaquine and its two metabolites after a single oral dose in human volunteers. *Arzneimittelforschung.* **1993**, *43*, 612–6.

(179) Churchill, F. C.; Patchen, L. C.; Campbell, C. C.; Schwartz, I. K.; Nguyen-Dinh, P.; Dickinson, C. M. Amodiaquine as a prodrug: importance of metabolite(s) in the antimalarial effect of amodiaquine in humans. *Life Sci.* **1985**, *36*, 53–62.

(180) Mount, D. L.; Patchen, L. C.; Nguyen-Dinh, P.; Barber, A. M.; Schwartz, I. K.; Churchill, F. C. Sensitive analysis of blood for amodiaquine and three metabolites by high-performance liquid chromatography with electrochemical detection. *J. Chromatogr.* **1986**, *383*, 375–86.

(181) Pussard, E.; Verdier, F.; Faurisson, F.; Scherrmann, J. M.; Bras, J.; Blayo, M. C. Disposition of monodesethylamodiaquine after a single oral dose of amodiaquine and three regimens for prophylaxis againstPlasmodium falciparum malaria. *Eur. J. Clin. Pharmacol.* **1987**, *33*, 409–414.

(182) Mariga, S. T.; Gil, J. P.; Sisowath, C.; Wernsdorfer, W. H.; Björkman, A. Synergism between amodiaquine and its major metabolite, desethylamodiaquine, against Plasmodium falciparum in vitro. *Antimicrob. Agents Chemother.* **2004**, *48*, 4089–96.

(183) Li, X.-Q.; Björkman, A.; Andersson, T. B.; Ridderström, M.; Masimirembwa, C. M. Amodiaquine clearance and its metabolism to N-desethylamodiaquine is mediated by CYP2C8: a new high affinity and turnover enzyme-specific probe substrate. *J. Pharmacol. Exp. Ther.* **2002**, *300*, 399–407.

(184) Li, X.-Q.; Björkman, A.; Andersson, T. B.; Gustafsson, L. L.; Masimirembwa, C. M. Identification of human cytochrome P(450)s that metabolise anti-parasitic drugs and predictions of in vivo drug hepatic clearance from in vitro data. *Eur. J. Clin. Pharmacol.* **2003**, *59*, 429–42.

(185) Hayeshi, R.; Masimirembwa, C.; Mukanganyama, S.; Ungell, A. B. Lysosomal trapping of amodiaquine: impact on transport across intestinal epithelia models. *Biopharm. Drug Dispos.* **2008**, *29*, 324–34.

(186) Hayeshi, R.; Masimirembwa, C.; Mukanganyama, S.; Ungell, A.-L. B. The potential inhibitory effect of antiparasitic drugs and natural products on P-glycoprotein mediated efflux. *Eur. J. Pharm. Sci.* **2006**, *29*, 70–81.

(187) Bapiro, T. E.; Egnell, A. C.; Hasler, J. A.; Masimirembwa, C. M. Application of higher throughput screening (HTS) inhibition assays to evaluate the interaction of antiparasitic drugs with cytochrome P450s. *Drug Metab. Dispos.* **2001**, *29*, 30–5.

(188) Neftel, K. A.; Woodtly, W.; Schmid, M.; Frick, P. G.; Fehr, J. Amodiaquine induced agranulocytosis and liver damage. *Br. Med. J. (Clin. Res. Ed).* **1986**, *292*, 721–3.

(189) Schulthess, H. K.; von Felten, A.; Gmür, J.; Neftel, K. Amodiaquine-induced agranulocytosis in malaria prevention: demonstration of an amodiaquine-induced cytotoxic antibody against granulocytes. *Schweiz. Med. Wochenschr.* **1983**, *113*, 1912–3.

(190) Tafazoli, S.; O'Brien, P. J. Amodiaquine-induced oxidative stress in a hepatocyte inflammation model. *Toxicology* **2009**, *256*, 101–9.

(191) Durrani, N.; Leslie, T.; Rahim, S.; Graham, K.; Ahmad, F.; Rowland, M. Efficacy of combination therapy with artesunate plus amodiaquine compared to monotherapy with chloroquine, amodiaquine or sulfadoxine-pyrimethamine for treatment of uncomplicated Plasmodium falciparum in Afghanistan. *Trop. Med. Int. Health* **2005**, *10*, 521–9.

(192) O'Neill, P. M.; Ward, S. A.; Berry, N. G.; Jeyadevan, J. P.; Biagini, G. A.; Asadollaly, E.; Park, B. K.; Bray, P. G. A medicinal chemistry perspective on 4-aminoquinoline antimalarial drugs. *Curr. Top. Med. Chem.* **2006**, *6*, 479–507.

(193) Shimizu, S.; Atsumi, R.; Itokawa, K.; Iwasaki, M.; Aoki, T.; Ono, C.; Izumi, T.; Sudo, K.; Okazaki, O. Metabolism-dependent hepatotoxicity of amodiaquine in glutathione-depleted mice. *Arch. Toxicol.* **2009**, *83*, 701–7.

(194) Naisbitt, D. J.; Williams, D. P.; O'Neill, P. M.; Maggs, J. L.; Willock, D. J.; Pirmohamed, M.; Park, B. K. Metabolism-dependent neutrophil cytotoxicity of amodiaquine: A comparison with pyronaridine and related antimalarial drugs. *Chem. Res. Toxicol.* **1998**, *11*, 1586–95.

(195) Tingle, M. D.; Jewell, H.; Maggs, J. L.; O'Neill, P. M.; Park, B. K. The bioactivation of amodiaquine by human polymorphonuclear leucocytes in vitro: Chemical mechanisms and the effects of fluorine substitution. *Biochem. Pharmacol.* **1995**, *50*, 1113–1119.

(196) Clarke, J. B.; Maggs, J. L.; Kitteringham, N. R.; Park, B. K. Immunogenicity of Amodiaquine in the Rat. *Int. Arch. Allergy Immunol.* **1990**, *91*, 335–342.

(197) Maggs, J. L.; Tingle, M. D.; Kitteringham, N. R.; Park, B. K. Drug-protein conjugates—XIV: Mechanisms of formation of protein-arylating intermediates from amodiaquine, a myelotoxin and hepatotoxin in man. *Biochem. Pharmacol.* **1988**, *37*, 303–311.

(198) Clarke, J. B.; Neftel, K.; Kitteringham, N. R.; Park, B. K. Detection of antidrug IgG antibodies in patients with adverse drug reactions to amodiaquine. *Int. Arch. Allergy Appl. Immunol.* **1991**, *95*, 369–75.

(199) Shimada, T.; Oda, Y.; Gillam, E. M.; Guengerich, F. P.; Inoue, K. Metabolic activation of polycyclic aromatic hydrocarbons and other procarcinogens by cytochromes P450 1A1 and P450 1B1 allelic variants and other human

cytochromes P450 in Salmonella typhimurium NM2009. *Drug Metab. Dispos.* **2001**, *29*, 1176–82.

(200) Shimada, T.; Fujii-Kuriyama, Y. Metabolic activation of polycyclic aromatic hydrocarbons to carcinogens by cytochromes P450 1A1 and 1B1. *Cancer Sci.* **2004**, *95*, 1–6.

(201) O'Neill, P. M.; Harrison, A. C.; Storr, R. C.; Hawley, S. R.; Ward, S. A.; Park, B. K. The Effect of Fluorine Substitution on the Metabolism and Antimalarial Activity of Amodiaquine. *J. Med. Chem.* **1994**, *37*, 1362–1370.

(202) O'Neill, P. M.; Mukhtar, A.; Stocks, P. A.; Randle, L. E.; Hindley, S.; Ward, S. A.; Storr, R. C.; Bickley, J. F.; O'Neil, I. A.; Maggs, J. L.; Hughes, R. H.; Winstanley, P. A.; Bray, P. G.; Park, B. K. Isoquine and related amodiaquine analogues: a new generation of improved 4-aminoquinoline antimalarials. *J. Med. Chem.* **2003**, *46*, 4933–45.

(203) O'Neill, P. M.; Shone, A. E.; Stanford, D.; Nixon, G.; Asadollahy, E.; Park, B. K.; Maggs, J. L.; Roberts, P.; Stocks, P. A.; Biagini, G.; Bray, P. G.; Davies, J.; Berry, N.; Hall, C.; Rimmer, K.; Winstanley, P. A.; Hindley, S.; Bambal, R. B.; Davis, C. B.; Bates, M.; Gresham, S. L.; Brigandi, R. A.; Gomez-de-Las-Heras, F. M.; Gargallo, D. V; Parapini, S.; Vivas, L.; Lander, H.; Taramelli, D.; Ward, S. A. SI Synthesis, antimalarial activity, and preclinical pharmacology of a novel series of 4'-fluoro and 4'-chloro analogues of amodiaquine. Identification of a suitable "back-up" compound for N-tert-butyl isoquine. *J. Med. Chem.* **2009**, *52*, 1828–44.

(204) Biamonte, M. A.; Wanner, J.; Le Roch, K. G. Recent advances in malaria drug discovery. *Bioorg. Med. Chem. Lett.* **2013**, *23*, 2829–43.

(205) Miroshnikova, O. V; Hudson, T. H.; Gerena, L.; Kyle, D. E.; Lin, A. J. Synthesis and antimalarial activity of new isotebuquine analogues. *J. Med. Chem.* **2007**, *50*, 889–96.

(206) O'Neill, P. M.; Bray, P. G.; Hawley, S. R.; Ward, S. A.; Park, B. K. 4-Aminoquinolines--past, present, and future: a chemical perspective. *Pharmacol. Ther.* **1998**, *77*, 29–58.

(207) Wang, X.; Dong, Y.; Wittlin, S.; Charman, S. A.; Chiu, F. C. K.; Chollet, J.; Katneni, K.; Mannila, J.; Morizzi, J.; Ryan, E.; et al. Comparative antimalarial activities and ADME profiles of ozonides (1,2,4-trioxolanes) OZ277, OZ439, and their 1,2-dioxolane, 1,2,4-trioxane, and 1,2,4,5-tetraoxane isosteres. *J. Med. Chem.* **2013**, *56*, 2547–2555.

(208) Atkuri, K. R.; Mantovani, J. J.; Herzenberg, L. A.; Herzenberg, L. A. N -Acetylcysteine — A safe antidote for cysteine/glutathione deficiency. *Curr. Opin. Pharmacol.* **2007**, *7*, 355–359.

Chapter 2

DESIGN AND SYNTHESIS OF BENZOHETEROCYCLIC AND PYRIDYL AMODIAQUINE ANALOGUES

2.1 DESIGN

As mentioned in Chapter 1, the 4-aminophenol moiety of amodiaquine is essential for the quinone imine reactive metabolite formation while the presence of the Mannich side chain is a prerequisite for the formation of the aldehyde reactive metabolite. We postulated that incorporating the Mannich side chain and the hydroxyl group of amodiaquine into a second benzoheterocyclic ring system would potentially block the formation of the two reactive metabolites. The aromatic ring, which is known to impart activity against chloroquine resistant strains, would thus still be retained in the resulting molecules [1]. A second approach was to replace the aromatic aminophenol ring with an aminopyridyl ring thus designing out the toxicophore from the resulting molecules. In both cases, a good leaving group, such as a halogen, on the azole benzoheterocyclic (benzazole) or pyridyl ring would serve as a handle for the introduction of diversity in the target molecules (Figure 2.1).

The choice of the benzoheterocyclic ring system was informed by commercial availability and chemical tractability. Consequently, the readily available and tractable benzoheterocyles became the ring systems of interest. Molecules with the benzothiazole scaffold are known to possess diverse pharmacological activity which includes antimalarial, antitubercular, antifungal, anthelmintic, antitumoral, antibacterial, antifungal and analgesic activities [2–5]. Benzoxazole analogues possess, among other reported activities, antifungal [6], antibacterial [7–10], antitumor [11], antiviral, antitubercular

and anthelmintic activity [12]. The pharmacological activities of benzimidazole containing molecules have been comprehensively reviewed and include antiviral, antibacterial, antitumoral, anthelmintic, antihypertensive, antiallergic, gastric proton pump inhibition and analgesic [13]. The extensive biological profile and synthetic accessibility of benzothiazole, as well as the benzoxazole and benzimidazole compounds make these scaffolds attractive in the design of potential chemotherapeutics [14].

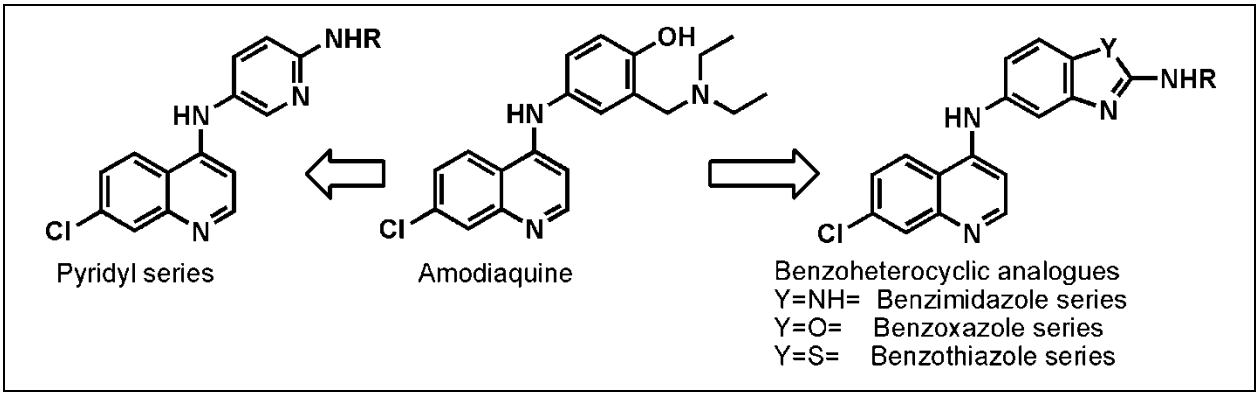

Figure 2.1: General chemical structures of the four series of amodiaquine analogues

The second aspect of the design was the choice of groups to introduce diversity in the molecules. The primary consideration was the fact that these compounds, being amodiaquine analogues, should have a protonatable tertiary nitrogen attached to the benzoheterocyclic or pyridyl rings. This would enhance accumulation in the parasitic food vacuole, assuming the mode of action of these compounds to primarily involve disruption of heme detoxification [15]. Different diamines were selected in which the tertiary nitrogen was part of an aliphatic or cyclic system. The second amine was a primary amine (or secondary amine in some compounds) that would take part in a substitution reaction with the leaving group on the tractable intermediates. The length of the linker between the two nitrogen atoms was varied and, in some molecules, a

piperazinyl linker was chosen instead of an alkyl linker. To more fully explore the groups tolerated on the side chain, different aromatic and simple alkyl amines were also incorporated in the side chain. The different amines selected are shown in Figure 2.2.

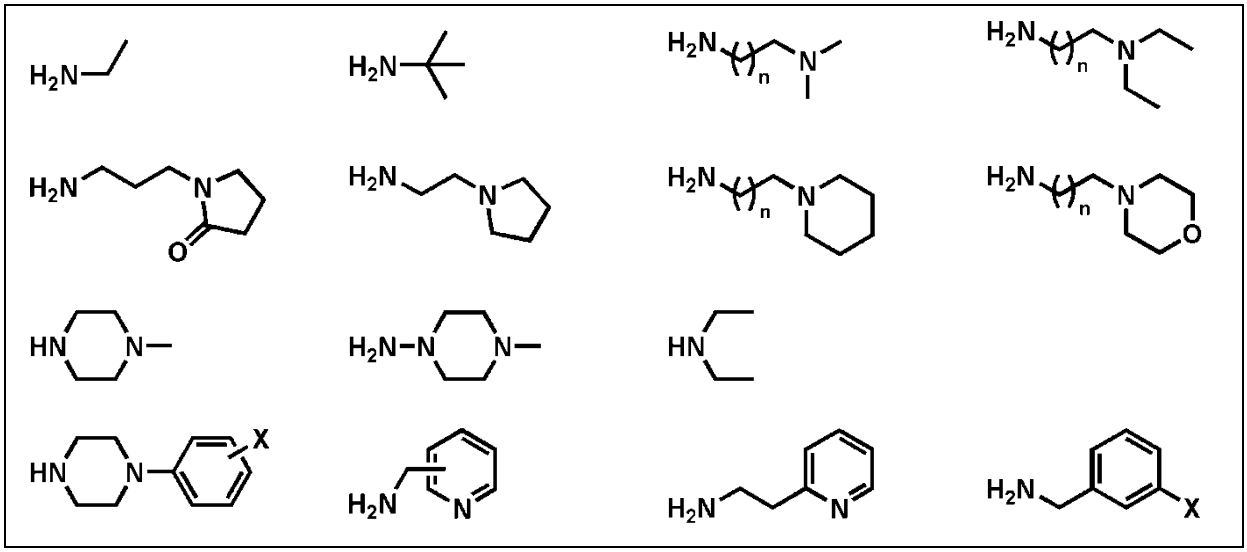

Figure 2.2: Amines employed in substitution reactions: n=1, 2, X= H, Cl, CF_3.

2.2 SYNTHESIS

After the introduction of the leaving group on the different ring systems, the synthesis of the four series of amodiaquine analogues proceeded through a common pathway: a substitution reaction on the leaving group to introduce the amino side chain, reduction of the aromatic nitro group to an aromatic amine and a second substitution reaction between the amine thus obtained and 4,7-dichloroquinoline to give the target molecules. The retrosynthetic analysis of the four series will be illustrated using the benzothiazole series (Scheme 2.1). The target molecule was envisaged to be obtained by disconnection of the 4-aminoquinoline bond. Commercially available 4,7-dichloroquinoline could then serve as the synthetic equivalent of the electrophilic synthon with the aromatic amine serving as the nucleophile. A functional group

interconversion (FGI) of the aromatic nitro compound by a variety of reduction techniques could readily furnish the aromatic amine. A second disconnection at the 2-amino position of the nitro intermediate revealed the starting molecules to be a substituted amine and a nitrobenzoheterocycle (or nitropyridine for the pyridyl series) with an appropriate leaving group.

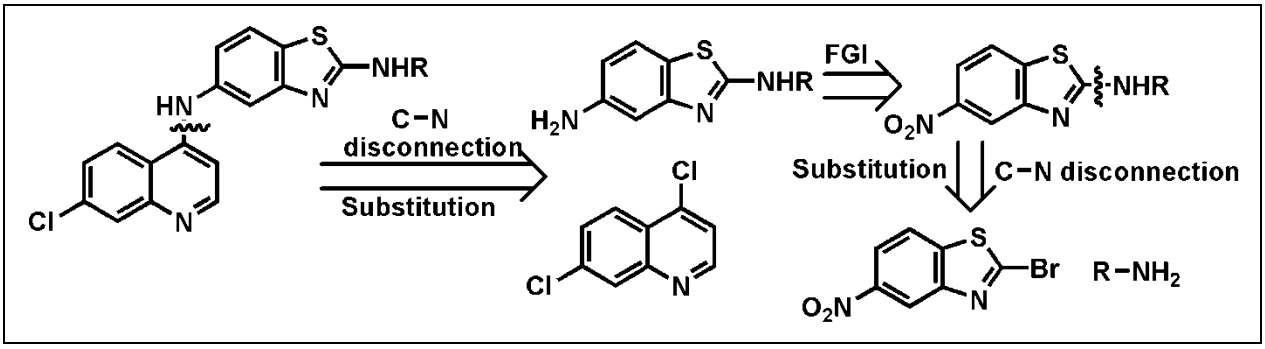

Scheme 2.1: Retrosynthetic scheme for the benzothiazole series

2.2.1 Towards chemically tractable intermediates

2.2.1.1 Bromo intermediates

The commercially available 6-nitrobenzothiazol-2-amine (**2.1**) was readily converted to 2-bromo-6-nitrobenzothiazole (**2.2**) at room temperature using the Sandmeyer reaction [16]. The mechanism for this reaction is well known, involving diazotization, loss of nitrogen gas and probably reaction of the resulting radical C-center on benzene with a bromide radical supplied by copper bromide to give the bromo substituted intermediate [17]. The same approach was applied to the conversion of 2-amino-5-nitropyridine (**2.3**) to 2-bromo-5-nitropyridine (**2.4**). However, this conversion did not go to completion and silica gel chromatography was required to separate the product from the starting material. The downfield shift of the proton attached to C3 to 7.7 ppm (it usually

resonates at <7.0 ppm in 2-aminopyridine) confirmed successful substitution. Bromination of the commercially available 5-nitrobenzimidazole-2-thiol (**2.5**) using bromine and HBr in acetic acid, as reported in literature, afforded 2-bromo-5-nitrobenzimidazole (**2.6**) [18]. The reaction conditions are illustrated in Scheme 2.2.

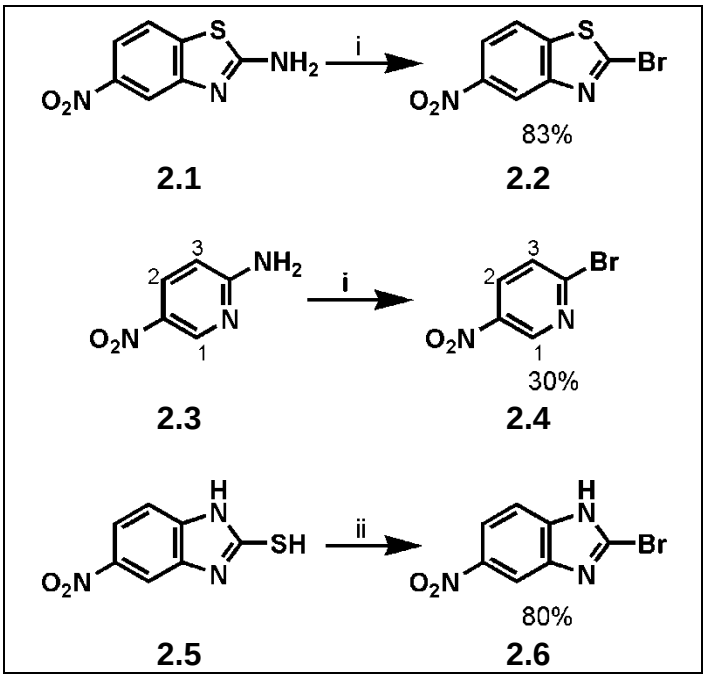

Scheme 2.2: *Reagents and conditions:* (i) 48% HBr, $NaNO_2$, CuBr, H_2O, 4h, r.t. (ii) Br_2, 48 % HBr, AcOH, 5°C-r.t., 4.5h, r.t.-0°C, H_2O, NaOH, pH 4.

2.2.1.2 2-(Methylthio)-5-nitrobenzoxazole

Cyclization of the readily available 2-amino-4-nitrophenol (**2.7**) using potassium ethyl xanthate in ethanol was carried out under reflux to give 5-nitrobenzoxazole-2-thione (**2.8**) [19]. Pyridine has also been used as a solvent for this reaction but its use necessitates prolonged drying of the product at elevated temperatures under vacuum [4]. Both solvents give excellent yields and thus ethanol was preferred. After completion of the reaction, which was monitored by TLC, the reaction mixture was cooled, diluted with

water and acidified to precipitate the product as a yellow solid. The benzoxazole-2-thione can also be obtained by reacting 2-aminophenol with carbon disulfide usually in the presence of base with ethanol or methanol as solvent [20,21]. In the second step, thiol (**2.8**) was converted to 2-(methylthio)-5-nitrobenzoxazole (**2.9**) by reaction with iodomethane in acetonitrile in the presence of a base at room temperature as shown in Scheme 2.3 [22]. The product was obtained after aqueous work-up and used without further purification after drying. The methylthio was envisaged to act as a better leaving group compared to the thione [23]. The structure of the target intermediate was confirmed by the presence of a characteristic deshielded methyl singlet at 2.8 ppm in the ^{1}H NMR spectrum.

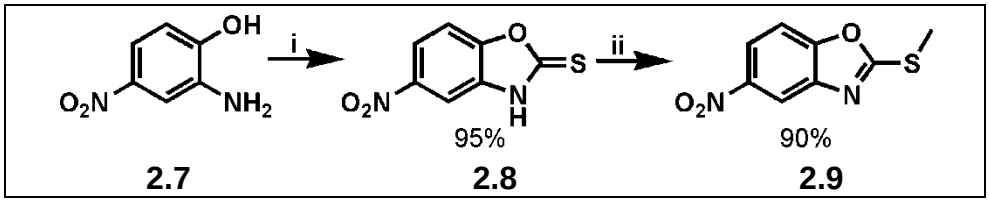

Scheme 2.3: *Reagents and conditions:* (**i**) Potassium ethyl xanthate, EtOH, reflux, 4.5 h, AcOH, pH 5 (**ii**) MeI, ACN, 25 °C, 4 h.

2.2.2 First nucelophilic substitution step

With the appropriately substituted intermediates in hand, the next step involved a nucleophilic substitution reaction with different amines to introduce diversity. For the simple alkyl amines (*tert*-butylamine and ethylamine), the reaction with 2-bromo-6-nitrobenzothiazole (**2.2**) took place at room temperature in THF. On the other hand, only ethylamine reacted with 2-(methylthio)-5-nitrobenzoxazole (**2.9**) in DMF at 80 °C to give the desired product. Attempts to react 2-bromo-5-nitrobenzimidazole (**2.6**) with ethylamine proved unsuccessful. Furthermore, reactions between 2-bromo-6-nitrobenzothiazole (**2.2**) and bulkier amines were found to be extremely slow and low

yielding while these amines did not react at all with 2-(methylthio)-5-nitrobenzoxazole (**2.9**). In a search for alternative synthetic schemes, it was noted that microwave assisted synthesis and the use of sealed tubes under thermal conditions have been reported in many amination reactions [24]. The microwave approach was adopted because of the associated short reaction times. After successfully applying microwave synthesis to obtain *N*-ethyl-5-nitro-benzimidazol-2-amine in only 20 minutes at 120 °C, we were encouraged to employ these conditions for all the other amination reactions. Except for aryl-substituted amines, the products were obtained after aqueous work-up and silica gel column chromatography. The aryl-substituted amines were observed to crystallize out of the reaction mixture after standing overnight and were obtained by filtration. In all these reactions, the starting heterocyclic intermediates had three well resolved aromatic proton signals in their ^{1}H NMR spectra. In the benzoxazole, benzimidazole and benzothiazole series, proton A was the most deshielded and appeared as a doublet with a small coupling constant (J≈2.2 Hz due to *meta* coupling with proton B), followed by protons B and C in that order (Figure 2.3). Proton B appeared as a doublet of doublets due to *meta* coupling with A (J≈2.2 Hz) and *ortho* coupling with C (J≈8.7 Hz). Generally, the nature of heteroatom X was seen to influence deshielding in the order S>O>NH.

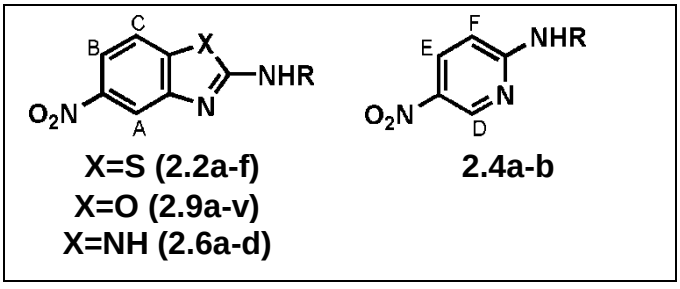

Figure 2.3: General structures of amine intermediates

In the pyridyl series (Figure 2.3), the presence of the electron withdrawing nitro group and the pyridyl nitrogen combined to make proton D the most deshielded (a doublet with a small coupling constant due to *meta* coupling at >9.1 ppm). Proton F was the most shielded due to its proximity to the amino group and appeared as a doublet with a large coupling constant (J≈9.0 Hz) due to *ortho* coupling with E. Proton E, as expected, appeared as a doublet of doublets due to coupling with D (J≈2.7 Hz) and F (J≈9.0 Hz).

Successful amination was easily confirmed by the appearance of additional aliphatic or aromatic signals at the expected chemical shifts as illustrated using the spectrum of **2.2d** in Figure 2.4. In this case, the ethylene protons 4 and 5 couple with each other and appear as triplets (J=6.7 Hz) at 3.57 and 2.61, respectively. These two pairs of protons appear more downfield compared to normal ethylene protons owing to the deshielding effect of the benzothiazolamine NH and piperidine nitrogen atom. The localization of the NH electrons into the benzothiazole ring results in proton pair D being the more deshielded. The multiplets for the piperidinyl protons 6, 7 and 8 appear progressively upfield as the deshielding effect of the piperidine nitrogen decreases. The diastereotopic nature of the axial and equatorial protons on the piperidine ring splits the signals of both geminal and vicinal protons thus explaining the appearance of proton groups 6, 7 and 8 as multiplets. Mass spectroscopy and ^{13}C NMR were utilized to more fully characterize novel intermediates.

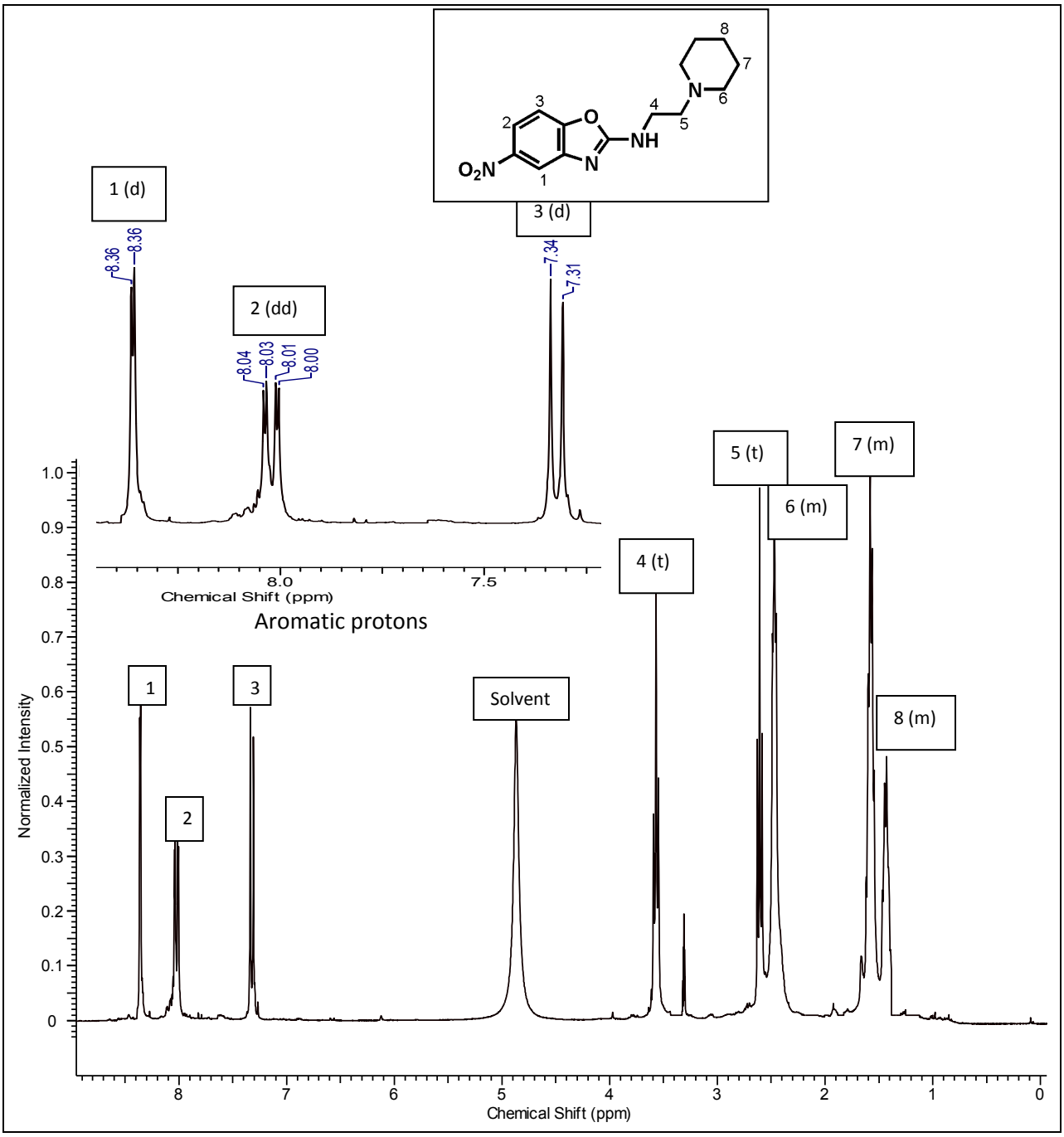

Figure 2.4: The ^{1}H NMR spectrum of **2.2d** showing an expansion of the aromatic region.

The isolated yields of the nitro intermediates are reported in Tables 2.1 through 2.4. In general, only the benzoxazole intermediates bearing aliphatic and alicyclic side chains were subjected to silica gel column chromatography.

Table 2.1: Yields of benzothiazole analogues

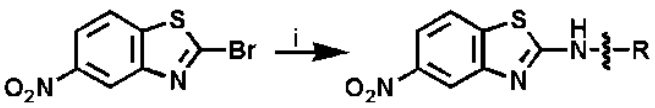

2.2 **2.2a-f**

Reagents and conditions: (i) RNH_2, THF, r.t., 15h or RNH_2, acetonitrile, MW, 120 °C, 20 min

Compound	-R	Yield %
2.2a (DS1B)		78
2.2b (DS1C)		93
2.2c (DS11)	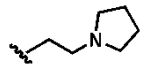	87
2.2d (DS12)	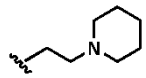	90
2.2e (DS13)	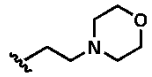	81
2.2f (DS18)	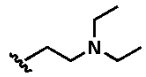	76

Table 2.2: Yields of benzimidazole analogues

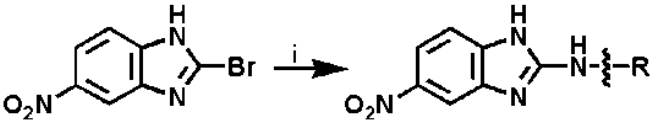

2.6 **2.6a-d**

Reagents and conditions: (i) RNH_2, acetonitrile, MW, 120 °C, 20 min

Compound	-R	Yield %
2.6a (DS5C)		92
2.6b (DS21)	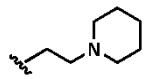	86
2.6c (DS22)	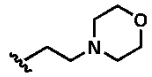	84
2.6d (DS24)	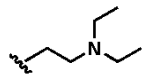	83

Table 2.3: Yields of pyridyl analogues

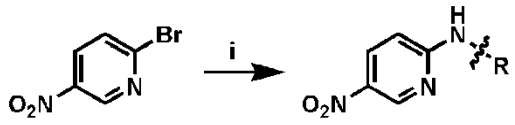

2.4 **2.4a-b**

Reagents and conditions: (i) RNH_2, acetonitrile, MW, 120 °C, 20 min

Compound	-R	Yield %
2.4a (DS26)	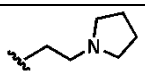	65
2.4b (DS27)	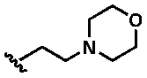	77

Table 2.4: Yields of benzoxazole analogues

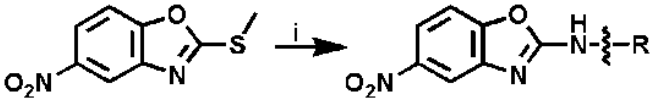

2.9 **2.9a-r**

Reagents and conditions: (i) RNH_2, acetonitrile, MW, 120 °C, 20 min

Compound	-R	Yield %
2.9a (DS4C)		87
2.9b (DS23)	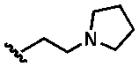	80
2.9c (DS46)	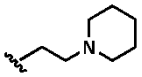	62
2.9d (DS31)	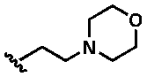	62
2.9e (DS33)	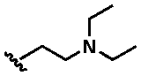	65
2.9f (DS50)	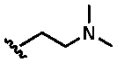	52
2.9g (DS34)	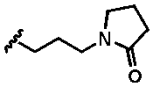	41
2.9h (DS36)	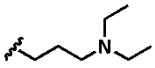	68
2.9i (DS37)	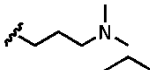	61
2.9j (DS48)	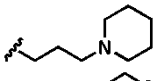	69
2.9k (DS56)	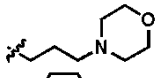	53
2.9l (DS41)	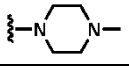	76

2.9m (DS42)	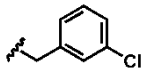	59
2.9n (DS54)	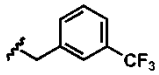	84
2.9o (DS32)	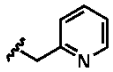	52
2.9p (DS35)	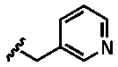	81
2.9q (DS47)	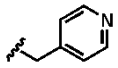	38
2.9r (DS49)	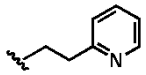	60

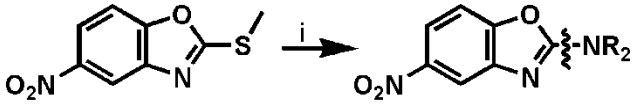

2.9 **2.9s-v**

Reagents and conditions: (i) R_2NH, acetonitrile, MW, 120 °C, 20 min

Compound	**-NR_2**	**Yield %**
2.9s (DS39)		56
2.9t (DS51)	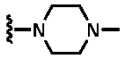	70
2.9u (DS52)	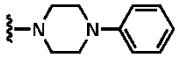	77
2.9v (DS53)	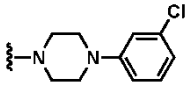	72

2.2.3 Reduction of the nitro group

Aromatic nitro groups can be reduced by a variety of methods. The use of combinations of metal and acid is a common approach. Zn/HCl and Sn/HCl require basic work-up and generate large amounts of residue thus making their use environmentally unfriendly when used in large scale synthesis or in routine syntheses. The combination of iron and HCl or acetic acid offers two advantages: it requires only catalytic amounts of acid and the iron (III) oxide by-product formed precipitates out of solution making product purification easy. In catalytic hydrogenation, the nitro compound is dissolved in an alcohol in which finely divided metal catalyst is suspended and maintained under an

atmosphere of hydrogen gas, usually under pressure. The catalysts used include palladium or platinum on carbon or alumina and the Raney catalysts comprising nickel, cobalt or copper. A hydrogen donor, such as hydrazine can be used instead of hydrogen gas. At the end of reaction, the hydrogenation vessel is vented and the catalyst simply filtered off leaving the product in solution [25]. Several other nitro reduction methods are available, including selective methods that can be employed when the nitro compound also contains other reducible groups [26,27]. We opted to use catalytic hydrogenation because the method consistently gave quantitative yields and did not require further work-up after filtration. The typical reaction time was between 8 and 10 hours. To monitor completion of the reaction, TLC was employed. Upon completion of the reduction, the reaction mixture was filtered through Celite® and the solvent evaporated *in vacuo* to obtain the aromatic amines. Selected amines were subjected to ^{1}H NMR spectroscopy to confirm the reduction of the nitro group. The typical difference in the spectra was the expected shielding of all aromatic protons, with a dramatic effect being observed on protons A and B that are adjacent to the amino group, as illustrated by the NMR spectra of **2.2d** before and after the hydrogenation reaction in Figure 2.5.

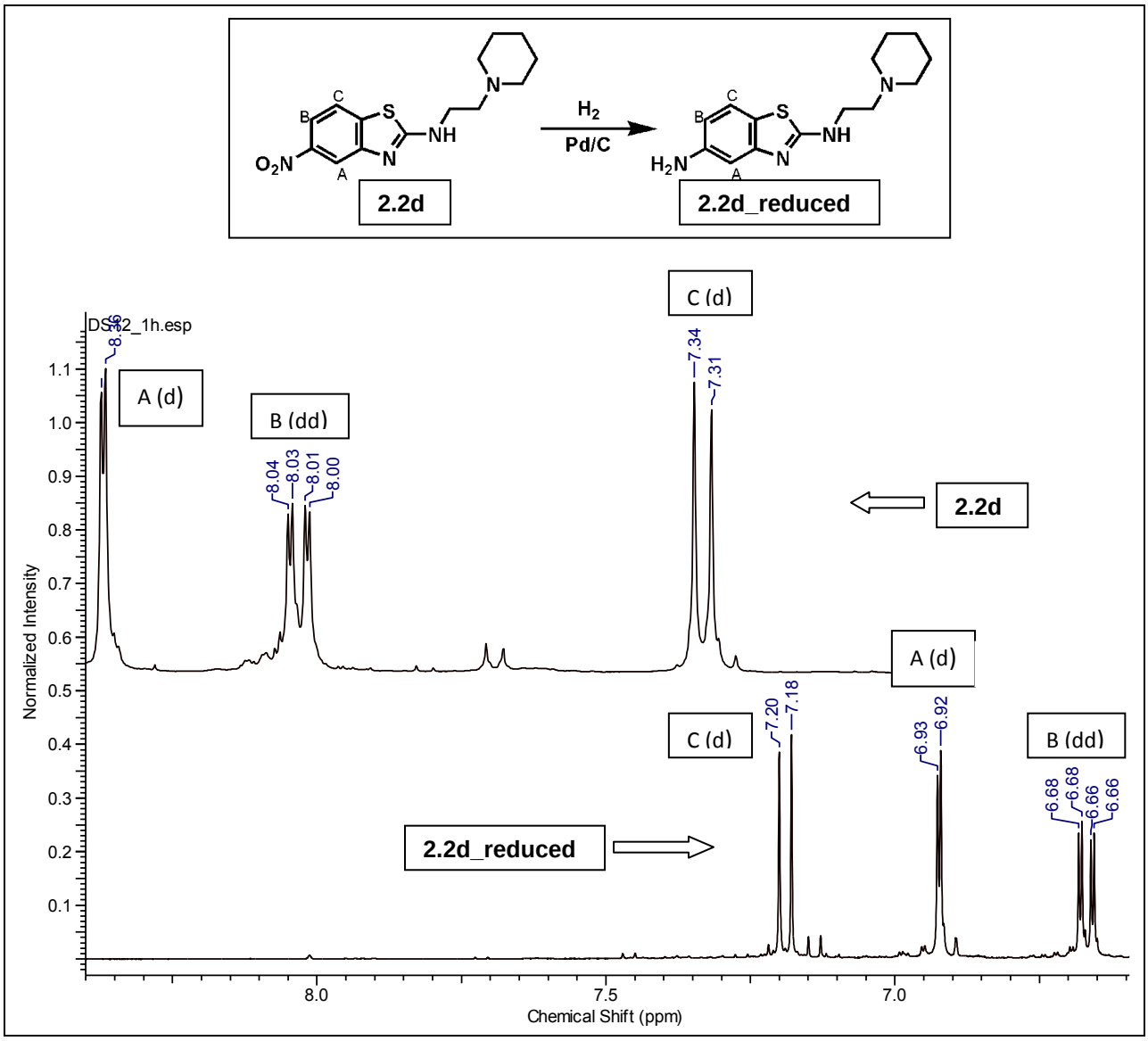

Figure 2.5: The aromatic region of the ^{1}H NMR spectra of **2.2d** and its reduced intermediate

2.2.4 Second substitution reaction (coupling with 4,7-dichloroquinoline)

The aromatic amines obtained in the previous step were coupled to position 4 of 4,7-dichloroquinoline by a nucleophilic aromatic substitution reaction to give the target molecules. The obvious starting point was to use the conditions employed in the synthesis of amodiaquine, namely reflux in ethanol [28]. However, these conditions gave

poor yields. In their synthesis of amodiaquine and amopyroquine analogues, Paunescu and coworkers reported good yields when they refluxed the reactants in acidified acetonitrile [29]. We adopted this method and reacted a slight excess of 4,7-dichloroquinoline with the amine to obtain the product, as the hydrochloride salt, in moderate yields. Typically, the reaction mixture was refluxed for 15 to 24 hours and then cooled to room temperature. The product was isolated after work-up involving basification with saturated sodium bicarbonate and silica gel column chromatography. Characterization of the target molecules was carried out using ^{1}H NMR, ^{13}C NMR and mass spectroscopy. Purity was assayed using HPLC.

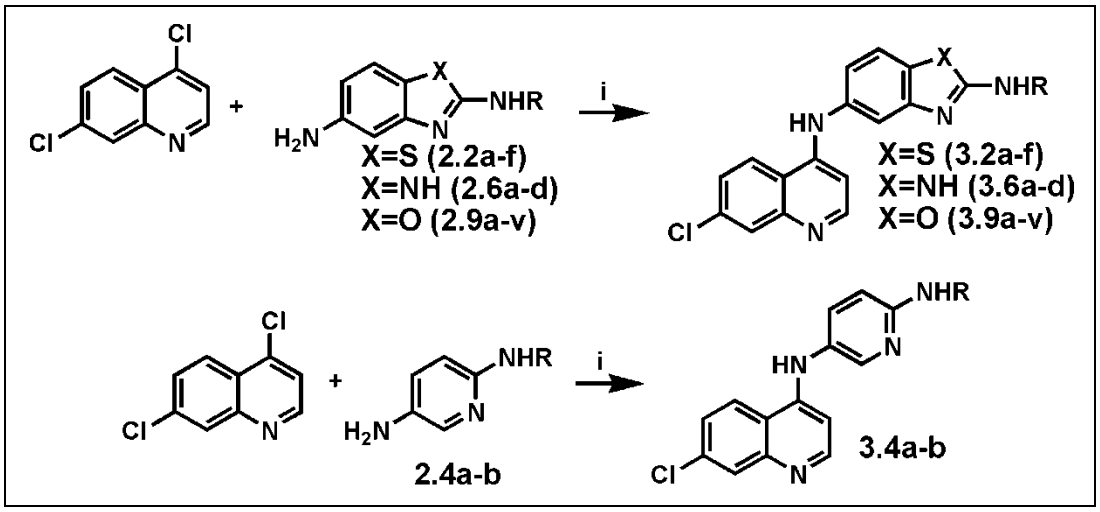

Scheme 2.4: *Reagents and conditions:* (i) Acetonitrile, HCl, reflux, 24 h.

2.3 CHARACTERIZATION OF TARGET MOLECULES

The aromatic region in the NMR spectra of all target molecules except those with additional aromatic rings attached to the benzoheterocylic or pyridine ring were similar. The spectrum of **3.9k** (Figure 2.6) will be used to discuss the characterization of target molecules with an aliphatic (or cyclic aliphatic) side chain. The quinolinyl protons were

generally more deshielded compared to the protons on the other aromatic rings. The proton attached to the α carbon of the quinoline ring (proton A) was the most deshielded, typically appearing at 8.3-8.4 ppm. This is explained by the fact that the quinolinyl nitrogen acts as an electron sink and leaves a partial positive charge on the α carbon. Conversely, the proton on the β carbon (proton H) was the most shielded of all the aromatic protons and appeared at ≈ 6.7 ppm, mainly due to the *ortho* directing effect of the 4-amino group which increases the electron density around carbon H. The two protons appeared as doublets with a coupling constant of approximately 5.6 Hz. Proton B was the second most deshielded and appeared as a doublet with a large coupling constant of 9.0 Hz due to *ortho* coupling. Proton C could only experience *meta* coupling with proton D and accordingly had a small coupling constant of ≈2.2 Hz. Finally proton D coupled with both proton B (*ortho* coupling, J = 9.0 Hz) and proton C (*meta* coupling, J =2.2 Hz) and appeared as a doublet of doublets. The aromatic region of the ^{1}H NMR spectrum of **3.9k** below illustrates these facts. The coupling of protons E, F and G has been discussed previously. The aliphatic region of the spectrum, in this case a propylmorpholino chain, has a multiplet for the deshielded morpholino protons I adjacent to the electronegative O, two triplets for the methylene protons J and K, which only couple with protons M, a second multiplet for the less deshielded morpholino protons L and an upfield multiplet signal for protons M due to coupling with both protons J and K.

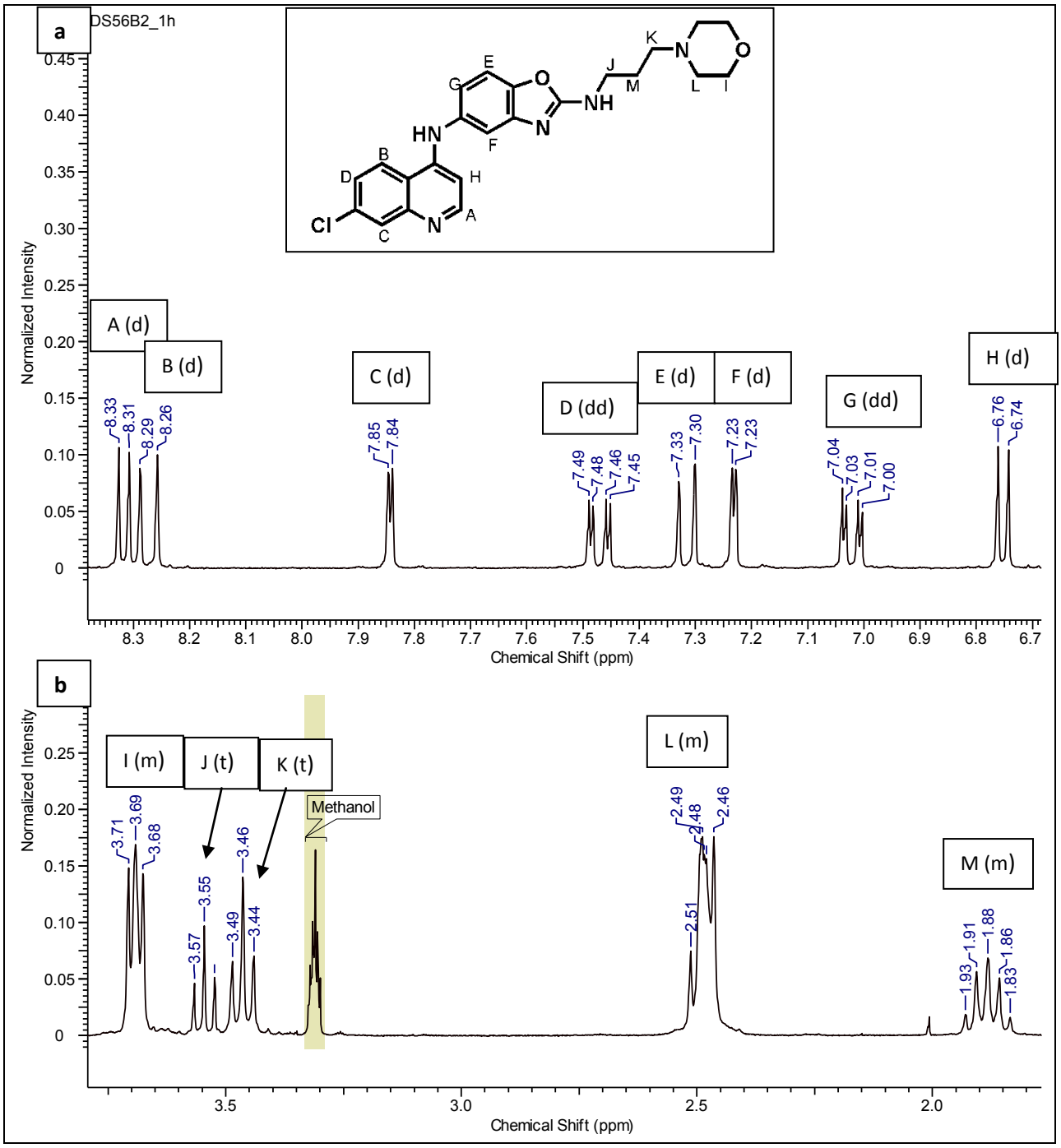

Figure 2.6: The ^{1}H NMR spectrum of **3.9k** in CD_3OD: a=aromatic, b=aliphatic

The ^{13}C spectrum of **3.9k** (Figure 2.7) has 16 aromatic carbon signals, 8 low intensity signals for the quaternary carbon atoms and 8 high intensity signals for the proton-bearing carbon atoms. In the aliphatic region, two intense signals due to the equivalent pairs of morpholino carbon atoms are clearly visible at 54.88 and 67.85 ppm, along with three low intensity signals for the propyl chain.

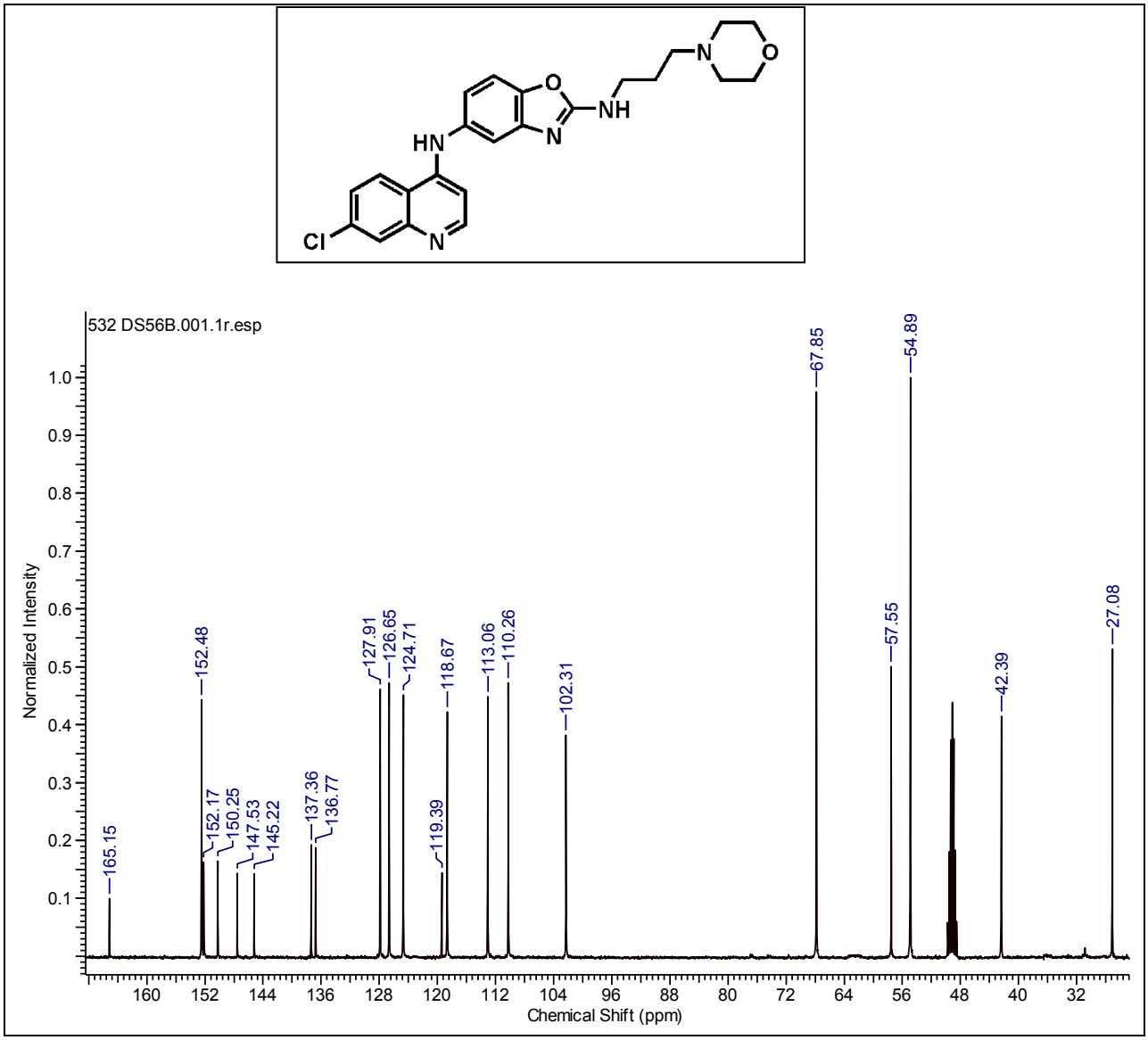

Figure 2.7: The ^{13}C spectrum of **3.9k** in CD_3OD.

The ^{1}H NMR spectrum of pyridyl analogue **3.9r** (Figure 2.8) was expected to have 12 aromatic protons: 5 from the quinolinyl ring, 3 from the benzoxazolyl ring and 4 from the pyridyl ring. However, the DMSO-d6 spectrum shows 14 protons in the aromatic region, the extra two protons coming from the two NH protons in the molecule. The NH proton at position 4 of the quinoline ring is the most deshielded and appears as singlet O at 9.01 ppm. After assigning all the aromatic protons, we were left with triplet D at 8.06 ppm. In the aliphatic region, two triplets were expected due to interaction between the two sets of ethylene protons. However, the more deshielded pair of ethylene protons (L) appear as a multiplet. This was attributed to coupling with both D and M. Such interaction would be expected to split the NH proton into a triplet and thus triplet D at 8.06 ppm was accordingly assigned.

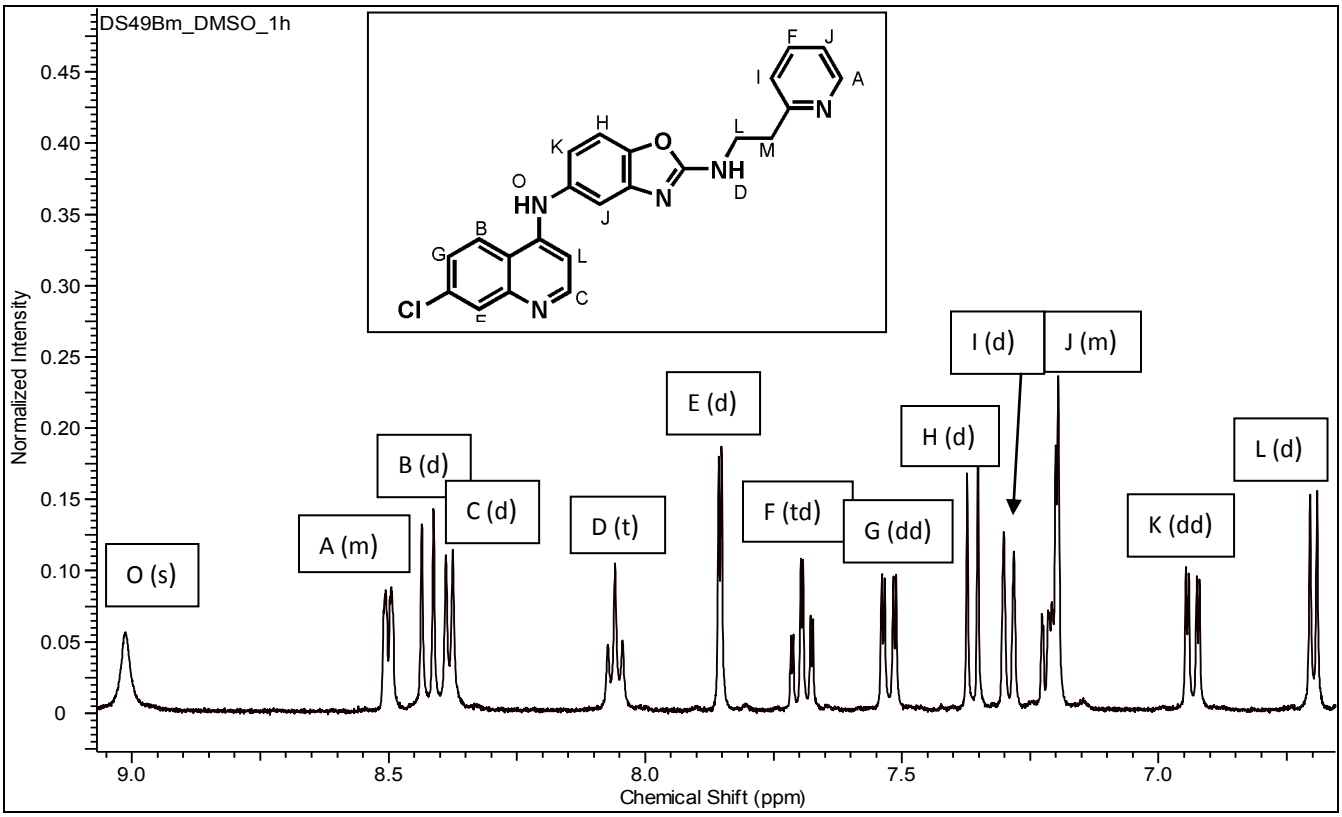

Figure 2.8: The aromatic region of the ^{1}H NMR spectrum of **3.9r.**

The ^{13}C spectrum of **3.9r** (Figure 2.9) has the expected 21 aromatic carbon signals, including a cluster of 3 signals at 149.58, 149.82 and 149.92 ppm. Of these, there are 12 high intensity signals for the CH carbon atoms. Seven low intensity signals are visible in the spectrum. These, together with the signals at 149.82 and 149.92 ppm which are seen on expanding the spectrum correspond to the nine quaternary carbon atoms. Finally, there are two signals for the ethylene carbon atoms in the aliphatic region at 37.56 and 42.53 ppm.

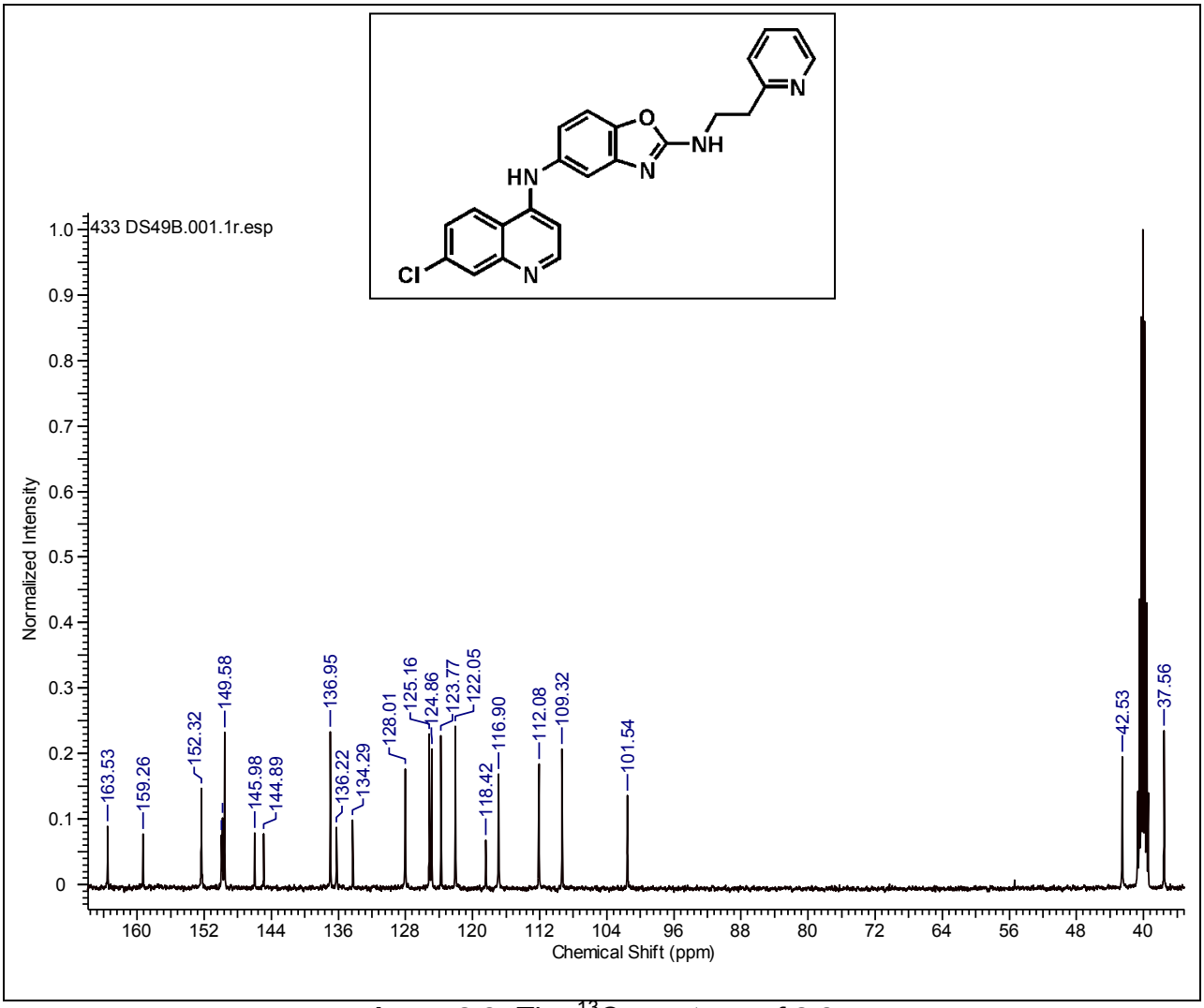

Figure 2.9: The ^{13}C spectrum of **3.9r**

The isolated yields of the target molecules are given in the tables 2.5 to 2.8 below. The greatest contributor to low yield was the difficulty encountered in purifying tertiary amine containing products which tended to co-elute with the aromatic amine reactant during column chromatography.

Table 2.5: Isolated yields of benzothiazole target molecules

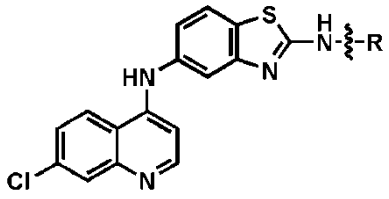

3.2a-f

Compound	-R	Yield %
3.2a (DS1F)		58
3.2b (DS1G)		42
3.2c (DS11B)	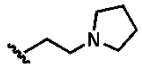	47
3.2d (DS12B)	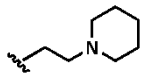	53
3.2e (DS13B)	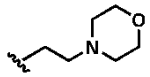	45
3.2f (DS18B)	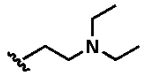	49

Table 2.6: Isolated yields of benzimidazole targets

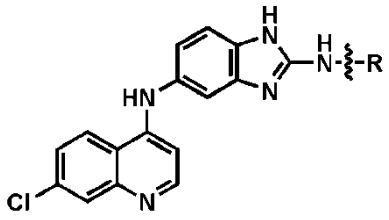

3.6a-d

Compound	-R	Yield %
3.6a (DS5G)		60
3.6b (DS21B)	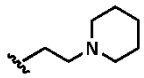	50

3.6c (DS22B)	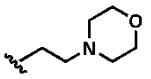	71
3.6d (DS24B)	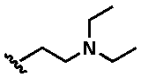	65

Table 2.7: Isolated yields of pyridyl targets

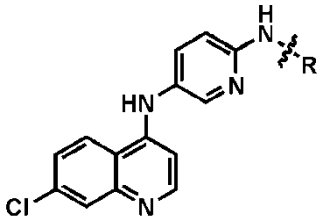

3.4a-b

Compound	-R	Yield %
3.4a (DS26B)	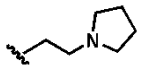	58
3.4b (DS27B)	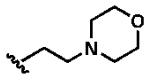	61

Table 2.8: Isolated yields of benzoxazole targets

General structure	Compound	-R or -NR_2	Yield %
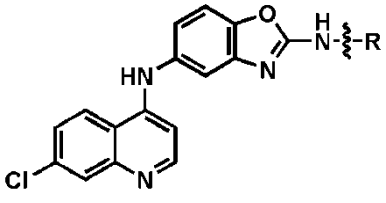 **3.9a-r**	**3.9a (DS4F)**		51
	3.9b (DS23B)	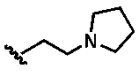	61
	3.9c (DS46B)	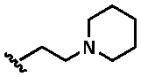	60
	3.9d (DS31B)	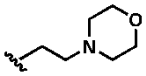	57
	3.9e (DS33B)	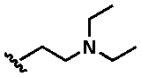	55
	3.9f (DS50B)	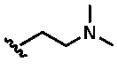	44
	3.9g (DS34B)	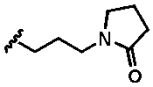	65
	3.9h (DS36B)	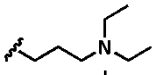	46
	3.9i (DS37B)	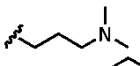	52
	3.9j (DS48B)	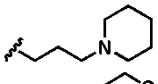	58
	3.9k (DS56B)	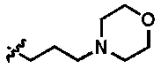	53

	3.9l (DS41B)	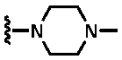	55
	3.9m (DS42B)	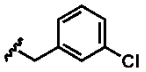	52
	3.9n (DS54B)	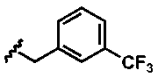	46
	3.9o (DS32B)	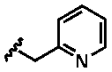	61
	3.9p (DS35B)	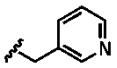	58
	3.9q (DS47B)	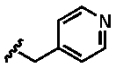	23
	3.9r (DS49B)	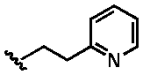	67
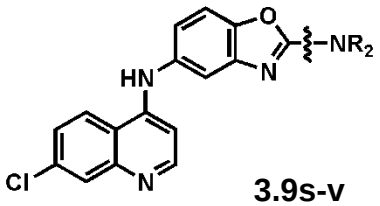 **3.9s-v**	**3.9s (DS39B)**		58
	3.9t (DS51B)	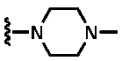	47
	3.9u (DS52B)	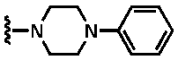	74
	3.9v (DS53B)	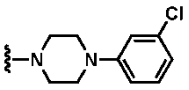	40

2.4 CONCLUSION

This chapter described the rational design and synthesis of the four series of amodiaquine analogues that formed the basis of this project. The synthesis was carried out in two phases. A limited number of representative compounds were synthesized from each of the four series and assayed for their bioactivation potential as reported in Chapter 3. Results from this assay led to the selection of the benzoxazole series for expanded antiplasmodial SAR studies. *In vitro* antiplasmodial and metabolic stability as well as *in vivo* antimalarial data are presented in Chapter 4.

REFERENCES

(1) Schlitzer, M. Malaria chemotherapeutics part I: History of antimalarial drug development, currently used therapeutics, and drugs in clinical development. *ChemMedChem.* **2007**, *2*, 944–86.

(2) Singh, M. K.; Tilak, R.; Nath, G.; Awasthi, S. K.; Agarwal, A. Design, synthesis and antimicrobial activity of novel benzothiazole analogs. *Eur. J. Med. Chem.* **2013**, *63*, 635–44.

(3) Bowyer, P. W.; Gunaratne, R. S.; Grainger, M.; Withers-Martinez, C.; Wickramsinghe, S. R.; Tate, E. W.; Leatherbarrow, R. J.; Brown, K. A.; Holder, A. A.; Smith, D. F. Molecules incorporating a benzothiazole core scaffold inhibit the N-myristoyltransferase of Plasmodium falciparum. *Biochem. J.* **2007**, *408*, 173–80.

(4) Xiang, P.; Zhou, T.; Wang, L.; Sun, C.; Hu, J.; Zhao, Y.; Yang, L. Novel benzothiazole, benzimidazole and benzoxazole derivatives as potential antitumor agents: synthesis and preliminary in vitro biological evaluation. *Molecules.* **2012**, *17*, 873–83.

(5) Bondock, S.; Fadaly, W.; Metwally, M. A. Synthesis and antimicrobial activity of some new thiazole, thiophene and pyrazole derivatives containing benzothiazole moiety. *Eur. J. Med. Chem.* **2010**, *45*, 3692–701.

(6) Kuroyanagi, J.; Kanai, K.; Horiuchi, T.; Takeshita, H.; Kobayashi, S.; Achiwa, I.; Yoshida, K.; Nakamura, K.; Kawakami, K. Structure-activity relationships of 1,3-benzoxazole-4-carbonitriles as novel antifungal agents with potent in vivo efficacy. *Chem. Pharm. Bull. (Tokyo).* **2011**, *59*, 341–52.

(7) Temiz-Arpaci, O.; Ozdemir, A.; Yalçin, I.; Yildiz, I.; Aki-Sener, E.; Altanlar, N. Synthesis and antimicrobial activity of some 5-[2-(morpholin-4-yl)acetamido] and/or 5-[2-(4-substituted piperazin-1-yl)acetamido]-2-(p-substituted phenyl)benzoxazoles. *Arch. Pharm.* **2005**, *338*, 105–11.

(8) Alper-Hayta, S.; Arisoy, M.; Temiz-Arpaci, O.; Yildiz, I.; Aki, E.; Ozkan, S.; Kaynak, F. Synthesis, antimicrobial activity, pharmacophore analysis of some new 2-(substitutedphenyl/benzyl)-5-[(2-benzofuryl)carboxamido]benzoxazoles. *Eur. J. Med. Chem.* **2008**, *43*, 2568–78.

(9) Temiz-Arpaci, O.; Yildiz, I.; Ozkan, S.; Kaynak, F.; Aki-Sener, E.; Yalçin, I. Synthesis and biological activity of some new benzoxazoles. *Eur. J. Med. Chem.* **2008**, *43*, 1423–31.

(10) Vinsová, J.; Horák, V.; Buchta, V.; Kaustová, J. Highly lipophilic benzoxazoles with potential antibacterial activity. *Molecules.* **2005**, *10*, 783–93.

(11) Rida, S. M.; Ashour, F. A.; El-Hawash, S. A. M.; ElSemary, M. M.; Badr, M. H.; Shalaby, M. A. Synthesis of some novel benzoxazole derivatives as anticancer, anti-HIV-1 and antimicrobial agents. *Eur. J. Med. Chem.* **2005**, *40*, 949–59.

(12) Jauhari, P. K.; Bhavani, A.; Varalwar, S.; Singhal, K.; Raj, P. Synthesis of some novel 2-substituted benzoxazoles as anticancer, antifungal, and antimicrobial agents. *Med. Chem. Res.* **2008**, *17*, 412–424.

(13) Spasov, A. A.; Yozhitsa, I. N.; Bugaeva, L. I.; Anisimova, V. A. Benzimidazole derivatives: Spectrum of pharmacological activity and toxicological properties (a review). *Pharm. Chem. J.* **1999**, *33*, 232–243.

(14) Ahmed, K.; Yellamelli Valli Venkata, S.; Mohammed, N. A. K.; Sultana, F.; Methuku, K. R. Recent advances on structural modifications of benzothiazoles

and their conjugate systems as potential chemotherapeutics. *Expert. Opin. Investig. Drugs.* **2012**, *21*, 619–35.

(15) Kumar, S.; Guha, M.; Choubey, V.; Maity, P.; Bandyopadhyay, U. Antimalarial drugs inhibiting hemozoin (beta-hematin) formation: a mechanistic update. *Life Sci.* **2007**, *80*, 813–28.

(16) Larina, L.; Lopyrev, V. *Nitroazoles: Synthesis, Structure and Applications*; Springer: New York, NY, 2009.

(17) Smith, M. B.; March, J. *March's advanced organic chemistry*; 6th ed.; John Wiley & Sons, Inc.: Hoboken, NJ, USA., 2007.

(18) Okolotowicz, K. J.; Shi, R.; Zheng, X.; MacDonald, M.; Reed, J. C.; Cashman, J. R. Selective benzimidazole inhibitors of the antigen receptor-mediated NF-kappaB activation pathway. *Bioorg. Med. Chem.* **2010**, *18*, 1918–24.

(19) Yamazaki, Y.; Ogawa, S.; Shibuya, K. Synthesis of highly deuterium-labeled (R)-K-13675, PPAR alpha agonist, for use as an internal standard for low-level quantification of drugs in plasma. *Bioorg. Med. Chem.* **2009**, *17*, 1911–7.

(20) Guntreddi, T.; Allam, B. K.; Singh, K. N. Utilization of carbon disulfide as a powerful building block for the synthesis of 2-aminobenzoxazoles. *RSC Advances* **2013**, *3*, 9875.

(21) Chen, W.; Jin, G. Synthesis of N-(thio)phosphoryl-N'-2-benzoxazolyl semicarbazides. *Heteroat. Chem.* **2001**, *12*, 151–155.

(22) Bethge, L.; Jarikote, D. V.; Seitz, O. New cyanine dyes as base surrogates in PNA: forced intercalation probes (FIT-probes) for homogeneous SNP detection. *Bioorg. Med. Chem.* **2008**, *16*, 114–25.

(23) Fujita, R.; Watanabe, N.; Tomisawa, H. Reaction of 1-alkylthioisoquinolinium salts with active methylene compounds. *Chem. Pharm. Bull. (Tokyo).* **2002**, *50*, 225–8.

(24) Peddibhotla, S.; Shi, R.; Khan, P.; Smith, L. H.; Mangravita-Novo, A.; Vicchiarelli, M.; Su, Y.; Okolotowicz, K. J.; Cashman, J. R.; Reed, J. C.; Roth, G. P. Inhibition of protein kinase C-driven nuclear factor-kappaB activation: synthesis, structure-activity relationship, and pharmacological profiling of pathway specific benzimidazole probe molecules. *J. Med. Chem.* **2010**, *53*, 4793–7.

(25) Hepworth, J. D.; Waring, D. R. *Aromatic Chemistry*; The Royal Society of Chemistry: Cambridge, 2002.

(26) Lee, H.; An, M. Selective Reduction of the Nitro-group Using Co 2 (CO) 8 -H 2 O. *Bull. Korean. Chem. Soc.* **2004**, *25*, 1717–1719.

(27) Rahaim, R. J.; Maleczka, R. E. Pd-catalyzed silicon hydride reductions of aromatic and aliphatic nitro groups. *Org. Lett.* **2005**, *7*, 5087–90.

(28) O'Neill, P. M.; Mukhtar, A.; Stocks, P. A.; Randle, L. E.; Hindley, S.; Ward, S. A.; Storr, R. C.; Bickley, J. F.; O'Neil, I. A.; Maggs, J. L.; Hughes, R. H.; Winstanley, P. A.; Bray, P. G.; Park, B. K. Isoquine and related amodiaquine analogues: a new generation of improved 4-aminoquinoline antimalarials. *J. Med. Chem.* **2003**, *46*, 4933–45.

(29) Păunescu, E.; Susplugas, S.; Boll, E.; Varga, R.; Mouray, E.; Grosu, I.; Grellier, P.; Melnyk, P. Replacement of the 4'-hydroxy group of amodiaquine and amopyroquine by aromatic and aliphatic substituents: synthesis and antimalarial activity. *ChemMedChem.* **2009**, *4*, 549–61.

Chapter 3

REACTIVE METABOLITE STUDIES

3.1 INTRODUCTION

In this chapter, the bioactivation potential of the four series of amodiaquine analogues previously described is assessed using representative compounds. Two methods are employed: trapping reactions using glutathione, potassium cyanide and methoxylamine as well as time-dependent CYP inhibition. Based on findings from this evaluation, the best series is selected for further exploration.

As mentioned in Chapter 1, reactive metabolites readily form covalent bonds with nucleophiles, a phenomenon that underlies both their detoxification and toxicity [1]. This reactivity is taken advantage of in trapping reactions where the test compound is exposed to conditions conducive for bioactivation in the presence of selected nucleophiles [2,3]. The formation of adducts with the nucleophiles is then detected using mass spectroscopic techniques and is a measure of the bioactivation potential of the test compound [4]. In our project, we were privileged to have a working collaboration with Dr Jurva Ulrik at AstraZeneca, Sweden, who gladly offered to carry out on-line Electrochemistry /Electrospray Ionization Mass Spectrometry (EC/ESI-MS) on the first batch of compounds.

Time-dependent CYP inhibition can be used as an indicator of the ability of a compound to form reactive metabolites as discussed in Chapter 1. In such cases, the metabolite is so reactive that it reacts directly with enzyme when it is formed resulting in inactivation of the enzyme [5]. To assess this type of inhibition, it was first necessary to determine whether the test compounds inhibited any of the five major CYP isoforms involved in

xenobiotic metabolism namely CYP1A2, CYP2C9, CYP2C19, CYP2D6 and CYP3A4 [6]. These studies were conducted at the African Institute of Biomedical Science and Technology (AiBST) in Harare, Zimbabwe.

3.1.1 The EC/ESI-MS procedure

This method involved infusion of the substrate solution through the electrochemical cell via a syringe pump (Figure 3.1). A pH adjusted make-up flow was added before the cell. The electrochemical cell was controlled using a potentiostat, at a fixed or varying potential of between 0 and 1500 V. The sample was collected in glass vials containing glutathione, methoxylamine or potassium cyanide as the trapping agents for subsequent analysis by LC/MS [7].

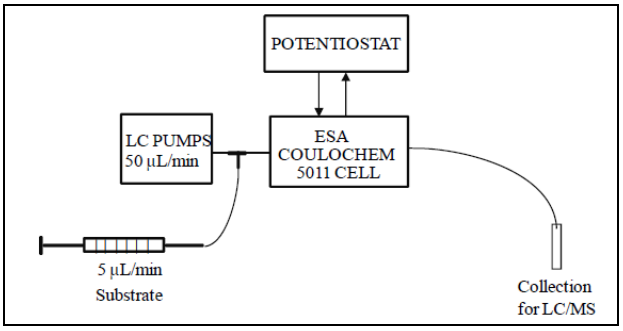

Figure 3.1: Schematic overview of the electrochemical system [7].

3.1.2 The CYP inhibition assay procedure

This assay was carried out according to the method by Crespi and Stresser in 96-well microtiter plates at high (20µM) and low (3µM) concentrations [8]. Enzyme substrates that are metabolized to fluorescent compounds were employed. After incubation for 15 minutes at 37 °C, the reaction was quenched using 1 mM Tris solution in 80% acetonitrile and the formation of fluorescent metabolites was measured. Ketoconazole, thioridazine, sulfaphenazole and α-naphthoflavone are known inhibitors of CYP3A4,

CYP2D6, CYP1A2 and CYP2C9, respectively, and were used as positive controls for these enzymes [9].

In the time-dependent CYP inhibition assay, a two-step incubation scheme consisting of an inactivation assay and an activity assay was used according to the method by Thelingwani *et al*. [10]. In the inactivation assay, the test compounds (at concentrations of 2 and 10 µM) were incubated with recombinant enzyme. The assay was performed both in the presence and absence of NADPH for 15 min at 37°C. An aliquot was then transferred to the activity assay plate consisting of buffer, NADPH and a substrate that is metabolized to a fluorescent compound. The mixture was incubated for a further 15 min at 37°C and the reaction was terminated by addition of an ice-cold 20% Tris base/80% acetonitrile solution. Enzyme activity was measured as described for the one step CYP inhibition assay. Troleandomycin, a known mechanism-based inhibitor of CYP3A4, was used as the positive control in this assay [11].

3.1.3 Treatment of results

In the glutathione trapping experiments, the mass spectrometer was set to detect glutathione adducts of the test compounds (305.32 mass units above the molecular weight of the test compound). Clozapine was used as the positive control compound. Clozapine is a neuroleptic drug that readily forms glutathione adducts following its bioactivation to a reactive nitrenium metabolite (figure) [12].

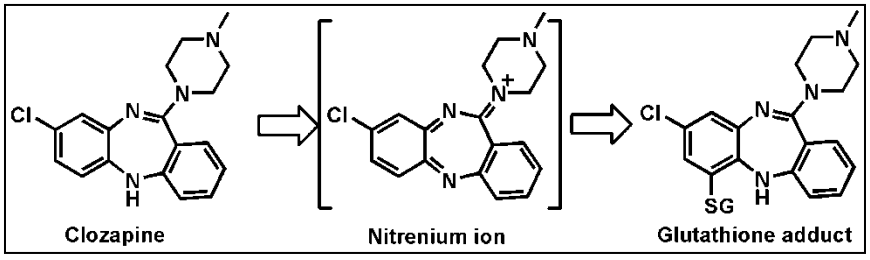

Figure 3.2: Bioactivation of clozapine and detoxification by glutathione.

The results of the trapping experiment were semi-quantitatively expressed using as a ratio of the peak areas of test compound and clozapine adducts as shown in equation 1 below.

$$\text{Glutathione ratio} = \frac{\text{Sum of areas of glutathione adducts of test compound}}{\text{Area of major glutatione adduct of clozapine}} \qquad \text{Equation 1}$$

Methoxylamine and potassium cyanide trapping was assessed by directly scanning for the masses of methoxylamine and cyanide adduct formation and were qualitatively expressed as yes (adduct detected) or no (adduct not detected) observations.

In the CYP inhibition assays, enzyme activity was estimated by comparing the level of fluorescence in wells containing test compounds with that in wells containing no inhibitor. Results were presented as % of remaining enzyme activity. Finally, mechanism-based inhibition (MBI) results were presented as a normalized ratio (Equation 2) as previously described [10].

$$\text{Normalized ratio} = \frac{(R+I^{+NADPH})/(R-I^{+NADPH})}{(R+I^{-NADPH})/(R-I^{-NADPH})} \qquad \text{Equation 2}$$

where $R+I^{+NADPH}$ and $R+I^{-NADPH}$ refer the rates of reaction when incubation is performed in the presence of the inhibitor with and without NADPH, respectively, while $R-I^{+NADPH}$ and $R-I^{-NADPH}$ refer to the rate when incubation is performed in the absence of inhibitor with and without NADPH, respectively.

3.2 RESULTS AND DISCUSSION

3.2.1 Glutathione trapping

Table 3.1: Glutathione trapping results

General structure	Compound	R	GSH ratio
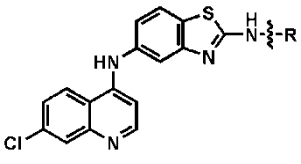	**3.2a (DS1F)**		0.74
	3.2c (DS11B)	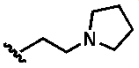	0.39
	3.2d (DS12B)	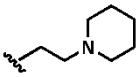	0.88
	3.2e (DS13B)	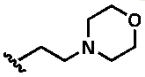	1.13
	3.2f (DS18B)	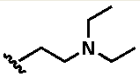	0.54
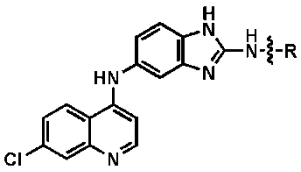	**3.6a (DS5G)**		0.54
	3.6b (DS21B)	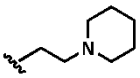	0.19
	3.6c (DS22B)	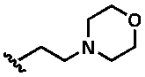	0.24
	3.6d (DS24B)	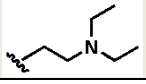	0.17
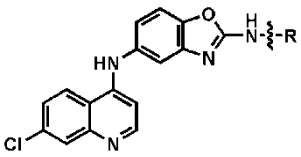	**3.9a (DS4F)**		0.07
	3.9b (DS23B)	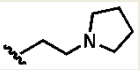	0.00
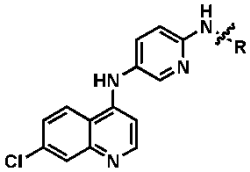	**3.4a (DS26B)**	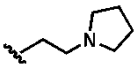	0.10
	3.4b (DS27B)	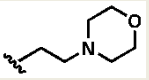	0.33
Amodiaquine			0.22

The results of the GSH trapping results showed the benzothiazole compounds to have the highest bioactivation potential. The highest GSH ratio, 1.13, was seen for the morpholine compound **3.2e**, indicating that this compound could be more reactive than clozapine itself. The second and third highest ratios were seen for **3.2d** and **3.2a**, respectively. In this series of compounds, **3.2c** had the lowest bioactivation potential

(GSH ratio 0.39). Thus all the compounds had a GSH ratio greater than that of amodiaquine, with the least reactive compound having a GSH ratio 1.8 times that of the amodiaquine. Among the remaining three series of compounds, **3.6a** and **3.4b** had GSH ratios 2.5 and 1.5 times that of amodiaquine, respectively. The rest of the compounds had GSH ratios equal to or less than amodiaquine. The least reactive compounds were the benzoxazole analogues of which **3.9a** had a low ratio of 0.07 while no adducts were detected for **3.9b**.

The HSAB (Hard Soft Acid Base) theory states that a hard electrophile will have increased reactivity towards hard nucleophiles and decreased reactivity towards soft nucleophiles and, conversely, a soft electrophile will have increased reactivity towards soft nucleophiles and decreased reactivity towards hard nucleophiles [13]. Glutathione contains a free sulfhydryl group that is classified as a soft nucleophile because the large atomic radius of the sulfur atom results in highly polarized valence electrons [14]. As such, glutathione will preferentially react with soft electrophiles including quinones, quinone imines, iminoquinone methides, epoxides, arene oxides and nitrenium ions [15]. Considering the chemical structures of the four series of compounds, the most probable reactive species that would trap glutathione are imine or quinone-like metabolites as illustrated in Figure 3.3.

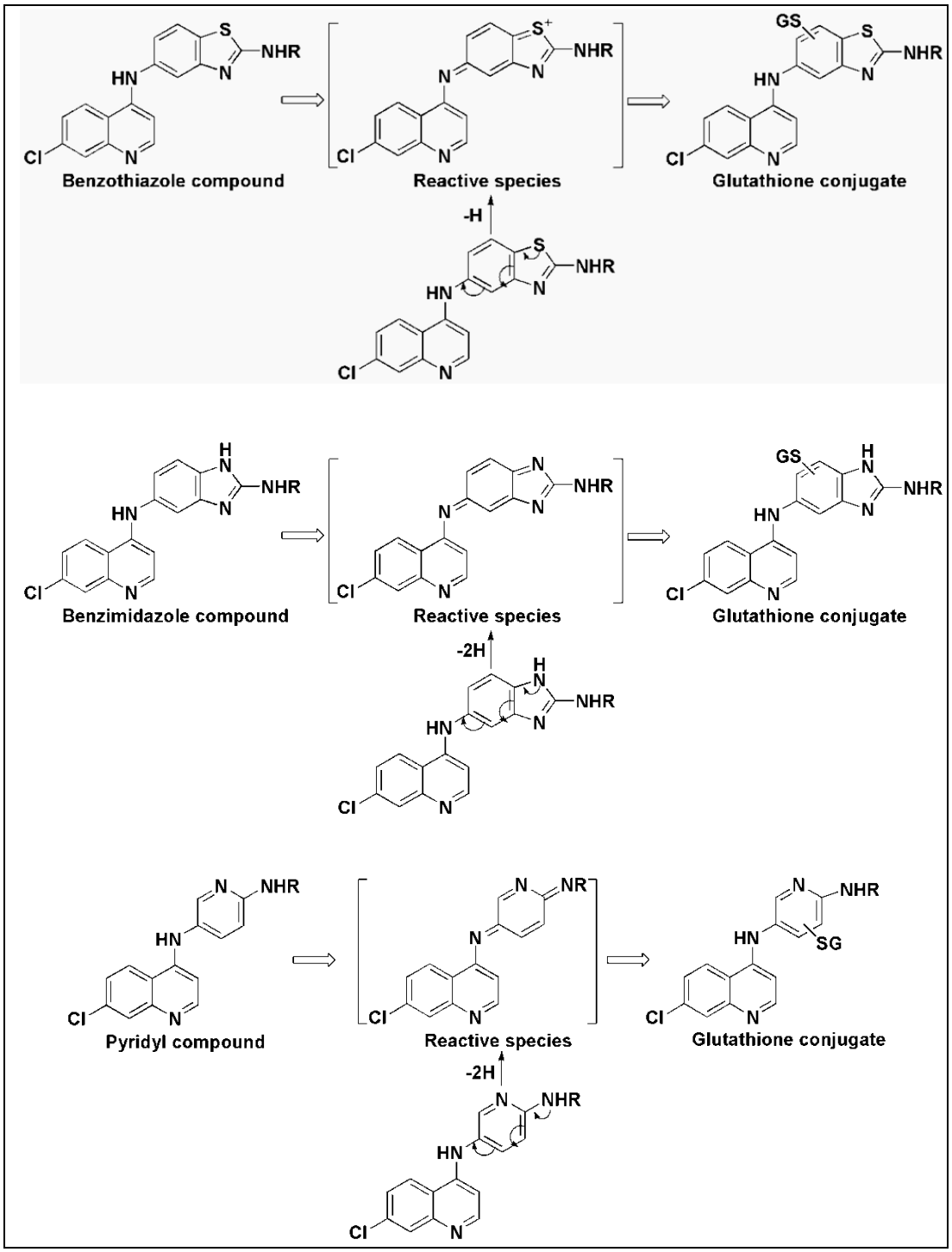

Figure 3.3: Proposed bioactivation of the pyridyl and benzazole analogues to soft electrophiles and their conjugation with GSH.

We postulate that, in the case of the benzothiazole compounds, the nucleophilic sulfur atom donates electrons into the ring efficiently to form a quinone-like positively charged reactive intermediate on account of the 1,4-relationship with the 4-amino group on the

quinoline ring. The benzimidazole and pyridyl compounds have two *para* nitrogen atoms which form the reactive quinone diimine metabolite. Evidence of this reactive metabolite is available in the literature [16]. The main biliary metabolite of the antileukemic drug amsacrine in rats was found to be the glutathione conjugate which was postulated to arise from reaction with amsacrine quinone diimine (Figure 3.4) [16]. Subsequent synthesis of the quinone diimine, which could not be detected in cellular matrix, demonstrated the high reactivity of this metabolite towards nucleophiles and thus confirmed the initial hypothesis [17]. Mitoxantrone, a drug used in the management of advanced breast cancer and acute leukemia, has also been shown to form glutathione conjugates following its metabolism to a metabolite containing a quinone dimine (Figure 3.5), whose structure has been confirmed using microsomal and electrochemical oxidation methods [18,19].

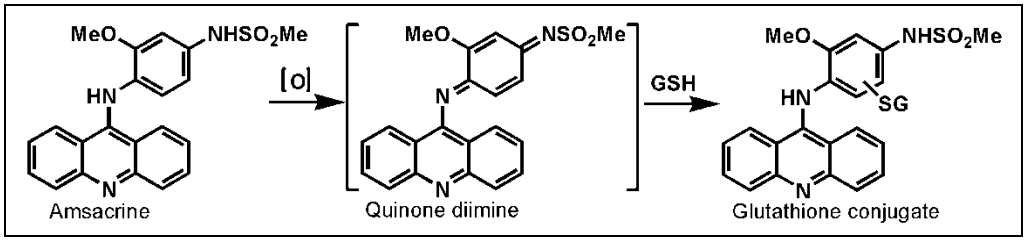

Figure 3.4: Bioactivation of amsacrine

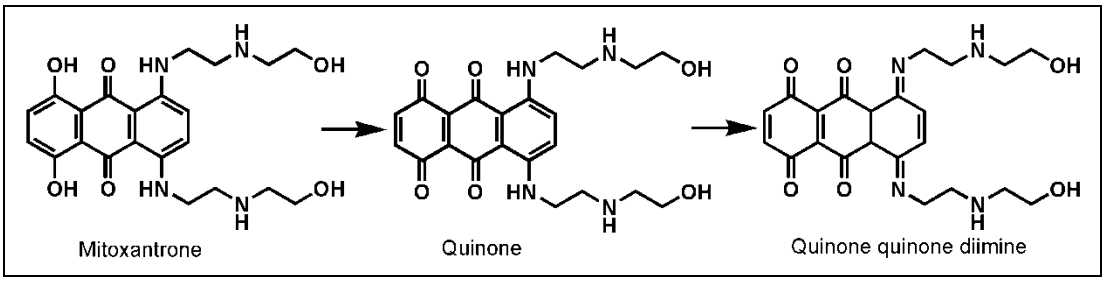

Figure 3.5: Bioactivation of mitoxantrone

It appears that in the benzoxazole series, despite the *para* position of the oxygen atom relative to the 4-aminoquinoline nitrogen, the high electronegativity, and hence reduced nuceophilicity, of oxygen makes the formation of a quinone imine reactive species less

likely. As expected, amodiaquine was confirmed to form glutathione conjugates in this study. The variations in the glutathione ratios appear significant, especially among the benzothiazole analogues as well as between the ethyl and the other analogues in the benzimidazole series. This may imply that the side chains have a role to play in influencing the overall reactivity of the benzazole nucleus.

3.2.2 Trapping with cyanide and methoxylamine

Table 3.2: Potassium cyanide and methoxyalmine trapping experiment results

General structure	CODE	R	KCN adduct?	Methoxylamine adduct?
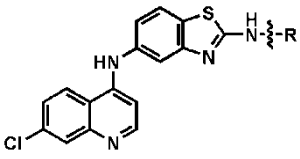	**3.2a (DS1F)**		No	No
	3.2c (DS11B)	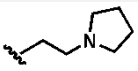	Yes	Yes
	3.2d (DS12B)	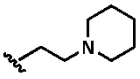	Yes	Yes
	3.2e (DS13B)	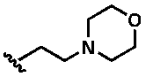	Yes	Yes
	3.2f (DS18B)	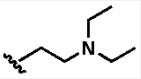	Yes	Yes
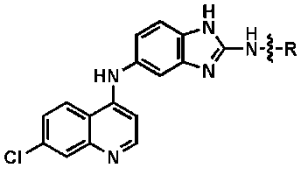	**3.6a (DS5G)**		No	No
	3.6b (DS21B)	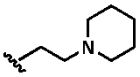	No	Yes
	3.6c (DS22B)	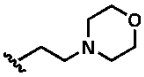	Yes	Yes
	3.6d (DS24B)	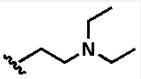	Yes	Yes
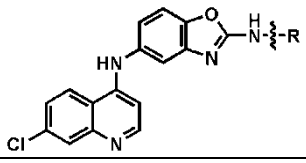	**3.9a (DS4F)**		No	No
	3.9b (DS23B)	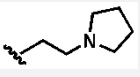	Yes	Yes
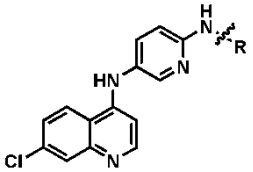	**3.4a (DS26B)**	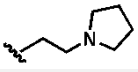	Yes	Yes
	3.4b (DS27B)	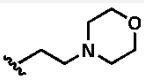	Yes	Yes
Amodiaquine			No	Yes

The most obvious observation in the results from the cyanide and methoxylamine trapping experiments was the fact that analogues bearing ethyl (**3.9a** and **3.6a**) or *tert*-butyl (**3.2a**) did not form adducts with the two trapping agents. The rest of the molecules formed adducts with both trapping agents except for benzimidazole analogue **3.6b** and amodiaquine which did not form adducts with potassium cyanide, or whose adducts were not detected under the experimental conditions. The two observations were consistent regardless of the nature of the aromatic ring system. It follows, therefore, that the observed trapping was purely dependent on the nature of the side chain, and that only molecules with a tertiary protonatable amine on the side chain could form reactive species capable of reacting with potassium cyanide and methoxylamine.

Trapping with methoxylamine and potassium cyanide is commonly used in the detection of hard nucelophiles, specifically the highly reactive iminium and aldehyde metabolites [20,21]. The bioactivation of cyclic and aliphatic tertiary amines to iminium and aldehyde metabolites is a well established metabolic pathway [22]. Figure 3.6, using piperidine as an example, illustrates the formation and trapping of the iminium and aldehyde metabolites. It can, therefore, be concluded that the bioactivation of compounds bearing a tertiary amine is an unavoidable outcome. As mentioned in earlier chapters, the presence of a tertiary amine in the side chain of aminoquinoline antimalarials enhances vacuolar trapping in the parasite and is essential for enhanced potency. There is thus an overlap between the pharmacophore and toxicophore. This makes it difficult to design out this part of the molecule without affecting activity, as the antiplasmodial results will later confirm.

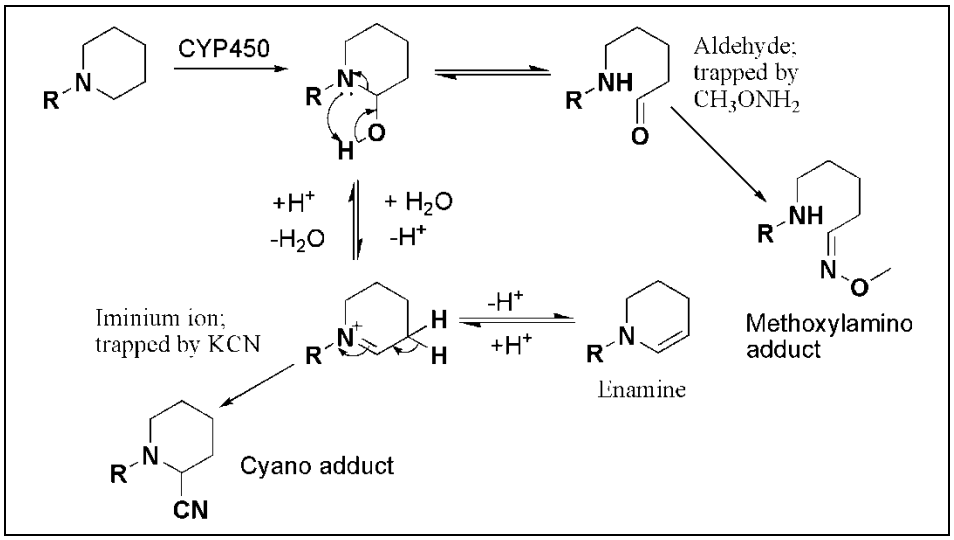

Figure 3.6: Bioactivation of piperidinyl compounds

3.2.3 CYP inhibition assays

The CYP inhibition assay results for four CYP isoforms are graphically presented in figures 3.7 to 3.10. The CYP2C19 assay did not give conclusive results even after repeated testing, probably due to background fluorescence interference.

3.2.3.1 CYP3A4 inhibition

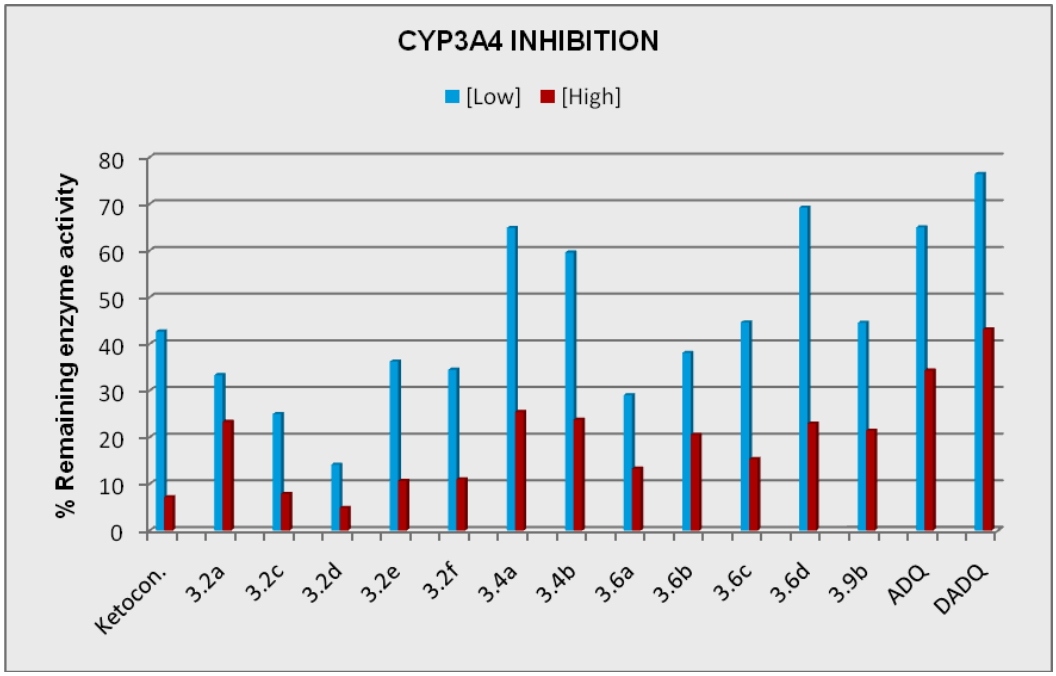

Figure 3.7: Results for the CYP3A4 inhibition assay. [Low] = 3 µM and [High] =20 µM. Ketocon= ketoconazole, ADQ = Amodiaquine, DADQ = Desethylamodiaquine.

Potent CYP3A4 inhibition was observed for all the compounds tested (Figure 3.7). In general, the analogues inhibited CYP3A4 more potently than amodiaquine and desethylamodiaquine (except for **3.6d**, a benzimidazole analogue, and **3.4a**, a pyridyl analogue). At 20 μM, **3.6d**, **3.4a** and **3.4b** inhibited the enzyme to the same extent as amodiaquine. At both concentrations, the benzothiazole analogues with a tertiary amine side chain (**3.2c**, **3.2d**, **3.2e** and **3.2f**) were the most potent inhibitors of the enzyme. **3.2d**, the piperidine benzothiazole analogue, was the most potent CYP3A4 inhibitor of all the compounds tested with only 14.1 % and 4.9 % remaining enzymatic activity at 3 μM and 20 μM, respectively. In the benzimidazole class, **3.6a** with a simple ethyl side chain was comparable to the benzimidazole morpholino analogue **3.6c** in its inhibition of the enzyme at 20 μM. Interestingly, the other two benzimidazole analogues **3.6b** and **3.6d** had virtually the same level of % remaining enzymatic activity at 20 μM as well. The pyridine analogs **3.4a** and **3.4b** were among the weakest inhibitors of all the compounds tested, along with **3.6d**, at both concentrations. The benzoxazole analogue **3.9b**, with 21.4% remaining enzyme activity, was one of only five compounds that had >20% remaining enzyme activity at 20 μM.

3.2.3.2 CYP2D6 inhibition

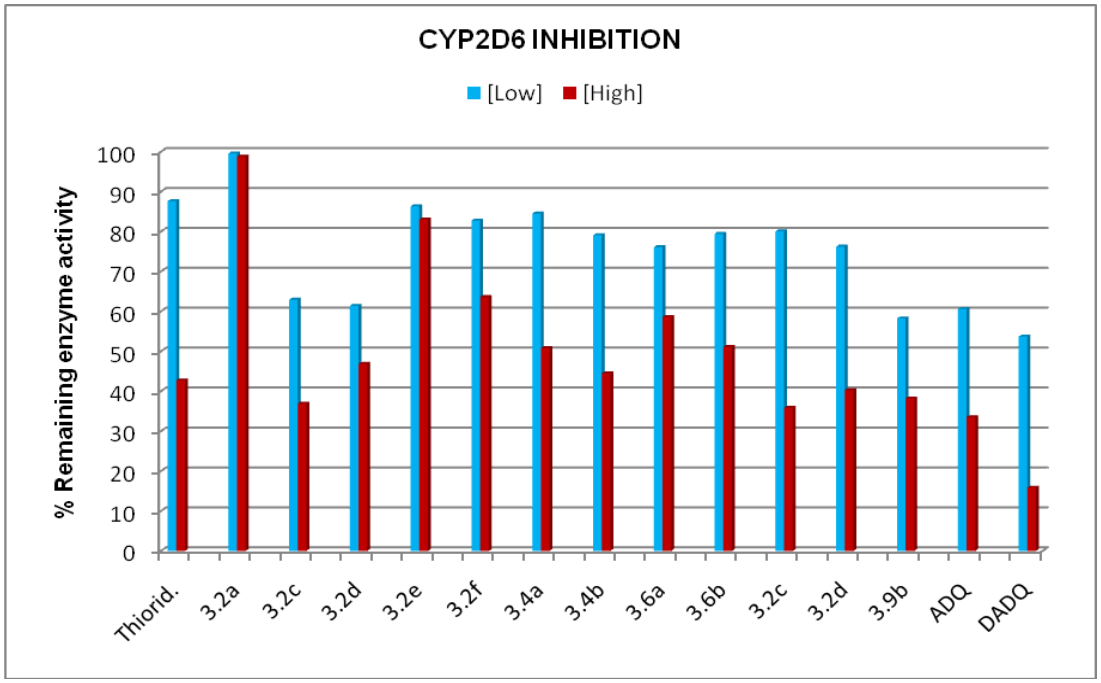

Figure 3.8: Results for the CYP2D6 inhibition assay. [Low] = 3 μM and [High] =20 μM. Thiorid = Thioridazine, ADQ = Amodiaquine, DADQ = Desethylamodiaquine.

All analogues were less potent than amodiaquine as CYP2D6 inhibitors (Figure 3.8). The benzothiazole analogues **3.2a** and **3.2e** were very weak CYP2D6 inhibitors with >80 % remaining enzyme activity at both concentrations. Less than 40 % remaining enzyme activity was seen for **3.2c** (benzothiazole analogue), **3.6c**, **3.6d** (benzimidazole analogues) and **3.9b** (benzoxazole analogue) at 20 μM. However, all the compounds had a level of enzyme activity at this concentration greater than the 33.5 % seen with amodiaquine. Desethylamodiaquine was found to be a more potent inhibitor of CYP2D6 than amodiaquine, in agreement with the literature [23].

3.2.3.3 CYP2C9 inhibition

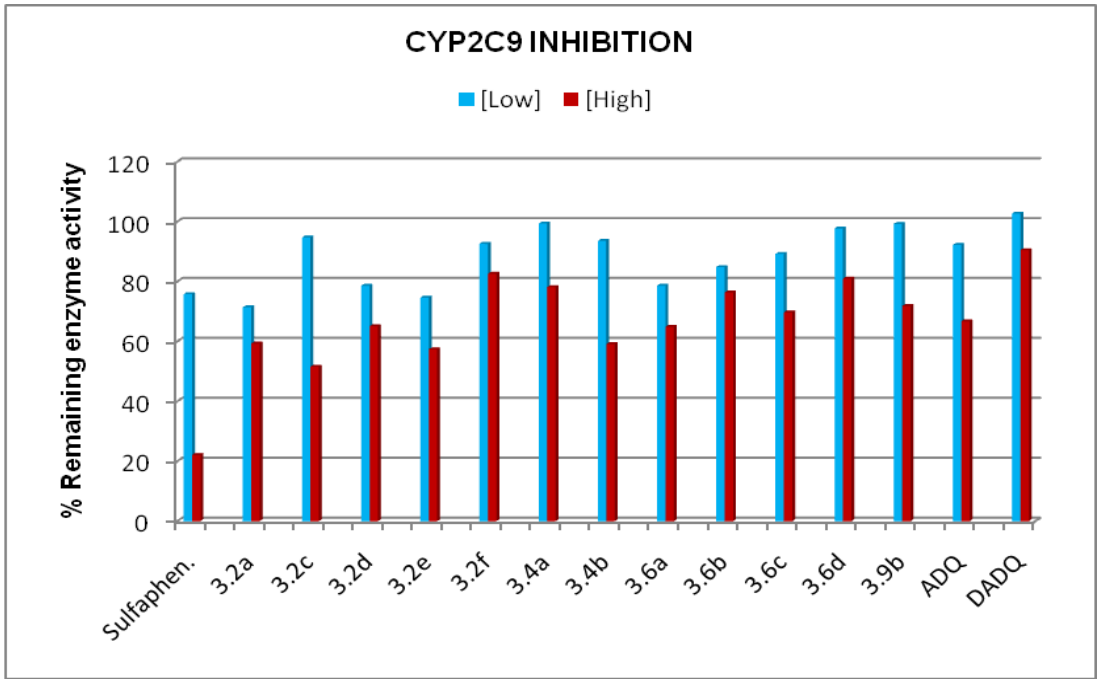

Figure 3.9: Results for the CYP2C9 inhibition assay. [Low] = 3 µM and [High] =20 µM. Sulfaphen = Sulfaphenazole, ADQ = Amodiaquine, DADQ = Desethylamodiaquine.

From Figure 3.9, it can be seen that **3.2a**, **3.2c**, **3.2e** (benzothiazole analogues) and **3.4b** (a pyridine analogue) inhibited CYP2C9 marginally more potently than amodiaquine at 20 µM. Only **3.2a**, **3.2d** and **3.2e** (benzothiazole analogues) and **3.6a** (a benzimidazole analogue) resulted in >20% inhibition of the enzyme at 3 µM. However, the inhibition remained less than 50 % at both 3 and 20 µM. Thus all the compounds tested were considered weak inhibitors of CYP2C9, especially when compared to the positive control inhibitor sulfaphenazole.

3.2.3.4 CYP1A2 inhibition

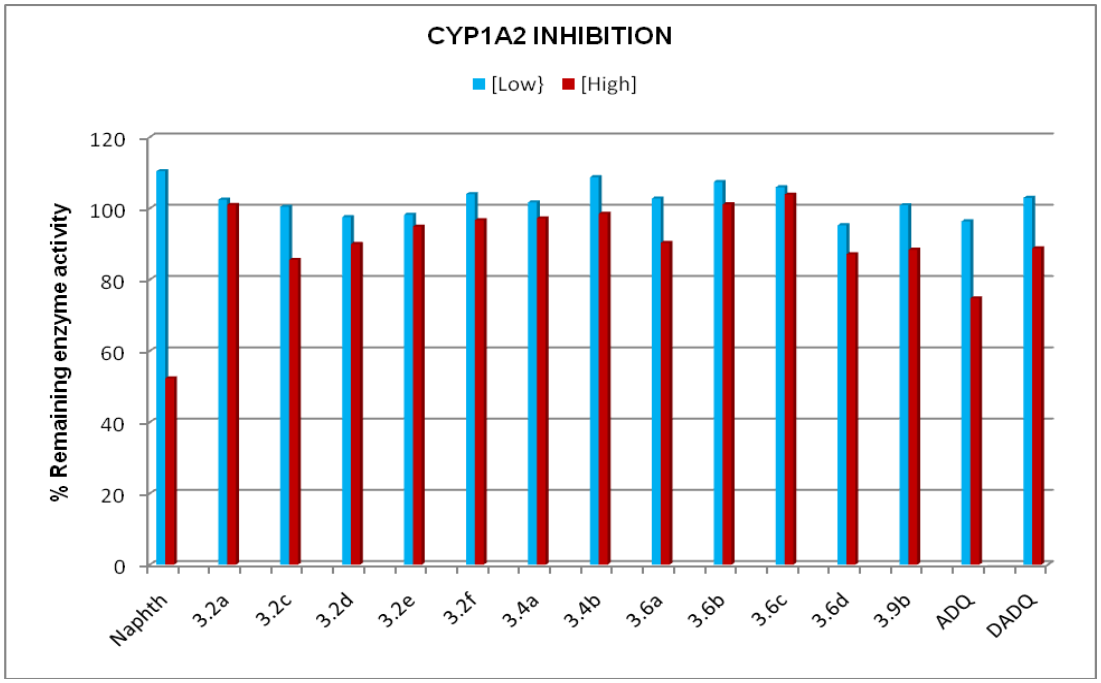

Figure 3.10: Results for the CYP1A2 inhibition assay. [Low] = 3 μM and [High] =20 μM. Naphth = α-naphthoflavone, ADQ = Amodiaquine, DADQ = Desethylamodiaquine.

None of the compounds tested inhibited CYP1A2 by >15% even at 20 μM, except amodiaquine which had 74.8% remaining activity at that concentration. This led to the conclusion that all the analogues tested were not CYP1A2 inhibitors.

3.2.4 Time-dependent inhibition results

From the foregoing results, the analogues tested were potent inhibitors of CYP3A4 and the time-dependent inhibition TDI) assay was thus carried out using this enzyme. The results obtained are graphically presented in Figure 3.11. In interpreting these results, we used the criteria set by Thelingwani et al. [10] whereby a normalized ratio <0.7 was taken to indicate MBI, a ratio between 0.7 and 0.9 was considered to be indeterminate while a ratio >0.9 implied lack of MBI.

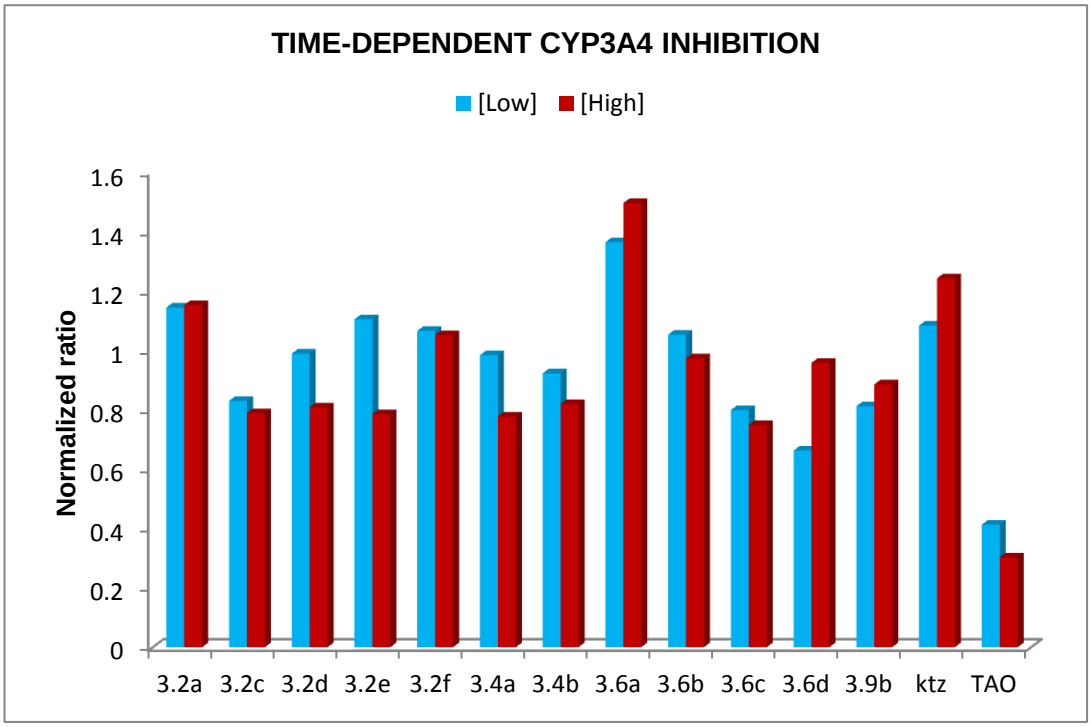

Figure 3.11: Results for the CYP3A4 time dependent inhibition assay. [Low] = 2 μM and [High] =10 μM. Ktz ketoconazole, TAO = troleandomycin.

The results showed that none of the analogues tested were mechanism-based inhibitors of CYP3A4. There is a clear distinction between the ratios seen for the positive control troleandomycin and those seen for the test compounds at both the high and low concentrations. Although the normalized ratio for **3.6d** at 2 μM fell below 0.7, the concentration-dependent nature of MBI was absent since at the high concentration, the ratio is greater than 0.9. At 10 μM, the normalized ratios for **3.2c**, **3.2d**, **3.2e**, **3.4a, 3.4b, 3.6c** and **3.9b** representing compounds from all the four series lay in the indeterminate region. Again, the concentration dependency requirement for MBI was lacking with compound **3.9b**.

3.3 DISCUSSION

Metabolism is one of the most important determinants of the pharmacokinetic disposition of a drug [24]. The liver is the primary site of drug metabolism, with cytochrome P450 enzymes being responsible for over 90 % of drug metabolism [25]. Identification of enzymes responsible for the metabolism of a test compound is, therefore, important in understanding the compounds' clearance mechanisms. Drug-drug interactions at metabolic level, particularly those involving CYP inhibition, have also been shown to result in undesirable adverse drug reactions [26–28]. Competitive and non-competitive inhibition have been shown to be the most common mechanisms of CYP inhibition [29]. There are also a significant number of compounds that have been shown to cause time-dependent inhibition which usually involves the generation of a reactive metabolite which reacts covalently with the enzyme, thus irreversibly inactivating it (mechanism based inhibition – MBI) or binding strongly to the heme in a quasi-irreversible manner (metabolite intermediate complex – MIC) [30,31]. Metabolism, inhibition and enzyme crystal structure studies have resulted in extensive knowledge of the active sites of major drug metabolizing enzymes [25,32].

The CYP1A2 active site has been modeled as an approximately rectangular slot composed of several aromatic side chains, including the coplanar rings of Phe181 and Tyr437, which restrict the size and shape of the cavity such that only planar structures (approximately 6 Å in width) are able to occupy the binding site [33]. CYP1A2 substrates /inhibitors are, therefore, generally lipophilic planar polyaromatic/heteroaromatic molecules defined by a small depth and a large area-to-depth ratio [33]. A 3D presentation of the simplest target molecule tested (**3.6a**, Figure 3.12) reveals a lack of planarity due

to the trigonal pyramidal arrangement at the quinolinyl 4-amino group. The resulting increased depth of the molecule may partly explain the lack of CYP1A2 inhibition observed among all the compounds tested.

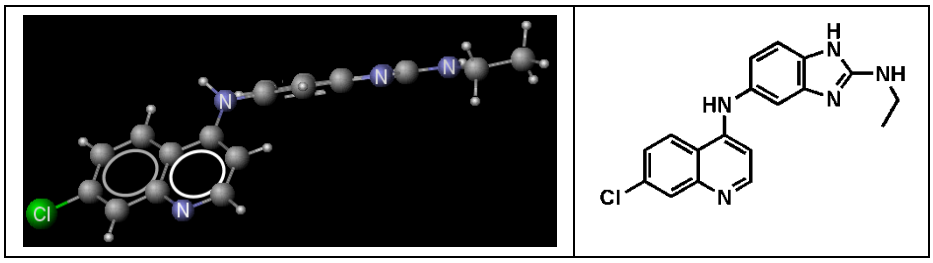

Figure 3.12: 3D view (Marvin Sketch®) of **3.6a** with the benzimidazole ring out of plane with the quinoline ring

A majority of CYP2C9 substrates are acidic and ionized at physiological pH or have a region that can act as a hydrogen bond donor [34]. The weak to moderate inhibition observed with CYP2C9 may be attributed to the lack of these properties in the compounds screened against this enzyme. Our findings that amodiaquine weakly inhibits CYP2C9 are in agreement with those by Wennerholm and coworkers who reported inhibition of CYP2C9-mediated metabolism of losartan by amodiaquine and desethylamodiaquine [35]. The binding and subsequent inhibition of CYP2C9 observed may involve interaction with water molecules at the active site. Such interactions have been reported for compounds like sulfaphenazole and warfarin [33,36].

Typical CYP2D6 substrates are lipophilic bases with a planar hydrophobic aromatic ring, a nitrogen atom which can be protonated at physiological pH and a negative molecular electrostatic potential above the planar part of the molecule [37,38]. It is not surprising then that a number of quinoline compounds such as chloroquine, amodiaquine and its major metabolite, desethylamodiaquine, are known inhibitors of

CYP2D6 [23,39]. This finding was confirmed in our study. The compounds screened were generally found to moderately inhibit CYP2D6, which was expected considering their structural similarity with amodiaquine. Potent CYP2D6 inhibition (up to 77 %) has been reported for chloroquine analogues with an aromatic substituent as one of the groups on the tertiary amine [40]. The researchers found secondary amines to be less potent CYP2D6 inhibitors than secondary amines. In our study, the two secondary amines screened, **3.2a** and **3.6a**, were the weakest inhibitors in their series, namely the benzothiazole and benzimidazole analogues, respectively. Indeed **3.2a** showed virtually no inhibition of the enzyme at both 3 and 20 μM. It can, consequently, be concluded that none of the series of compounds tested were potent CYP2D6 inhibitors to the extent exhibited by amodiaquine and desethylamodiaquine. Amodiaquine has a short half life (5.7-7.9 hours) and acts as a prodrug for desethylamodiaquine which has a much longer half life (7-9 days) [41]. After a single 600 mg dose of amodiaquine, its main metabolite desethylamodiaquine attains high circulating concentrations in blood (maximum concentration 660 mmol/l compared to 47 mmol/l for amodiaquine) [35]. In addition to the high circulating concentrations and long half life, desethylamodiaquine inhibits CYP2D6 by up to 99% and can change an individual's metabolism status from extensive to poor metabolizer status [23]. In the clinical setting, this can lead to high circulating concentrations of CYP2D6 substrate drugs and could result in adverse effects [42,43].

Potent inhibition of CYP3A4 was observed among all the compounds tested, including the antimalarial drug amodiaquine. It is worth noting that the four series of compounds screened meet the requirements for typical CYP3A4 substrates: lipophilic neutral or

basic molecules whose metabolism will primarily involve N-dealkylation [34]. As mentioned earlier in the section on trapping reactions, this metabolic pathway proceeds via reactive intermediates, namely aldehydes and iminium ions. A number of secondary and tertiary amine containing compounds such as diltiazem, N-desmethyl-diltiazem, fluoxetine, nortriptyline, phencyclidine and verapamil are known to be mechanism-based inhibitors of CYP3A4 [5]. Our results, however, showed that the analogues tested did not result in CYP3A4 MBI although the formation of reactive aldehyde and iminium metabolite formation was observed under electrochemical oxidation conditions. Thus there appears to be a difference in outcome between the electrochemical and the biological system. In the latter, the protein matrix and enzyme affinity, among other factors, influence the fate of a substrate. The lack of MBI observed may be attributed to efficient conversion of the reactive metabolic intermediates to less reactive species such as the carboxylic acid or, in the case of the cyclic tertiary amines, some degree of metabolic stability such that dealkylation occurs very slowly. CYP3A4 catalyzes the metabolism of a wide range of drugs [44,45]. Its inhibition is likely to result in elevated blood levels of co-administered drugs that are substrates of the isozyme, leading to toxicity and drug-drug interactions [46,47]. Further thorough investigation of these findings will therefore be necessary for any lead compound arising from this project.

In interpreting these results, it is important to note that CYP3A4 inhibition is substrate dependent, a factor that is attributed to the possible existence of more than one substrate binding pocket or the ability of the enzyme to exist in multiple conformations [48]. To get a more conclusive picture, the need to carry out the assay using multiple substrates has been recommended [8,48]. Furthermore, the fluorescence-based CYP

inhibition assay relies on substrates that are not exactly drug-like. Consequently, the pharmaceutical industry is switching to assays that employ drug substrates such as midazolam and testosterone which tend to be more specific for CYP3A4, as well as LC/MS analysis [49]. For rapid screening in early drug development, however, fluorescence-based assays are an affordable and readily accessible tool for the medicinal chemist [50].

3.4 CONCLUSION

The methoxylamine and cyanide trapping experiments revealed the potential for formation of reactive aldehyde and iminium intermediates by all tertiary nitrogen containing compounds, regardless of their series. The overall conclusion of the CYP inhibition assays was that benzothiazole analogues had the greatest inhibition potential of all the four series. Thus these two assays could not be used to select the safest series but gave useful information on which series to drop. Glutathione trapping results clearly revealed that the benzoxazole series has the least potential for formation of soft electrophilic metabolites. In light of these findings, the benzoxazole series was selected for further SAR expansion.

REFERENCES

(1) Guengerich, F. P. Cytochrome P450s and other enzymes in drug metabolism and toxicity. *AAPS. J.* **2006**, *8*, E101–11.

(2) Johansson, T.; Weidolf, L.; Jurva, U. Mimicry of phase I drug metabolism--novel methods for metabolite characterization and synthesis. *Rapid. Commun. Mass. Spectrom.* **2007**, *21*, 2323–31.

(3) Ma, S.; Subramanian, R. Detecting and characterizing reactive metabolites by liquid chromatography/tandem mass spectrometry. *J. Mass. Spectrom.* **2006**, *41*, 1121–39.

(4) Park, B. K.; Boobis, A.; Clarke, S.; Goldring, C. E. P.; Jones, D.; Kenna, J. G.; Lambert, C.; Laverty, H. G.; Naisbitt, D. J.; Nelson, S.; Nicoll-Griffith, D. a; Obach, R. S.; Routledge, P.; Smith, D. a; Tweedie, D. J.; Vermeulen, N.; Williams, D. P.; Wilson, I. D.; Baillie, T. a Managing the challenge of chemically reactive metabolites in drug development. *Nat. Rev. Drug Discov.* **2011**, *10*, 292–306.

(5) Fontana, E.; Dansette, P. M.; Poli, S. M. Cytochrome p450 enzymes mechanism based inhibitors: common sub-structures and reactivity. *Curr. Drug Metab.* **2005**, *6*, 413–54.

(6) Evans, W. E. Pharmacogenomics: Translating Functional Genomics into Rational Therapeutics. *Science* **1999**, *286*, 487–491.

(7) Mali'n, T. J. Electrochemical and Enzymatic In Vitro Studies on Reactive Drug Metabolites, University of Gothenburg, 2010, pp. 1–64.

(8) Crespi, C. L.; Stresser, D. M. Fluorometric screening for metabolism-based drug--drug interactions. *J. Pharmacol. Toxicol. Methods.* **2001**, *44*, 325–31.

(9) Wójcikowski, J.; Maurel, P.; Daniel, W. A. Characterization of human cytochrome p450 enzymes involved in the metabolism of the piperidine-type phenothiazine neuroleptic thioridazine. *Drug Metab. Dispos.* **2006**, *34*, 471–6.

(10) Thelingwani, R. S.; Zvada, S. P.; Dolgos, H.; Ungell, A. B.; Masimirembwa, C. M. In vitro and in silico identification and characterization of thiabendazole as a mechanism-based inhibitor of CYP1A2 and simulation of possible pharmacokinetic drug-drug interactions. *Drug Metab. Dispos.* **2009**, *37*, 1286–94.

(11) McGinnity, D. F.; Berry, A. J.; Kenny, J. R.; Grime, K.; Riley, R. J. Evaluation of time-dependent cytochrome P450 inhibition using cultured human hepatocytes. *Drug Metab. Dispos.* **2006**, *34*, 1291–300.

(12) Park, B. K.; Naisbitt, D. J.; Gordon, S. F.; Kitteringham, N. R.; Pirmohamed, M. Metabolic activation in drug allergies. *Toxicology* **2001**, *158*, 11–23.

(13) Meschkat, E.; Barratt, M. D.; Lepoittevin, J. Studies of the chemical selectivity of hapten, reactivity, and skin sensitization potency. 2. nmr studies of the covalent binding of the ^{13}C-labeled skin sensitizers 2-[^{13}C]- and 3-[^{13}C]hex-1-ene- and 3-[^{13}C]hexane-1,3-sultones to human serum albumin. *Chem. Res. Toxicol.* **2001**, *14*, 118–26.

(14) LoPachin, R. M.; Barber, D. S.; Gavin, T. Molecular mechanisms of the conjugated alpha,beta-unsaturated carbonyl derivatives: relevance to neurotoxicity and neurodegenerative diseases. *Toxicol. Sci.* **2008**, *104*, 235–49.

(15) Yan, Z.; Maher, N.; Torres, R.; Huebert, N. Use of a trapping agent for simultaneous capturing and high-throughput screening of both “soft” and “hard” reactive metabolites. *Anal. Chem.* **2007**, *79*, 4206–14.

(16) Lee, H. H.; Palmer, B. D.; Denny, W. A. Reactivity of quinone imine and quinone diimine metabolites of the antitumor drug amsacrine and related compounds to nucleophiles. *J. Org. Chem.* **1988**, *53*, 6042–6047.

(17) Clark, G. R.; Robinson, K.; Denny, W. a.; Lee, H. H. Structures of quinone imine metabolites related to the anti-cancer drug amsacrine. *Acta Crystallogr. B* **1993**, *49*, 342–347.

(18) Duthie, S. J.; Grant, M. H. The role of reductive and oxidative metabolism in the toxicity of mitoxantrone, adriamycin and menadione in human liver derived Hep G2 hepatoma cells. *Br. J. Cancer* **1989**, *60*, 566–71.

(19) Lohmann, W.; Karst, U. Generation and identification of reactive metabolites by electrochemistry and immobilized enzymes coupled on-line to liquid chromatography/mass spectrometry. *Anal. Chem.* **2007**, *79*, 6831–9.

(20) Johansson, T.; Jurva, U.; Grönberg, G.; Weidolf, L.; Masimirembwa, C. Novel metabolites of amodiaquine formed by CYP1A1 and CYP1B1: structure elucidation using electrochemistry, mass spectrometry, and NMR. *Drug Metab. Dispos.* **2009**, *37*, 571–9.

(21) Argoti, D.; Liang, L.; Conteh, A.; Chen, L.; Bershas, D.; Yu, C.-P.; Vouros, P.; Yang, E. Cyanide trapping of iminium ion reactive intermediates followed by detection and structure identification using liquid chromatography-tandem mass spectrometry (LC-MS/MS). *Chem. Res. Toxicol.* **2005**, *18*, 1537–44.

(22) Kalgutkar, A. S.; Dalvie, D. K.; O'Donnell, J. P.; Taylor, T. J.; Sahakian, D. C. On the diversity of oxidative bioactivation reactions on nitrogen-containing xenobiotics. *Curr. Drug Metab.* **2002**, *3*, 379–424.

(23) Bapiro, T. E.; Egnell, A. C.; Hasler, J. A.; Masimirembwa, C. M. Application of higher throughput screening (HTS) inhibition assays to evaluate the interaction of antiparasitic drugs with cytochrome P450s. *Drug Metab. Dispos.* **2001**, *29*, 30–5.

(24) Kumar, G. N.; Surapaneni, S. Role of drug metabolism in drug discovery and development. *Med. Res. Rev.* **2001**, *21*, 397–411.

(25) Sun, H.; Scott, D. O. Structure-based drug metabolism predictions for drug design. *Chem. Biol. Drug Des.* **2010**, *75*, 3–17.

(26) Obach, R. S.; Walsky, R. L.; Venkatakrishnan, K. Mechanism-based inactivation of human cytochrome p450 enzymes and the prediction of drug-drug interactions. *Drug Metab. Dispos.* **2007**, *35*, 246–55.

(27) Brown, H. S.; Galetin, A.; Hallifax, D.; Houston, J. B. Prediction of in vivo drug-drug interactions from in vitro data : factors affecting prototypic drug-drug interactions involving CYP2C9, CYP2D6 and CYP3A4. *Clin. Pharmacokinet.* **2006**, *45*, 1035–50.

(28) Wienkers, L. C.; Heath, T. G. Predicting in vivo drug interactions from in vitro drug discovery data. *Nat. Rev. Drug Discov.* **2005**, *4*, 825–33.

(29) Fowler, S.; Zhang, H. In vitro evaluation of reversible and irreversible cytochrome P450 inhibition: current status on methodologies and their utility for predicting drug-drug interactions. *AAPS. J.* **2008**, *10*, 410–24.

(30) Zhang, Z.-Y.; Wong, Y. N. Enzyme kinetics for clinically relevant CYP inhibition. *Curr. Drug Metab.* **2005**, *6*, 241–57.

(31) Taxak, N.; Desai, P. V; Patel, B.; Mohutsky, M.; Klimkowski, V. J.; Gombar, V.; Bharatam, P. V Metabolic-intermediate complex formation with cytochrome P450:

theoretical studies in elucidating the reaction pathway for the generation of reactive nitroso intermediate. *J. Comput. Chem.* **2012**, *33*, 1740–7.

(32) Denisov, I. G.; Makris, T. M.; Sligar, S. G.; Schlichting, I. Structure and chemistry of cytochrome P450. *Chem. Rev.* **2005**, *105*, 2253–77.

(33) Smith, D. a.; Ackland, M. J.; Jones, B. C. Properties of cytochrome P450 isoenzymes and their substrates Part 1: active site characteristics. *Drug Discov. Today* **1997**, *2*, 406–414.

(34) Smith, D. A.; Ackland, M. J.; Jones, B. C. Properties of cytochrome P450 isoenzymes and their substrates part 2: properties of cytochrome P450 substrates. *Drug Discov. Today* **1997**, *2*, 479–486.

(35) Wennerholm, A.; Nordmark, A.; Pihlsgård, M.; Mahindi, M.; Bertilsson, L.; Gustafsson, L. L. Amodiaquine, its desethylated metabolite, or both, inhibit the metabolism of debrisoquine (CYP2D6) and losartan (CYP2C9) in vivo. *Eur. J. Clin. Pharmacol.* **2006**, *62*, 539–46.

(36) Rao, S.; Aoyama, R.; Schrag, M.; Trager, W. F.; Rettie, a; Jones, J. P. A refined 3-dimensional QSAR of cytochrome P450 2C9: computational predictions of drug interactions. *J. Med. Chem.* **2000**, *43*, 2789–96.

(37) Zhou, S.-F.; Liu, J.-P.; Lai, X.-S. Substrate specificity, inhibitors and regulation of human cytochrome P450 2D6 and implications in drug development. *Curr. Med. Chem.* **2009**, *16*, 2661–805.

(38) De Groot, M. J.; Wakenhut, F.; Whitlock, G.; Hyland, R. Understanding CYP2D6 interactions. *Drug Discov. Today* **2009**, *14*, 964–72.

(39) Projean, D.; Baune, B.; Farinotti, R.; Flinois, J.; Beaune, P.; Taburet, A.; Ducharme, J. In vitro metabolism of chloroquine: identification of CYP2C8, CYP3A4, and CYP2D6 as the main isoforms catalyzing N-desethylchloroquine formation. *Drug Metab. Dispos.* **2003**, *31*, 748–54.

(40) Ray, S.; Madrid, P. B.; Catz, P.; LeValley, S. E.; Furniss, M. J.; Rausch, L. L.; Guy, R. K.; DeRisi, J. L.; Iyer, L. V; Green, C. E.; Mirsalis, J. C. Development of a new generation of 4-aminoquinoline antimalarial compounds using predictive pharmacokinetic and toxicology models. *J. Med. Chem.* **2010**, *53*, 3685–95.

(41) Adjei, G. O.; Kudzi, W.; Dodoo, A.; Kurtzhals, J. a. L. Artesunate plus amodiaquine combination therapy: reviewing the evidence. *Drug Dev. Res.* **2009**, *43*, 33–43.

(42) Brockmöller, J.; Kirchheiner, J.; Schmider, J.; Walter, S.; Sachse, C.; Müller-Oerlinghausen, B.; Roots, I. The impact of the CYP2D6 polymorphism on haloperidol pharmacokinetics and on the outcome of haloperidol treatment. *Clin. Pharmacol. Ther.* **2002**, *72*, 438–52.

(43) Shams, M. E. E.; Arneth, B.; Hiemke, C.; Dragicevic, a; Müller, M. J.; Kaiser, R.; Lackner, K.; Härtter, S. CYP2D6 polymorphism and clinical effect of the antidepressant venlafaxine. *J. Clin. Pharm. Ther.* **2006**, *31*, 493–502.

(44) Uno, Y.; Matsushita, A.; Osada, N.; Uehara, S.; Kohara, S.; Nagata, R.; Fukuzaki, K.; Utoh, M.; Murayama, N.; Yamazaki, H. Genetic variants of CYP3A4 and CYP3A5 in cynomolgus and rhesus macaques. *Drug Metab. Dispos.* **2010**, *38*, 209–14.

(45) Sun, H.; Bessire, A. J.; Vaz, A. Dirlotapide as a model substrate to refine structure-based drug design strategies on CYP3A4-catalyzed metabolism. *Bioorg. Med. Chem. Lett.* **2012**, *22*, 371–6.

(46) Chow, H.-H. S.; Garland, L. L.; Hsu, C.-H.; Vining, D. R.; Chew, W. M.; Miller, J. a; Perloff, M.; Crowell, J. a; Alberts, D. S. Resveratrol modulates drug- and carcinogen-metabolizing enzymes in a healthy volunteer study. *Cancer Prev. Res. (Phila).* **2010**, *3*, 1168–75.

(47) Hamon, V.; Horvath, D.; Gaudin, C.; Desrivot, J.; Junges, C.; Arrault, A.; Bertrand, M.; Vayer, P. QSAR Modelling of CYP3A4 Inhibition as a Screening Tool in the Context of Drug-Drug Interaction Studies. *Mol. Inform.* **2012**, *31*, 669–677.

(48) Ekins, S.; Stresser, D. M.; Andrew Williams, J. In vitro and pharmacophore insights into CYP3A enzymes. *Trends Pharmacol. Sci.* **2003**, *24*, 161–166.

(49) Lin, T.; Pan, K.; Mordenti, J.; Pan, L. In vitro assessment of cytochrome P450 inhibition: strategies for increasing LC/MS-based assay throughput using a one-point IC(50) method and multiplexing high-performance liquid chromatography. *J. Pharm. Sci.* **2007**, *96*, 2485–93.

(50) Yan, Z.; Rafferty, B.; Caldwell, G. W.; Masucci, J. a Rapidly distinguishing reversible and irreversible CYP450 inhibitors by using fluorometric kinetic analyses. *Eur. J. Drug Metab. Pharmacokinet.* **2002**, *27*, 281–7.

Chapter 4

EVALUATION OF PHYSICOCHEMICAL PROPERTIES, METABOLIC STABILITY AND ANTIPLASMODIAL ACTIVITY OF AMODIAQUINE ANALOGUES

4.1 CHAPTER OVERVIEW

This Chapter starts with an evaluation of the physicochemical properties of all the analogues synthesized in the project for their 'drug-likeness', specifically those properties that are predictive of good oral bioavailability. Results for antiplasmodial and cytotoxicity studies are then presented and discussed. Subsequently, mechanistic investigation of the benzoxazole analogues, based on the known mode of action of amodiaquine, is discussed. This is followed by *in vitro* metabolic stability evaluation of selected analogues and *in vivo* efficacy studies in *Plasmodium berghei* infected mice.

4.2 PHYSICOCHEMICAL PROPERTIES

4.2.1 Introduction and rationale

One of the underlying objectives of medicinal chemistry research is to discover new chemical entities which have similarities with existing drugs with respect to key physicochemical and biological properties (drug-like properties) with the understanding that such properties may help achieve good pharmacokinetic and pharmacodynamic properties [1]. Several computational approaches exist that enable the prediction of various physicochemical properties of complex organic molecules from their molecular structures without the need of any experimentally derived parameters [2]. Lipinski and co-workers were the first researchers to identify and then to list, in a formalized and simplified form, the molecular properties that contribute most to drug-likeness, based on

disposition criteria [3,4]. Since molecular properties can be estimated from computational molecular descriptors, Lipinski et al. postulated that computational methods in the early discovery setting could deal with large numbers of compounds and serve as filters to direct chemistry SAR towards compounds with greater probability of oral activity [4]. Currently, the chemical space can be navigated using a large number of physicochemical descriptors, with Volsurf+® for example using as many as 56 descriptors [5]. However, Lipinski's 'rule of 5' remains a useful guide in the design of molecules intended for oral administration [4]. The 'rule of 5' states that for good oral absorption and permeation (for compound classes that are not substrates for biological transporters) a compound should not have >5 H-bond donors (expressed as the sum of OHs and NHs), molecular weight >500, ClogP >5 (or MLogP >4.15) and >10 H-bond acceptors (expressed as the sum of Ns and Os) [4]. Veber and coworkers found the use of the rotatable bond count in conjunction with the polar surface area to give an effective rule for prediction of oral bioavailability [6]. According to the researchers, molecules with > 10 rotatable bonds generally had poor oral bioavailability [6]. Furthermore, the researchers observed that reduced polar surface area (PSA) correlated better with increased permeation rate than did lipophilicity (cLogP) [6]. Elsewhere, Palm and coworkers noted that the molecular descriptor PSA, which is related to the hydrogen-bonding capacity, was a good predictor of intestinal epithelial permeability [7]. Assessment of drug-likeness, therefore, includes the 'rule of 5' properties as well as rotatable bond count and PSA, among other properties [8]. In general, compounds that violate no more than one of Lipinski's guidelines, have less than 10 rotatable bonds and a PSA < 160 $Å^2$ are more likely to be orally bioavailable [9]. It is worth mentioning that

more and more drugs approved since 2002 are moving away from the traditional drug space making the application of semi-empirical rules derived from knowledge accumulated from historic, older molecules not necessarily valid [5].

The target molecules included in this project were assessed for drug-likeness using the 'rule of 5' properties as well as rotatable bond count and PSA in the design stages. In addition, the pKa was also predicted. This was done with a view to explaining any variations observed in antiplasmodial activity since a number of target molecules were envisaged to have the same mode of action as other 4-aminoquinoline antimalarials that rely on basicity for accumulation at the site of action. Prediction of cLogP was done using ChemDraw while MarvinSketch was employed for all the other predictions.

Lipophilicity and solubility are the two most important physicochemical factors affecting both the extent and rate of drug absorption [10]. Increasing lipophilicity generally enhances membrane permeability. However, a drug that is highly lipophilic is also likely to undergo rapid metabolic clearance, hence the need for a balance between permeability and clearance. Orally administered drugs need to dissolve in the aqueous environment before they can be absorbed [10].

To complement the results obtained from the prediction of drug-like properties, the turbidimetric solubility of the target molecules was assessed in 96-well microtiter plates as previously described [11,12]. Briefly, the turbidmetric solubility assay involved diluting the test compounds from 10 mM stock solutions in DMSO in phosphate buffered saline (PBS) at pH 7.4 as well as in DMSO to obtain final concentrations of between 0 and 200 **µ**M. After incubation at room temperature for two hours, absorbance was read at 620

nm. Since most organic compounds are not freely soluble in aqueous media, as the concentration of compound in PBS increased, precipitation would occur resulting in increased absorbance in the PBS wells relative to the DMSO containing wells. The absorbance readings were plotted against concentration and the point at which absorbance started rising was taken as the higher bound of solubility.

4.2.2 Results of physicochemical evaluation

The results of the predicted physicochemical properties and experimentally determined solubility are given in Tables 4.1 to 4.4. The average molecular weight was 408.98. The mean number of hydrogen bond donors, hydrogen bond acceptors and rotatable bonds was 1.94, 5.06 and 5.71, respectively. The PSA ranged between 49.84 $Å^2$ (**3.2a**) and 83.29 $Å^2$ (**3.9g**). The mean cLogP was 6.10 (range 4.44-7.70). Only analogues **3.4b**, **3.9w**, **3.9x** and **3.9t** had cLogP values less than 5. The high cLogP values observed for the rest of the molecules are attributable to the presence of the largely nonpolar quinoline and benzoheterocyclic rings.

Thus the analogues evaluated generally had only one ‘rule of 5’ violation. This was interpreted to imply that the compounds would most likely be orally bioavailable. With regard to the turbidmetric solubility results, compounds with a protonatable tertiary nitrogen tended to have excellent solubility compared to the rest of the analogues. Poor solubility was generally associated with compounds possessing additional aromatic rings.

Table 4.1: Physicochemical properties of benzothiazole, benzimidazole and pyridine analogues

General structure	Code	-R	MW	HBD	HBA	cLogP	RB	PSA (Å^2)	pKa	Soly* (µM)
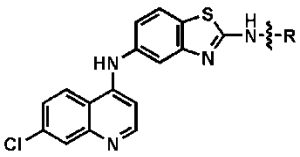	**3.2a (DS1F)**		382.91	2	4	7.22	4	49.84	-	10
	3.2c (DS11B)	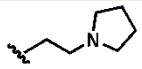	423.96	2	5	6.86	6	53.08	8.67	>100
	3.2d (DS12B)	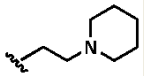	437.99	2	5	7.42	6	53.08	8.55	>100
	3.2e (DS13B)	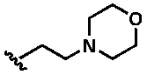	438.96	2	6	6.20	6	62.31	6.11	80
	3.2f (DS18B)	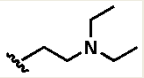	425.98	2	5	7.25	8	53.08	9.17	>100
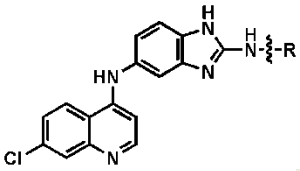	**3.6a (DS5G)**		337.81	3	4	5.92	4	65.63	-	40
	3.6b (DS21B)	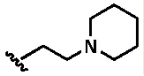	420.94	3	5	6.82	6	68.87	8.98	>100
	3.6c (DS22B)	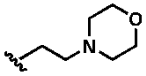	422.91	3	6	5.60	6	78.10	6.84	>100
	3.6d (DS24B)	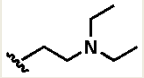	408.93	3	5	6.65	8	68.87	9.44	>100
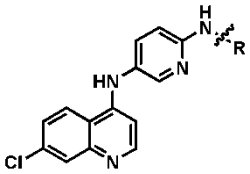	**3.4a (DS26B)**	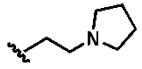	367.88	2	5	5.42	6	53.08	8.90	>100
	3.4b (DS27B)	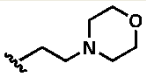	383.87	2	6	4.77	6	62.31	6.85	>100

MW = Molecular weight; HBD = hydrogen bond donor; HBA = hydrogen bond acceptor; cLogP = calculated log of partition coefficient; RB =rotatable bonds; PSA = polar surface area; Soly* = Experimental solubility

Table 4.2: Physicochemical properties of dialkylamino and cycloalkylamino benzoxazole analogues

General structure	Code	-R	MW	HBD	HBA	cLogP	RB	PSA (Å^2)	pKa	Soly* (µM)
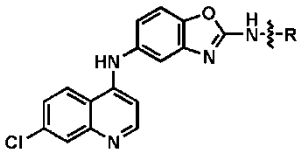	**3.9a (DS4F)**		338.79	2	4	5.77	4	62.98	-	40
	3.9b (DS23B)	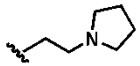	407.90	2	5	6.11	6	66.22	8.69	200
	3.9c (DS46B)	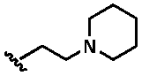	421.92	2	5	6.67	6	66.22	8.56	200
	3.9d (DS31B)	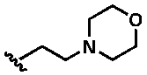	423.90	2	7	5.45	6	75.45	6.11	160
	3.9e (DS33B)	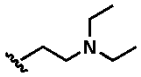	409.91	2	5	6.50	8	66.22	9.08	160
	3.9f (DS50B)	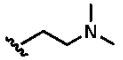	381.86	2	5	5.46	6	66.22	8.54	160
	3.9g (DS34B)	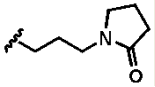	435.91	2	6	5.26	7	83.29	-	160
	3.9h (DS36B)	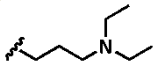	423.94	2	5	6.83	9	66.22	9.94	>200
	3.9i (DS37B)	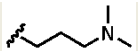	395.89	2	5	5.77	7	66.22	9.40	>200
	3.9j (DS48B)	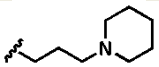	435.95	2	5	6.94	7	66.22	8.92	>200
	3.9k (DS56B)	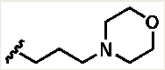	437.92	2	7	5.72	7	75.45	6.91	200
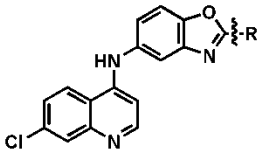	**3.9w (DS30B)**		352.82	1	4	4.60	4	54.19	7.75	>200
	3.9x (DS58B)	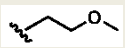	353.80	1	5	4.44	5	60.18	-	80
Amodiaquine			355.86	2	4	5.46	6	48.39	10.23	-

MW = Molecular weight; HBD = hydrogen bond donor; HBA = hydrogen bond acceptor; cLogP = calculated log of partition coefficient; RB =rotatable bonds; PSA = polar surface area; Soly = Experimental solubility

Table 4.3: Physicochemical properties of benzylamino and alkylpyridyl benzoxazole analogues

General structure	Code	-R	MW	HBD	HBA	cLogP	RB	PSA (Å^2)	Soly* (µM)
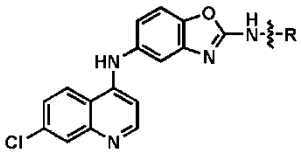	**3.9m (DS42B)**	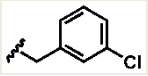	435.31	2	4	7.40	5	62.98	40
	3.9n (DS54B)	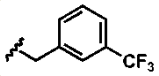	468.86	2	4	7.57	6	62.98	20
	3.9o (DS32B)	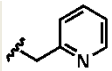	401.85	2	5	5.19	5	75.87	80
	3.9p (DS35B)	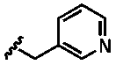	401.85	2	5	5.19	5	75.87	40
	3.9q (DS47B)	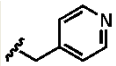	401.85	2	5	5.19	5	75.87	80
	3.9r (DS49B)	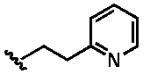	415.87	2	5	5.84	6	75.87	10

MW = Molecular weight; HBD = hydrogen bond donor; HBA = hydrogen bond acceptor; cLogP = calculated log of partition coefficient; RB =rotatable bonds; PSA = polar surface area; Soly = Experimental solubility

Table 4.4: Physicochemical properties of piperazinyl and dialkyl benzoxazole analogues

General structure	Code	-NR_2	MW	HBD	HBA	cLogP	RB	PSA (Å^2)	pKa	Soly* (µM)
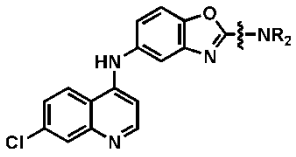	**3.9s (DS39B)**		366.84	1	4	6.54	5	54.19	-	80
	3.9l (DS41B)	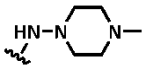	408.88	2	6	5.74	4	69.46	5.64	200
	3.9t (DS51B)	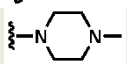	393.87	1	5	4.70	3	57.43	7.44	160
	3.9u (DS52B)	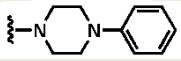	455.94	1	5	6.82	4	57.43	3.00	40
	3.9v (DS53B)	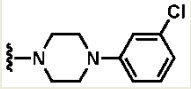	490.38	1	5	7.70	4	57.43	0.98	40

MW = Molecular weight; HBD = hydrogen bond donor; HBA = hydrogen bond acceptor; cLogP = calculated og of partition coefficient; RB =rotatable bonds; PSA = polar surface area; Soly = Experimental solubility

4.3 ANTIPLASMODIAL ACTIVITY

4.3.1 Introduction and rationale

In the medicinal chemistry rescue of drugs with unfavorable toxicity profiles by analogue design, improvement of the safety profile must not adversely affect the pharmacological efficacy of the resulting molecules. For amodiaquine analogues, therefore, the objective was to retain antimalarial activity, not just against chloroquine sensitive strains, but also against multi-drug resistant strains. The target compounds and selected intermediates were evaluated for activity against three *Plasmodium falciparum* strains: the drug sensitive NF54 strain and the drug resistant W2 and K1 strains. Testing was conducted at the University of California, San Francisco (W2) and the Swiss Tropical and Public Health Institute (NF54 and K1). Cytotoxicity assays were conducted against the L6 rat myoblasts (Swiss Tropical and Public Health Institute) and Chinese Hamster Ovarian (CHO) cells (University of Cape Town, Division of Pharmacology) to give an indication of the selectivity of the compounds for parasite cells.

4.3.2 Antiplasmodial activity results

4.3.2.1 Antiplasmodial activity of the initial library of benzoheterocyclic and pyridine analogues

The library of representative compounds synthesized for reactive metabolite studies was screened for antiplasmodial activity against the W2 and K1 *Plasmodium falciparum* strains. The results are shown in Table 4.5. The analogues could be divided into two main classes: those with a simple alkyl side chain (**3.2a**, **3.9a** and **3.6a**) and those with dialkylamino or cycloalkylamino moieties attached to the heterocyclic ring. The simple alkyl side chain analogues exhibited moderate antiplasmodial activity in the low

micromolar (**3.2a**) and submicromolar (**3.9a** and **3.6a**) ranges. In general, these analogs did not retain activity against the two chloroquine resistant *Plasmodium falciparum* strains. However, benzimidazole analogue **3.6a** (IC_{50} 0.249 μM) **w**as marginally more active than chloroquine against the K1 strain but was 31 times less active than amodiaquine against the same strain. Compounds with the dialkylamino and cycloalkylamino substituents displayed activity in the low nanomolar ranges except for the benzimidazole analogs which had activity in the low submicromolar to low micromolar range (0.189 μM-4.580 μM). The introduction of the tertiary amine was apparently responsible for a dramatic improvement in the potency of the benzothiazole and benzoxazole analogues but not the benzimidazole analogues. The benzoxazole analog **3.9b** (IC_{50} 8 nM) was the most potent analogue against the W2 strain, a 61-fold improvement over the activity observed for **3.9a**.

On the other hand, **3.2d** (IC_{50} 7 nM) was the most active compound against the K1 strain, representing a 131-fold increase in activity relative to **3.2a**. The two pyridyl analogues **3.4a** and **3.4b** exhibited modest activity against the W2 strain (IC_{50}s 21 and 41 nM, respectively). The morpholino pyridyl compound **3.4b** was only marginally more active than chloroquine (IC_{50} 49 nM) against the W2 strain. Interestingly, the morpholino benzothiazole analogue **3.2e** showed similar activity with **3.4b** against the W2 strain and was the least active tertiary amine containing benzothiazole analogue against both the W2 and K1 strains.

A chloroquine-like resistance pattern was observed from the resistance index (RI) data (calculated as K1 IC_{50}/W2 IC_{50} since the W2 strain used was more chloroquine sensitive compared to the K1 strain) among most compounds. However, for compounds with low

nanomolar activity, the benzothiazole analogues displayed the lowest RIs. The most active analogue, **3.2d**, was almost twice as active against the more resistant K1 strain as it was against the W2 strain (RI 0.54).

Table 4.5: Antiplasmodial activity of the initial library of benzoheterocyclic and pyridine analogues

General structure	Code	R	Antiplasmodial activity: IC_{50} (μM) W2	K1	Resistance index
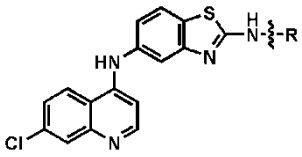	**3.2a (DS1F)**		1.158	0.917	0.79
	3.2c (DS11B)	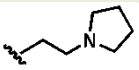	0.012	0.014	1.17
	3.2d (DS12B)	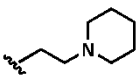	0.013	0.007	0.54
	3.2e (DS13B)	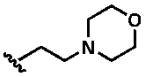	0.040	0.025	0.63
	3.2f (DS18B)	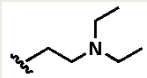	0.011	nt	-
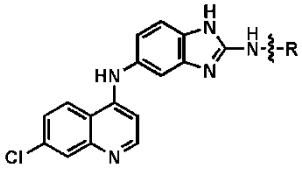	**3.6a (DS5G)**		0.501	0.249	0.50
	3.6b (DS21B)	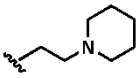	4.580	0.09	0.02
	3.6c (DS22B)	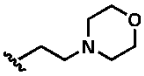	0.189	0.742	3.93
	3.6d (DS24B)	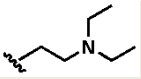	0.200	0.827	4.14
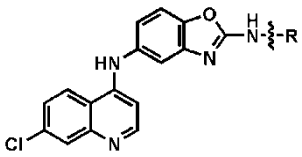	**3.9a (DS4F)**		0.491	0.921	1.88
	3.9b (DS23B)	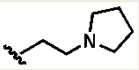	0.008	0.022	2.75
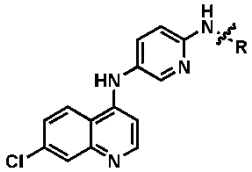	**3.4a (DS26B)**	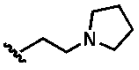	0.021	0.092	4.38
	3.4b (DS27B)	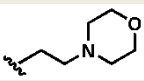	0.041	0.073	1.78
Amodiaquine			0.005	0.008	1.60
Chloroquine			0.049	0.344	7.02

4.3.2.2 Cytotoxicity and selectivity indexes of the initial library of benzoheterocyclic and pyridine analogues

Results of the cytotoxic activity against the L6 rat myoblast cell line, expressed as IC_{50}, are shown in Table 4.6. The selectivity index (SI) was calculated as the quotient of the cytotoxic IC_{50} divided by the antiplasmodial IC_{50}.

Table 4.6: Cytotoxicity and selectivity indexes of the initial library of benzoheterocyclic and pyridine analogues

General structure	Code	R	W2 IC_{50} (µM)	Cytotoxicity L6 IC_{50} (µM)	SI
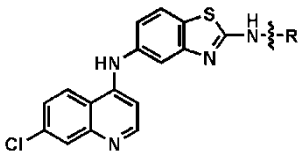	**3.2a DS1F**		1.158	4.126	3.56
	3.2c DS11B	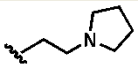	0.012	5.118	426.50
	3.2d (DS12B)	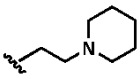	0.013	3.539	272.23
	3.2e (DS13B)	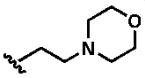	0.040	4.67	116.75
	3.2f (DS18B)	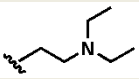	0.011	nt	-
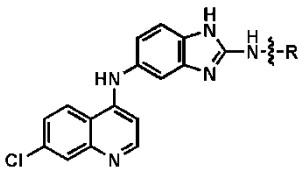	**3.6a (DS5G)**		0.501	5.713	11.40
	3.6b (DS21B)	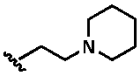	4.580	5.25	1.15
	3.6c (DS22B)	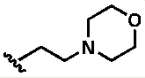	0.189	10.191	53.92
	3.6d (DS24B)	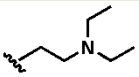	0.200	15.284	76.42
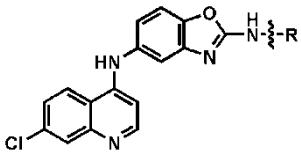	**3.9a (DS4F)**		0.491	16.352	33.30
	3.9b (DS23B)	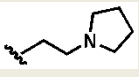	0.008	8.703	1087.88
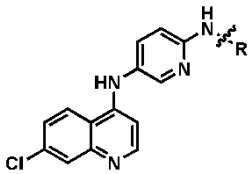	**3.4a (DS26B)**	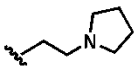	0.021	18.593	885.38
	3.4b (DS27B)	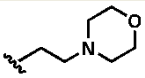	0.041	47.412	1156.39
Podophyllotoxin			-	0.021	
Amodiaquine			0.005	-	-
Chloroquine			0.049	-	-

An SI value of >1 is an indication that the compound is more cytotoxic to the parasite than the normal cells while a value of <1 implies that the compound will preferentially be lethal against the normal cells. In general, cytotoxicity was observed to decrease in the order pyridyl < benzoxazole < benzimidazole < benzothiazole. Pyridyl analogue **3.4b** had the highest SI (1156.39) followed by benzoxazole analogue **3.9b** (1087.88).

The potent benzothiazole compounds had better selectivity indexes (116.75-426.50) than the benzimidazole compounds. This was a clear indication that the superior antiplasmodial potency of the benzothiazole analogues outweighed their cytotoxicity. In spite of the encouraging SI observed for pyridyl analogue **3.4b**, this compound did not retain significant activity against the chloroquine resistant strains. Thus **3.9b** was the compound with the best balance of potent activity and low cytotoxicity.

As mentioned in Chapter 3, the benzoxazole analogues had the lowest bioactivation potential. The tertiary nitrogen containing compound **3.9b** displayed potent activity against the drug resistant W2 and K1 *Plasmodium falciparum* strains. These findings formed the basis for an expanded SAR study of this benzoxazole series. The antiplasmodial data for the benzoxazole targets are shown in the following tables.

4.3.2.3 Antiplasmodial activity of alkyl, amide, dialkylamino and cycloalkylamino analogues

When tested against the NF54 strain, the most potent compounds (**3.9b**, **3.9c**, **3.9e**, **3.9f**, **3.9h** and **3.9j**) had IC_{50} values equal to or comparable to that of chloroquine (10 nM) (Table 4.7). These potent compounds were all dialkylamino or cycloalkylamino

analogues with a protonatable tertiary nitrogen and could be classified as either ethyl (**3.9b**, **3.9c**, **3.9d**, **3.9e** and **3.9f**) or propyl (**3.9h**, **3.9i**, **3.9j** and **3.9k**) linker analogues. Activity against the NF54 strain did not vary widely, ranging between 10 and 19 nM, except for the morpholino analogues. The ethylmorpholino analogue **3.9d** was the least active compound against the NF54 strain within the protonatable tertiary nitrogen subset (IC_{50} 0.108 μM), followed by the propylmorpholino analogue **3.9k** (IC_{50} 0.039 μM).

Table 4.7: Antiplasmodial activity of alkyl, amide, dialkylamino and cycloalkylamino analogues

General structure	Code	-R	Activity , IC_{50} (μM)		RI
			NF54	K1	
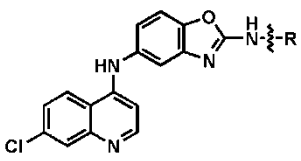	**3.9a (DS4F)**		0.466	1.003	2.15
	3.9b (DS23B)	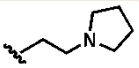	0.015	0.056	3.73
	3.9c (DS46B)	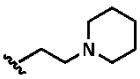	0.010	0.024	2.40
	3.9d (DS31B)	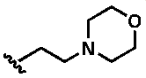	0.108	0.198	1.83
	3.9e (DS33B)	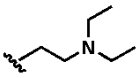	0.011	0.042	3.82
	3.9f (DS50B)	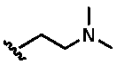	0.012	0.042	3.50
	3.9g (DS34B)	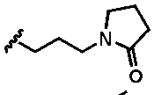	1.876	0.773	0.41
	3.9h (DS36B)	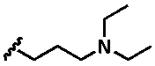	0.014	0.085	6.07
	3.9i (DS37B)	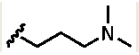	0.019	0.149	7.84
	3.9j (DS48B)	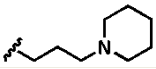	0.010	0.039	3.90
	3.9k (DS56B)	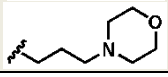	0.039	0.080	2.05
Amodiaquine			0.004	0.010	2.50
Chloroquine			0.010	0.275	27.50

Variations from which a tentative SAR could be derived were noticeable in K1 activity. Changing the dialkylamino group from diethyl to dimethyl did not have any effect on activity in ethyl linker analogues as both **3.9e** and **3.9f** had an IC_{50} of 42 nM. Changing to a propyl linker resulted in reduced activity. In addition, the diethyl analogue **3.9h** (IC_{50} 85 nM) was more active than the dimethyl analogue **3.9i** (IC_{50} 149 nM). A similar trend was observed for the piperidine analogues where the ethylpiperidine compound **3.9c** (24 nM) was more active than the propylpiperidine analogue **3.9j** (39 nM). However, this trend was reversed among the morpholino analogues **3.9d** and **3.9k** mentioned earlier where the propyl linker analogue was more potent. Converting the tertiary amine to an amide, as in **3.9g**, resulted in a drastic decline in activity against both strains, more so against the NF54 (IC_{50} 1.876 μM) than the K1 (IC_{50} 0.773 μM) strain. These results reinforced the importance of the protonatable nitrogen. Further exploratory studies involved the synthesis of analogues in which the side chain was attached to the benzoxazole group via a carbon instead of a nitrogen atom (Table 4.8). Although analogue **3.9w** had a protonatable nitrogen, it showed remarkably reduced activity against both strains compared to the alkylamino or cycloalkylamino analogues. The reduction in activity could not simply be accounted for by the low predicted pKa (7.75) since the morpholino analogues with even lower pKas showed better activity. Attachment to the benzoxazole ring via a carbon atom was, therefore, considered to adversely affect antiplasmodial activity. Analogue **3.9x** only exhibited micromolar activity, probably due to the lack of a protonatable nitrogen and the presence of a carbon linker.

Table 4.8: Antiplasmodial activity of carbon-linked analogues

General structure	Code	R	Activity, IC_{50} (μM)		RI
			NF54	K1	
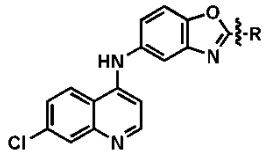	**3.9w (DS30B)**		0.213	0.411	1.93
	3.9x (DS58B)	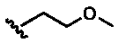	1.094	2.111	1.93

A chloroquine-like resistance pattern was generally observed among all the compounds. The exception was **3.9g** which, unfortunately, was less active than chloroquine against both *Plasmodium* strains. Nonetheless, the RIs were much lower than the 27.50 observed for chloroquine.

4.3.2.4 Antiplasmodial activity of benzylamino and alkylpyridyl benzoxazole analogues

When the alkylamino groups were replaced with substituted benzylamines (**3.9m** and **3.9n**) activity dropped to the low submicromolar range (Table 4.9). The benzylamine analogues were less active than chloroquine against the NF54 strain and virtually equipotent with the drug against the K1 strain. The methylpyridine analogues (**3.9o**, **3.9p** and **3.9q**) had activity in the mid-submicromolar to low micromolar range with activity increasing in the order 4-methyl < 2-methyl < 3-methyl (Table 4.9). Increasing the length of the linker from a methyl to an ethyl (**3.9r**) did not affect activity when compared to the corresponding 2-methylpyridine analogue **3.9o**. As with the rest of the analogues discussed above, these compounds were more active against the chloroquine sensitive strain as compared to the multi-drug resistant strain.

Table 4.9: Antiplasmodial activity of benzylamino and alkylpyridyl benzoxazole analogues

General structure	Code	-R	Activity , IC_{50} (μM)		RI
			NF54	K1	
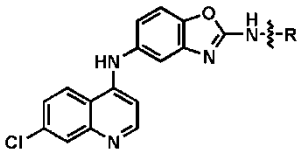	**3.9m (DS42B)**	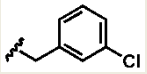	0.124	0.223	1.80
	3.9n (DS54B)	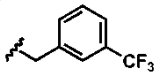	0.107	0.282	2.64
	3.9o (DS32B)	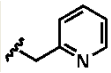	0.406	0.883	2.17
	3.9p (DS35B)	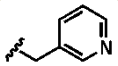	0.309	0.704	2.28
	3.9q (DS47B)	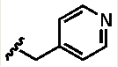	0.630	1.553	2.47
	3.9r (DS49B)	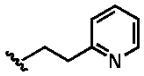	0.402	0.851	2.12
Amodiaquine			0.004	0.010	2.50
Chloroquine			0.010	0.275	27.50

4.3.2.5 Antiplasmoodial activity of piperazinyl and dialkyl benzoxazole analogues

As shown in Table 4.10, the methylpiperazine analogue with the piperazine ring directly attached to the benzoxazole ring (**3.9t**) was more active than the corresponding 1-amino-4-methylpiperazine analogue (**3.9l)**). Indeed **3.9t** retained activity against the multi-drug resistant K1 strain. Attachment of aromatic groups to the piperazine linker (**3.9u** and **3.9v**) resulted in further loss of activity against both the NF54 and K1 strains. The chloro substituted phenyl ring in **3.9v** resulted in a two-fold improvement in activity against the K1 strain over analogue **3.9u** with an unsubstituted phenyl ring. In all cases, the pattern of sensitivity observed with the other analogues was maintained. In terms of structure, analogue **3.9s** was closely related to the diethylamino analogues **3.9e** and

3.9h mentioned in Table 4.7 above and its reduced activity shows the importance of the alkyl linker in the antiplasmodial potency of these compounds.

Table 4.10: Antiplasmoodial activity of piperazinyl and dialkyl benzoxazole analogues

General structure	Code	-NR_2	Activity , IC_{50} (μM)		RI
			NF54	K1	
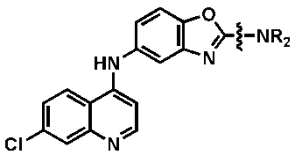	**3.9s (DS39B)**		0.512	1.379	2.69
	3.9l (DS41B)	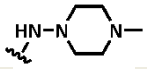	0.144	0.240	1.67
	3.9t (DS51B)	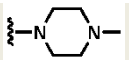	0.051	0.099	1.94
	3.9u (DS52B)	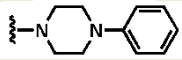	0.274	0.875	3.19
	3.9v (DS53B)	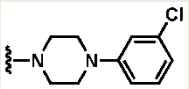	0.202	0.412	2.04
Amodiaquine			0.004	0.010	2.50
Chloroquine			0.010	0.275	27.50

4.3.2.6 Antiplasmodial activity of selected intermediates

A few nitrobenzoxazole intermediates were tested for activity against the NF54 and K1 strains (Table 4.11). It was immediately clear that the quinoline coupled analogues had far superior activity compared to the intermediates. Whereas all the intermediates were considered inactive (IC_{50}>20 μM), intermediate **2.9b** with a protonatable tertiary nitrogen showed low micromolar activity against both plasmodial strains. The other tertiary nitrogen containing intermediate, **2.9i**, displayed weak activity against the multi-drug resistant K1 strain but was inactive against the NF54 strain. These findings underscored the importance of the tertiary nitrogen in the activity of both the intermediates and the target molecules.

Table 4.11: Activity of selected benzoxazole intermediates

Compound	Structure	Activity, IC50 (μM)	
		NF54	K1
2.9b (DS23)	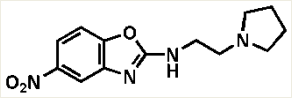	1.640	2.928
2.9o (DS32)	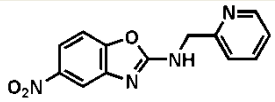	>20	>20
2.9i (DS37)	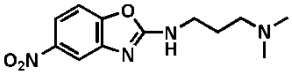	>20	10.992
2.9s (DS39)	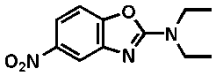	>20	>20
2.9r (DS49)	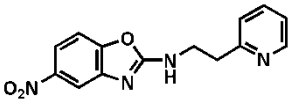	>20	>20
2.9t (DS51)	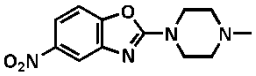	>20	>20
2.9u (DS52)	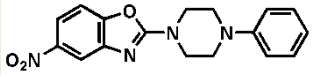	>20	>20
2.12b (DS62)	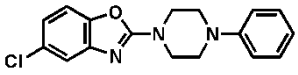	>20	>20

4.3.2.7 Cytotoxicity and selectivity indexes of benzoxazole analogues

The benzoxazole analogues with potent antiplasmodial activity were also the compounds with the most potent cytotoxicity (Table 4.12). Except for **3.9d**, all analogues with a protonatable tertiary nitrogen had cytotoxicity values less than 10 μg/ml. The pyridyl analogues **3.9o**, **3.9p**, **3.9q** and **3.9r** were the subclass with the lowest cytotoxic activity. In this subclass **3.9p** was the most cytotoxic (IC_{50} 66.0 μg/ml) while the other three analogues had IC_{50} values >100 μg/ml. The piperazine linker analogues were generally only weakly cytotoxic except for analogue **3.9u** (IC_{50} 13.1 μg/ml). It appears that the introduction of a chloro substituent as in **3.9v** drastically decreases cytotoxic activity. Overall, analogue **3.9b** had the highest cytotoxic activity at

2.0 µg/ml. However, all the active antiplasmodial compounds had high selectivity indexes ranging between 333 (**3.9b**) and 1175 (**3.9e**). These indexes were several magnitudes lower than that of amodiaquine in the CHO cell line but are not a cause for concern partly because there is still a sufficiently high enough *in vitro* safety window and partly because *in vivo* toxicity and *in vitro* cytoxicity on other mammalian cell lines are yet to be assessed.

Table 4.12: Cytotoxicity against CHO cells and selectivity indexes

General structure	Compound	-R or -NR_2	Activity, IC_{50} (µg/ml)		SI
			NF54	CHO	
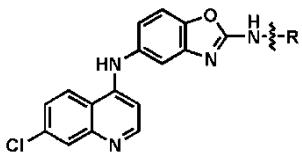	**3.9b (DS23B)**	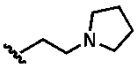	0.006	2.0	333
	3.9c (DS46B)	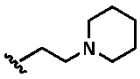	0.004	3.2	800
	3.9d (DS31B)	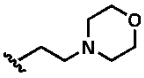	0.046	52.6	1143
	3.9e (DS33B)	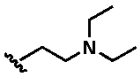	0.004	4.7	1175
	3.9f (DS50B)	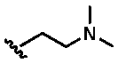	0.004	2.9	725
	3.9g (DS34B)	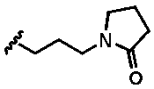	0.818	12.9	16
	3.9h (DS36B)	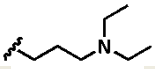	0.006	2.7	450
	3.9i (DS37B)	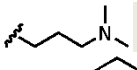	0.008	5.0	625
	3.9j (DS48B)	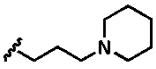	0.004	4.6	1150
	3.9k (DS56B)	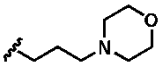	0.017	6.0	353
	3.9l (DS41B)	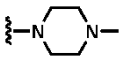	0.059	50.0	847
	3.9m (DS42B)	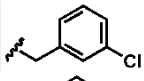	0.054	11.2	207
	3.9n (DS54B)	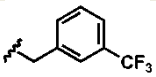	0.050	8.8	176
	3.9o (DS32B)	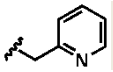	0.163	>100.0	-
	3.9p (DS35B)	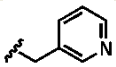	0.124	66.0	532

	3.9q (DS47B)	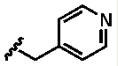	0.253	>100	-
	3.9r (DS49B)	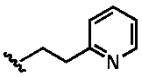	0.167	>100	-
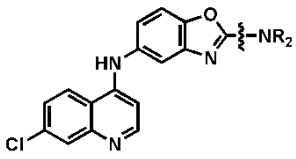	**3.9s (DS39B)**		0.188	84.1	447
	3.9t (DS51B)	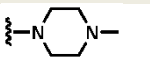	0.020	>100	-
	3.9u (DS52B)	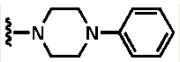	0.125	13.1	105
	3.9v (DS53B)	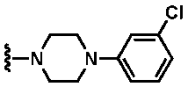	0.099	84.4	853
Amodiaquine HCl			0.002	68.4	34,200
Emetine			-	0.05	

4.3.2.8 Discussion of antiplasmodial activity data

From the antiplasmodial data, a number of observations were made. The 4-aminoquinoline ring was essential for activity. This pointed to a mode of action similar to that of other 4-aminoquinoline drugs, namely inhibition of heme detoxification by formation of the insoluble malaria pigment, hemozoin. Further support of this hypothesis was obtained from the observation that a tertiary nitrogen with a pKa greater than 8.00 was a necessary feature for potent antiplasmodial activity. This tertiary nitrogen could be part of a cycloalkylamino ring or a dialkylamino moiety. Such a nitrogen could be protonated inside the parasite's acidic food vacuole and result in increased accumulation of the compound. Among the most active compounds, there was no strong correlation between predicted pKa and antiplasmodial activity since compounds with a propyl linker had generally higher pKas but weaker antiplasmodial activity. This was a pointer to the involvement of other physicochemical and pharmacodynamic factors in the determination of antiplasmodial activity. However, in the overall picture, compounds without a protonatable tertiary nitrogen or those with a weakly basic tertiary

nitrogen, were found to have weak antiplasmodial activity. These observations informed the choice of β-hematin inhibition as the antiplasmodial mechanism to be studied.

4.4 BETA HEMATIN FORMATION INHIBITION ACTIVITY

4.4.1 Introduction

Synthetic or *in vitro* generated hemozoin, referred to as β-hematin, is used to estimate the hemozoin formation inhibition potential of compounds, which can be correlated to their antiplasmodial activity [13,14]. A number of *in vitro* assays using this approach have been described [15–17]. Such assays can be carried out in tube or microplate format with the latter being amenable to high throughput screening. Following incubation of the test compound in a solution containing hemin, the amount of β-hematin formed or that of hematin (in monomeric or aggregate form) remaining is quantified to give a direct or inverse colorimetric, radiometric, fluorometric or HPLC readout of β-hematin formation. The differential solubility between β-hematin and hematin in alkaline bicarbonate solutions (the former is insoluble) has been utilized in some assays to wash off unreacted hematin after the reaction and quantify the amount of β-hematin formed [18]. Alternatively, as in the assay described by Egan and Ncokazi, advantage is taken of the fact that free heme reacts with pyridine to form a pyridine–Fe(III)PPIX complex with a characteristic absorbance wavelength [15]. Thus the amount of free heme remaining at the end of experiment can be quantified. The results from these assays are presented as IC_{50} values defined as the number of molar equivalents of the test compound relative to hematin required to inhibit its conversion to β-hematin by 50 %.

Table 4.13: β-hematin inhibition activity of benzoxazole analogues

General structure	Compound	-R or -NR_2	Activity, IC_{50} (μM)	
			NF54	BHI[a]
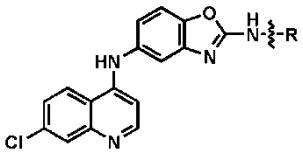	**3.9a (DS4F)**		0.466	80.2 ± 2.90
	3.9b (DS23B)	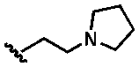	0.015	91.5 ± 1.69
	3.9c (DS46B)	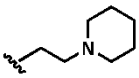	0.010	89 ± 0.48
	3.9d (DS31B)	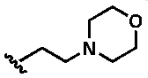	0.108	80.0 ± 2.36
	3.9e (DS33B)	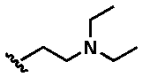	0.011	244.2 ± 7.26
	3.9f (DS50B)	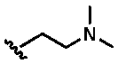	0.012	363.2 ± 17.6
	3.9g (DS34B)	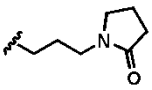	1.876	97.5 ± 3.43
	3.9h (DS36B)	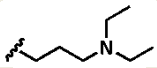	0.014	165.0 ± 9.10
	3.9i (DS37B)	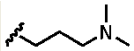	0.019	173.7 ± 6.99
	3.9j (DS48B)	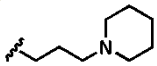	0.010	105 ± 8.32
	3.9k (DS56B)	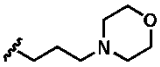	0.039	80.1 ± 0.93
	3.9l (DS41B)	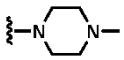	0.144	73.3 ± 1.93
	3.9m (DS42B)	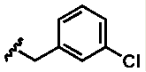	0.124	27.1 ± 1.03
	3.9n (DS54B)	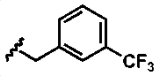	0.107	22.4 ± 3.02
	3.9o (DS32B)	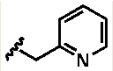	0.406	106.3 ± 1.06
	3.9p (DS35B)	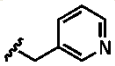	0.309	100.1 ± 2.58
	3.9q (DS47B)	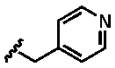	0.630	93.0 ± 0.91
	3.9r (DS49B)	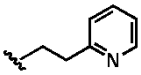	0.402	63.0 ± 1.61
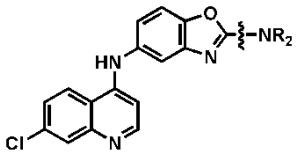	**3.9s (DS39B)**		0.512	50.7 ± 1.45
	3.9l (DS41B)	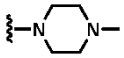	0.051	71.7 ± 4.06
	3.9u (DS52B)	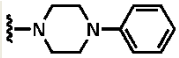	0.274	29.6 ± 1.47
	3.9v (DS53B)	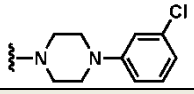	0.202	24.7 ± 1.28
Amodiaquine HCl			0.004	43.5 ± 5.32

[a]β-hematin inhibition

4.4.2 Results and discussion (β-hematin inhibition)

The β-hematin inhibition activity was observed to group the compounds according to their chemical structures (Table 4.13). The cycloalkylamine compounds (**3.9b**, **3.9c**, **3.9d**, **3.9j** and **3.9k**) had IC_{50} values lying between 80 and 105 μM. The dialkylamine analogues had higher IC_{50} values. Ethyldialkylamine analogues **3.9e** and **3.9f** (IC_{50}s 244.2 and 363.2 μM, respectively) had lower activity compared to the propyldialkylamine analogues **3.9h** and **3.9i** (IC_{50}s 165.0 and 173.7 μM, respectively). Since these tertiary amine compounds did not show a wide variation in antiplasmodial activity, these results indicated a lack of correlation between β-hematin inhibition and antiplasmodial activities. It is worth mentioning that antiplasmodial activity against the chloroquine-sensitive NF54 strain was utilized in attempting to correlate observed β-hematin inhibitory activity and antiplasmodial activity. This was done because in the resistant strain, the resistance mechanisms interfere with compound accumulation in the food vacuole.

The morpholino analogues **3.9d** and **3.9k** were among the most potent inhibitors of β-hematin formation (IC_{50} 80 μM) in the tertiary amine group of compounds but had the lowest antiplasmodial activity (0.108 and 0.039 μM, respectively). The γ-lactam analogue **3.9g** and the alkyl analogue **3.9a** showed good β-hematin formation inhibition activity although they only had weak antiplasmodial activity. The methylpiperazine analogues **3.9l** and **3.9t** were marginally more potent inhibitors of β-hematin formation than the tertiary amine analogues. A large increase in β-hematin inhibition activity was seen with the introduction of an aromatic ring in the piperazine class with **3.9u** and **3.9v** being more potent inhibitors than amodiaquine. The benzylamine analogues **3.9m** and

3.9n were equipotent with the arylpiperazine analogues, probably implying that the nature or length of linker was not as important a determinant of inhibition activity as was the presence of the aromatic ring. In the pyridine series, the methylpyridine analogues **3.9o**, **3.9p** and **3.9q** had activity about four-fold less than that observed among the benzylamines. The presence of the heteroatom, therefore appears to influence the efficiency of β-hematin inhibition. In this group, lengthening the linker by one carbon atom, as in **3.9r**, resulted in improved β-hematin inhibition. As seen in the previous section, compounds with an extra aromatic or heteroaromatic ring had weak antiplasmodial activity. Thus the excellent β-hematin inhibition observed in this subset of compounds did not translate to excellent antiplasmodial activity. Finally, the non-quinoline benzoxazole intermediates did not show any inhibitory activity even at the highest concentration of 1000 μM (data not tabulated). Thus it can be concluded, as expected, that the quinoline ring is essential for the β-hematin inhibition observed in this series of compounds.

Overall, it is apparent that the presence of an aromatic ring, in addition to the quinoline, imparts greater β-hematin inhibitory activity. This may be attributed to increased π-π stacking. However, since analogues with an extra aromatic ring did not have a protonatable tertiary amine, they could not accumulate in the food vacuole in the parasite where these compounds are believed to act.

Ferriprotoporphyrin IX can interact with drug molecules via two carboxyl groups (hydrogen bonding and electrostatic interactions) and a flat planar porphyrin ring (hydrophobic interactions). Potent amodiaquine analogues undergo a two-point attachment involving the H- bonding of the secondary amino group at one of the

carboxyl groups in such a way that the quinoline group is π-stacked on top of the FP ring [19]. This strong interaction may explain the high potency observed for the dialkylamino and cycloalkylamino analogues in this study. A high field NMR study showed that the aliphatic chain plays a key role in stabilizing heme-drug complexes with chains longer than three carbon chains forcing the end of the aliphatic chain outside the porphyrin rim and shorter chains reducing the stabilizing van der Waals contribution [20]. This may partly explain our observation that ethyl linker cycloalkylamino analogues were more potent β-hematin inhibitors than their corresponding propyl linker analogues. The inverse trend was, however, observed among the dialkylamino compounds. This may be explained by effective van der Waals interactions. It appears that the cycloalkyl rings have greater ability to interact with the porphyrin ring compared to the dialkyl groups. The interaction of the rings may play a more important role than the aliphatic linker chains. However, in the case of the dialkyl analogues, the aliphatic linkers more effectively interact with the porphyrin ring via van der Waals forces compared to the terminal alkyl groups and thus the propyl linker analogues have improved binding affinities over the ethyl linker analogues. Analogously, it can be argued that the introduction of the piperazine linker improves β-hematin inhibitory activity by increasing the van der Waals interaction of the linker with the porphyrin ring.

The observed lack of correlation between antiplasmodial and β-hematin inhibitory activity confirms one of the shortcomings of target-based drug discovery. Apart from having an effect on their target, in whole cell or organism assays, drugs need to traverse various biological spaces and membranes to access the target. A prerequisite for this is that drugs should possess appropriate physicochemical and pharmacokinetic

properties. In the case of drugs that inhibit β-hematin formation, drug accumulation in the acidic food vacuole is essential and is only possible for drugs with a tertiary nitrogen that is protonatable in the acidic pH in the food vacuole. The high β-hematin inhibitory activity of morpholino analogues is probably due to a favorable hydrogen bonding interaction with heme hydrogen atoms. However, the oxygen atom reduces the basicity of the morpholine nitrogen and results in reduced accumulation and antiplasmodial activity. Our findings are in agreement with those of other researchers who have reported reduced antiplasmodial activity for morpholine compared to other cycloalkylamine quinoline analogues [21,22].

4.5 MICROSOMAL STABILITY STUDIES

4.5.1 Introduction and rationale

It was mentioned in Chapter 3 that metabolism is one of the most important determinants of the pharmacokinetic disposition of a xenobiotic [23]. Pharmacokinetics is a term that encompasses the processes of absorption, distribution, metabolism and excretion (ADME) and is currently commonly studied in conjunction with toxicity, hence the acronym ADMET [24]. Prior to the year 2,000, poor pharmacokinetics was the major cause of attrition in drug development programs [25]. To address this issue, the pharmaceutical industry started including ADME/PK studies early in drug development, rather than simply utilizing it as a preclinical safety support function [26]. This approach is currently the accepted norm in rational drug design [27,28]. ADMET studies can be conducted using any combination of available *in silico*, *in vitro* and *in vivo* methods, depending on the volume and value of the test compounds [24,29].

Metabolic bioactivation has already been addressed in Chapter 3. In this section, the focus will be on metabolic stability. Extensive or extremely rapid metabolism of a compound to less active or inactive metabolites is a liability as it results in reduced efficacy [30]. *In vitro* metabolic stability can be assessed using individual recombinant CYP enzymes, microsomes, hepatocytes or liver slices [31,32]. Microsomes are the most widely employed system for metabolic stability studies [33]. This can be attributed to, among other factors, ease of preservation, amenability to high throughput screening and the fact that the enzymatic activity remains stable even after prolonged storage [34].

4.5.2 Procedure for microsomal stability studies

The general procedure for microsomal stability studies has been captured by Li [24]. For most of the compounds, the assay was carried out in 96-well plates at two time points, 0 and 30 minutes. The wells were preloaded with test and control compounds in phosphate buffer pH 7.4. Human liver and mouse liver microsomes were added to the appropriate wells. The reaction was initiated by the addition of NADPH and incubation was carried out at 37 °C for 30 minutes. The reaction was stopped using an ice-cold stop solution of Tris in acetonitrile. For the time 0 plate, the stop solution was added at the start of the experiment, followed by NADPH. After centrifugation and membrane filtration into a second 96-well plate, the amount of compound remaining in the mixture was quantified using LC/MS. Results were presented as percentage of compound remaining after incubation.

4.5.3 Results and discussion of microsomal stability studies

Table 4.14: Percentage of compound remaining after 30 min incubation with microsomes

General structure	Code	R	% remaining	
			HLM	MLM
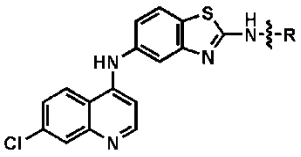	**3.2a (DS1F)**		>99	2
	3.2c (DS11B)	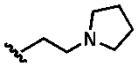	>99	85
	3.2d (DS12B)	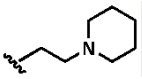	52	46
	3.2e (DS13B)	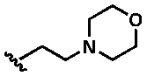	55	90
	3.2f (DS18B)	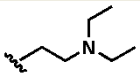	79	47
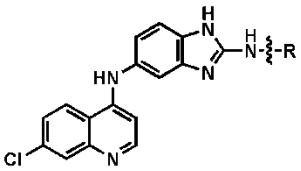	**3.6a (DS5G)**		>99	35
	3.6b (DS21B)	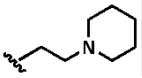	87	72
	3.6c (DS22B)	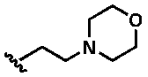	93	84
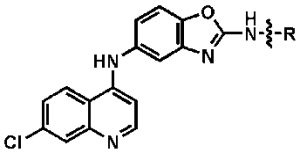	**3.9a (DS4F)**		81	1
	3.9b (DS23B)	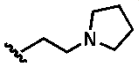	62	81
	3.9e (DS33B)	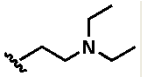	78	74
	3.9f (DS50B)	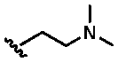	>99	>99
	3.9c (DS46B)	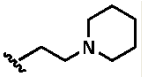	71	41
	3.9i (DS37B)	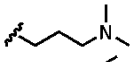	78	44
	3.9h (DS36B)	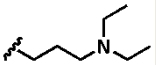	70	70
	3.9j (DS48B)	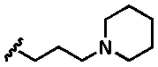	70	49
	3.9k (DS56B)	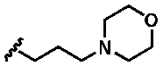	27	26
	3.9t (DS51B)	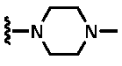	61	18
	3.9v (DS53B)	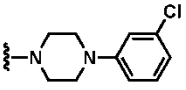	36	>99
	3.9n (DS54B)	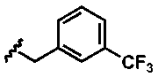	>99	71
Amodiaquine			60	22

HLM = Human liver microsomes; MLM = mouse liver microsomes

As can be seen from Table 4.14, alkyl analogues **3.2a** (benzothiazole) and **3.9a** (benzoxazole) were extremely unstable in MLMs but very stable in HLMs, probably as a result of species specific rapid dealkylation. However, the benzimidazole alkyl analogue **3.6a** was slightly more stable in MLMs. These analogues did not exhibit potent antiplasmodial activity and were not accorded further attention. The most stable compound was the dimethylamino analogue **3.9f**. This analogue was virtually not metabolized in the presence of MLMs and HLMs after 30 minutes of incubation. This was a surprising finding since N-demethylation would have been expected to occur with ease. Propylmorpholino benzoxazole analogue **3.9k** was the least metabolically stable analogue with <30% remaining after 30 minutes of incubation with both MLMs and HLMs. This was in stark contrast to the much more stable ethylmorpholino benzothiazole and benzimidazole analogues **3.2e** and **3.6c**. Ethyldialkylamino analogues **3.9e** and **3.9f** were also observed to be more metabolically stable than the corresponding propyldialkylamino analogues **3.9h** and **3.9i**, respectively. This may be construed to imply that the propyl linker is the source of metabolic liability. The methylpiperazine analogue **3.9t** was moderately stable in HLMs but unstable in MLMs, with only 18 % of the compound remaining after 30 minutes, possibly as a result of rapid N-demethylation. Except for **3.2e**, **3.9b** and **3.9v**, the analogues were generally more stable in HLMs than in MLMs. Overall, benzoxazole analogues with potent antiplasmodial activity (**3.9b**, **3.9c**, **3.9e**, **3.9f** and **3.9j**) exhibited metabolic stability equal to or greater than amodiaquine in HLMs. In MLM incubations, the analogues were at least twice as stable as amodiaquine except for **3.9c** which had only 41 % of the parent compound remaining after 30 minutes. It was apparent that in MLMs, the

metabolic stability of the cycloalkylamino compounds decreased in the order morpholine > pyrollidine > piperidine.

4.6 *IN VIVO* EFFICACY STUDIES

4.6.1 Introduction

It is an established fact that *in vitro* potency does not necessarily translate to *in vivo* efficacy. This inconsistency may arise as a result of several whole organism factors coming into play. For this reason, compounds with desirable *in vitro* potency and ADMET characteristics usually undergo *in vivo* efficacy tests before advancing any further in the drug development process.

Plasmodium falciparum only infects human beings and a small number of primates [35]. Since widespread use of primates in malaria research is impractical, the use of avian and rodent plasmodial species that are non-pathogenic to humans as surrogates of *P. falciparum* offers a valuable alternative [36]. The rodent malaria parasites *P. berghei*, *P. vinckei*, *P. yoelii* and *P. chabaudii* readily infect laboratory mice and are, consequently, extensively used in early drug discovery and development [37]. The use of rodent models is not without its own challenges. First, the parasite species used is different from the human malaria parasite and as such may present with a dissimilar sensitivity to the antimalarial compound. Secondly, biological differences between the rodent and man may make interpretation of results obtained tentative at best. As an attempt to address the first challenge, *P. falciparum* infected humanized mouse models, usually immunodeficient mice engrafted with hematopoietic cells or tissues, or mice that transgenically express human genes, have been developed [38]. Nonetheless, ready availability and ease of handling make the traditional rodent models an attractive choice

in early drug development studies. The most widely used initial *in vivo* test is the Peters' four-day suppressive test in which the efficacy of four daily doses of compounds is measured by comparison of blood parasitemia (on day four after infection) and mouse survival time in treated and untreated mice [36].

In this project three compounds, **3.9b**, **3.9c** and **3.9j** were selected for *in vivo* efficacy studies based on their potent antiplasmodial activity, high selectivity indexes and improved metabolic stability over amodiaquine. Testing was carried out at the Swiss Tropical and Public Health Institute. Compounds were administered in four daily oral doses of 50 mg/kg.

4.6.2 Results and discussion

Table 4.15 shows the suppression of parasitemia by the three analogues tested as a percentage of the untreated control while Table 4.16 presents results on the effects of the analogues on mouse survival. A compound was considered curative if the animal survived to day 30 after infection with no detectable parasites.

Table 4.15: *In vivo* suppression of parasitemia by **3.9b, 3.9c** and **3.9j**.

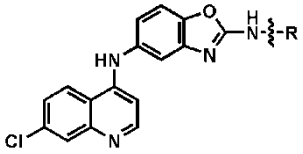

General structure

Compound	R	Parasitized RBC over 100						% of control	% Activity
		M1	M2	M3	M4	M5	Avg		
3.9b (DS23B)	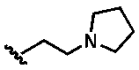	0.10	0.20	0.10	-	-	0.13	0.17	99.83
3.9c (DS46B)	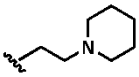	0.10	0.10	0.10	-	-	0.10	0.13	99.87
3.9j (DS48B)	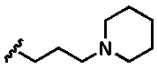	0.10	0.10	0.20	-	-	0.13	0.17	99.83
Control		84.70	84.30	75.50	71.30	80.50	79.26		
CQ[41]									99.9

M1, M2...=Mouse 1, Mouse 2…; CQ=Chloroquine (Data from reference 41, dosed at 4 x 30 mg/kg)

Table 4.16: Effect of **3.9b, 3.9c** and **3.9j** on mouse survival.

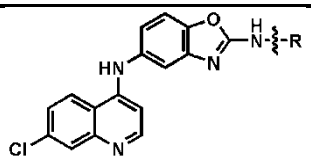

General structure

Compound	R	Mouse survival days (MSDs)						Cured
		M1	M2	M3	M4	M5	Avg	
3.9b (DS23B)	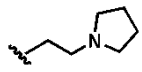	**30**	**30**	**30**	-	-	30	3/3
3.9c (DS46B)	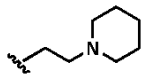	30[a]	**30**	21[b]	-	-	27	1/3
3.9j (DS48B)	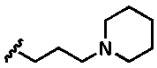	**30**	**30**	30[a]	-	-	30	2/3
Control		4	4	4	4	4	4	0
CQ[41]							24	

M1, M2...=Mouse 1, Mouse 2…; [a]Mouse euthanized at end of 30 days due to presence of parasitemia; [b]Mouse found dead; CQ=Chloroquine (Data from reference 41, dosed at 4 x 30 mg/kg)

The results show that the three analogues tested suppressed parasitemia by >99% on the third day post-infection compared to the control. All the three mice treated with **3.9b** survived the entire 30-day duration of the experiment. On their part, **3.9c** and **3.9j** cured 1/3 and 2/3 of treated mice, respectively. One of the mice treated with **3.9b** died on day 21 while the rest of the mice in the experiment survived for the entire 30 days. However, at the end of 30 days, one mouse each from the groups treated with **3.9c** and **3.9j** showed parasitemia when a drop of blood was examined under the microscope.

The potent oral *in vivo* efficacy of the three analogues was encouraging both from the antimalarial and pharmacokinetic perspectives. It was an indication of good oral bioavailability possibly due to lack of the first pass effect whereby compounds are rapidly converted to less active metabolites after oral administration [39]. It could also imply a reasonably low volume of distribution affording sufficient free unbound drug

concentration in circulating blood to achieve parasitemia reduction in parasitized RBCs. The reduced efficacy of **3.9c** and **3.9j** as characterized by reduced MSDs (**3.9c**) and proportion of cured mice (**3.9j**) suggests parasite recrudescence. This may result from high clearance leading to short elimination half-lives for these two analogues. This finding may be supported by the observation that these two compounds had lower metabolic stability compared to **3.9b**. The ideal profile for new antimalarials comprises orally active compounds that can cure the disease with a 3-day regimen using once-a-day dosing [40]. These analogues, especially **3.9b**, have demonstrated the potential to meet these requirements. Detailed *in vivo* pharmacokinetic studies are ongoing to provide more information on the fate of these compounds. In addition, these analogues have been earmarked for single and lower multiple dose studies in the *in vivo* murine model. These studies will also include compounds from the dialkylamino class which had good microsomal stability.

4.7 CONCLUSION

The four series of analogues synthesized and developed in this study generally possessed drug-like properties suitable for oral absorption. In all the series, potent antiplasmodial activity was observed in 4-aminoquinoline compounds with dialkylamino and cycloalkylamino moieties whose tertiary nitrogen could be protonated at neutral or acidic pH. Among the benzoxazole analogues, there was generally a weak correlation between β-hematin activity and antiplasmodial potency against the chloroquine-sensitive NF54 strain even though most of the potent antiplasmodial compounds were also potent β-hematin formation inhibitors. The lack of correlation was especially evident among the dialkylamino analogues which showed potent antiplasmodial activity and

weak β-hematin activity. Compounds with potent antiplasmodial activity were also found to possess high cytotoxic activity against CHO cells. However, these compounds had high selectivity indexes. With regard to *in vitro* metabolic stability, moderate to excellent stability was observed in compounds with potent antiplasmodial activity. These data informed the selection of three analogues for *in vivo* efficacy studies in *P*. *berghei* infected mice. The three analogues proved to be very potent in suppressing parasitemia (>99%) and resulted in oral cures in treated mice.

REFERENCES

(1) Testa, B.; Pedretti, A.; Vistoli, G. Reactions and enzymes in the metabolism of drugs and other xenobiotics. *Drug Discov. Today* **2012**, *17*, 549–60.

(2) Blake, J. F. Chemoinformatics - predicting the physicochemical properties of "drug-like" molecules. *Curr. Opin. Biotechnol.* **2000**, *11*, 104–7.

(3) Vistoli, G.; Pedretti, A.; Testa, B. Assessing drug-likeness--what are we missing? *Drug Discov. Today* **2008**, *13*, 285–94.

(4) Lipinski, C. A.; Lombardo, F.; Dominy, B. W.; Feeney, P. J. Experimental and computational approaches to estimate solubility and permeability in drug discovery and development settings. *Adv. Drug Deliv. Rev.* **1997**, *23*, 3–25.

(5) Faller, B.; Ottaviani, G.; Ertl, P.; Berellini, G.; Collis, A. Evolution of the physicochemical properties of marketed drugs: can history foretell the future? *Drug Discov. Today* **2011**, *16*, 976–84.

(6) Veber, D. F.; Johnson, S. R.; Cheng, H.-Y.; Smith, B. R.; Ward, K. W.; Kopple, K. D. Molecular properties that influence the oral bioavailability of drug candidates. *J. Med. Chem.* **2002**, *45*, 2615–23.

(7) Palm, K.; Luthman, K.; Ungell, A.-L.; Strandlund, G.; Beigi, F.; Lundahl, P.; Artursson, P. Evaluation of dynamic polar molecular surface area as predictor of drug absorption: comparison with other computational and experimental predictors. *J. Med. Chem.* **1998**, *41*, 5382–92.

(8) Leeson, P. D.; Springthorpe, B. The influence of drug-like concepts on decision-making in medicinal chemistry. *Nat. Rev. Drug Discov.* **2007**, *6*, 881–90.

(9) Hooft van Huijsduijnen, R.; Sauer, W. H. B.; Bombrun, A.; Swinnen, D. Prospects for inhibitors of protein tyrosine phosphatase 1B as antidiabetic drugs. *J. Med. Chem.* **2004**, *47*, 4142–6.

(10) Lin, J. H.; Lu, A. Y. Role of pharmacokinetics and metabolism in drug discovery and development. *Pharmacol. Rev.* **1997**, *49*, 403–49.

(11) Pérez, J.; Díaz, C.; Salado, I. G.; Pérez, D. I.; Peláez, F.; Genilloud, O.; Vicente, F. Evaluation of the effect of compound aqueous solubility in cytochrome P450 inhibition assays. *Adv. Biosci. Biotechnol.* **2013**, *04*, 628–639.

(12) Kerns, E. H.; Di, L.; Carter, G. T. In vitro solubility assays in drug discovery. *Curr. Drug Metab.* **2008**, *9*, 879–85.

(13) Thomas, V.; Góis, A.; Ritts, B.; Burke, P.; Hänscheid, T.; McDonnell, G. A novel way to grow hemozoin-like crystals in vitro and its use to screen for hemozoin inhibiting antimalarial compounds. *PLoS One* **2012**, *7*, e41006.

(14) Coban, C.; Yagi, M.; Ohata, K.; Igari, Y.; Tsukui, T.; Horii, T.; Ishii, K. J.; Akira, S. The malarial metabolite hemozoin and its potential use as a vaccine adjuvant. *Allergol. Int.* **2010**, *59*, 115–24.

(15) Ncokazi, K. K.; Egan, T. J. A colorimetric high-throughput β-hematin inhibition screening assay for use in the search for antimalarial compounds. *Anal. Biochem.* **2005**, *338*, 306–319.

(16) Huy, N. T.; Uyen, D. T.; Maeda, A.; Trang, D. T. X.; Oida, T.; Harada, S.; Kamei, K. Simple Colorimetric Inhibition Assay of Heme Crystallization for High-Throughput Screening of Antimalarial Compounds. *Antimicrob. Agents Chemother.* **2006**, *51*, 350–353.

(17) Gorka, A. P.; Alumasa, J. N.; Sherlach, K. S.; Jacobs, L. M.; Nickley, K. B.; Brower, J. P.; de Dios, A. C.; Roepe, P. D. Cytostatic versus Cytocidal Activities of Chloroquine Analogues and Inhibition of Hemozoin Crystal Growth. *Antimicrob. Agents Chemother.* **2012**, *57*, 356–364.

(18) Tripathi, A. K.; Khan, S. I.; Walker, L. A.; Tekwani, B. L. Spectrophotometric determination of de novo hemozoin/β-hematin formation in an in vitro assay. *Anal. Biochem.* **2004**, *325*, 85–91.

(19) O'Neill, P. M.; Ward, S. A.; Berry, N. G.; Jeyadevan, J. P.; Biagini, G. A.; Asadollaly, E.; Park, B. K.; Bray, P. G. A medicinal chemistry perspective on 4-aminoquinoline antimalarial drugs. *Curr. Top. Med. Chem.* **2006**, *6*, 479–507.

(20) Leed, A.; DuBay, K.; Ursos, L. M. B.; Sears, D.; de Dios, A. C.; Roepe, P. D. Solution structures of antimalarial drug-heme complexes. *Biochemistry* **2002**, *41*, 10245–55.

(21) O'Neill, P. M.; Shone, A. E.; Stanford, D.; Nixon, G.; Asadollahy, E.; Park, B. K.; Maggs, J. L.; Roberts, P.; Stocks, P. A.; Biagini, G.; Bray, P. G.; Davies, J.; Berry, N.; Hall, C.; Rimmer, K.; Winstanley, P. A.; Hindley, S.; Bambal, R. B.; Davis, C. B.; Bates, M.; Gresham, S. L.; Brigandi, R. A.; Gomez-de-Las-Heras, F. M.; Gargallo, D. V; Parapini, S.; Vivas, L.; Lander, H.; Taramelli, D.; Ward, S. A. Synthesis, antimalarial activity, and preclinical pharmacology of a novel series of 4'-fluoro and 4'-chloro analogues of amodiaquine. Identification of a suitable "back-up" compound for N-tert-butyl isoquine. *J. Med. Chem.* **2009**, *52*, 1828–44.

(22) Gemma, S.; Camodeca, C.; Sanna Coccone, S.; Joshi, B. P.; Bernetti, M.; Moretti, V.; Brogi, S.; de Marcos, M. C. B.; Savini, L.; Taramelli, D.; Basilico, N.; Parapini,

S.; Rottmann, M.; Brun, R.; Lamponi, S.; Caccia, S.; Guiso, G.; Summers, R. L.; Martin, R. E.; Saponara, S.; Gorelli, B.; Novellino, E.; Campiani, G.; Butini, S. Optimization of 4-aminoquinoline/clotrimazole-based hybrid antimalarials: further structure-activity relationships, in vivo studies, and preliminary toxicity profiling. *J. Med. Chem.* **2012**, *55*, 6948–67.

(23) Kumar, G. N.; Surapaneni, S. Role of drug metabolism in drug discovery and development. *Med. Res. Rev.* **2001**, *21*, 397–411.

(24) Li, A. P. Screening for human ADME/Tox drug properties in drug discovery. *Drug Discov. Today* **2001**, *6*, 357–366.

(25) Kola, I.; Landis, J. Can the pharmaceutical industry reduce attrition rates? *Nat. Rev. Drug Discov.* **2004**, *3*, 711–5.

(26) Eddershaw, P.; Beresford, A.; Bayliss, M. ADME/PK as part of a rational approach to drug discovery. *Drug Discov. Today* **2000**, *5*, 409–414.

(27) Kassel, D. B. Applications of high-throughput ADME in drug discovery. *Curr. Opin. Chem. Biol.* **2004**, *8*, 339–45.

(28) Koh, H.-L.; Yau, W.-P.; Ong, P.-S.; Hegde, A. Current trends in modern pharmaceutical analysis for drug discovery. *Drug Discov. Today* **2003**, *8*, 889–97.

(29) Yu, H.; Adedoyin, A. ADME-Tox in drug discovery: integration of experimental and computational technologies. *Drug Discov. Today* **2003**, *8*, 852–61.

(30) Pritchard, J. F.; Jurima-Romet, M.; Reimer, M. L. J.; Mortimer, E.; Rolfe, B.; Cayen, M. N. Making better drugs: Decision gates in non-clinical drug development. *Nat. Rev. Drug Discov.* **2003**, *2*, 542–53.

(31) Panchagnula, R.; Thomas, N. S. Biopharmaceutics and pharmacokinetics in drug research. *Int. J. Pharm.* **2000**, *201*, 131–50.

(32) Brandon, E. F. .; Raap, C. D.; Meijerman, I.; Beijnen, J. H.; Schellens, J. H. . An update on in vitro test methods in human hepatic drug biotransformation research: pros and cons. *Toxicol. Appl. Pharmacol.* **2003**, *189*, 233–246.

(33) Ekins, S.; Ring, B. J.; Grace, J.; McRobie-Belle, D. J.; Wrighton, S. A. Present and future in vitro approaches for drug metabolism. *J. Pharmacol. Toxicol. Methods* **2001**, *44*, 313–24.

(34) Baranczewski, P.; Stańczak, A.; Sundberg, K.; Svensson, R.; Wallin, A.; Jansson, J.; Garberg, P.; Postlind, H. Introduction to in vitro estimation of metabolic stability and drug interactions of new chemical entities in drug discovery and development. *Pharmacol. Rep.* **2006**, *58*, 453–72.

(35) Angulo-Barturen, I.; Jiménez-Díaz, M. B.; Mulet, T.; Rullas, J.; Herreros, E.; Ferrer, S.; Jiménez, E.; Mendoza, A.; Regadera, J.; Rosenthal, P. J.; Bathurst, I.; Pompliano, D. L.; Gómez de las Heras, F.; Gargallo-Viola, D. A murine model of falciparum-malaria by in vivo selection of competent strains in non-myelodepleted mice engrafted with human erythrocytes. *PLoS One* **2008**, *3*, e2252.

(36) Fidock, D. A.; Rosenthal, P. J.; Croft, S. L.; Brun, R.; Nwaka, S. Antimalarial drug discovery: efficacy models for compound screening. *Nat. Rev. Drug Discov.* **2004**, *3*, 509–20.

(37) Perkins, S. L.; Sarkar, I. N.; Carter, R. The phylogeny of rodent malaria parasites: simultaneous analysis across three genomes. *Infect. Genet. Evol.* **2007**, *7*, 74–83.

(38) Shultz, L. D.; Ishikawa, F.; Greiner, D. L. Humanized mice in translational biomedical research. *Nat. Rev. Immunol.* **2007**, *7*, 118–30.

(39) Lin, J. H.; Chiba, M.; Baillie, T. A. Is the role of the small intestine in first-pass metabolism overemphasized? *Pharmacol. Rev.* **1999**, *51*, 135–58.

(40) Ridley, R. G. Medical need, scientific opportunity and the drive for antimalarial drugs. *Nature* **2002**, *415*, 686–93.

(41) González Cabrera, D.; Douelle, F.; Feng, T.-S.; Nchinda, A. T.; Younis, Y.; White, K. L.; Wu, Q.; Ryan, E.; Burrows, J. N.; Waterson, D.; et al. Novel orally active antimalarial thiazoles. *J. Med. Chem.* **2011**, *54*, 7713–7719.

Chapter 5

SUMMARY, CONCLUSIONS AND RECOMMENDATIONS FOR FUTURE WORK

5.1 SUMMARY AND CONCLUSIONS

This project aimed to discover analogues of the 4-aminoquinoline drug amodiaquine with potentially improved safety and efficacy profiles using the present and available knowledge of the drug metabolism and pharmacokinetics (DMPK), toxicity and efficacy profile of the drug.

The first objective was to design and synthesize analogues of amodiaquine which potentially prevent bioactivation to the quinone imine and aldehyde metabolites which could be associated with hepatotoxicity and agranulocytosis. The molecules designed would retain most of the features of amodiaquine necessary for retention of activity against chloroquine resistant *Plasmodium falciparum* strains. A representative set of compounds in four different series was synthesized in which the 4-aminoquinoline ring was coupled with benzothiazole, benzimidazole, benzoxazole and pyridyl rings bearing different aliphatic amines and diamines. The chemistry mainly involved aromatic nucleophilic substitution reactions and reductive hydrogenation of nitro aromatic compounds which could be carried out with relative facility and using affordable starting materials.

The second objective was to use EC-ESI/MS and CYP inhibition studies to assess the bioactivation potential of the amodiaquine analogues synthesized. Potent non-time-dependent CYP3A4 inhibition was observed amongst all analogues tested. The benzothiazole analogues were the most potent inhibitors. Additionally, most of the analogues were moderate inhibitors of CYP2D6, though to a lesser extent than

amodiaquine and desethylamodiaquine. In EC-ESI/MS trapping experiments using potassium cyanide and methoxylamine, all analogues with a protonatable tertiary nitrogen formed reactive metabolites that were subsequently trapped. This finding was expected as it occurs for tertiary amine containing compounds. In the glutathione trapping experiments, the benzoxazole analogues did not form reactive metabolites that could be trapped. The benzothiazole analogues showed the highest potential for bioactivation as evidenced by high glutathione trapping ratios when compared to clozapine, the positive control. The benzimidazole and pyridyl analogues showed successively lower potentials for bioactivation. From these results, it was concluded that the benzoxazole series had the lowest bioactivation risk.

The third objective was to carry out antiplasmodial assays on the synthesized analogues. For the representative set of compounds, this was done in parallel with the bioactivation studies. The results showed that benzothiazole and benzoxazole analogues with protonatable tertiary nitrogens had potent antiplasmodial acitivity against two chloroquine resistant *P*. *falciparum* strains. Weaker but noteworthy activity was also observed in the benzimidazole and pyridyl series. Based on the antiplasmodial data and results from the bioactivation studies, the benzothiazole series was selected for expanded SAR studies.

The second synthetic campaign involved the synthesis of 4-amino-7-chloroquinoline-coupled benzoxazole analogues bearing diverse amino groups on the benzoxazole ring. These included simple alkyl, cycloalkylamino, dialkylamino, aminobenzyl, aminopyridyl, alkylpiperazine and arylpiperazine groups.

Antiplasmodial assays on the expanded benzoxazole series confirmed that the tertiary protonatable nitrogen was essential for potent antiplasmodial activity, as was the 4-amino-7-chloroquinoline ring. Ethyldialkylamino and ethylcycloalkylamino analogues were generally more potent than their corresponding propyl linker analogues. Mechanistic evaluation was conducted using the β-hematin formation inhibition assay, premised on the fact that these compounds would act similarly to amodiauine. There was generally a weak correlation between β-hematin activity and antiplasmodial potency even though most of the potent antiplasmodial compounds were also potent β-hematin formation inhibitors. Dialkylamino analogues with potent antiplasmodial activity exhibited weak β-hematin formation inhibition activity.

In vitro metabolic stability studies revealed moderate to excellent stability in compounds with potent antiplasmodial activity. This informed the selection of analogues **3.9b**, **3.9c** and **3.9j** for *in vivo* evaluation.

As a final objective, *in vivo* efficacy studies were conducted on analogues **3.9b**, **3.9c** and **3.9j** in *P*. *berghei* infected mice at four daily oral doses of 50 mg/kg. All the three compounds efficiently suppressed parasitemia by >99% relative to the control. Analogue **3.9b** cured all three treated mice while analogues **3.9c** and **3.9j** cured 1/3 and 2/3 of treated mice, respectively. Mice treated with **3.9b** and **3.9j** survived the entire thirty day duration of the experiment while one of the three mice treated with **3.9c** died on day 21 resulting in an average of 27 mouse survival days for this compound.

5.2 RECOMMENDATIONS FOR FUTURE WORK

The potent *in vitro* antiplasmodial and *in vivo* antimalarial activity of benzoxazole amodiaquine analogues demonstrated in this project necessitates further more detailed toxicity studies on these compounds. In particular, the use of MS methods and actual drug substrates for CYP3A4 inhibition studies will provide useful information to guide any further development of this class of compounds. At the same time, *in vivo* pharmacokinetic studies will be provide valuable insights into the performance of these compounds in animal models.

Further structural modifications to incorporate secondary instead of tertiary amines are needed. Other modifications will include the lengthening of the carbon linker in analogue **3.9w** as this may result in improved activity due to an increase in the pKa of the tertiary nitrogen. The effect of replacing the 7-chloro group on the quinoline ring with various groups also needs to be investigated.

Finally, only cycloalkylamino compounds were selected for *in vivo* efficacy studies in this project. However, the dialkylamino analogues **3.9e** and **3.9f** also showed high potency and, especially in the case of **3.9f** which would have been expected to be demethylated with ease, surprisingly excellent metabolic stability. These analogues would be interesting candidates for future *in vivo* efficacy studies.

Chapter 6

EXPERIMENTAL

6.1 REAGENTS AND SOLVENTS

2-((dimethylamino)methyl)benzoxazol-5-amine and 2-(2-methoxyethyl)benzoxazol-5-amine were sourced from Ukrorgsyntez Ltd, Riga, Latvia.. The rest of the commercially available chemicals and reagents were purchased from Sigma Aldrich and were of analytical grade quality. Acetonitrile, tetrahydrofuran and DMF were purchased from Sigma-Aldrich. South Africa. Methanol, ethanol, ethyl acetate, dichloromethane and hexane were obtained from Kimix Chemicals or Protea Chemicals, South Africa. Bulk solvents were purchased either as Chemically Pure (CP) grade solvents and distilled prior to use or as Analytical Reagent (AR) grade solvents and used as such.

6.2 CHROMATOGRAPHY

Reactions were monitored by thin layer chromatography (TLC) using Fluka or Merck F_{254} aluminium-backed pre-coated silica gel plates and were visualized under ultraviolet light at 254 nm. Silica gel column chromatography was performed using Merck kieselgel 60: 70-230 mesh by gravity column chromatography or flash column chromatography on a Biotage Isolera™ system (Biotage AB, Uppsala, Sweden). HPLC purity checks were performed as per the methods listed in Table 6.1.

Table 6.1: HPLC conditions

Method	Time (min)	% A	% B	Composition A	Composition B	Reversed phase column parameters
A	0.0-14.5 14.5-19.5 19.5-20.0 20.0-25.0	75 0 0 75	25 100 100 25	10 mM NH_4OAc in HPLC grade H_2O	10 mM NH_4OAc in 90 % HPLC grade CH_3OH in H_2O	Kinetex™ 2.6 µ C_{18} 100Å LC column, 150 x 2.1 mm (Phenomenex, Torrance, CA, USA)
B	0.0-7.0 7.0-10.0 10.0-12.0 12.0-15.0	100 0 0 100	0 100 100 0	5% CH_3CN in H_2O	5% H_2O in CH_3CN	Luna® 3µm C_{18} 100Å LC column, 150 x 4.6 mm (Phenomenex, Torrance, CA, USA)
C	0.0-0.5 0.5-2.5 2.5-6.0 6.0-8.0	90 90 10 90	10 10 90 10	10 mM NH_4OAc in HPLC grade H_2O	10 mM NH_4OAc in 90 % HPLC grade CH_3OH in H_2O	Zorbax SB-C_{18} 2.7 µm, LC column, 50 x2.1 mm, (Agilent Technologies, Santa Clara, CA, USA)
D	0.0-4.0 4.0-7.0 7.0-14.0 14.0-15.0	20 5 100 20	80 95 0 80	01 % NH_4OH in HPLC grade H_2O	0.1 % NH_4OH in HPLC grade CH_3OH	Luna® 3µm C_{18} 100Å LC column, 150 x 4.6 mm (Phenomenex, Torrance, CA, USA)

6.3 PHYSICAL AND SPECTROSCOPIC CHARACTERIZATION

Melting points were determined using a Reichert-Jung Thermovar hot stage microscope and are uncorrected. ^{1}H NMR spectra were recorded on a Varian Mercury (300MHz), a Varian Unity (400 MHz) or a Bruker Ultrashield-Plus (400MHz) spectrometer. NMR samples were dissolved in deuterated chloroform ($CDCl_3$), dimethylsulfoxide (DMSO-d6) or methanol (CD_3OD) with tetramethylsilane as the internal standard. ^{13}C NMR spectra were recorded on the same instruments at 75 or 100 MHz. Chemical shifts (δ) are reported in parts per million (ppm) to 2 decimal places downfield from the internal standard tetramethylsilane (TMS). Coupling constants (*J*) are reported in Hertz (Hz) to one decimal place. Abbreviations used in assigning ^{l}H-NMR signals are: d (doublet), dd (doublet of doublets), ddd (doublet of doublet of doublets), m (multiplet), q (quartet), s (singlet), t (triplet) or td (triplet of doublets). High resolution mass spectrometry (ESI) was performed using a Waters API Q-TOF Ultima instrument at Stellenbosch University,

Cape Town, while low resolution mass spectrometry (LRMS) (EI^+) was performed on a JEOL GC Mate III instrument at the University of Cape Town.

6.4 SYNTHESIS

2-Bromo-5-nitrobenzothiazole, 2.2

CuBr (64.5 mg, 0.45 mmol, 1 eq) and 2-amino-6-nitrobenzothiazole (701.5 mg, 3.60 mmol, 8 eq) were added to a solution of 3 ml of 48% HBr in 12 ml of water. The suspension was stirred at room temperature for 10 minutes. Sodium nitrate (2140.0 mg, 31.00 mmol, 69 eq) was slowly added in small portions into the suspension, allowing for the evolution of nitrogen gas to stop before each addition, and the reaction mixture was stirred for a further 4 h. The mixture was filtered under suction and washed with water until the filtrate appeared colorless. The product was dried for 48 hour and used without further purification.

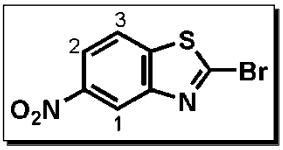

As a brown solid (0.773 g, 83 %); m.p. 189-190 °C; R_f (EtOAc: Hexane, 7:3) 0.5; δ_H (300 MHz, DMSO-*d6*) 9.14 (1H, s, H1), 8.33 (1H, d, *J* = 8.4 Hz, H2), 8.17 (1H, d, *J* = 8.4 Hz, H3).

2-Bromo-5-nitropyridine, 2.4 (DS25)

CuBr (362.2 mg, 2.52 mmol, 1 eq) and 2-amino-5-nitropyridine (2810.11 mg, 20.20 mmol, 8 eq) were added to a solution of 18 ml of 48% HBr in 32 ml of water. The suspension was stirred at room temperature for 10 minutes. Sodium nitrate (12020.0 mg, 174.21 mmol, 69 eq) was slowly added in small portions into the suspension, allowing for the evolution of nitrogen gas to stop before each addition, and the reaction

mixture was stirred for a further 4 h. The reaction mixture was filtered, washed with water, dried and purified using silica gel column chromatography (EtOAC: Hexane 2:3 to 3:2).

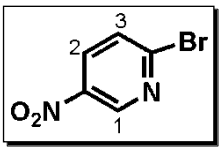

As an off-white powder (1,230 mg, 30 %); m.p. 132-134 °C; R_f (EtOAc: Hexane, 3:2) 0.4; δ_H (300 MHz, $CDCl_3$) 9.20 (1H, d, *J* = 2. 8 Hz, H1), 8.32 (1H, dd, *J* = 8.7, 2.8 Hz, H2), 7.71 (1H, d, *J* = 8.7 Hz, H3).

General procedure for the synthesis of benzoxazole-2-thiol compounds

Potassium ethyl xanthate (1872.4 mg, 11.7 mmol, 2 eq) was added to a solution of 2-amino-4-nitrophenol or 2-amino-4-chloronitrophenol (5.8 mmol, 1 eq) in 25 ml of absolute ethanol. The reaction was heated at reflux for 4 h. The reaction mixture was then cooled to room temperature and concentrated to dryness under vacuum. The residue was dissolved in water and acidified to pH 5 using acetic acid. The resulting precipitate was filtered, washed with water and dried for 48 h to give the products which were used without further purification.

5-Nitrobenzoxazole-2-thiol, 2.8

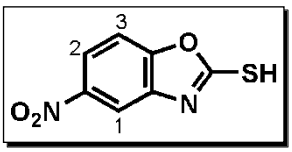

As a yellow powder (1,091 mg, 95 %); m.p. 239-240 °C; R_f (EtOAc: Hexane, 2:3) 0.63; δ_H (300 MHz, DMSO-*d6*) 8.16 (1H, dd, *J* = 8.9, 2.4 Hz, H2), 7.92 (1H, d, *J* = 2.4 Hz, H1), 7.69 (1H, d, *J* = 8.9 Hz, H3).

5-Chlorobenzoxazole-2-thiol, 2.11 (DS59)

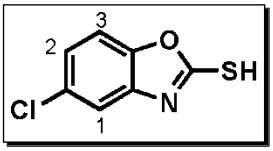

As a pale pink powder (970 mg, 89 %); m.p. 247-250 °C; R_f (EtOAc: Hexane, 2:3) 0.63; δ_H (400 MHz, DMSO-*d6*) 8.16 (1H, d, *J* = 9.0 Hz, H3), 7.30 (1H, dd, *J* = 9.0, 2.4 Hz, H2), 7.29 (1H, s, H1).

General procedure for synthesis of 2-(methylthio)-benzoxazole analogues

Iodomethane (1.2 eq) and anhydrous potassium carbonate (1 eq) were added to a solution of 5-nitrobenzoxazole-2-thiol or 5-chlorobenzoxazole-2-thiol (1 eq) in acetonitrile (15 ml). The reaction mixture was stirred at room temperature for 4h. The reaction was quenched with a drop of water and the solvent removed under vacuum. The residue was suspended in water and extracted three times with ethyl acetate. The combined organic fractions were washed with brine (1x10ml) and dried over $MgSO_4$. Solvent evaporation under vacuum yielded the products which were used without further purification.

2-(Methylthio)-5-nitrobenzoxazole, 2.9

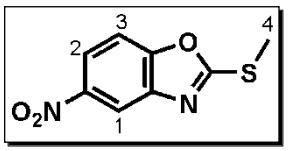

As a pale pink powder (483 mg, 90 %); m.p. 147-148 °C; R_f (EtOAc: Hexane, 2:3) 0.83; δ_H (400 MHz, $CDCl_3$) 8.49 (1H. d, *J* = 2.5 Hz, H1), 8.24 (1H, dd, *J* = 8.9, 2.3 Hz, H2), 7.54 (1H, d, *J* = 8.9 Hz, H3), 2.82 (3H, s, H4).

5-Chloro-2-(methylthio)benzoxazole, 2.12 (DS60)

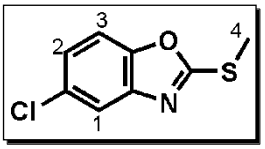

As a yellowish pink solid (2,920 mg, 91 %); m.p. 89-90 °C; R_f (Hexane: EtOAc, 3:7) 0.70; δ_H ($CDCl_3$, 400 MHz) 7.60 (1H, d, *J* = 2.1 Hz, H1), 7.24 (1H, dd, *J* = 8.6, 2.1 Hz, H2), 7.37 (1H, d, *J* = 8.6 Hz, H3), 2.79 (3H, s, H4)

2-Bromo-5-nitro-1H-benzimidazole, 2.6

2-mercapto-5-nitrobenzimidazole (546.6 mg, 2.8 mmol, 1 eq)) was added to a cooled solution of acetic acid (4 ml) and 48% aqueous HBr (0.42 ml, 3.7 mmol, 1.3 eq).

Bromine (0.52 ml, 10.1 mmol, 3.6 eq) was slowly added dropwise to this slurry. The reaction mixture solidified after addition of a few drops and was manually agitated to break up the solids. When all the bromine was added, acetic acid (8 ml) was added and the mixture was stirred at room temperature. After 4.5 h, the mixture was diluted with water and cooled to 0 °C. The pH of the mixture was adjusted to pH 4 using solid NaOH. The solid that precipitated out of solution was filtered under suction, washed with water, dried for 48 h and used without further purification.

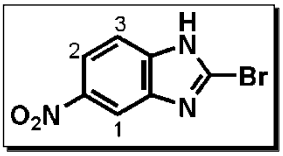

As a grey powder (0.543 g, 80 %); m.p. 229-230 °C; R_f (EtOAc: Hexane, 3:2) 0.6; δ_H (400 MHz, DMSO) 8.32 (1H, d, *J* = 2.3 Hz, H1), 8.03 (1H, dd, *J* = 8.9, 2.3 Hz, H2), 7.60 (1H, d, *J* = 8.9 Hz, H3).

General procedure for the synthesis of alkylamine substituted nitrobenzothiazoles

2-bromo-5-nitrobenzothiazole (1 eq) was dissolved in THF with warming. Ethylamine solution (70 % in water) or *tert*-butylamine (3 eq) and anhydrous potassium carbonate (1.5 eq) were added to the solution and the reaction mixture was stirred at 40-50 °C for 15 hours. The solvent was removed under vacuum. The residue was suspended in water, extracted with EtOAC (3 x 20 ml) and washed with brine (1 x 20 ml). The combined organic extracts were dried over anhydrous $MgSO_4$ and purified by silica gel column chromatography eluting with EtOAC: Hexane (10% to 70%).

***N-Tert-butyl-5-nitrobenzothiazol-2-amine*, 2.2a (DS1B)**

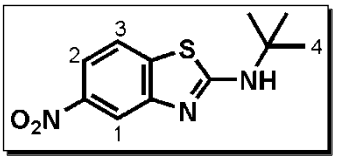

As a yellow solid (254 mg, 78 %); m.p. 64-65 °C; R_f (EtOAc: Hexane, 1:7) 0.40; δ_H (400 MHz, $CDCl_3$) 8.43 (1H, s, H1), 8.12 (1H, d, *J* = 8.2 Hz, H2), 7.46 (1H, d, *J* = 8.2 Hz, H3) 1.50 (9H, s, H4); δ_C (101 MHz, $CDCl_3$) 168.22, 157.93, 142.04, 131.01, 122.27, 118.25, 116.93, 54.41, 28.92; LRMS (EI) *m/z,* 251.05 (M^+ $C_{11}H_{13}N_3O_2S$ requires 251.07).

***N-Ethyl-5-nitrobenzothiazol-2-amine,* 2.2b (DS1C)**

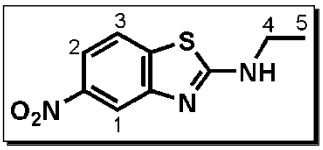

As a yellow powder (224 mg, 93 %); m.p. 208-209 °C; R_f (EtOAc: Hexane, 7:3) 0.60; δ_H (300 MHz, DMSO-*d6*) 8.65 (1H, d, *J* = 2.5 Hz, H1), 8.09 (1H, dd, *J* = 8.9, 2.5 Hz, H2), 7.45 (1H, d, *J* = 8.9 Hz, H3), 3.44 (2H, q, *J* = 7.2 Hz, H4), 1.23 (3H, t, *J* = 7.2 Hz, H5); δ_C (101 MHz, $CDCl_3$) 170.87, 157.84, 142.25, 133.68, 122.39, 118.15, 117.23, 40.56, 14.63;

***N-Ethyl-5-nitrobenzoxazol-2-amine,* 2.9a (DS4C)**

Ethylamine solution (70 % in water) (3 eq) was added to a solution of 2-(methylthio)-5-nitrobenzoxazole (1 eq) in 20 ml of DMF. The reaction mixture was heated at 80 °C for 15 hours after which the solvent was removed under vacuum. The residue was purified by silica gel column chromatography eluting with 50 % EtOAC:Hexane.

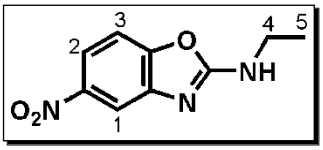

As a yellow powder (191 mg, 87 %); m.p. 130-131 °C; R_f (EtOAc: Hexane, 3:2) 0.30; δ_H (300 MHz, $CDCl_3$) 8.17 (1H, d, *J* = 2.3 Hz, H1), 8.00 (1H, dd, *J* = 8.8, 2.3 Hz, H2), 7.29 (1H, d, *J* = 8.8 Hz, H3), 3.57 (2H, q, *J* = 7.2 Hz, H4), 1.35 (3H, t, *J* = 7.2 Hz, H5); δ_C (101 MHz, $CDCl_3$) 163.66, 152.52, 145.20, 144.08, 117.36, 111.85, 108.33, 38.22, 15.01; LRMS (EI) *m/z,* 207.05 (M^+ $C_9H_9N_3O_3$requires 207.06).

General procedure for amination reactions

A mixture of 2-bromo-5-nitrobenzothiazole, 2-bromo-5-nitro-1H-benzimidazole, 2-bromo-5-nitropyridine, 2-(methylthio)-5-nitrobenzoxazole, 5-chloro-2-(methylthio)-benzoxazole, (1 eq) and the appropriate amine (3 eq) in acetonitrile was heated in a microwave reactor at 120 °C for 20-30 min. The solvent was removed under vacuum and the residue dissolved in EtOAc, washed with water (2x10 ml), a solution of saturated $NaHCO_3$ (only employed when bromo-substituted reactants were used to neutralize HBr), brine (10 ml) and dried over $MgSO_4$. The solvent was removed under vacuum to obtain the products in crude mixture. Column chromatography using a MeOH: EtOAc (0-20%) (for tertiary amine products) or a hexane: EtOAc gradient afforded the pure products.

***5-Nitro-N-(2-(pyrrolidin-1-yl)ethyl)benzothiazol-2-amine,* 2.2c (DS11)**

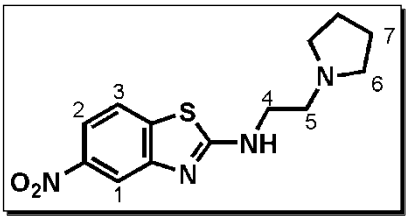

As a yellow powder (230 mg, 87 %), m.p. 133-135 °C; R_f (MeOH: DCM: NH_4OH, 10:88:2) 0.50; δ_H (400 MHz, $CDCl_3$) 8.48 (1H, d, *J* = 2.4 Hz, H1), 8.18 (1H, dd, *J* = 8.9, 2.34 Hz, H2), 7.50 (1H, d, *J* = 8.9 Hz, H3), 6.57, 3.57 (2H, t, *J* = 5.9 Hz, H4), 2.80 (2H, t, *J* = 5.9 Hz, H5), 2.59 (4H, m, H6), 1.81 (4H, m, H7); δ_C (101 MHz, $CDCl_3$) 170.75, 164.01, 157.99, 122.45, 117.95, 117.24, 53.81, 53.69, 43.51 (x2), 23.56 (x2); LRMS (EI) *m/z,* 292.09 (M^+ $C_{13}H_{16}N_4O_2S$ requires 292.10).

***5-Nitro-N-(2-(piperidin-1-yl)ethyl)benzothiazol-2-amine,* 2.2d (DS12)**

As a yellow powder (258 mg, 90 %), m.p. 130-131 °C; R_f (MeOH: DCM: NH_4OH, 10:88:2) 0.50; δ_H (400 MHz, CD_3OD) 8.49 (1H, d, *J* = 2.4 Hz, H1), 8.11 (1H, dd, *J* = 8.9

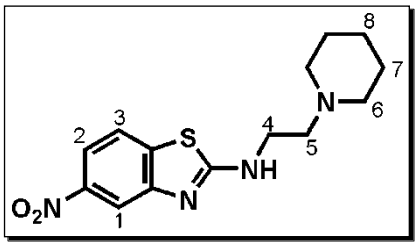

Hz, 2.4 Hz, H2), 7.42 (1H, d, *J* = 8.9 Hz, H3), 3.62 (2H, t, *J* = 6.7 Hz, H4), 2.66 (2H, t, *J* = 6.7 Hz, H5), 2.53 (4H, m, H6), 1.61 (4H, m, H7), 1.46 (2H, m, H8); δ_C (101 MHz, CD_3OD) 171.36, 157.61, 141.78, 130.83, 121.77, 116.93, 116.90, 57.06, 54.13, 41.31 (x2), 25.10 (x2), 23.63; LRMS (EI) *m/z,* 306.12 (M^+ $C_{14}H_{18}N_4O_2S$ requires 306.12).

***N-(2-Morpholinoethyl)-5-nitrobenzothiazol-2-amine,* 2.2e (DS13)**

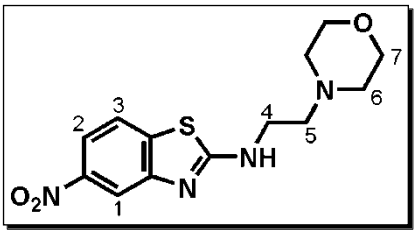

As a yellow powder (228 mg, 81 %), m.p. 128-130 °C; R_f (MeOH: DCM: NH_4OH, 10:88:2) 0.60; δ_H (400 MHz, CD_3OD) 8.34 (1H, d, *J* = 2.4 Hz, H1), 8.00 (1H, dd, *J* = 8.9, 2.4 Hz, H2), 7.30 (1H, d, *J* = 8.9 Hz, H3), 3.65 (4H, m, H7), 3.55 (2H, t, *J* = 6.5 Hz, H4), 2.60 (2H, t, *J* = 6.5 Hz, H5), 2.48 (4H, m, H6); δ_C (101 MHz, CD_3OD) 171.20, 157.48, 141.60, 130.68, 121.64, 116.753, 110.89, 66.28 (x2), 56.67, 53.18 (x2), 41.07; LRMS (EI) *m/z,* 308.10 (M^+ $C_{13}H_{16}N_4O_3S$ requires 308.09).

***N^1,N^1-Diethyl-N^2-(5-nitrobenzothiazol-2-yl)ethane-1,2-diamine,* 2.2f (DS18)**

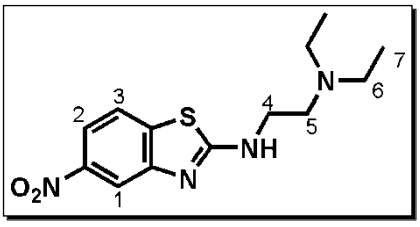

As a yellow powder (218 mg, 76 %), m.p. 94-96 °C; R_f (MeOH: DCM: NH_4OH, 10:88:2) 0.40; δ_H (400 MHz, $CDCl_3$) 8.42 (1H, d, *J* = 2. 4 Hz, H1), 8.07 (1H, dd, *J* = 8.9, 2.4 Hz, H2), 7.37 (1H, d, *J* = 8.9 Hz, H3), 3.57 (2H, t, *J* = 6.9 Hz, H4), 2.78 (2H, t, *J* = 6.9 Hz, H5), 2.65 (4H, q, *J* = 7.2 Hz, H6), 1.07 (6H, t, *J* = 7.2 Hz, H7). δ_C (101 MHz, CD_3OD) 171.19, 157.50, 141.56, 130.68, 121.62, 116.79,

116.72, 50.86, 46.70, 41.74 (x2), 10.12 (x2); LRMS (EI) *m/z,* 294.13 (M^+ $C_{13}H_{18}N_4O_2S$ requires 294.12).

***N-Ethyl-5-nitro-1H-benzimidazol-2-amine,* 2.6a (DS5C)**

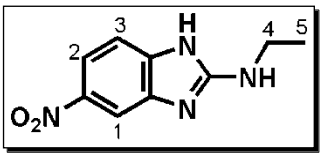

As a yellow powder (188 mg, 92 %); m.p. 204-205 °C; R_f (EtOAc: Hexane, 3:2) 0.24; δ_H (300 MHz, DMSO-*d6*) 7.94 (1H, d, *J* = 2.6 Hz, H1), 7.86 (1H, dd, *J* = 8.7, 2.6 Hz, H2), 7.20 (1H, d, *J* = 8.7 Hz, H3), 2.83 (2H, q, *J* = 7.6 Hz, H4), 1.19 (3H, t, *J* = 7.6 Hz, H5); LRMS (EI) *m/z,* 206.06 (M^+ $C_9H_{10}N_4O_2$ requires 206.08).

***5-Nitro-N-(2-(piperidin-1-yl)ethyl)-1H-benzimidazol-2-amine,* 2.6b (DS21)**

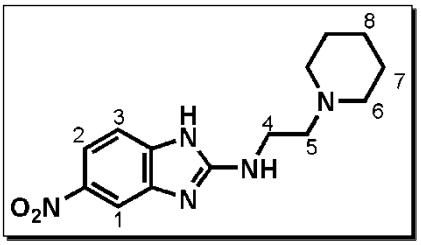

As a yellow powder (202 mg, 86 %), m.p. 155-158 °C; R_f (MeOH: DCM: NH_4OH, 10:86:4) 0.50; δ_H (400 MHz, $CDCl_3$) 8.01 (1H, d, *J* = 2.2 Hz, H1), 7.93 (1H, dd, *J* = 8.7, 2.2 Hz, H2), 7.16 (1H, d, *J* = 8.7 Hz, H3), 3.59 (2H, t, *J* = 5.0 Hz, H4), 2.87 (2H, t, *J* = 5.0 Hz, H5), 2.79 (4H, m, H6), 1.77 (4H, m, H7), 1.59 (2H, m, H8); δ_C (101 MHz, $CDCl_3$) 159.84, 145.32, 141.38, 136.69, 117.60, 111.76, 107.34, 59.62, 54.39, 39.90 (x2), 25.18 (x2), 23.21; LRMS (EI) *m/z,* 289.17 (M^+ $C_{14}H_{19}N_5O_2$ requires 289.15).

***N-(2-Morpholinoethyl)-5-nitro-1H-benzimidazol-2-amine,* 2.6c (DS22)**

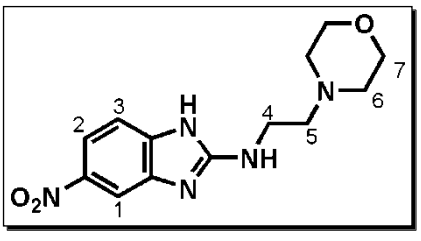

As a yellow powder (215 mg, 84 %), m.p. 186-187 °C; R_f (MeOH: DCM: NH_4OH, 10:86:4) 0.60; δ_H (300 MHz, $CDCl_3$) 7.82 (1H, d, *J* = 2.2 Hz, H1), 7.68 (1H, dd, *J* =

8.7, 2.2 Hz, H2), 6.99 (1H, d, *J* = 8.7 Hz, H3), 3.43 (4H, m, H7), 3.36 (2H, t, *J* = 5.9 Hz, H4), 2.42 (2H, t, *J* = 5.9 Hz, H5), 2.27 (4H, m, H6); δ_C (101 MHz, $CDCl_3$) 158.33, 145.05, 140.30, 136.15, 116.72, 110.96, 106.38, 66.10 (x2), 56.90, 52.71 (x2), 38.94; LRMS (EI) *m/z,* 291.13, (M^+ $C_{13}H_{17}N_5O_3$ requires 291.13).

***N^1,N^1-Diethyl-N2-(5-nitro-1H-benzimidazol-2-yl)ethane-1,2-diamine,* 2.6d (DS24)**

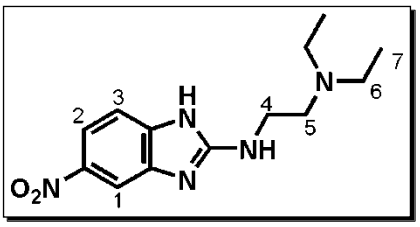

As a yellow powder (241 mg, 83 %), m.p. 93-94 °C; R_f (MeOH: DCM: NH_4OH, 10:86:4) 0.50; δ_H (400 MHz, $CDCl_3$) 8.07 (1H, d, *J* = 2. 2 Hz, H1), 8.02 (1H, dd, *J* = 8.7, 2.2 Hz, H2), 7.22 (1H, d, *J* = 8.7 Hz, H3), 3.53 (2H, t, *J* = 4.5 Hz, H4), 2.86 (2H, t, *J* = 4.5 Hz, H5), 2.80 (4H, q, *J* = 7.2 Hz, H6), 1.20 (6H, t, *J* = 7.2 Hz, H7); δ_C (101 MHz, CD_3OD) 171.63, 162.09, 158.33, 142.01, 117.20, 111.73, 107.19, 60.24, 53.44, 38.11 (x2), 8.03 (x2); LRMS (EI) *m/z,* 277.16 (M^+ $C_{13}H_{19}N_5O_2$ requires 277.15).

5-Nitro-N-(2-(pyrrolidin-1-yl)ethyl)pyridin-2-amine, 2.4a (DS26)

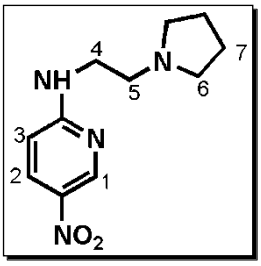

As a yellow powder (238 mg, 65 %), m.p. 195-196 °C; R_f (MeOH: DCM: NH_4OH, 10:88:2) 0.50; δ_H (300 MHz, CD_3OD) 8.97 (1H, d, *J* = 2.7 Hz, H1), 8.17 (1H, dd, *J* = 9.3, 2.7 Hz, H2), 6.69 (1H, d, *J* = 9.3 Hz, H3), 3.86 (2H, t, *J* = 6.0 Hz, H4), 3.46 (2H, t, *J* = 6.0 Hz, H5), 3.43 (4H, m, H6), 2.09 (4H, m, H7); δ_C (101 MHz, CD_3OD) 161.58, 145.95, 136.19, 132.15, 108.83, 54.52, 54.35, 37.65 (x2), 22.73 (x2); LRMS (EI) *m/z,* 236.07 (M^+ $C_{11}H_{16}N_4O_2$ requires 236.13).

N-(2-Morpholinoethyl)-5-nitropyridin-2-amine, 2.4b (DS27)

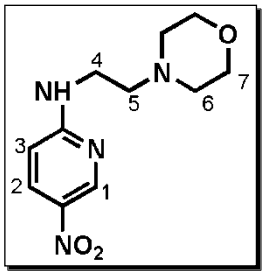

As a yellow powder (202 mg, 77 %), m.p. 56-58 °C; R_f (MeOH: DCM: NH_4OH, 10:88:2) 0.60; δ_H (400 MHz, $CDCl_3$) 8.91 (1H, d, *J* = 2.7 Hz, H1), 8.07 (1H, d, *J* = 9.0 Hz, H2), 6.34 (1H, d, *J* = 9.0 Hz, H3), 3.66 (4H, m, H7), 3.44 (2H, t, *J* = 6.4 Hz, H4), 2.59 (2H, t, *J* = 6.4 Hz, H5), 2.44 (4H, m, H6); δ_C (101 MHz, $CDCl_3$) 161.00, 147.00 (x2), 135.85, 132.79, 66.87 (x2), 56.54, 53.28 (x2), 38.04; LRMS (EI) *m/z,* 252.09 (M^+ $C_{11}H_{16}N_4O_3$ requires 252.12).

***5-Nitro-N-(2-(pyrrolidin-1-yl)ethyl)benzoxazol-2-amine,* 2.9b (DS23)**

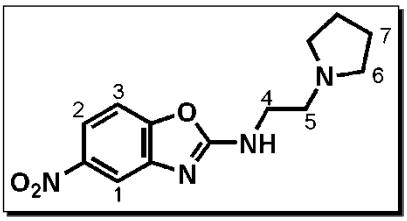

As a yellow powder (222 mg, 80 %), m.p. 89-90 °C; R_f (MeOH: DCM: NH_4OH, 10:86:4) 0.70; δ_H (400 MHz, $CDCl_3$) 7.86 (1H, d, *J* = 2.3 Hz, H1), 7.59 (1H, dd, *J* = 8.7, 2.3 Hz, H2), 6.82 (1H, d, *J* = 8.7 Hz, H3), 3.52 (2H, t, *J* = 5.6 Hz, H4), 2.81 (2H, t, *J* = 5.6 Hz, H5), 2.60 (4H, m, H6), 1.74 (4H, m, H7); δ_C (101 MHz, $CDCl_3$) 163.84, 152.48, 144.98, 144.08, 117.02, 111.51, 108.02, 54.31, 53.78, 41.29 (x2), 23.46 (x2); LRMS (EI) *m/z,* 276.15 (M^+ $C_{13}H_{16}N_4O_3$ requires 276.12).

***5-Nitro-N-(2-(piperidin-1-yl)ethyl)benzoxazol-2-amine,* 2.9c (DS46)**

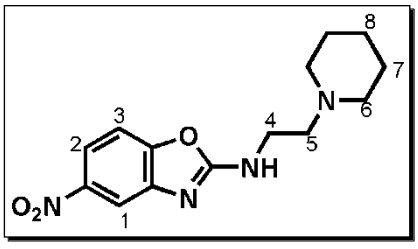

As a yellow solid (213 mg, 62 %); m.p. 82-84 °C; R_f (MeOH: EtOAc, 20:80) 0.30; δ_H ($CDCl_3$, 300 MHz) 8.08 (1H, d, *J*=2.0 Hz, H1), 7.91 (1H, dd, *J*=8.7, 2.0 Hz, H2), 7.18 (1H, d, *J*=8.7 Hz, H3), 3.52 (2H, t, *J*=5.8 Hz, H4), 2.60 (2H, t, *J*=5.8 Hz, H5), 2.51 – 2.35 (4H, m, H6), 1.70 – 1.50 (4H, m, H7), 1.46 – 1.31 (2H, m, H8); δ_C (101 MHz, $CDCl_3$) 163.76, 152.50, 145.01, 143.98, 117.17, 111.53,

108.17, 56.86, 54.27, 39.23 (x2), 25.57 (x2), 24.04; LRMS (EI) *m/z,* 290.14 (M^+ $C_{14}H_{18}N_4O_3$ requires 290.14).

***N-(2-Morpholinoethyl)-5-nitrobenzoxazol-2-amine,* 2.9d (DS31)**

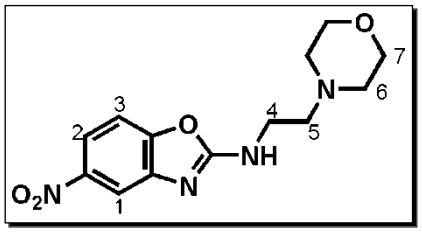

As yellow crystals (250 mg, 62 %); m.p. 151-153 °C; R_f (MeOH: EtOAc, 20:80) 0.57; δ_H ($CDCl_3$, 400 MHz) 8.08 (1H, d, *J*=2.3 Hz, H1), 7.92 (1H, dd, *J*=8.8, 2.3 Hz, H2), 7.20 (1H, d, *J*=8.8 Hz, H3), 3.66 (4H, t, *J*=4.6 Hz, H7), 3.52 (2H, t, *J*=5.7 Hz, H4), 2.60 (2H, t, *J*=5.7 Hz, H5), 2.45 (4H, t, *J*=4.6 Hz, H6); δ_C (101 MHz, $CDCl_3$) 163.66, 152.59, 145.34, 144.17, 117.33, 111.98, 108.22, 66.85 (x2), 56.69, 53.35 (x2), 39.26; LRMS (EI) *m/z,* 292.00 (M^+ $C_{13}H_{16}N_4O_4$ requires 292.12).

***N^1,N^1-Diethyl-N^2-(5-nitrobenzoxazol-2-yl)ethane-1,2-diamine,* 2.9e (DS33)**

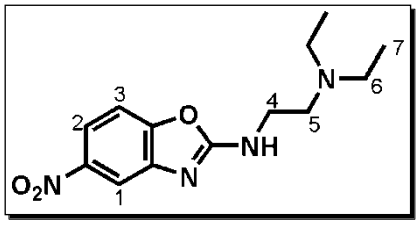

As a yellow solid (182 mg, 65%); m.p. 58-60 °C; R_f (MeOH: EtOAc, 20:80) 0.31; δ_H ($CDCl_3$, 400 MHz) 8.01 (1H, d, *J*=2.3 Hz, H1), 7.84 (1H, dd, *J*=8.7, 2.3 Hz, H2), 7.13 (1H, d, *J*=8.7 Hz, H3), 3.43 (2H, t, *J*=5.9 Hz, H4), 2.65 (2H, t, *J*=5.9 Hz, H5), 2.51 (4H, q, *J*=7.1 Hz, H6), 0.94 (6H, t, *J*=7.1 Hz, H7); δ_C (101 MHz, $CDCl_3$)163.84, 152.60, 145.02, 144.17, 117.15, 111.59, 108.19, 51.17, 46.61, 40.26 (x2), 11.46 (x2); LRMS (EI) *m/z,* 278.14 (M^+ $C_{13}H_{18}N_4O_3$ requires 278.14).

***N^1,N^1-Dimethyl-N^2-(5-nitrobenzoxazol-2-yl)ethane-1,2-diamine,* 2.9f (DS50)**

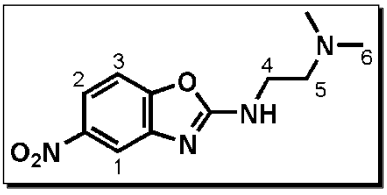

As an orange solid (161 mg, 52 %); m.p. 123-126 °C; R_f (MeOH: EtOAc, 20:80) 0.60; δ_H ($CDCl_3$, 400 MHz) 8.14

(1H, d, *J*=2.3 Hz, H1), 7.93 (1H, dd, *J*=8.7, 2.3 Hz, H2), 7.19 (1H, d, *J*=8.7 Hz, H3), 3.56 (2H, t, *J*=5.8 Hz, H4), 2.61 (2H, t, *J*=5.8 Hz, H5), 2.30 (6H, s, H6); δ_C (101 MHz, CD_3OD) 164.56, 152.45, 145.07, 143.69, 116.91, 114.25, 112.74, 110.22, 109.01, 108.21, 57.56, 44.04, 39.96 (x2); LRMS (EI) *m/z,* 250.10 (M^+ $C_{11}H_{14}N_4O_3$ requires 250.11).

***1-(3-(5-Nitrobenzoxazol-2-ylamino)propyl)pyrrolidin-2-one,* 2.9g (DS34)**

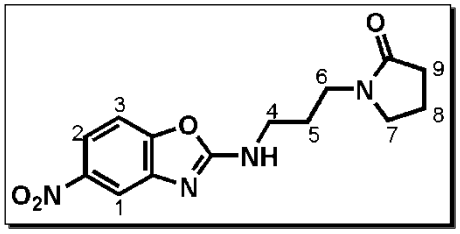

As a brown solid (125 mg, 41%); m.p. 116-118 °C; R_f (EtOAc) 0.61; δ_H ($CDCl_3$, 400 MHz) 8.05 (1H, d, *J*=2.3 Hz, H1), 7.89 (1H, dd, *J*=8.7, 2.3 Hz, H2), 7.18 (1H, d, *J*=8.7 Hz, H3), 3.42 – 3.29 (6H, m, H4, H6, H7), 2.37 (2H, t, *J*=8.1 Hz, H9), 1.95 – 2.04 (2H, m, H8), 1.85 – 1.73 (2H, m, H5); δ_C (101 MHz, $CDCl_3$) δ 176.38, 163.87, 152.65, 145.06, 144.14, 117.24, 111.55, 108.24, 47.57, 39.46, 39.42, 30.84, 26.21, 17.97; LRMS (EI) *m/z,* 304.13 (M^+ $C_{14}H_{16}N_4O_4$ requires 304.12).

***N^1,N^1-Diethyl-N^3-(5-nitrobenzoxazol-2-yl)propane-1,3-diamine,* 2.9h (DS36)**

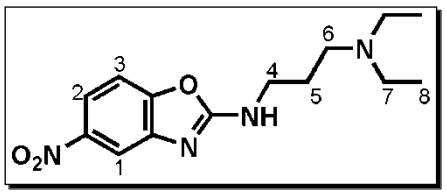

As a yellow resin (201 mg, 68 %); R_f (MeOH: EtOAc, 20:80) 0.32; δ_H ($CDCl_3$, 400 MHz) 8.03 (1H, d, *J*=2.3 Hz, H1), 7.87 (1H, dd, *J*=8.6, 2.3 Hz, H2), 7.16 (1H, d, *J*=8.6 Hz, H3), 3.53 (2H, t, *J*=5.9 Hz, H4), 2.63 (2H, t, *J*=5.9 Hz, H6), 2.55 (4H, q, *J*=7.2 Hz, H7), 1.80 – 1.74 (2H, m, H5), 1.03 (6H, t, *J*=7.2 Hz, H8); δ_C (101 MHz, $CDCl_3$) 163.88, 152.65, 145.14, 144.49, 116.91, 111.45, 107.96, 52.67, 46.93, 43.70 (x2), 24.83, 11.31 (x2); LRMS (EI) *m/z,* 292.22 (M^+ $C_{14}H_{20}N_4O_3$ requires 292.15).

***N^1,N^1-Dimethyl-N^3-(5-nitrobenzoxazol-2-yl)propane-1,3-diamine,* 2.9i (DS37)**

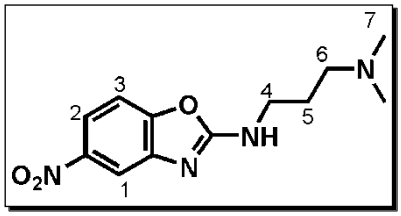

As a yellow solid (192 mg, 61 %); m.p. 67-69 °C; R_f (MeOH: EtOAc, 20:80) 0.31; δ_H ($CDCl_3$, 400 MHz) 7.93 (1H, d, *J*=2.2 Hz, H1), 7.76 (1H, dd, *J*=8.8, 2.2 Hz, H2), 7.07 (1H, d, *J*=8.8 Hz, H3), 3.42 (2H, t, *J*=6.3 Hz, H4), 2.34 (2H, t, *J*=6.3 Hz, H6), 2.11 (6H, s, H7), 1.72 – 1.65 (2H, m, H5); δ_C (101 MHz, $CDCl_3$) 163.99, 152.50, 144.85, 144.25, 116.83, 111.13, 108.00, 58.35, 45.21, 43.10, 25.61 (x2); LRMS (EI) *m/z,* 264.11 (M^+ $C_{12}H_{16}N_4O_3$ requires 264.12).

***5-Nitro-N-(3-(piperidin-1-yl)propyl)benzoxazol-2-amine,* 2.9j (DS48)**

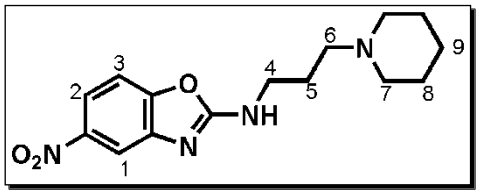

As a yellow solid (207 mg, 69 %); m.p. 95-97 °C; R_f (MeOH: EtOAc, 20:80) 0.31; δ_H ($CDCl_3$, 400 MHz) 8.01 (1H, d, *J*=2.3 Hz, H1), 7.86 (1H, dd, *J*=8.7, 2.3 Hz, H2), 7.17 (1H, d, *J*=8.7 Hz, H3), 3.53 (2H, t, *J*=6.0 Hz, H4), 2.56 (2H, t, *J*=6.1 Hz, H6), 2.53 – 2.39 (4H, m, H7), 1.82 (1H, p, *J*=6.1 Hz, H5), 1.67 – 1.56 (4H, m, H8), 1.48 – 1.38 (2H, m, H9); δ_C (101 MHz, $CDCl_3$) 163.97, 152.61, 144.99, 144.42, 116.83, 111.25, 107.96, 57.71, 54.33, 43.28 (x2), 25.53, 24.20 (x2), 23.88; LRMS (EI) *m/z,* 304.13 (M^+ $C_{15}H_{20}N_4O_3$ requires 304.15).

***5-Nitro-N-(3-(piperidin-1-yl)propyl)benzo[d]oxazol-2-amine,* 2.9k (DS56)**

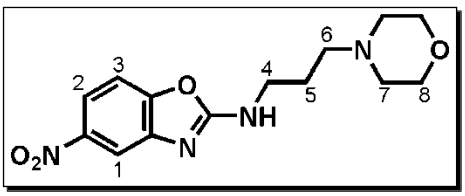

As a yellow solid (162 mg, 53 %); m.p. 94-96 °C; R_f (MeOH: EtOAc, 20:80) 0.65; δ_H ($CDCl_3$, 400 MHz) 8.11 (1H, d, *J*=2.3 Hz, H1), 7.97 (1H, dd, *J*=8.7, 2.3 Hz, H2), 7.26 (1H, d, *J*=8.7 Hz, H3), 3.80 – 3.70 (4H, m, H8), 3.61 (2H, t, *J*=6.0 Hz, H4), 2.59 (2H, t, *J*=6.0 Hz, H6), 2.55 – 2.49 (4H, m, H7), 1.93 – 1.78 (2H, m, H5); δ_C (101

MHz, $CDCl_3$) 163.73, 152.58, 145.10, 144.31, 117.20, 111.67, 108.13, 67.03 (x2), 58.20, 53.72 (x2), 43.82, 24.02; LRMS (EI) *m/z,* 306.12 (M^+ $C_{14}H_{18}N_4O_4$ requires 306.13).

***N-(4-Methylpiperazin-1-yl)-5-nitrobenzoxazol-2-amine,* 2.9l (DS41)**

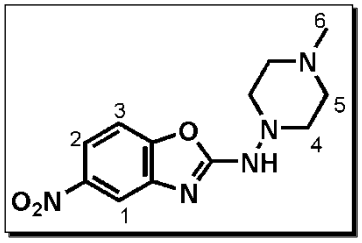

As a yellow solid (210 mg, 76 %); m.p. 129-131 °C; R_f (MeOH: EtOAc, 20:80) 0.60; δ_H ($CDCl_3$, 400 MHz) 8.10 (1H, d, *J*=2.2 Hz, H1), 7.94 (1H, dd, *J*=8.7, 2.2 Hz, H2), 7.26 (1H, d, *J*=8.7 Hz, H3), 3.74 (4H, t, *J*=5.1 Hz, H4), 2.53 (4H, t, *J*=5.1 Hz, H5), 2.34 (3H, s, H6); δ_C (101 MHz, $CDCl_3$) 163.58, 152.66, 145.33, 144.16, 117.01, 111.67, 108.23, 54.05 (x2), 46.00, 45.51 (x2); LRMS (EI) *m/z,* 262.08 (M-15) (M^+ $C_{12}H_{15}N_5O_3$ requires 277.12).

***N-(3-Chlorobenzyl)-5-nitrobenzoxazol-2-amine,* 2.9m (DS42)**

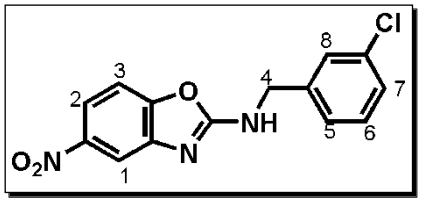

As yellow crystals (180 mg, 59 %); m.p. 140-142 °C; R_f (EtOAc: Hexane, 30:70) 0.14; δ_H (DMSO, 400 MHz) 8.01 (1H, d, *J*=2.4 Hz, H1), 7.94 (1H, dd, *J*=8.7, 2.4 Hz, H2), 7.58 (1H, d, *J*=8.7 Hz, H3), 7.43 (1H, s, H8), 7.28 – 7.38 (3H, m, H5, H6, H7), 4.56 (2H, s, H4); δ_C (101 MHz, DMSO) 164.70, 152.96, 144.98, 144.50, 141.45, 133.59, 130.82, 127.66, 127.54, 126.38, 117.49, 110.91, 109.38, 45.69; LRMS (EI) *m/z,* 303.01 (M^+ $C_{14}H_{10}ClN_3O_3$ requires 303.04).

***5-Nitro-N-(3-(trifluoromethyl)benzyl)benzoxazol-2-amine,* 2.9n (DS54)**

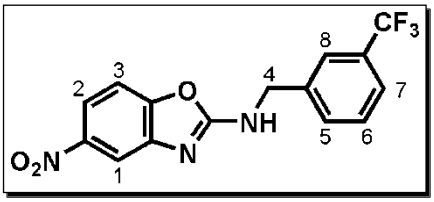

As a brown solid (221 mg, 84 %); m.p. 156-158 °C; R_f (Hexane: EtOAc, 30:70) 0.20; δ_H (DMSO, 400 MHz) 8.02 (1H, d, *J*=2.4 Hz, H1), 7.95 (1H, dd, *J*=9.2, 2.4 Hz, H2), 7.75 – 7.67 (2H, m, H3, H7), 7.65 – 7.55 (3H, m, H5, H6, H8), 4.66 (2H, s, H4); δ_C (101 MHz, DMSO) 164.72, 152.97, 144.99, 144.47, 140.38, 131.88, 130.04, 124.49, 124.45, 124.32, 124.27, 117.53, 110.93, 109.41, 45.79; LRMS (EI) *m/z,* 337.08 (M^+ $C_{15}H_{10}F_3N_3O_3$ requires 337.07).

***5-Nitro-N-(pyridin-2-ylmethyl)benzoxazol-2-amine,* 2.9o (DS32)**

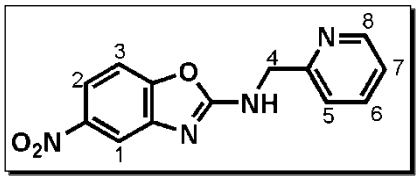

As a yellow solid (140 mg, 52 %); m.p. 142-144 °C; R_f (EtOAc) 0.70; δ_H (DMSO, 400 MHz) 8.52 (1H, d, *J*=4.8 Hz, H8), 8.00 (1H, d, *J*=2.4 Hz, H1), 7.94 (1H, dd, *J*=8.7, 2.4 Hz, H2), 7.76 (1H, td, *J*=7.8 (x2), 1.8 Hz, H6), 7.58 (1H, d, *J*=8.7 Hz, H3), 7.41 (1H, d, *J*=7.8 Hz, H5), 7.28 (1H, dd, *J*=7.3, 5.1 Hz, H7), 4.65 (2H, s); δ_C (101 MHz, DMSO) 164.94, 158.00, 152.99, 149.55, 144.98, 144.58, 137.38, 122.95, 121.59, 117.44, 110.87, 109.36, 47.99; LRMS (EI) *m/z,* 270.06 (M^+ $C_{13}H_{10}N_4O_3$ requires 270.08).

***5-Nitro-N-(pyridin-3-ylmethyl)benzoxazol-2-amine,* 2.9p (DS35)**

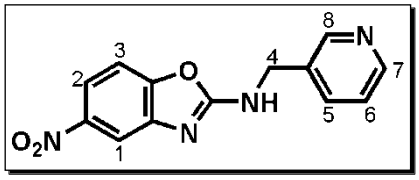

As brown crystals (218 mg, 81%); m.p. 189-191 °C; R_f (EtOAc) 0.70; δ_H (CD_3OD, 400 MHz) 8.61 (1H, d, *J*=2.2 Hz, H8), 8.47 (1H, dd, *J*=4.9, 1.6 Hz, H7), 8.07 (1H, d, *J*=2.3 Hz, H1), 8.01 (1H, dd, *J*=8.8, 2.3 Hz, H2), 7.95 – 7.87 (1H, m, H6), 7.44 (1H, d, *J*=8.8 Hz, H3), 7.45 – 7.41 (m, 1H, H5), 4.67 (4H, s, H4); δ_C (101 MHz, DMSO) 164.65,

152.97, 149.31, 149.03, 144.97, 144.48, 135.66, 134.30, 124.03, 117.50, 110.93, 109.36, 43.98; LRMS (EI) *m/z,* 270.11 (M^+ $C_{13}H_{10}N_4O_3$ requires 270.08).

***5-Nitro-N-(pyridin-4-ylmethyl)benzoxazol-2-amine,* 2.9q (DS47)**

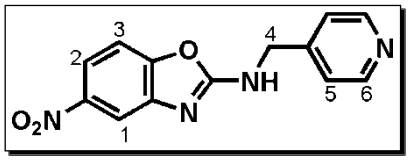

As an orange solid (127 mg, 38 %); m.p. 206-208 °C; R_f (EtOAc) 0.70; δ_H ($CDCl_3$, 400 MHz) 8.61 (2H, d, *J*=6.1 Hz, H6), 8.21 (1H, d, *J*=2.3 Hz, H1), 8.05 (1H, dd, *J*=8.8, 2.3 Hz, H2), 7.34 (1H, d, *J*=8.8 Hz, H3), 7.32 (2H, d, *J*=6.1 Hz, H5), 4.74 (2H, s, H4); δ_C (101 MHz, DMSO) 164.74, 152.99, 150.16 (x2), 147.83, 144.99, 144.42, 122.49 (x2), 117.56, 111.00, 109.43, 45.20; LRMS (EI) *m/z,* 270.04 (M^+ $C_{13}H_{10}N_4O_3$ requires 270.08).

***5-Nitro-N-(2-(pyridin-2-yl)ethyl)benzoxazol-2-amine,* 2.9r (DS49)**

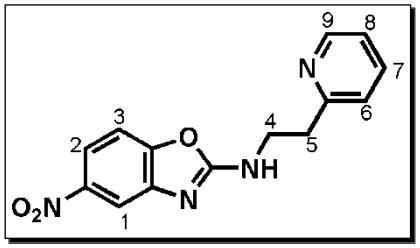

As an orange solid (254 mg, 60 %); m.p. 179-180 °C; R_f (EtOAc) 0.80; δ_H (DMSO, 400 MHz) 8.49 (1H, ddd, *J*=4.8, 1.8, 1.0 Hz, H9), 8.00 (1H, d, *J*=2.4 Hz, H1), 7.92 (1H, dd, *J*=8.7, 2.4 Hz, H2), 7.68 (1H, td, *J*=7.6, 1.9 Hz, H7), 7.53 (1H, d, *J*=8.7 Hz, H3), 7.28 (1H, m, H6), 7.20 (1H, ddd, *J*=7.6, 4.9, 1.0 Hz, H8), 3.71 (2H, t, *J*=7.2 Hz, H4), 3.07 (2H, t, *J*=7.2 Hz, H5); δ_C (101 MHz, DMSO) 164.59, 159.01, 152.85, 149.58, 144.92, 144.79, 136.95, 123.77, 122.08, 117.22, 110.63, 109.15, 42.54, 37.33; LRMS (EI) *m/z,* 284.10 (M^+ $C_{14}H_{12}N_4O_3$ requires 284.09).

***N,N-Diethyl-5-nitrobenzoxazol-2-amine,* 2.9s (DS39)**

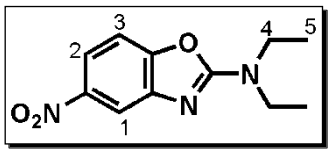

As a brown solid (132 mg, 56 %); m.p. 79-80°C; R_f (EtOAc: Hexane, 20:80) 0.31; δ_H ($CDCl_3$, 400 MHz) 8.02 (1H, d, *J*=2.3 Hz, H1), 7.84 (1H, dd, *J*=8.7, 2.3 Hz, H2), 7.17 (1H, d, *J*=8.7 Hz, H3), 3.52 (4H, q, *J*=7.2 Hz, H4), 1.21 (6H, t, *J*=7.2 Hz, H5); δ_C (101 MHz, $CDCl_3$) 163.72, 152.84, 145.16, 144.63, 116.56, 111.25, 108.02, 43.27 (x2), 13.35 (x2); LRMS (EI) *m/z,* 235.03 (M^+ $C_{11}H_{13}N_3O_3$ requires 235.10).

***2-(4-Methylpiperazin-1-yl)-5-nitrobenzoxazole,* 2.9t (DS51)**

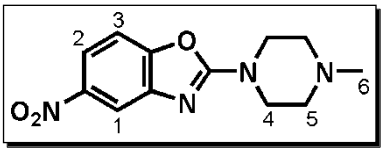

As a yellow solid (191 mg, 70 %); m.p. 135-136 °C; R_f (EtOAc) 0.60; δ_H ($CDCl_3$, 300 MHz) 8.03 (1H, d, *J*=2.3 Hz, H1), 7.88 (1H, dd, *J*=8.7, 2.3 Hz, H2), 7.20 (1H, d, *J*=8.7 Hz, H3), 3.68 (4H, t, *J*=5.1 Hz, H4), 2.46 (4H, t, *J*=5.1 Hz, H5), 2.28 (3H, s, H6); δ_C (101 MHz, $CDCl_3$) 163.58, 152.70, 145.27, 144.21, 117.13, 111.77, 108.28, 54.13 (x2), 46.18, 45.57 (x2); LRMS (EI) *m/z,* 262.10 (M^+ $C_{12}H_{14}N_4O_3$ requires 262.11).

***5-Nitro-2-(4-phenylpiperazin-1-yl)benzoxazole,* 2.9u (DS52)**

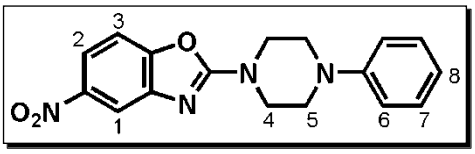

As a yellow solid (234 mg, 77 %); m.p. 178-180 °C; R_f (Hexane: EtOAc, 40:60) 0.50; δ_H ($CDCl_3$, 300 MHz) 8.13 (1H, d, *J*=2.4 Hz, H1), 7.95 (1H, dd, *J*=9.0, 2.4 Hz, H2), 7.38 – 7.14 (3H, m, H3, H7), 7.03 – 6.76 (3H, m, H6, H8), 3.98 – 3.71 (4H, m, H5), 3.41 – 3.15 (4H, m, H4); δ_C (101 MHz, $CDCl_3$) 163.50, 152.72, 150.88, 145.33, 144.12, 129.34 (x2), 121.02, 117.28, 117.06 (x2), 111.91, 108.40, 49.21 (x2), 45.64 (x2); LRMS (EI) *m/z,* 324.14 (M^+ $C_{17}H_{16}N_4O_3$ requires 324.12).

2-(4-(3-Chlorophenyl)piperazin-1-yl)-5-nitrobenzoxazole, 2.9v (DS53)

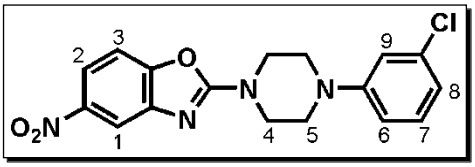

As a yellow solid (202 mg, 72 %); m.p. 155-157 °C; R_f (Hexane: EtOAc, 40:60) 0.60; δ_H ($CDCl_3$, 400 MHz) 8.19 (1H, d, *J*=2.2 Hz, H1), 8.02 (1H, dd, *J*=8.8, 2.2 Hz, H2), 7.33 (2H, d, *J*=8.8 Hz, H3), 7.21 (1H, t, *J*=8.1 Hz, H7), 6.97 – 6.77 (3H, m, H6, H8, H9), 3.89 (4H, t, *J*=5.2 Hz, H5), 3.33 (4H, t, *J*=5.2 Hz, H4); δ_C (101 MHz, $CDCl_3$) 163.41, 152.70, 151.89, 145.36, 144.03, 135.18, 130.27, 120.69, 117.39, 116.86, 114.85, 112.03, 108.46, 48.72 (x2), 45.44 (x2); LRMS (EI) *m/z,* 358.11 (M^+ $C_{17}H_{15}ClN_4O_3$ requires 358.08).

***N^1-(5-Chlorobenzoxazol-2-yl)-N^2,N^2-diethylethane-1,2-diamine,* 2.12a (DS61)**

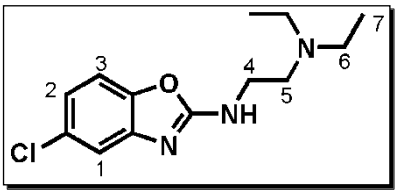

As an off-white solid (121 mg, 33 %) m.p. 54-56 °C; R_f (MeOH: EtOAc, 20:80) 0.36; δ_H (CD_3OD, 400 MHz) 7.19 (1H, d, *J*=2.0 Hz, H1) 7.17 (1H, d, *J*=8.4 Hz, H3) 6.96 (1H, dd, *J*=8.4, 2.0 Hz, H2) 3.44 - 3.50 (2H, m, H4) 2.68 - 2.74 (2H, m, H5) 2.60 (4H, q, *J*=7.1 Hz, H6) 1.04 (6H, t, *J*=7.1 Hz, H7); δ_C (CD_3OD, 75 MHz) 163.80, 147.10, 144.15, 129.08, 120.36, 115.19, 109.21, 51.67, 47.05, 40.31 (x2), 10.70 (x2); LRMS (EI) *m/z,* 267.08 (M^+ $C_{13}H_{18}ClN_3O$ requires 267.11).

***5-Chloro-2-(4-phenylpiperazin-1-yl)benzoxazole,* 2.12b (DS62)**

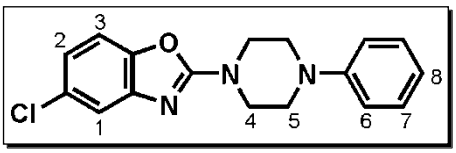

As a pink solid (127 mg, 46 %); m.p. 145-146 °C; R_f (Hexane: EtOAc, 30:70) 0.70; δ_H ($CDCl_3$, 400 MHz) 7.33 (1H, d, *J*=1.9 Hz), 7.32 – 7.24 (2H, m, H7), 7.16 (1H, d, *J*=8.4 Hz), 7.00 (1H, dd, *J*=8.1, 1.9 Hz), 6.98 – 6.90 (3H, m, H6, H8), 3.86 (4H, t, *J*=5.2 Hz, H5), 3.30 (4H, t, *J*=5.2 Hz, H6); δ_C (101 MHz, $CDCl_3$) 162.83, 151.01, 147.44,

144.49, 129.30 (x2), 120.85, 120.65, 116.99 (x2), 116.53, 109.28, 49.19 (x2), 45.58 (x2); LRMS (EI) *m/z,* 313.07 (M^+ $C_{17}H_{16}ClN_3O$ requires 313.10).

General procedure for the coupling of aromatic amines with 4,7-dichloroquinoline

The aromatic nitro-compound (1 mmol) was dissolved in ethanol (8 ml) with warming in a hydrogenator bottle. 10% Pd/C (0.3 times the weight of the compound being reduced) was added to this solution. The reaction bottle was sealed, filled with H_2 and evacuated twice. It was then shaken on a Parr shaker for 12 h at 60 psi of H_2 until completion of the reaction (monitored by TLC). The reaction mixture was filtered through Celite and the solvent removed under vacuum to obtain the aromatic amine. The aromatic amine (1 mmol, 1 eq) was mixed with 4,7-dichloroquinoline (1.1 eq) in acetonitrile (25 ml). The mixture was acidified with 3-5 drops of HCl and stirred at reflux for 24 h. The solvent was removed under vacuum after which the residue was dissolved in EtOAc (or 20% methanol in dichloromethane for tertiary amine compounds) and washed with saturated $NaHCO_3$ (3x20 ml) and brine (1x10ml). The combined organic fractions were dried over anhydrous $MgSO_4$, adsorbed onto silica gel (5g) and subjected to silica gel column chromatography to afford the target compounds.

***N^5-(7-Chloroquinolin-4-yl)-N^2-ethylbenzothiazole-2,5-diamine,* 3.2a (DS1F)**

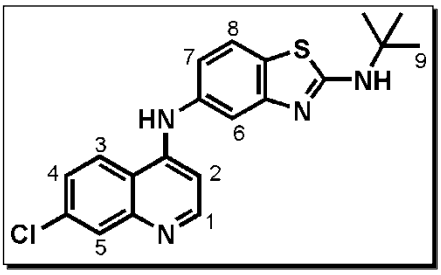

As a yellow powder (41 mg, 21 %); m.p. 209-210 °C; R_f (MeOH:DCM, 10:90) 0.58; δ_H (400 MHz, $CDCl_3$) 8.51 (1H, d, *J* = 5.3 Hz, H1), 8.04 (1H, d, *J* = 2.1 Hz, H5), 7.88 (1H, d, *J* = 8.9 Hz, H3), 7.58 (1H, d, *J* = 8.5 Hz, H8), 7.50 (1H, d, *J* = 2.2 Hz, H6), 7.43 (1H, dd, *J* = 8.9, 2.1 Hz, H4), 7.19 (1H, dd, *J* =

8.5, 2.2 Hz, H7), 6.74 (1H, d, *J* = 5.3 Hz, H2), 1.54 (9H, s, H9); δ_C (101 MHz, $CDCl_3$) 164.59, 151.91, 150.92, 149.73, 148.94, 135.20, 133.12, 132.09, 129.03, 125.84, 122.86, 121.05, 119.82, 117.75, 116.57, 102.01, 53.61, 29.10 (3C); HRMS (ESI) *m/z*, 383.1097 ($[M+H]^+$ $C_{20}H_{20}N_4SCl$ requires 383.1097); HPLC Purity (Method A): >99 %, t_R = 13.70 min.

***N^5-(7-Chloroquinolin-4-yl)-N^2-ethylbenzo[d]thiazole-2,5-diamine,* 3.2b (DS1G)**

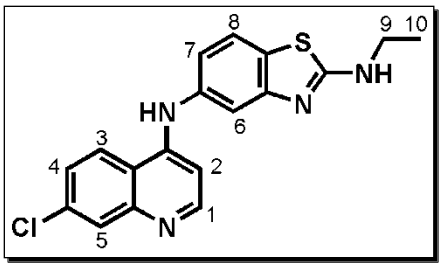

As a yellow powder (52 mg, 42 %); m.p. 281-282 °C; R_f (MeOH: DCM) 0.59; δ_H (400 MHz, DMSO) 8.43 (1H, d, *J* = 9.1 Hz, H3), 8.40 (1H, d, *J* = 5.4 Hz, H1), 7.86 (1H, d, *J* = 2..2 Hz, H5), 7.65 (1H, d, *J* = 2.2 Hz, H6), 7.52 (1H, dd, *J* = 9.1, 2.2 Hz, H4), 7.43 (1H, d, *J* = 8.5 Hz, H8), 7.20 (1H, dd, *J* = 8.5, 2.2 Hz, H7), 6.68 (1H, d, *J* = 5.4 Hz, H2), 3.41 (2H, q, *J* = 7.2 Hz, H9), 1.22 (3H, t, *J* = 7.2 Hz, H10); δ_C (101 MHz, DMSO) 166.47, 152.40, 150.76, 149.96, 149.68, 134.24, 133.41, 131.62, 128.06, 125.13, 124.77, 122.99, 118.77, 118.36, 117.42, 101.45, 29.43, 14.92; LRMS (EI) *m/z,* 354.05 (M^+ $C_{18}H_{15}ClN_4S$ requires 354.07); HPLC Purity (Method A): >99 %, t_R = 12.70 min.

***N^5-(7-Chloroquinolin-4-yl)-N^2-(2-(pyrrolidin-1-yl)ethyl)benzo[d]thiazole-2,5-diamine,* 3.2c (DS11B)**

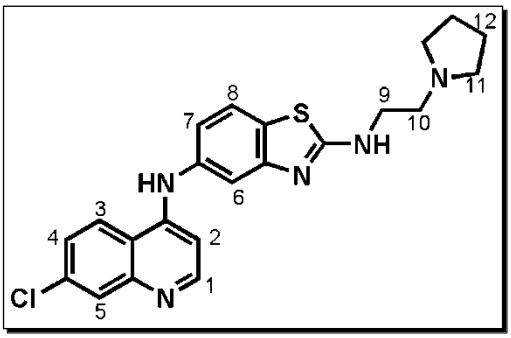

As a yellow powder (96 mg, 47 %); m.p. 126-128 °C; R_f (MeOH: DCM: NH_4OH, 10:88:2) 0.47; m.p. δ_H (400 MHz, CD_3OD) 8.32 (1H, d, *J* = 5.6 Hz, H1), 8.26 (1H, d, *J* = 9.0 Hz, H3), 7.84 (1H, d, *J* =

2.2 Hz, H5), 7.60 (1H, d, *J* = 2.1 Hz, H6), 7.50 (1H, d, *J* = 8.5 Hz, H8), 7.47 (1H, dd, *J* = 9.0, 2.2 Hz, H4), 7.26 (1H, dd, *J* = 8.5, 2.2 Hz, H7), 6.73 (1H, d, *J* = 5.6 Hz, H2), 3.66 (2H, t, *J* = 6.6 Hz, H9), 2.93 (2H, t, *J* = 6.6 Hz, 10), 2.79 (4H, m, H11), 1.88 (4H, m, H12); δ_C (101 MHz, CD_3OD) 169.61, 157.30, 152.81, 144.15, 141.15, 140.58, 133.48, 131.99, 128.97, 126.51, 124.84, 120.47, 119.59, 117.20, 101.52, 55.54, 55.39, 41.58 (x2), 24.04 (x2); HRMS (ESI) *m/z*, 424.1361 ($[M+1]^+$ $C_{22}H_{23}N_5SCl$ requires 424.1363); HPLC Purity (Method D): >99 %, t_R = 9.46 min.

***N^5-(7-Chloroquinolin-4-yl)-N^2-(2-(piperidin-1-yl)ethyl)benzo[d]thiazole-2,5-diamine,* 3.2d (DS12B)**

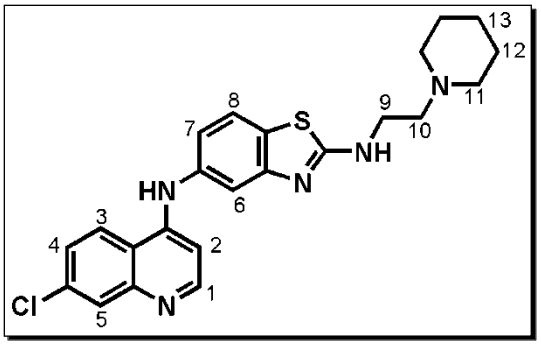

As a yellow powder (106 mg, 53 %); m.p. 170-174 °C; R_f (MeOH: DCM: NH_4OH, 10:88:2) 0.40; δ_H (400 MHz, CD_3OD) 8.33 (1H, d, *J* = 5.8 Hz, H1), 8.29 (1H, d, *J* = 8.6 Hz, H3), 7.85 (1H, d, *J* = 2.1 Hz, H5), 7.64 (1H, d, *J* = 2.1 Hz, H6), 7.52 (1H, d, *J* = 8.5 Hz, H8), 7.49 (1H, dd, *J* = 8.6, 2.2 Hz, H4), 7.23 (1H, dd, *J* = 8.5, 2.2 Hz, H7), 6.75 (1H, d, *J* = 5.8 Hz, H2), 3.74 (2H, t, *J* = 6.03 Hz, H13), 3.04 (2H, t, *J* = 6.03 Hz, H14), 2.96 (4H, m, H15), 1.79 (4H, m, H16), 1.62 (2H, m, H17); δ_C (101 MHz, $CDCl_3$) 167.19, 151.58, 150.75, 149.25, 149.11, 135.34, 132.33, 131.86, 128.57, 125.90, 123.01, 121.43, 119.41, 117.61, 116.95, 101.73, 56.78, 54.23, 41.22 (x2), 25.56 (x2), 24.05; HRMS (ESI) *m/z*, 438.1516 ($[M+H]^+$ $C_{23}H_{25}N_5SCl$ requires 438.1519); HPLC Purity (Method D): >99 %, t_R = 9.76 min.

***N^5-(7-Chloroquinolin-4-yl)-N^2-(2-morpholinoethyl)benzo[d]thiazole-2,5-diamine,* 3.2e (DS13B)**

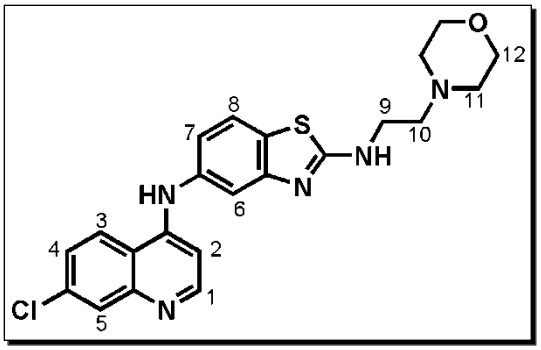

As a yellow powder (91 mg, 45 %); m.p. 162-166 °C; R_f (MeOH: DCM: NH_4OH, 10:88:2) 0.54; δ_H (400 MHz, CD_3OD) 8.27 (1H, d, *J* = 5.6 Hz, H1), 8.20 (1H, d, *J* = 9.0 Hz, H3), 7.81 (1H, d, *J* = 2.2 Hz, H5), 7.53 (1H, d, *J* = 2.2 Hz, H6), 7.45 (1H, d, *J* = 8.5 Hz, H8), 7.41 (1H, dd, *J* = 9.0, 2.2 Hz, H4), 7.21 (1H, dd, *J* = 8.5, 2.2 Hz, H7), 6.69 (1H, d, *J* = 5.6 Hz, H2), 3.68 (4H, m, H12), 3.56 (2H, t, *J* = 6.5 Hz, H9), 2.62 (2H, t, *J* = 6.5 Hz, H10), 2.50 (4H, m, H11); δ_C (101 MHz, CD_3OD) 169.23, 152.60, 151.53, 151.35, 149.01, 137.06, 134.42, 132.49, 126.91, 126.67, 124.54, 124.24, 119.59, 118.95, 118.38, 102.16, 67.79 (x2), 58.40, 54.74, 42.58 (x2); HRMS (ESI) *m/z*, 440.1300 ($[M+H]^+$ $C_{22}H_{23}N_5OSCl$ requires 440.1312); HPLC Purity (Method D): >99 %, t_R = 4.96 min.

***N^5-(7-Chloroquinolin-4-yl)-N^2-(2-(diethylamino)ethyl)benzo[d]thiazole-2,5-diamine,* 3.2f (DS18B)**

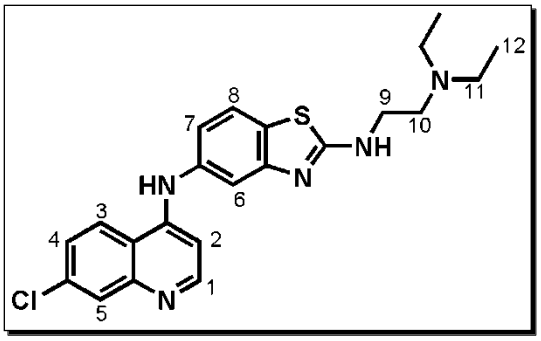

As a yellow powder (66 mg, 49 %); m.p. 136-137 °C; R_f (MeOH: DCM: NH_4OH, 10:88:2) 0.40; δ_H (400 MHz, CD_3OD) 8.32 (1H, d, *J* = 5.6 Hz, H1), 8.26 (1H, d, *J* = 9.0 Hz, H3), 7.84 (1H, d, *J* = 2.2 Hz, H5), 7.59 (1H, d, *J* = 2.2 Hz, H6), 7.48 (1H, d, *J* = 8.5 Hz, H8), 7.47 (1H, dd, *J* = 9.0, 2.2 Hz, H4), 7.26 (1H, dd, *J* = 8.5, 2.2 Hz, H7), 6.73 (1H, d, *J* = 5.6 Hz, H2), 3.56 (2H, t, *J* = 6.9 Hz, H9), 2.78 (2H, t, *J* = 6.9 Hz, H10), 2.65 (4H, q, *J* = 7.2 Hz, H11), 1.09 (6H, t, *J* = 7.2 Hz, H12); δ_C (101 MHz, $CDCl_3$)

167.38, 151.81, 150.83, 149.66, 149.18, 135.15, 133.15, 128.3, 125.69, 122.99, 121.53, 119.42, 117.85, 116.85, 101.92, 51.44, 46.78, 42.74 (x2), 11.75 (x2); HRMS (ESI) *m/z*, 426.1518, ($[M+H]^+$ $C_{22}H_{25}N_5SCl$ requires 426.1519); HPLC Purity (Method A): >99 %, t_R = 13.04 min.

***N^5-(7-Chloroquinolin-4-yl)-N^2-ethyl-1H-benzimidazole-2,5-diamine,* 3.6a (DS5G)**

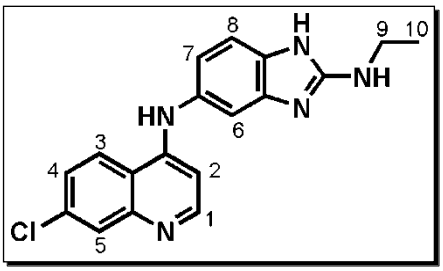

As an orange powder (350 mg, 26 %); m.p. 189-190 °C; R_f (MeOH:DCM, 10:90) 0.61; δ_H (300 MHz, CD_3OD) 8.38 (1H, d, *J* = 9.1 Hz, H3), 8.25 (1H, d, *J* = 6.3 Hz, H1), 7.82 (1H, d, *J* = 2.1 Hz, H5), 7.53 (1H, dd, *J* = 9.1, 2.1 Hz, H4), 7.29 (1H, d, *J* = 8.3 Hz, H8), 7.24 (1H, d, *J* = 2.0 Hz, H6), 7.03 (1H, dd, *J* = 8.3, 2.0 Hz, H7), 6.72 (1H, d, *J* = 6.3 Hz, H2), 3.43 (2H, q, *J* = 7.3 Hz, H9), 1.30 (3H, t, *J* = 7.3 Hz, H10); δ_C (101 MHz, CD_3OD) δ 155.43, 153.25, 147.24, 144.74, 137.14, 134.74, 131.51, 126.07, 123.99, 123.11, 117.47, 111.63, 111.37, 108.62, 100.40, 97.84, 37.36, 13.84; HRMS (ESI) *m/z*, 338.1164 ($[M+H]^+$ $C_{18}H_{17}N_5Cl$ requires 338.1172); HPLC Purity (Method D): >99 %, t_R = 4.90 min.

***N^5-(7-Chloroquinolin-4-yl)-N^2-(2-(piperidin-1-yl)ethyl)-1H-benzo[d]imidazole-2,5-diamine,* 3.6b (DS21B)**

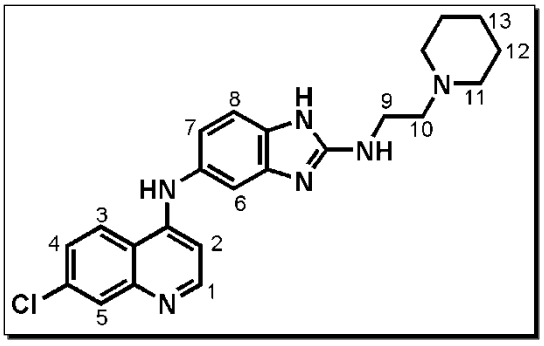

As a yellow powder (80 mg, 63 %); m.p. 153-156 °C; R_f (MeOH: DCM: NH_4OH, 10:88:2) 0.42; δ_H (400 MHz, CD_3OD) 8.27 (1H, d, *J* = 9.0 Hz, H3), 8.26 (1H, d, *J* = 5.6 Hz, H1), 7.82 (1H, d, *J* = 2.1 Hz, H5), 7.44 (1H, dd, *J* = 9.0, 2.2 Hz, H4), 7.25 (1H, d, *J* = 8.3 Hz, H8), 7.20 (1H, d, *J* = 2.0 Hz, H6), 6.98 (1H, dd, *J* = 8.3, 2.0

Hz, H7), 6.66 (1H, d, *J* = 5.6 Hz, H2), 3.54 (2H, t, *J* = 6.2 Hz, H9), 2.70 (2H, t, *J* = 6.2 Hz, H10), 2.60 (4H, m, H11), 1.67 (4H, m, H12), 1.53 (2H, m, H13); δ_C (101 MHz, CD_3OD) 156.52, 151.51, 150.62, 148.44, 135.32, 132.33, 126.05, 125.95, 125.02, 123.25, 117.73, 117.65, 111.75, 108.96, 100.48, 58.28, 53.92, 39.01 (x2), 24.80 (x2), 23.12; HRMS (ESI) *m/z*, 421.1900 ($[M+H]^+$ $C_{23}H_{26}N_6Cl$ requires 421.1907); HPLC Purity (Method D): >99 %, t_R = 9.04 min.

***N^5-(7-Chloroquinolin-4-yl)-N^2-(2-morpholinoethyl)-1H-benzo[d]imidazole-2,5-diamine,* 3.6c (DS22B)**

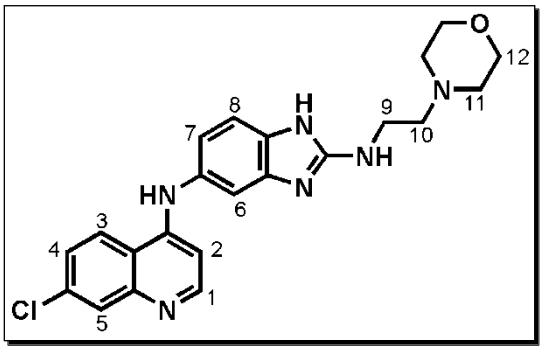

As a yellow powder (124 mg, 71 %); m.p. 149-150 °C; R_f (MeOH: DCM: NH_4OH, 10:88:2) 0.63; δ_H (400 MHz, CD_3OD) 8.20 (1H, d, *J* = 9.2 Hz, H3), 8.19 (1H, d, *J* = 5.6 Hz, H1), 7.77 (1H, d, *J* = 2.2 Hz, H5), 7.16 (1H, d, *J* = 2.1 Hz, H6), 7.20 (1H, d, *J* = 8.4 Hz, H8), 7.36 (1H, dd, *J* = 9.1, 2.2 Hz, H4), 6.92 (1H, dd, *J* = 8.4, 2.1 Hz, H7), 6.61 (1H, d, *J* = 5.6 Hz, H2), 3.65 (4H, m, H12), 3.47 (2H, t, *J* = 6.28 Hz, H9), 2.58 (2H, t, *J* = 6.28 Hz, H10), 2.46 (4H, m, H11); δ_C (101 MHz, CD_3OD) 157.79, 152.76, 152.24, 150.05, 136.54, 133.56, 127.62, 126.30, 124.58, 119.07, 118.92, 113.03, 110.33, 101.85, 67.84 (x2), 58.86, 54.70, 40.50 (x2); HRMS (ESI) *m/z*, 423.1699 ($[M+H]^+$ $C_{22}H_{24}N_6OCl$ requires 423.1700); HPLC Purity (Method D): 99 %, t_R = 5.26 min.

***N^5-(7-Chloroquinolin-4-yl)-N^2-(2-(diethylamino)ethyl)-1H-benzo[d]imidazole-2,5-diamine,* 3.6d (DS24B)**

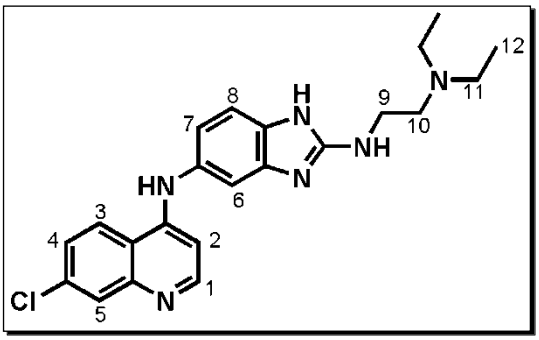

As an orange resin (98 mg, 65 %); m.p. 79-80 °C; R_f (MeOH: DCM: NH_4OH, 10:88:2) 0.37; δ_H (400 MHz, CD_3OD) 8.24 (1H, d, *J* = 9.0 Hz, H3), 8.23 (1H, d, *J* = 5.6 Hz, H1), 7.80 (1H, d, *J* = 2.2 Hz, H5), 7.39 (1H, dd, *J* = 9.0, 2.2 Hz, H4), 7.23 (1H, d, *J* = 8.3 Hz, H8), 7.18 (1H, d, *J* = 1.9 Hz, H6), 6.95 (1H, dd, *J* = 8.3, 1.9 Hz, H7), 6.64 (1H, d, *J* = 5.6 Hz, H2), 3.46 (2H, t, *J* = 6.4 Hz, H9), 2.71 (2H, t, *J* = 6.4 Hz, H10), 2.60 (4H, q, *J* = 7.2 Hz, H11), 1.05 (6H, t, *J* = 7.2 Hz, H12); δ_C (101 MHz, CD_3OD) 172.91, 157.90, 152.68, 152.25, 150.07, 136.48, 133.52, 127.64, 126.24, 124.55, 119.05, 118.85, 112.98, 110.30, 101.83, 53.44, 48.06, 41.46 (x2), 11.72 (x2); HRMS (ESI) *m/z*, 409.1897 ($[M+H]^+$, $C_{22}H_{26}N_6Cl$ requires 409.1907); HPLC Purity (Method D): >99 %, t_R = 10.19 min.

***N^5-(7-Chloroquinolin-4-yl)-N^2-(2-(pyrrolidin-1-yl)ethyl)pyridine-2,5-diamine,* 3.4a (DS26B)**

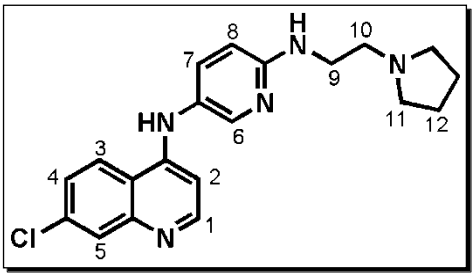

As a yellow powder (54 mg, 58 %); m.p. 143-145 °C; R_f (MeOH: DCM: NH_4OH, 10:88:2) 0.48; δ_H (400 MHz, CD_3OD) 8.29 (1H, d, *J* = 5.6 Hz, H1), 8.24 (1H, d, *J* = 9.0 Hz, H3), 7.98 (1H, d, *J* = 2.7 Hz, H6), 7.81 (1H, d, *J* = 2.2 Hz, H5), 7.46 (1H, dd, *J* = 8.8, 2.7 Hz, H7), 7.45 (1H, dd, *J* = 9.0, 2.2 Hz, H4), 6.67 (1H, d, *J* = 8.8 Hz, H8), 6.49 (1H, d, *J* = 5.6 Hz, H2), 3.56 (2H, t, *J* = 6.46 Hz, H9), 2.95 (2H, t, *J* = 6.48 Hz, H10), 2.86 (4H, m, H11), 1.90 (4H, m, H12); δ_C (101 MHz, CD_3OD) 157.26, 151.43, 150.96, 148.64, 144.44, 136.00, 135.33, 126.36, 125.59,

125.17, 123.16, 123.09, 117.60, 109.24, 100.28, 55.19, 53.79, 39.57 (x2), 22.79 (x2); HRMS (ESI) *m/z*, 368.1642 ([M+H]$^+$ $C_{20}H_{23}N_5Cl$ requires 368.1642); HPLC Purity (Method D): 91%, t_R = 6.48 min.

***N^5-(7-Chloroquinolin-4-yl)-N^2-(2-morpholinoethyl)pyridine-2,5-diamine,* 3.4b (DS27B)**

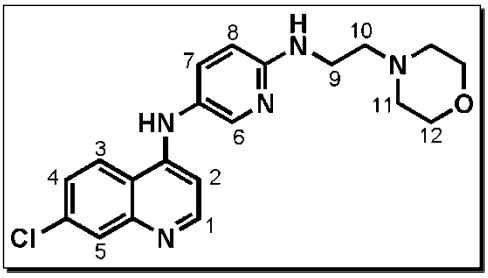

As a yellow powder (73 mg, 61 %); m.p. 92-94 °C; R_f (MeOH: DCM: NH_4OH, 10:88:2) 0.64; δ_H (400 MHz, CD_3OD) 8.30 (1H, d, *J* = 5.7 Hz, H1), 8.26 (1H, d, *J* = 9.0 Hz, H3), 7.97 (1H, d, *J* = 2.6 Hz, H6), 7.83 (1H, d, *J* = 2.1 Hz, H5), 7.48 (1H, dd, *J* = 9.0, 2.1 Hz, H4), 7.46 (1H, dd, *J* = 8.9, 2.6 Hz, H7), 6.66 (1H, d, *J* = 8.9 Hz, H8), 6.51 (1H, d, *J* = 5.7 Hz, H2), 3.72 (4H, m, H12), 3.48 (2H, t, *J* = 6.47 Hz, H9), 2.66 (2H, t, *J* = 6.49 Hz, H10), 2.57 (4H, m, H11); δ_C (101 MHz, CD_3OD) 158.83, 153.31, 151.58, 145.84, 137.34, 137.13, 127.07, 126.77, 126.43, 124.64, 110.29, 101.63, 67.67 (x2), 58.74, 54.69, 39.39 (x2); 384.1584; HRMS (ESI) *m/z*, 384.1584 ([M+H]$^+$ $C_{20}H_{23}N_5Cl$ requires 384.1591); HPLC Purity (Method D): >99 %, t_R = 4.40 min.

***N^5-(7-Chloroquinolin-4-yl)-N^2-ethylbenzoxazole-2,5-diamine,* 3.9a (DS4F)**

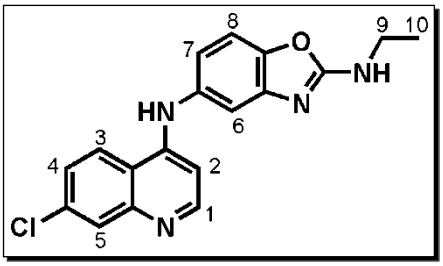

As a light pink powder (33 mg, 24 %); m.p. 227-228 °C; R_f (MeOH:DCM, 10:90%) 0.55; δ_H (400 MHz, CD_3OD) 8.34 (1H, d, *J* = 5.6 Hz, H1), 8.27 (1H, d, *J* = 9.0 Hz, H3), 7.88 (1H, d, *J* = 2.2 Hz, H5), 7.48 (1H, dd, *J* = 9.0, 2.2 Hz, H4), 7.32 (1H, d, *J* = 8.4 Hz, H8), 7.25 (1H, d, *J* = 2.1 Hz, H6), 7.03 (1H, dd, *J* = 8.4, 2.1 Hz, H7), 6.75 (1H, d, *J* = 5.6 Hz, H2), 3.47 (2H, q, *J* = 7.2 Hz, H9), 1.31 (3H, t, *J*

= 7.2 Hz, H10); δ_C (101 MHz, CD_3OD) 151.04, 149.70, 148.89, 135.99, 134.99, 126.79, 125.51, 122.81, 117.97, 117.72, 111.62, 108.57, 100.74, 37.26, 13.70; HRMS (ESI) *m/z*, 339.1002 ($[M+H]^+$ $C_{18}H_{16}N_4OCl$ requires 339.1013); HPLC Purity (Method A): >99 %, t_R = 11.98 min.

***N^5-(7-Chloroquinolin-4-yl)-N^2-(2-(pyrrolidin-1-yl)ethyl)-benzoxazole-2,5-diamine,* 3.9b (DS23B)**

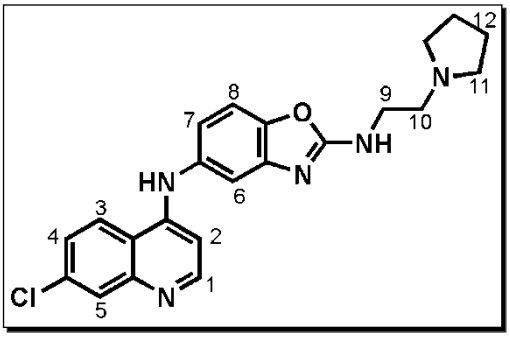

As a yellow powder (102 mg, 61 %); m.p. 98-102 °C; R_f (MeOH: DCM: NH_4OH, 10:88:2) 0.60; δ_H (400 MHz, CD_3OD) 8.26 (1H, d, *J* = 5.6 Hz, H1), 8.21 (1H, d, *J* = 9.0 Hz, H3), 7.79 (1H, d, *J* = 2.2 Hz, H5), 7.40 (1H, dd, *J* = 9.0, 2.2 Hz, H4), 7.24 (1H, d, *J* = 8.4 Hz, H8), 7.20 (1H, d, *J* = 2.1 Hz, H6), 6.96 (1H, dd, *J* = 8.4, 2.1 Hz, H7), 6.70 (1H, d, *J* = 5.6 Hz, H2), 3.52 (2H, t, *J* = 6.7 Hz, H9), 2.74 (2H, t, *J* = 6.7 Hz, H10), 2.58 (4H, m, H11), 1.77 (4H, m, H12); δ_C (101 MHz, CD_3OD) 163.56, 150.98, 150.62, 148.76, 146.07, 143.68, 135.85, 135.24, 126.40, 125.12, 123.18, 117.87, 117.19, 111.62, 108.76, 100.79, 54.72, 53.66, 41.21 (x2), 22.88 (x2); HRMS (ESI) *m/z*, 408.1577 ($[M+H]^+$ $C_{22}H_{23}N_5OCl$ requires 408.1591); HPLC Purity (Method D): 97 %, t_R = 8.64 min.

***N^5-(7-Chloroquinolin-4-yl)-N^2-(2-(piperidin-1-yl)ethyl)benzoxazole-2,5-diamine,* 3.9c (DS46B)**

As a dark yellow-brown powder (123 mg, 69 %); m.p. 89-91 °C; R_f (MeOH: EtOAc, 20:80) 0.35; δ_H (CD_3OD, 400 MHz) δ 8.28 (1H, d, *J*=5.6 Hz, H1), 8.24 (1H, d, *J*=9.0 Hz, H3), 7.81 (1H, d, *J*=2.2 Hz, H5), 7.43 (1H, dd, *J*=9.0, 2.2 Hz, H4), 7.27 (1H, d, *J*=8.4 Hz,

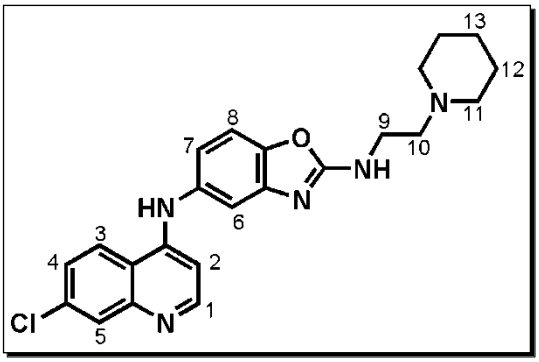

H8), 7.22 (1H, d, *J*=2.1 Hz, H6), 6.99 (1H, dd, *J*=8.4, 2.2 Hz, H7), 6.73 (1H, d, *J*=5.6 Hz, H2), 3.54 (2H, t, *J*=6.7 Hz, H9), 2.63 (2H, t, *J*=6.7 Hz, H10), 2.56 – 2.42 (4H, m, H11), 1.66 – 1.53 (4H, m, H12), 1.49 – 1.40 (4H, m, H13); δ_C (101 MHz, CD_3OD) 163.59, 150.92, 150.68, 148.69, 146.09, 143.65, 135.85, 135.29, 126.35, 125.16, 123.21, 117.87, 117.24, 111.64, 108.80, 100.79, 57.46, 54.16, 39.34, 25.14, 23.68; LRMS (EI) *m/z,* 421.12 (M^+ $C_{22}H_{16}ClN_5O$ requires 421.17); HPLC Purity (Method A): >99 %, t_R = 8.79 min.

N^5-(7-Chloroquinolin-4-yl)-N^2-(2-morpholinoethyl)benzoxazole-2,5-diamine, **3.9d (DS31B)**

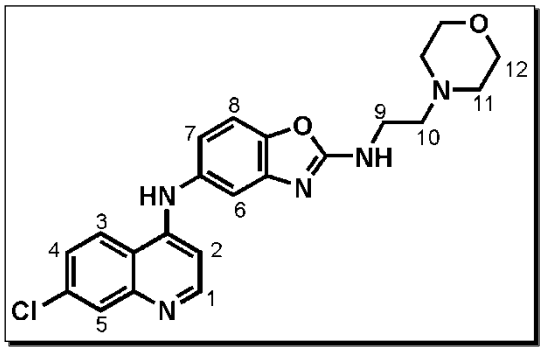

As a yellow solid (107 mg, 57 %); m.p. 107-109 °C; R_f (MeOH: EtOAc, 20:80) 0.36; δ_H ($CDCl_3$, 300 MHz) δ 8.27 (1H, d, *J*=5.8 Hz, H1), 8.07 (1H, d, *J*=9.2 Hz, H3), 7.96 (1H, d, *J*=2.0 Hz, H5), 7.36 (1H, dd, *J*=9.2, 2.0 Hz, H4), 7.20 (1H, d, *J*=2.2 Hz, H6), 7.16 (1H, d, *J*=8.4 Hz, H8), 6.92 (1H, dd, *J*=8.4, 2.2 Hz, H7), 6.65 (1H, d, *J*=5.8 Hz, H2), 3.57 – 3.74 (4H, m, H12), 3.49 (2H, t, *J*=5.8 Hz, H9), 2.61 (2H, t, *J*=5.8 Hz, H10), 2.43 – 2.50 (4H, m, H11); δ_C (101 MHz, $CDCl_3$) 163.00, 150.75, 149.81, 148.45, 146.48, 144.35, 135.59, 135.27, 127.59, 125.87, 122.10, 117.60, 117.28, 112.47, 109.23, 101.53, 66.84 (x2), 56.86, 53.30, 39.14 (x2); LRMS (EI) *m/z,* 422.99 (M^+ $C_{22}H_{22}ClN_5O_2$ requires 423.15); HPLC Purity (Method C): >99 %, t_R = 2.82 min.

***N^5-(7-Chloroquinolin-4-yl)-N^2-(2-(diethylamino)ethyl)benzoxazole-2,5-diamine,* 3.9e (DS33B)**

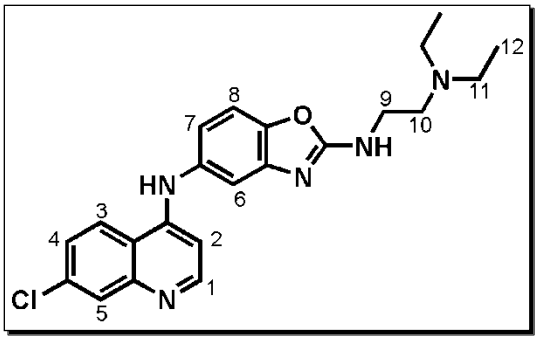

As a yellow solid (89 mg, 61 %); m.p. 91-93 °C; R_f (MeOH: EtOAc, 20:80) 0.30; δ_H (CD_3OD, 300 MHz) 8.27 (1H, d, *J*=5.6 Hz, H1), 8.23 (1H, d, *J*=9.0 Hz, H3), 7.80 (1H, d, *J*=2.2 Hz, H5), 7.42 (1H, dd, *J*=9.0, 2.2 Hz, H4), 7.27 (1H, d, *J*=8.4 Hz, H8), 7.21 (1H, d, *J*=2.1 Hz, H6), 6.98 (1H, dd, *J*=8.4, 2.1 Hz, H7), 6.72 (1H, d, *J*=5.6 Hz, H2), 3.49 (2H, t, *J*=6.9 Hz, H9), 2.73 (2H, t, *J*=6.9 Hz, H10), 2.61 (4H, q, *J*=7.2 Hz, H11), 1.05 (6H, t, *J*=7.2 Hz, H12); δ_C (101 MHz, CD_3OD) 163.62, 150.97, 150.67, 148.75, 146.10, 143.71, 135.87, 135.26, 126.39, 125.14, 123.20, 117.89, 117.23, 111.66, 108.78, 100.80, 51.44, 46.78, 39.97, 10.29; LRMS (EI) *m/z,* 409.16 (M^+ $C_{22}H_{24}ClN_5O$ requires 409.17); HPLC Purity (Method A): >99 %, t_R = 11.34 min.

***N^5-(7-Chloroquinolin-4-yl)-N^2-(2-(dimethylamino)ethyl)benzoxazole-2,5-diamine,* 3.9f (DS50B)**

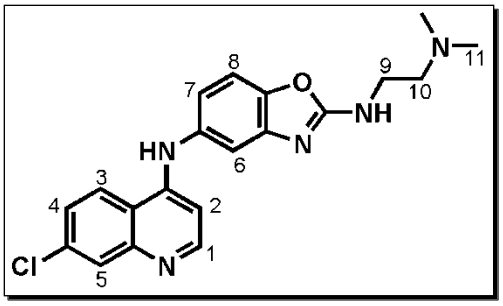

As a dark brown resin (51 mg, 44 %); R_f (MeOH: EtOAc, 20:80) 0.32; δ_H (CD_3OD, 300 MHz) 8.30 (1H, d, *J*=5.6 Hz, H1), 8.26 (1H, d, *J*=9.0 Hz, H3), 7.83 (1H, d, *J*=2.2 Hz, H5), 7.46 (1H, dd, *J*=9.0, 2.2 Hz, H4), 7.31 (1H, d, *J*=8.4 Hz, H8), 7.23 (1H, d, *J*=2.2 Hz, H6), 7.01 (1H, dd, *J*=8.4, 2.2 Hz, H7), 6.74 (1H, d, *J*=5.6 Hz, H2), 3.54 (2H, t, *J*=6.6 Hz, H9), 2.65 (2H, t, *J*=6.6 Hz, H10), 2.33 (8H, s, H11); δ_C (101 MHz, CD_3OD) 163.61, 150.90, 150.80, 148.67, 146.16, 143.68, 135.86, 135.33, 126.31, 125.18, 123.23, 117.87, 117.35, 111.73, 108.82, 100.80, 57.72, 44.11, 39.96; LRMS (EI) *m/z,*

381.13 (M^+ $C_{20}H_{20}ClN_5O$ requires 381.14); HPLC Purity (Method B): 99 %, t_R = 8.56 min.

***1-(3-(5-(7-Chloroquinolin-4-ylamino)benzoxazol-2-ylamino)propyl)pyrrolidin-2-one,* 3.9g (DS34B)**

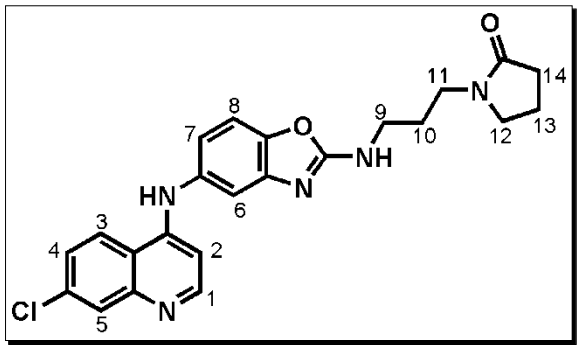

As a yellow solid (102 mg, 65 %); m.p. 95-97 °C; R_f (EtOAc) 0.57; δ_H ($CDCl_3$, 400 MHz) 8.39 (1H, d, *J*=5.5 Hz, H1), 8.02 (1H, d, *J*=9.0 Hz, H3), 7.98 (1H, d, *J*=2.1 Hz, H5), 7.40 (1H, dd, *J*=9.0, 2.1 Hz, H4), 7.24 (1H, d, *J*=2.0 Hz, H6), 7.19 (1H, d, *J*=8.4 Hz, H8), 6.92 (1H, dd, *J*=8.4, 2.0 Hz, H7), 6.72 (1H, d, *J*=5.5 Hz, H2), 3.34 - 3.45 (6H, m, H9, H11, H12), 2.42 (2H, t, *J*=8.1 Hz, H14), 2.14 – 1.99 (2H, m, H13), 1.93 – 1.80 (2H, m, H10); δ_C (101 MHz, $CDCl_3$) 176.16, 163.15, 150.70, 149.82, 148.38, 146.55, 144.51, 135.64, 135.04, 127.68, 125.94, 122.00, 117.54, 117.15, 112.39, 109.20, 101.52, 47.50, 39.57, 39.53, 30.89, 26.44, 17.95; HPLC Purity: 96 %, t_R = 9.95 min; LRMS (EI) *m/z,* 435.10 (M^+ $C_{23}H_{22}ClN_5O_2$ requires 435.15); HPLC Purity (Method B): 97 %, t_R = 9.95 min.

***N^5-(7-Chloroquinolin-4-yl)-N^2-(3-(diethylamino)propyl)benzoxazole-2,5-diamine,* 3.9h (DS36B)**

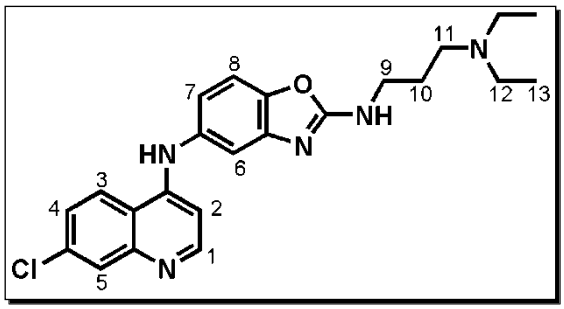

As a yellow solid (125 mg, 46 %); m.p. 79-80 °C; R_f (MeOH: EtOAc, 20:80) 0.33; δ_H (CD_3OD, 400 MHz) 8.25 (1H, d, *J*=5.6 Hz, H1), 8.21 (1H, d, *J*=9.0 Hz, H3), 7.78 (1H, d, *J*=2.2 Hz, H5), 7.37 (1H, dd, *J*=9.0, 2.2 Hz, H4), 7.23

(1H, d, *J*=8.4 Hz, H8), 7.20 (1H, d, *J*=2.2 Hz, H6), 6.95 (1H, dd, *J*=8.4, 2.2 Hz, H7), 6.70 (1H, d, *J*=5.6 Hz, H2), 3.40 (2H, t, *J*=6.8 Hz, H9), 2.68 – 2.45 (6H, m, H11, H12), 1.92 – 1.71 (2H, m, H10), 1.02 (6H, t, *J*=7.2 Hz); δ_C (101 MHz, CD_3OD) 163.58, 150.95, 150.53, 148.73, 145.96, 143.65, 135.83, 135.21, 126.42, 125.11, 123.20, 117.87, 117.08, 111.49, 108.74, 100.78, 49.96, 46.46, 41.03, 25.60, 9.98; LRMS (EI) *m/z,* 423.16 (M^+ $C_{23}H_{26}ClN_5O$ requires 423.18); HPLC Purity (Method A): >99 %, t_R = 9.02 min.

***N^5-(7-Chloroquinolin-4-yl)-N^2-(3-(dimethylamino)propyl)benzoxazole-2,5-diamine,* 3.9i (DS37B)**

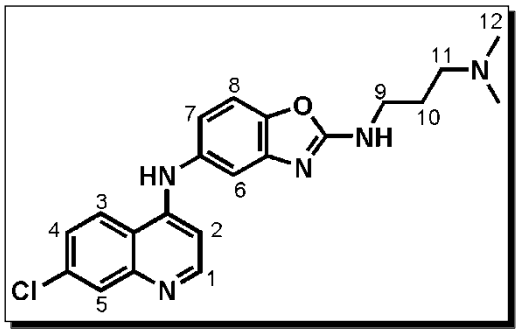

As a yellow solid (113 mg, 52 %); m.p. 55-56 °C; R_f (MeOH: EtOAc, 20:80) 0.27; δ_H (CD_3OD, 400 MHz) 8.28 (1H, d, *J*=5.6 Hz, H1), 8.24 (1H, d, *J*=9.0 Hz, H3), 7.81 (1H, d, *J*=2.2 Hz, H5), 7.43 (1H, dd, *J*=9.0, 2.2 Hz, H4), 7.28 (1H, d, *J*=8.4 Hz, H8), 7.22 (1H, d, *J*=2.0 Hz, H6), 6.99 (1H, dd, *J*=8.4, 2.1 Hz, H7), 6.72 (H, d, *J*=5.6 Hz, H2), 3.43 (2H, t, *J*=6.9 Hz, H9), 2.53 (2H, t, *J*=7.7 Hz, H11), 2.33 (6H, s, H12), 1.92 – 1.85 (2H, m, H10); δ_C (101 MHz, CD_3OD) 163.64, 150.90, 150.71, 148.67, 146.06, 143.65, 135.84, 135.29, 126.32, 125.16, 123.23, 117.86, 117.25, 111.61, 108.79, 100.79, 56.42, 43.81 (x2), 40.55, 26.43; LRMS (EI) *m/z,* 395.12 (M^+ $C_{21}H_{22}ClN_5O$ requires 395.15); HPLC Purity (Method C): 95 %, t_R = 2.65 min.

N^5-(7-Chloroquinolin-4-yl)-N^2-(3-(piperidin-1-yl)propyl)benzoxazole-2,5-diamine, **3.9j (DS48B)**

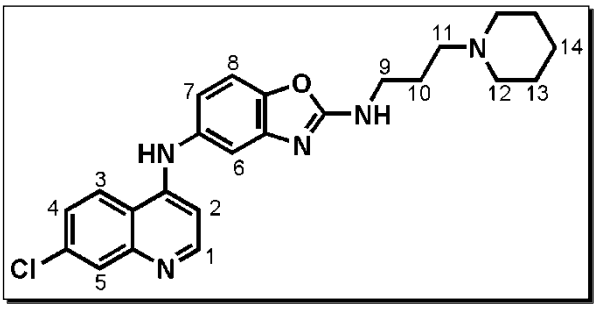

As a yellow-brown solid (96 mg, 58 %); m.p. 87-89 °C; R_f (MeOH: EtOAc, 20:80) 0.30; δ_H (CD_3OD, 300 MHz) 8.26 (1H, d, *J*=5.6 Hz, H1), 8.21 (1H, d, *J*=9.0 Hz, H3), 7.79 (1H, d, *J*=2.2 Hz, H5), 7.39 (1H, dd, *J*=9.0, 2.2 Hz, H4), 7.24 (1H, d, *J*=8.4 Hz, H8), 7.20 (1H, d, *J*=2.1 Hz, H6), 6.96 (1H, dd, *J*=8.4, 2.1 Hz, H7), 6.71 (1H, d, *J*=5.6 Hz, H2), 3.39 (2H, t, *J*=6.8 Hz, H9), 2.45 – 2.32 (6H, m, H11, H12), 1.93 – 1.75 (1H, m, H10), 1.63 – 1.49 (4H, m, H13), 1.48 – 1.34 (2H, m, H14); δ_C NMR (101 MHz, CD_3OD) 163.66, 151.02, 150.77, 148.80, 146.08, 143.70, 135.89, 135.28, 126.40, 125.16, 123.22, 117.90, 117.28, 111.62, 108.77, 100.81, 56.38, 54.12, 41.03, 25.76, 25.18, 23.79; LRMS (EI) *m/z,* 435.13 (M^+ $C_{24}H_{26}ClN_5O$ requires 435.18); HPLC Purity (Method A): >99 %, t_R = 9.11 min.

N^5-(7-Chloroquinolin-4-yl)-N^2-(3-morpholinopropyl)benzoxazole-2,5-diamine, **3.9k (DS56B)**

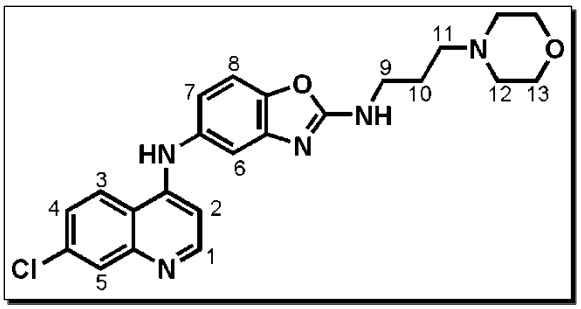

As a yellow solid (88 mg, 53 %); m.p. 182-183 °C; R_f (MeOH: EtOAc, 20:80) 0.52; δ_H (CD_3OD, 300 MHz) 8.28 (1H, d, *J*=5.6 Hz, H1), 8.23 (1H, d, *J*=9.0 Hz, H3), 7.81 (1H, d, *J*=2.2 Hz, H5), 7.42 (1H, dd, *J*=9.0, 2.2 Hz, H4), 7.26 (1H, d, *J*=8.4 Hz, H8), 7.21 (1H, d, *J*=2.1 Hz, H6), 6.98 (1H, dd, *J*=8.4, 2.1 Hz, H7), 6.72 (1H, d, *J*=5.6 Hz, H2), 3.74 – 3.62 (4H, m, H13), 3.53 (2H, t, *J*=6.6 Hz, H9), 3.43 (2H, t, *J*=6.6 Hz, H11), 2.51 – 2.37 (4H, m, H12), 1.91 – 1.78 (2H, m, H10); δ_C (101

MHz, CD_3OD) 163.63, 150.96, 150.64, 148.73, 146.01, 143.70, 135.85, 135.25, 126.39, 125.14, 123.19, 117.88, 117.15, 111.55, 108.74, 100.80, 66.35, 56.04, 53.38, 40.88, 25.58; LRMS (EI) *m/z,* 437.13 (M^+ $C_{23}H_{24}ClN_5O_2$ requires 437.16); HPLC Purity (Method A): >99 %, t_R = 11.52 min.

***N^5-(7-Chloroquinolin-4-yl)-N^2-(4-methylpiperazin-1-yl)benzoxazole-2,5-diamine,* 3.9l (DS41B)**

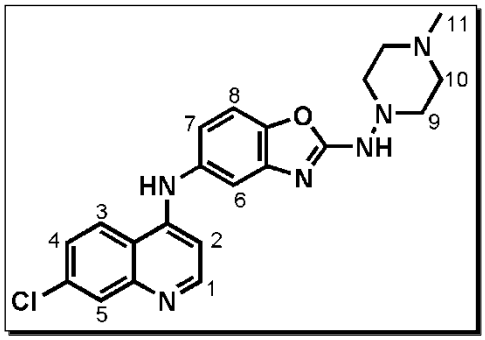

As a yellow solid (106 mg, 49 %); m.p. 80-81 °C; R_f (MeOH: EtOAc, 20:80) 0.56; δ_H (CD_3OD, 400 MHz) 8.29 (1H, d, *J*=5.6 Hz, H2), 8.25 (1H, d, *J*=9.0 Hz, H3), 7.82 (1H, d, *J*=2.1 Hz, H5), 7.44 (1H, dd, *J*=9.0, 2.1 Hz, H4), 7.34 (1H, d, *J*=8.5 Hz, H8), 7.25 (1H, d, *J*=2.1 Hz, H6), 7.03 (1H, dd, *J*=8.5, 2.1 Hz, H7), 6.74 (1H, d, *J*=5.6 Hz, H2), 3.75 – 3.64 (4H, m, H9), 2.60 – 2.51 (4H, m, H10), 2.33 (3H, s, H11); δ_C (101 MHz, $CDCl_3$) 163.15, 151.79, 149.49, 149.08, 146.81, 145.15, 135.31, 135.17, 128.76, 127.75, 125.76, 121.39, 116.30, 112.03, 109.01, 101.85, 43.05 (x2), 13.46 (x2); LRMS (EI) *m/z,* 408.13 (M^+ $C_{21}H_{21}ClN_6O$ requires 408.15); HPLC Purity (Method A): >99 %, t_R = 8.87 min.

***N^2-(3-Chlorobenzyl)-N^5-(7-chloroquinolin-4-yl)benzoxazole-2,5-diamine,* 3.9m (DS42B)**

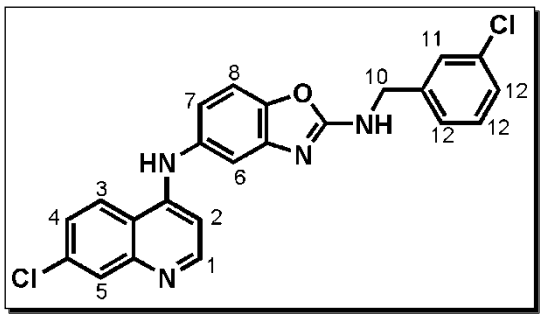

As a yellow solid (71 mg, 39 %); m.p. 98-99 °C; R_f (Hexane: EtOAc, 20:80) 0.61; δ_H ($CDCl_3$, 400 MHz) 8.50 (1H, d, *J*=5.4 Hz, H1), 8.04 (1H, d, *J*=2.1 Hz, H5), 7.91 (1H, d, *J*=9.0 Hz, H3), 7.46 (1H, dd, *J*=9.0, 2.1 Hz, H4), 7.41 (1H, s, H11),

7.34 – 7.23 (5H, m, H6, H8, H12), 7.00 (2H, dd, *J*=8.4, 2.1 Hz, H7), 6.79 (1H, d, *J*=5.4 Hz), 4.70 (2H, s, H10); δ_C (101 MHz, $CDCl_3$) 162.75, 151.79, 149.63, 148.84, 146.65, 144.40, 139.63, 135.77, 135.28, 130.07, 128.98, 128.10, 127.75, 127.65, 125.92, 125.58, 121.06, 117.49, 112.87, 109.42, 102.10, 46.63; LRMS (EI) *m/z,* 434.04 (M^+ $C_{23}H_{16}Cl_2N_4O$ requires 434.07); HPLC Purity (Method A): >99 %, t_R = 13.93 min.

***N^5-(7-Chloroquinolin-4-yl)-N^2-(3-(trifluoromethyl)benzyl)benzoxazole-2,5-diamine,* 3.9n (DS54B)**

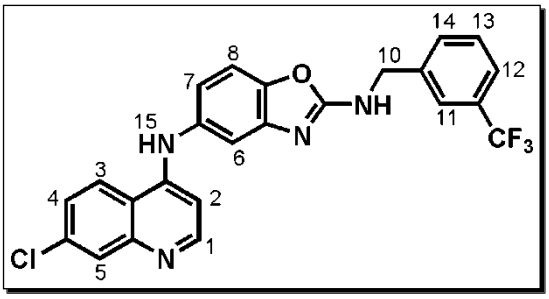

As a yellow solid (73 mg, 43 %); m.p. 108-110 °C; R_f (Hexane: EtOAc, 20:80) 0.64; δ_H (CD_3OD, 400 MHz) 8.31 (1H, d, *J*=5.6 Hz, H1), 8.26 (1H, d, *J*=9.0 Hz, H3), 7.84 (1H, d, *J*=2.2 Hz, H5), 7.73 – 7.70 (1H, m, H11), 7.69 – 7.65 (1H, m, H12), 7.60 – 7.51 (2H, m, H13, H14), 7.46 (1H, dd, *J*=9.0, 2.2 Hz, H4), 7.34 (1H, d, *J*=8.4 Hz, H8), 7.24 (1H, d, *J*=2.1 Hz, H6), 7.04 (1H, dd, *J*=8.4, 2.1 Hz, H7), 6.75 (1H, d, *J*=5.6 Hz, H2), 4.67 (2H, s, H10); δ_C NMR (101 MHz, CD_3OD) 163.62, 150.99, 150.75, 148.75, 146.22, 143.50, 139.81, 136.00, 135.30, 130.69, 129.06, 126.35, 125.17, 123.89, 123.85, 123.81, 123.63, 123.59, 123.21, 117.89, 117.59, 111.90, 108.95, 100.84, 45.41; LRMS (EI) *m/z,* 468.10 (M^+ $C_{24}H_{16}ClF_3N_4O$ requires 468.10); HPLC Purity (Method A): >99 %, t_R = 14.84 min.

N^5-(7-Chloroquinolin-4-yl)-N^2-(pyridin-2-ylmethyl)benzoxazole-2,5-diamine, **3.9o (DS32B)**

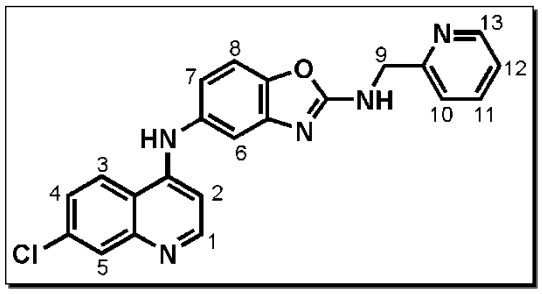

As a yellow solid (80 mg, 61 %); m.p. 118-120 °C; R_f (MeOH: EtOAc, 5:95) 0.59; δ_H ($CDCl_3$, 400 MHz) 8.57 (1H, d, *J*=4.7 Hz, H13), 8.41 (1H, d, *J*=5.5 Hz, H1), 7.99 (1H, d, *J*=2.0 Hz, H5), 7.97 (1H, d, *J*=9.0 Hz, H3), 7.69 (1H, td, *J*=7.8 (x2), 1.8 Hz, H11), 7.40 (1H, dd, *J*=9.0, 2.0 Hz, H4), 7.33 (1H, d, *J*=7.8 Hz, H10), 7.29 (1H, d, *J*=2.0 Hz, H6), 7.20 – 7.26 (2H, m, H8, H12), 6.95 (1H, dd, *J*=8.4, 2.0 Hz, H7), 6.74 (1H, d, *J*=5.5 Hz, H2), 4.78 (2H, s, H9); δ_C (101 MHz, $CDCl_3$) 162.96, 155.51, 151.22, 149.33, 149.14, 149.01, 146.84, 144.63, 136.79, 135.50, 135.38, 128.40, 125.96, 122.62, 121.76, 121.40, 117.66, 117.37, 112.80, 109.34, 101.89, 47.47; LRMS (EI) *m/z,* 400.93 (M^+ $C_{24}H_{26}ClN_5O$ requires 401.10); HPLC Purity (Method A): >99 %, t_R = 11.29 min.

N^5-(7-Chloroquinolin-4-yl)-N^2-(pyridin-3-ylmethyl)benzo[d]oxazole-2,5-diamine, **3.9p (DS35B)**

As a yellow solid (86 mg, 58 %); m.p. 108-109 °C; R_f (MeOH: EtOAc, 5:95) 0.78; δ_H ($CDCl_3$, 400 MHz) 8.66 (1H, d, *J*=2.2 Hz, H13), 8.54 (1H, dd, *J*=4.8, 1.6 Hz, H12), 8.46

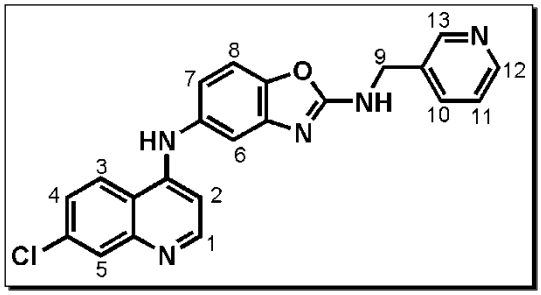

(1H, d, *J*=5.4 Hz, H1), 8.00 (1H, d, *J*=2.1 Hz, H5), 7.90 (1H, d, *J*=9.0 Hz, H3), 7.78 – 7.71 (1H, m, H11), 7.42 (1H, dd, *J*=9.0, 2.2 Hz, H4), 7.30 – 7.25 (2H, m, H8, H10), 7.24 (1H, d, *J*=2.2 Hz, H6), 6.96 (1H, dd, *J*=8.4, 2.2 Hz, H7), 6.76 (1H, d, *J*=5.4 Hz, H2), 4.70 (2H, s, H9); δ_C (101 MHz, $CDCl_3$) 162.66, 151.84, 149.66, 149.40, 149.19, 148.79, 146.63, 144.29, 135.79, 135.26, 133.17, 129.01, 125.92,

123.58, 121.07, 117.79, 117.58, 112.90, 109.47, 102.08, 77.25, 76.93, 76.61, 44.76; LRMS (EI) *m/z,* 401.10 (M^+ $C_{24}H_{26}ClN_5O$ requires 401.10); HPLC Purity (Method A): >99 %, t_R = 10.87 min.

N^5-(7-Chloroquinolin-4-yl)-N^2-(pyridin-4-ylmethyl)benzoxazole-2,5-diamine, **3.9q (DS47B)**

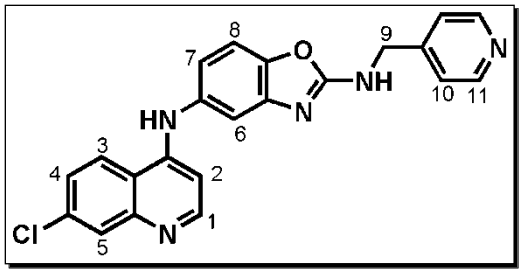

As a yellow solid (26 mg, 23 %); m.p. 202-204 °C; R_f (MeOH: EtOAc, 5:95) 0.68; δ_H (CD_3OD, 300 MHz) 8.52 – 8.43 (2H, m, H11), 8.31 (1H, d, *J*=5.6 Hz, H1), 8.27 (1H, d, *J*=9.0 Hz, H3), 7.84 (1H, d, *J*=2.1 Hz, H5), 7.51 – 7.42 (3H, m, H4, H10), 7.36 (1H, d, *J*=8.4 Hz, H8), 7.23 (1H, d, *J*=2.1 Hz, H6), 7.05 (1H, dd, *J*=8.4, 2.1 Hz, H7), 6.75 (1H, d, *J*=5.6 Hz, H2), 4.67 (2H, s, H9); δ_C (101 MHz, CD_3OD) 163.58, 150.96, 150.78, 149.12, 148.86, 148.72, 146.29, 143.44, 136.05, 135.34, 126.33, 125.20, 123.22, 122.26, 117.89, 117.72, 111.99, 109.03, 100.83, 44.73; LRMS (EI) *m/z,* 401.07 (M^+ $C_{24}H_{26}ClN_5O$ requires 401.10); HPLC Purity (Method B): 96 %, t_R = 10.06 min.

N^5-(7-Chloroquinolin-4-yl)-N^2-(2-(pyridin-2-yl)ethyl)benzoxazole-2,5-diamine, **3.9r (DS49B)**

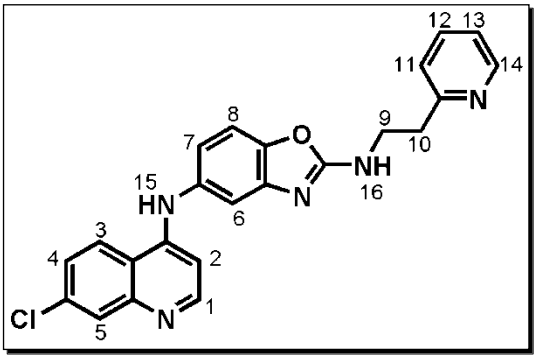

As a yellow solid (131 mg, 67 %); m.p. 89-91 °C; R_f (MeOH: EtOAc, 5:95) 0.70; δ_H (DMSO, 400 MHz) 9.01 (1H, s, H15), 8.52 – 8.47 (1H, m, H14), 8.42 (1H, d, *J*=9.0 Hz, H3), 8.38 (1H, d, *J*=5.4 Hz, H1), 8.06 (1H, t, *J*=5.7 Hz, H16), 7.85 (1H, d, *J*=2.2 Hz, H5), 7.69 (1H, td, *J*=7.8 (x2), 1.9 Hz, H12), 7.52 (1H, dd, *J*=9.0, 2.2

Hz, H4), 7.36 (1H, d, *J*=8.4 Hz, H8), 7.29 (1H, d, *J*=7.8 Hz, H11), 7.24 – 7.17 (2H, m, H6, H13), 6.93 (1H, dd, *J*=8.4, 2.1 Hz, H7), 6.70 (1H, d, *J*=5.4 Hz, H2), 3.74 – 3.63 (2H, m, H9), 3.07 (2H, t, *J*=7.2 Hz, H10); δ_C (101 MHz, DMSO) 163.51, 159.25, 152.31, 149.90, 149.81, 149.57, 145.97, 144.88, 136.94, 136.21, 134.28, 128.01, 125.15, 124.85, 123.76, 122.04, 118.41, 116.89, 112.08, 109.31, 101.54, 42.53, 37.56; LRMS (EI) *m/z,* 415.09 (M^+ $C_{23}H_{18}ClN_5O$ requires 415.12); HPLC Purity (Method A): >99 %, t_R = 13.20 min.

N^5-(7-Chloroquinolin-4-yl)-N^2,N^2-diethylbenzoxazole-2,5-diamine, **3.9s (DS39B)**

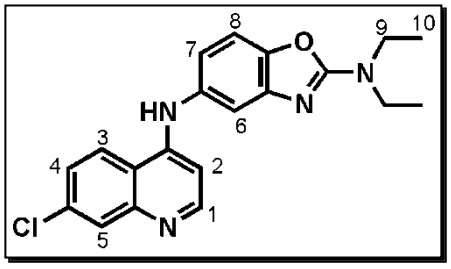

As a yellow solid (76 mg, 58%); m.p. 189-190 °C; R_f (Hexane: EtOAc, 20:80) 0.60; δ_H ($CDCl_3$, 400 MHz) 8.45 (1H, d, *J*=5.4 Hz, H1), 7.99 (1H, d, *J*=2.2 Hz, H5), 7.90 (1H, d, *J*=8.9 Hz, H3), 7.39 (1H, dd, *J*=8.9, 2.2 Hz, H4), 7.23 – 7.25 (2H, m, H6, H8), 6.88 (1H, dd, *J*=8.3, 2.2 Hz, H7), 6.76 (1H, d, *J*=5.4 Hz, H2), 3.59 (3H, q, *J*=7.2 Hz, H9), 1.29 (4H, t, *J*=7.2 Hz, H10) δ_C (101 MHz, $CDCl_3$) 163.15, 151.79, 151.67, 149.49, 149.08, 146.81, 145.15, 135.31, 135.17, 128.76, 125.76, 121.39, 116.30, 112.03, 109.01, 101.85, 43.05 (x2), 13.46 (x2); LRMS (EI) *m/z,* 366.11 (M^+ $C_{20}H_{19}ClN_4O$ requires 366.12); HPLC Purity (Method A): >99 %, t_R = 12.97 min.

N-(7-Chloroquinolin-4-yl)-2-(4-methylpiperazin-1-yl)benzoxazol-5-amine, **3.9t (DS51B)**

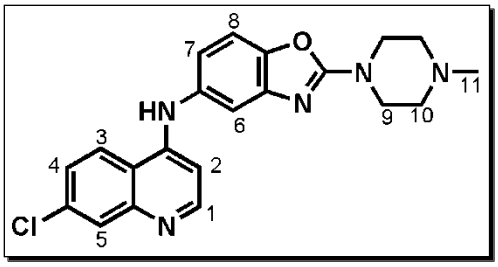

As a yellow solid (77 mg, 47 %); m.p. 113-115 °C; R_f (MeOH: EtOAc, 20:80) 0.55; δ_H (DMSO, 400 MHz) 9.02 (1H, s, quinolinyl NH), 8.41 (1H, d, *J*=9.0 Hz, H3), 8.38 (1H, d, *J*=5.4 Hz, H2), 7.85 (1H, d, *J*=2.2 Hz, H5), 7.52 (1H, dd, *J*=9.0, 2.2 Hz, H4), 7.43 (1H, d, *J*=8.2 Hz, H8), 7.23 (1H, d, *J*=2.0 Hz, H6), 6.98 (1H, dd, *J*=8.2, 2.0 Hz, H7), 6.70 (1H, d, *J*=5.4 Hz, H2), 3.60 (4H, t, *J*=5.0 Hz, H9), 2.42 (4H, t, *J*=5.0 Hz, H10), 2.22 (3H, s, H11); δ_C (101 MHz, DMSO) 163.04, 152.38, 150.03, 149.68, 146.20, 144.55, 136.64, 134.27, 128.10, 125.15, 124.82, 118.49, 117.21, 112.20, 109.72, 101.64, 54.18, 46.21, 45.66; LRMS (EI) *m/z,* 393.12 (M^+ $C_{21}H_{20}ClN_5O$ requires 393.14); HPLC Purity (Method A): >99 %, t_R = 11.50 min.

N-(7-Chloroquinolin-4-yl)-2-(4-phenylpiperazin-1-yl)benzoxazol-5-amine, **3.9u (DS52B)**

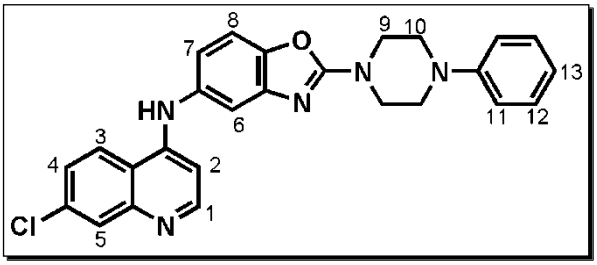

As a yellow solid (222 mg, 74 %); m.p. 96-98 °C; R_f (EtOAc) 0.49; δ_H (DMSO, 400 MHz) 9.03 (1H, s, quinolinyl NH), 8.42 (1H, d, *J*=9.0 Hz, H3), 8.39 (1H, d, *J*=5.3 Hz, H1), 7.86 (1H, d, *J*=2.2 Hz, H5), 7.52 (1H, dd, *J*=9.0, 2.2 Hz, H4), 7.45 (1H, d, *J*=8.4 Hz, H8), 7.29 – 7.16 (3H, m, H6, H12), 7.05 – 6.94 (3H, m, H7, H11), 6.82 (1H, t, *J*=7.2 Hz, H13), 6.72 (1H, d, *J*=5.3 Hz, H2), 3.75 (4H, t, *J*=5.0 Hz, H, H10), 3.27 (4H, t, *J*=5.0 Hz, H9); δ_C (101 MHz, DMSO) 163.07, 152.34, 151.29, 150.17, 149.80, 146.38, 144.64, 136.96, 134.29, 129.46, 128.17, 125.08, 124.80, 119.98, 118.68, 117.29, 116.60,

112.33, 109.69, 101.94, 48.52, 45.73; LRMS (EI) *m/z,* 455.12 (M^+ $C_{26}H_{22}ClN_5O$ requires 455.15); HPLC Purity (Method A): >99 %, t_R = 15.41 min.

***2-(4-(3-Chlorophenyl)piperazin-1-yl)-N-(7-chloroquinolin-4-yl)benzoxazol-5-amine,* 3.9v (DS53B)**

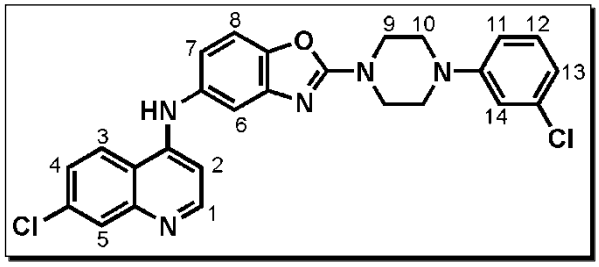

As a yellow solid (39 mg, 40 %); m.p. 90-92 °C; R_f (EtOAc) 0.52; δ_H ($CDCl_3$, 400 MHz) 8.46 (1H, d, *J*=5.3 Hz, H1), 8.00 (1H, d, *J*=2.1 Hz, H5), 7.89 (1H, d, *J*=9.0 Hz, H3), 7.40 (1H, dd, *J*=9.0, 2.1 Hz, H4), 7.31 – 7.25 (2H, m, H6, H7), 7.24 – 7.15 (1H, m, H11), 6.95 (1H, dd, *J*=8.4, 2.1 Hz, H7), 6.92 (1H, t, *J*=2.2 Hz, H14), 6.89 – 6.86 (1H, m, H12), 6.84 – 6.80 (1H, m, H13), 6.77 (1H, d, *J*=5.4 Hz, H2), 3.92 – 3.80 (4H, m, H10), 3.38 – 3.22 (4H, m, H9); δ_C (101 MHz, $CDCl_3$) 162.89, 152.03, 151.82, 149.68, 148.89, 146.77, 144.54, 135.89, 135.21, 130.16, 128.93, 125.82, 121.22, 120.45, 117.86, 117.19, 116.73, 114.69, 112.61, 109.36, 102.07, 48.67, 45.47; LRMS (EI) *m/z,* 489.10 (M^+ $C_{26}H_{21}Cl_2N_5O$ requires 489.11); HPLC Purity (Method A): >99 %, t_R = 15.94 min.

***N-(7-Chloroquinolin-4-yl)-2-((dimethylamino)methyl)benzoxazol-5-amine,* 3.9w (DS30B)**

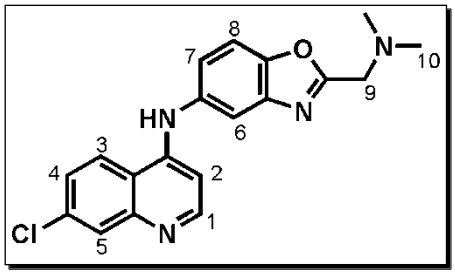

As an off white powder, (63 mg, 49 %); m.p. 156-158 °C; R_f (MeOH: EtOAc, 20:80) 0.27; δ_H (300 MHz, $CDCl_3$) δ 8.37 (1H, d, *J* = 5.4 Hz, H1), 7.88 – 7.94 (2H, m, H3, H5), 7.54 (1H, d, *J* = 2.1 Hz, H6), 7.46 (d, *J* = 8.6 Hz, H8), 7.30 (1H, dd, *J* = 9.0, 2.2 Hz, H4), 7.21 (1H, dd, *J* = 8.6, 2.1 Hz, H7), 6.68 (1H, d, *J* = 5.4 Hz, H2), 3.73 (2H, s, H9), 2.34 (6H, s, H10); δ_C (101 MHz, CD_3OD)

164.75, 151.11, 150.36, 148.82, 148.48, 141.53, 136.86, 135.39, 126.47, 125.36, 123.21, 122.28, 118.03, 115.03, 111.18, 100.96, 55.09, 44.04; LRMS (EI) *m/z,* 352.01 (M^+ $C_{19}H_{17}ClN_4O$ requires 352.11); HPLC Purity (Method C): 98 %, t_R = 2.78 min.

***N-(7-Chloroquinolin-4-yl)-2-(2-methoxyethyl)benzoxazol-5-amine,* 3.9x (DS58B)**

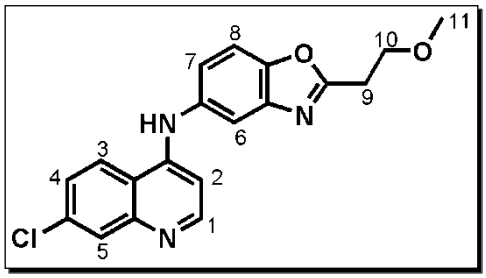

As a light pink solid (106 mg, 65 %); m.p. 165-166 °C; R_f (MeOH: EtOAc, 20:80) 0.62; δ_H (CD_3OD, 300 MHz) 8.33 (1H, d, *J*=5.5 Hz, H1), 8.27 (1H, d, *J*=9.0 Hz, H3), 7.84 (1H, d, *J*=2.1 Hz, H5), 7.63 – 7.59 (2H, m, H6, H8), 7.47 (1H, dd, *J*=9.0, 2.2 Hz, H4), 7.35 (1H, dd, *J*=8.6, 2.2 Hz, H7), 6.77 (1H, d, *J*=5.5 Hz, H2), 3.89 (2H, t, *J*=6.2 Hz), 3.37 (2H, s), 3.21 (2H, t, *J*=6.2 Hz); δ_C (101 MHz, CD_3OD) 167.58, 156.58, 150.21, 142.90, 142.26, 140.17, 139.21, 133.37, 127.89, 124.91, 122.88, 119.14, 116.70, 115.91, 111.71, 100.24, 68.50, 57.54, 28.89; LRMS (EI) *m/z,* 353.08 (M^+ $C_{19}H_{16}ClN_3O_2$ requires 353.09); HPLC Purity (Method A): >99 %, t_R = 12.83 min.

6.5 ANTIPLASMODIAL ACTIVITY ASSAYS

6.5.1 In vitro antiplasmodial assay against K1 and NF54 strains of P. falciparum[1,2] (Swiss Tropical and Public Health Institute)

In vitro activity against the erythrocytic stages of the K1 (chloroquine and pyrimethamine resistant, originated in Thailand) and NF54 *P. falciparum* strains was determined using a ^{3}H-hypoxanthine incorporation assay. Compounds were dissolved in DMSO at 10 mg/ml and added to parasite cultures incubated in RPMI 1640 medium without hypoxanthine, supplemented with HEPES (5.94 g/l), $NaHCO_3$ (2.1 g/l), neomycin (100 U/mL), AlbumaxR (5 g/l) and washed A^+ human red cells at 2.5 % hematocrit (0.3% parasitemia). Serial drug dilutions of eleven three-fold dilution steps covering a range from 100 to 0.002 µg/ml were prepared. The 96-well plates were incubated in a humidified atmosphere at 37 °C; 4 % CO_2, 3 % O_2 and 93 % N_2. After 48 h, 50 µl of ^{3}H-hypoxanthine (=0.5 µCi) was added to each well of the plate. The plates were incubated for a further 24 h under the same conditions. The plates were then harvested with a Betaplate™ cell harvester (Wallac, Zurich, Switzerland), and the red blood cells transferred onto a glass fiber filter then washed with distilled water. The dried filters were inserted into a plastic foil with 10 ml of scintillation fluid, and counted in a Betaplate™ liquid scintillation counter (Wallac, Zurich, Switzerland). IC_{50} values were calculated from sigmoidal inhibition curves by linear regression using Microsoft Excel.

6.5.2 *In vitro* antiplasmodial assay against the W2 strain [3,4]

(Department of Medicine, San Francisco General Hospital, University of San Francisco)

The protocol described by Rosenthal et al. was used in this assay [3]. The chloroquine-resistant W2 strain of *P. falciparum* (1 % parasitemia, 2 % hematocrit) was cultured in 0.5 ml of medium in 48-well culture dishes. Stock solutions of inhibitors (10 mM) in DMSO were added to cultured parasites to a final concentration of 20 µM. From the 48-well plate*s,* 125 µM of culture was transferred to two 96-well plates. Serial dilutions of inhibitors were made to final concentrations of 10 µ*M,* 2 µ*M,* 0.4 µ*M,* 80 n*M,* 16 n*M,* and 3.2 nM. Cultures were maintained at 37 °C for 2 days after which the parasites were washed and fixed with 1 % formaldehyde in PBS. After 2 days parasitemia was measured by flow cytometry using the DNA stain YOYO-1 as a marker of cell survival.

6.6 *IN VIVO* ANTIMALARIAL EFFICACY STUDIES [5,6]

(Swiss Tropical and Public Health Institute)

All efficacy studies were approved by the institutional animal experimentation ethics committee. *In vivo* antimalarial activity was usually assessed for groups of three (treatment group) or five (untreated control group) female NMRI mice (20–22 g) intravenously infected on day 0 with a GFP-transfected *P. berghei* ANKA strain (donated by A. P. Waters and C. J. Janse, Leiden University, The Netherlands) (2 x 10^7 parasitized erythrocytes per ml) (Roche). Compounds formulated in SSV (70/30 Tween 80/ethanol and diluted 10 x with water) were administered orally in a volume of 10 ml/kg as four consecutive daily doses (24, 48, 72 and 96 h after infection). Blood smears were collected and stained on day 4 after infection. The degree of infection (parasitemia

expressed as per cent infected erythrocytes) was determined using microscopy. Activity was calculated as the difference between the mean per cent parasitemia for the control and treated groups expressed as a per cent relative to the control group. The survival time in days was also recorded up to 30 days after infection. A compound was considered curative if the animal survived to day 30 after infection with no detectable parasites.

6.7 CYTOTOXICITY ASSAYS

6.7.1 *In vitro* cytotoxicity against L6 cells [7,8]

(Swiss Tropical and Public Health Institute)

Assays were performed in 96-well microtiter plates, each well containing 100 µl of RPMI 1640 medium supplemented with 1 % L-glutamine (200 mM) and 10 % fetal bovine serum, and 40,000 L6 cells (a primary cell line derived from rat skeletal myoblasts). Serial drug dilutions of eleven three-fold dilution steps covering a range from 100 to 0.002 µg/mL were prepared. After 72 hours of incubation the plates were inspected under an inverted microscope to assure growth of the controls and sterile conditions. 10 µl of Alamar Blue was then added to each well and the plates incubated for another 2 hours. The plates were then read with a Spectramax Gemini XS microplate fluorometer (Molecular Devices Cooperation, Sunnyvale, CA, USA) using an excitation wavelength of 536 nm and an emission wavelength of 588 nm. The IC_{50} values were calculated by linear regression from the sigmoidal dose inhibition curves using SoftmaxPro software (Molecular Devices Cooperation, Sunnyvale, CA, USA).

6.7.2 *In vitro* cytotoxicity against CHO cells

(Division of Pharmacology, University of Cape Town)

Test samples were screened for *in vitro* cytotoxicity against a mammalian cell-line, Chinese Hamster Ovarian (CHO) using the 3-(4,5-dimethylthiazol-2-yl)-2,5-diphenyltetrazoliumbromide (MTT)-assay. The MTT-assay is used as a colorimetric assay for cellular growth and survival, and compares well with other available assays [9,10]. The tetrazolium salt MTT was used to measure all growth and chemosensitivity. Test samples were tested in triplicate on one occasion. The test samples were prepared to a 20 mg/ml stock solution in 100 % DMSO. Stock solutions were stored at -20ºC. Further dilutions were prepared in complete medium on the day of the experiment. Samples were tested as a suspension if not completely dissolved. Emetine was used as the reference drug in all experiments. The initial concentration of emetine was 100 µg/ml, which was serially diluted in complete medium with 10-fold dilutions to give 6 concentrations, the lowest being 0.001 µg/ml. The same dilution technique was applied to the all test samples. The highest concentration of solvent to which the cells were exposed to had no measurable effect on the cell viability (data not shown). The 50% inhibitory concentration (IC_{50}) values were obtained from full dose-response curves, using a non-linear dose-response curve fitting analysis via GraphPad Prism v.4 software.

6.8 DETERGENT MEDIATED *B*-HEMATIN FORMATION INHIBITION ASSAY

(Department of Chemistry, University of Cape Town)

The β-hematin formation inhibition assay method described by Carter et al. was modified for manual liquid delivery [11,12]. Two stock solutions of the samples were prepared by dissolving the pre-weighed compound in DMSO with sonication to give 20 mM and 2 mM solutions of each sample. These were delivered to a 96-well plate in duplicate to give concentrations ranging from 0–1000 μM (final well concentration) with a total DMSO volume of 10 μL in each well, after which deionised H_2O (70 μL) and NP-40 (20 μL; 30.55 μM) were added. Plates containing coloured compounds were pre-read on a on a SpectraMax plate reader for blanking purposes. A 25 mM haematin stock solution was prepared by sonicating hemin in DMSO for one minute and then suspending 178 μL of this in 1M acetate buffer (pH 4.8). The homogenous suspension (100 μL) was then added to the wells to give final buffer and hematin concentrations of 0.5 M and 100 μM respectively. The plate was covered and incubated at 37°C for 5–6 hrs. Free heme was detected using the pyridine-ferrichrome method developed by Ncokazi and Egan [13]. A solution of 50 % (v/v) pyridine, 30 % (v/v) H_2O, 20 % (v/v) acetone and 0.2 M HEPES buffer (pH 7.4) was prepared and 32 μL added to each well to give a final pyridine concentration of ~5 % (v/v). Acetone (60 μL) was then added to assist with haematin dispersion. The UV-vis absorbance of the plate wells was read on a SpectraMax® 340 PC^{384} Absorbance Microplate Reader (Molecular Devices, Sunnyvale, CA, USA). Sigmoidal dose-response curves were fitted to the absorbance data using GraphPad Prism v3.02 to obtain a 50 % inhibitory concentration (IC_{50}) for each compound.

6.9 TURBIDIMETRIC SOLUBILITY ASSAY[14]

Stock solutions of samples and control compounds were prepared in DMSO at a concentration of 10 mM. The assay was carried out using flat-bottomed transparent 96-well microtiter plates. A predilution plate was prepared by adding 20 µl of DMSO into row G and 50 µl of DMSO into rows B to F. Using a micropipette 80 µl of the stock solution was transferred into row G and mixed with the DMSO already in the well. Subsequently, the solution in row G was serially diluted by taking 50 µl from one row to the next all the way to row B. This was done in triplicate to give concentrations of 0.25, 0.50, 1.00, 2.00, 4.00 and 8.00 mM.

The actual dilution for the solubility assay was carried out in triplicate separately in DMSO and PBS. The dilution plate was preloaded with the DMSO (200 µl in row A wells and 196 µl in the rest of the wells) and 196 µl of PBS. Aliquots of 4 µl were then transferred from the corresponding wells in the predilution plate to the dilution plate. DMSO (4 µl) was added to the row A PBS wells while 4 µl of the stock solution were added in triplicate to the row H DMSO and PBS wells. The final concentrations in the wells were 0, 5, 10, 20, 40, 80, 160 and 200 µM, in rows A through H, rescpetively. The plate was covered and incubated at room temperature for two hours after which absorbance was read at 620 nm on a SpectraMax® 340 PC^{384} Absorbance Microplate Reader (Molecular Devices, Sunnyvale, CA, USA). The means of the DMSO and PBS readings for the different concentrations were separately calculated using Microsoft Excel. The figures for rows B to H were each subtracted from the mean for row A. The results for the DMSO and PBS solutions were plotted against concentration and the point of deflection from the origin was taken as the upper bound of solubility.

6.10 CYP INHIBITION ASSAY

Recombinant enzymes were obtained from Cypex Limited, Dundee, Scotland, UK. Inhibitors and NADPH were purchased from Sigma Aldrich, St. Louis, MO, USA. The marker substrates were from BD Gentest Corporation, Woburn, MA, USA. Absorbance readings were taken on a Wallac Victor^{2}™ Multilabel Counter (Wallac AB, Oxfordhuset, Upplands Vasby, Sweden).

Incubations were carried out in black 96 well microtiter plates. A master mix was prepared by mixing ice cold water, buffer, substrate and enzyme, in that order. The master mix was added to all the 96 wells. Inhibitor was added to the appropriate wells and solvent to the wells without inhibitor and the blanks. Test compounds were added to the rest of the wells. The plate was pre-incubated for 10 min at 37 °C. NADPH was added to all wells except the blanks. The plate was incubated for 15 min at 37 °C. Reaction was stopped by adding 75 µl of 1 mM Tris solution in 80% ACN. NADPH was added to the blanks. Fluorescence was measured appropriate excitation and emission wavelengths. The setups for the various enzymes are given in Tables 6.2-6.6.

Table 6.2: CYP1A2 incubation setup

Component	[Stock]	Vol/well (µl)	Conc/well	Master mix (µl) (105 wells)
CYP1A2	13.3 pmol/µl	0.04	0.5 pmol	3.9
CEC in 40% ACN	120 µM	5	3 µM	525
α-naphthaoflavone (or test compound)	100 µM (150, 1000 µM)	4	0.001, 0.01 µM (3, 20 µM)	
KPO_4 buffer	1 M	20	0.1 M	2100
NADPH	20 mM	10	1 mM	
Water		160.96		16901
Exc/Emission λ (nm)	405/460			

Table 6.3: CYP3A4 incubation setup

Component	[Stock]	Vol/well (µl)	Conc/well	Master mix (µl) (105 wells)
CYP3A4	3.9 pmol/µl	0.51	2 pmol	53.8
BFC in 40% ACN	400 µM	5	10 µM	525
Ketoconazole (or test compound)	150, 1000 µM	4	0.01, 0.1 µM (3, 20 µM)	
KPO_4 buffer	1 M	20	0.1 M	2100
NADPH	20 mM	10	1 mM	
Water		160.49		16901
Exc/Emission λ (nm)	405/535			

Table 6.4: CYP2C9 incubation setup

Component	[Stock]	Vol/well (µl)	Conc/well	Master mix (µl) (105 wells)
CYP2C9	2.1 pmol/µl	2.38	5 pmol	250
MFC in 40% ACN	3.4 mM	5	85 µM	525
Sulfaphenazole (or test compound)	150, 1000 µM	4	0.1, 1 µM (3, 20 µM)	
KPO_4 buffer	1 M	20	0.1 M	2100
NADPH	20 mM	10	1 mM	
Water		158.62		16655.2
Exc/Emission λ (nm)	405/535			

Table 6.5: CYP2C19 incubation setup

Component	[Stock]	Vol/well (µl)	Conc/well	Master mix (µl) (105 wells)
CYP2C19	4.9 pmol/µl	0.41	2 pmol	42.86
MFC in 40% ACN	1400 µM	5	35 µM	525
Ticlopidine (or test compound)	150, 1000 µM	4	1, 10 µM (3, 20 µM)	
KPO_4 buffer	1 M	20	0.1 M	2100
NADPH	20 mM	10	1 mM	
Water		160.59		16861.95
Exc/Emission λ (nm)	405/535			

Table 6.6: CYP2D6 incubation setup

Component	[Stock]	Vol/well (µl)	Conc/well	Master mix (µl) (105 wells)
CYP2D6	3.8 pmol/µl	1.31	5 pmol	138.16
MAMC in 40% ACN	600 µM	5	10 µM	525
Thioridazine (or test compound)	150, 1000 µM	4	0.1, 1 µM (3, 20 µM)	
KPO_4 buffer	1 M	20	0.1 M	2100
NADPH	8 mM	10	0.4 mM	
Water		159.69		16767.45
Exc/Emission λ (nm)	390/460			

6.11 TIME DEPENDENT CYP3A4 INHIBITION ASSAY

6.11.1 Incubation 1 (Inactivation assay)

A two-step incubation scheme consisting of an inactivation assay and an activity assay was used according to the method by Thelingwani et al. [15]. In the inactivation assay, the master mix comprising buffer, water and enzyme was added to all wells. A 5 µl aliquot of test compound or control was added to columns 1-4, 7-10 and solvent to columns 5, 6, 11 and 12 of the 96-well plate according to the format shown in Table 6.7. The plate was pre-warmed for 5 min at 37 °C. Water (10 µl) was added to columns 1-6 and NADPH (10 µl) to columns 7-12. The plate was incubated for 15 min at 37 °C.

Table 6.7: Inactivation assay setup

	Stock conc.	Vol / well(µl)	Final conc.	Master mix (315 wells)
Enzyme	3.9 pmol/µl	1.28	5 pmol/well	404 µl
inhibitor	40, 200 µM	5	2, 10 µM	
NADPH	10 mM	10	1 mM	
KPO_4	0.4 M	50	0.2 M	15750 µl
Water		33.7		10621 µl
Final volume		100		
Volume of master mix/well				85 µl

6.11.2 Incubation 2 (Activity assay)

The master mix, prepared as indicated in Table 6.8, was added to all wells. The plate was pre-warmed for 5 min at 37 °C. A 20 µl aliquot was transferred from plate 1 into the corresponding wells in plate 2. NADPH was added to all wells except columns 6 and 12 (blanks). The plate was incubated for 15 min at 37 °C. Reaction was stopped by adding 75 µl of 1 mM Tris solution in 80% ACN. NADPH was added to the blanks. Fluorescence was measured appropriate excitation and emission wavelengths. Results were analyzed as previously described [15].

Table 6.8: Activity assay setup

	Stock conc.	Vol / well(µl)	Final conc.	Master mix (315 wells)
BFC	520 µM	5	13 µM	1575 µl
incubate 1		20		
NADPH	20 mM	10	1 mM	
KPO_4	0.4 M	100	0.2 M	31500 µl
Water		65.0		20475 µl
Final volume		200		
Volume of master mix/well				170 µl

6.12 EC-ESI/MS TRAPPING EXPERIMENTS

The EC/ESI-MS system setup was based on the method previously reported [16,17] Samples were infused through an ESA Coulochem 5011 analytical cell (ESA Inc., Bedford, MA, USA). The electrochemical cell was controlled by an ESA Coulochem II potentiostat (ESA Inc.). Samples were infused through the electrochemical cell by a syringe pump at a flow rate of 5 ml/min. A make-up flow of 50 ml/min was added before the electrochemical cell by a HP1050 high-performance liquid chromatography (HPLC) system (Hewlett Packard, Palo Alto, CA, USA). The sample was collected in glass vials

containing glutathione, methoxylamine or potassium cyanide as the trapping agents for subsequent analysis by LC/MS [17].

6.13 METABOLIC STABILITY ASSAY [18]

This assay was conducted in 96-well plate format. Test compounds and controls were prepared from 10 mM DMSO stock solutions. 0.40 mg protein/ml microsomes (pooled Human mixed gender, male Mouse BALB/c) from XenoTech were incubated with 1 mM test compound at 37 °C. Metabolic reactions were initiated by the addition of the co-factor NADPH and the plates were incubated for 30 minutes. The reactions were quenched with triple the volume of acetonitrile containing carbamazepine as internal standard. The centrifuged and filtered samples were analysed by HPLC-MS/MS to determine the remaining concentrations of the test compounds. Control standards (midazolam and propranolol) were included in the assay to provide quality control and an indication of the metabolic capacity of the microsomes used.

REFERENCES

(1) Thaithong, S.; Beale, G. H.; Chutmongkonkul, M. Susceptibility of Plasmodium falciparum to five drugs: an in vitro study of isolates mainly from Thailand. *Trans. R. Soc. Trop. Med. Hyg.* **1983**, *77*, 228–31.

(2) Desjardins, R. E.; Canfield, C. J.; Haynes, J. D.; Chulay, J. D. Quantitative assessment of antimalarial activity in vitro by a semiautomated microdilution technique. *Antimicrob. Agents Chemother.* **1979**, *16*, 710–8.

(3) Rosenthal, P. J.; Olson, J. E.; Lee, G. K.; Palmer, J. T.; Klaus, J. L.; Rasnick, D. Antimalarial effects of vinyl sulfone cysteine proteinase inhibitors. *Antimicrob. Agents Chemother.* **1996**, *40*, 1600–3.

(4) Greenbaum, D. C.; Mackey, Z.; Hansell, E.; Doyle, P.; Gut, J.; Caffrey, C. R.; Lehrman, J.; Rosenthal, P. J.; McKerrow, J. H.; Chibale, K. Synthesis and structure-activity relationships of parasiticidal thiosemicarbazone cysteine protease inhibitors against Plasmodium falciparum, Trypanosoma brucei, and Trypanosoma cruzi. *J. Med. Chem.* **2004**, *47*, 3212–9.

(5) Vennerstrom, J. L.; Arbe-Barnes, S.; Brun, R.; Charman, S. A.; Chiu, F. C. K.; Chollet, J.; Dong, Y.; Dorn, A.; Hunziker, D.; Matile, H.; McIntosh, K.; Padmanilayam, M.; Santo Tomas, J.; Scheurer, C.; Scorneaux, B.; Tang, Y.; Urwyler, H.; Wittlin, S.; Charman, W. N. Identification of an antimalarial synthetic trioxolane drug development candidate. *Nature* **2004**, *430*, 900–4.

(6) González Cabrera, D.; Douelle, F.; Feng, T.-S.; Nchinda, A. T.; Younis, Y.; White, K. L.; Wu, Q.; Ryan, E.; Burrows, J. N.; Waterson, D.; Witty, M. J.; Wittlin, S.;

Charman, S. A.; Chibale, K. Novel orally active antimalarial thiazoles. *J. Med. Chem.* **2011**, *54*, 7713–9.

(7) Ahmed, S. A.; Gogal, R. M.; Walsh, J. E. A new rapid and simple non-radioactive assay to monitor and determine the proliferation of lymphocytes: an alternative to [3H]thymidine incorporation assay. *J. Immunol. Methods* **1994**, *170*, 211–24.

(8) Page, B.; Page, M.; Noel, C. A new fluorometric assay for cytotoxicity measurements in-vitro. *Int. J. Oncol.* **1993**, *3*, 473–6.

(9) Rubinstein, L. V; Shoemaker, R. H.; Paull, K. D.; Simon, R. M.; Tosini, S.; Skehan, P.; Scudiero, D. A.; Monks, A.; Boyd, M. R. Comparison of in vitro anticancer-drug-screening data generated with a tetrazolium assay versus a protein assay against a diverse panel of human tumor cell lines. *J. Natl. Cancer Inst.* **1990**, *82*, 1113–8.

(10) Mosmann, T. Rapid colorimetric assay for cellular growth and survival: application to proliferation and cytotoxicity assays. *J. Immunol. Methods* **1983**, *65*, 55–63.

(11) Carter, M. D.; Phelan, V. V; Sandlin, R. D.; Bachmann, B. O.; Wright, D. W. Lipophilic mediated assays for beta-hematin inhibitors. *Comb. Chem. High Throughput Screen.* **2010**, *13*, 285–92.

(12) Sandlin, R. D.; Carter, M. D.; Lee, P. J.; Auschwitz, J. M.; Leed, S. E.; Johnson, J. D.; Wright, D. W. Use of the NP-40 detergent-mediated assay in discovery of inhibitors of beta-hematin crystallization. *Antimicrob. Agents Chemother.* **2011**, *55*, 3363–9.

(13) Ncokazi, K. K.; Egan, T. J. A colorimetric high-throughput β-hematin inhibition screening assay for use in the search for antimalarial compounds. *Anal. Biochem.* **2005**, *338*, 306–319.

(14) Pérez, J.; Díaz, C.; Salado, I. G.; Pérez, D. I.; Peláez, F.; Genilloud, O.; Vicente, F. Evaluation of the effect of compound aqueous solubility in cytochrome P450 inhibition assays. *Adv. Biosci. Biotechnol.* **2013**, *04*, 628–639.

(15) Thelingwani, R. S.; Zvada, S. P.; Dolgos, H.; Ungell, A. B.; Masimirembwa, C. M. In vitro and in silico identification and characterization of thiabendazole as a mechanism-based inhibitor of CYP1A2 and simulation of possible pharmacokinetic drug-drug interactions. *Drug Metab. Dispos.* **2009**, *37*, 1286–94.

(16) Johansson, T.; Weidolf, L.; Jurva, U. Mimicry of phase I drug metabolism--novel methods for metabolite characterization and synthesis. *Rapid Commun. Mass Spectrom.* **2007**, *21*, 2323–31.

(17) Mali'n, T. J. Electrochemical and Enzymatic In Vitro Studies on Reactive Drug Metabolites, University of Gothenburg, 2010, pp. 1–64.

(18) Di, L.; Kerns, E. H.; Gao, N.; Li, S. Q.; Huang, Y.; Bourassa, J. L.; Huryn, D. M. Experimental design on single-time-point high-throughput microsomal stability assay. *J. Pharm. Sci.* **2004**, *93*, 1537–44.

APPENDIX 1

ANTIPLASMODIAL ACTIVITY (WITH STANDARD DEVIATION)AGAINST THE NF54 (CHLOROQUINE SENSITIVE), K1 AND W2 (DRUG RESISTANT) *PLASMODIUM FALCIPARUM* STRAINS

K1 AND NF54 STRAINS

Code	Structure	Antiplasmodial IC_{50} (nM)			
		K1	sd*	NF54	sd*
3.9a (DS4F)	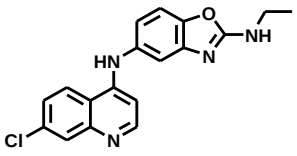	1003	29.2202	466	29.2202
3.9b (DS23B)	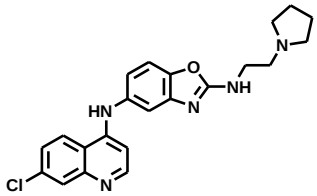	56.4	13.9403	15.4	2.0560
3.9w (DS30B)	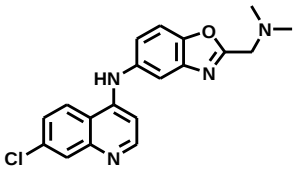	411	16.0333	213	8.5029
3.9d (DS31B)	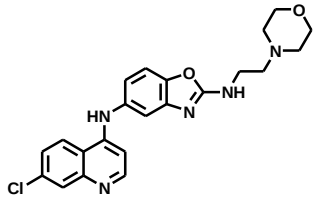	198	3.3362	108	17.8624
3.9o (DS32B)	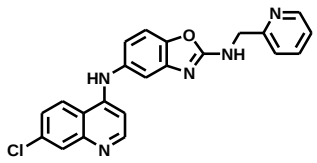	883	14.0770	406	1.7596
3.9e (DS33B)	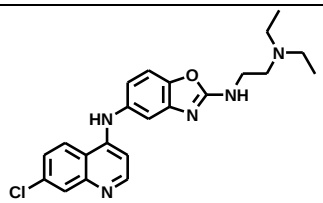	41.5	2.4396	10.7	0.0000
3.9g (DS34B)	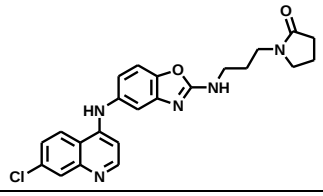	773	82.7291	1876	206.0117

Code	Structure	Antiplasmodial IC_{50} (nM)			
		K1	sd*	NF54	sd*
3.9p (DS35B)	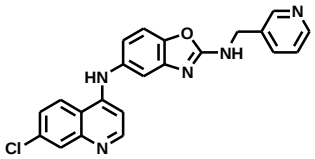	**704**	**42.2311**	**309**	**22.8752**
3.9h (DS36B)	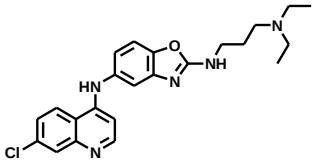	**84.9**	**15.1651**	**14.2**	**2.6583**
3.9i (DS37B)	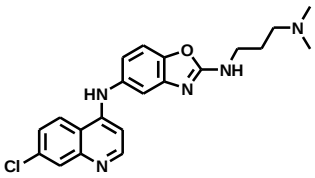	**149.0)**	**13.9122**	**18.9**	**1.1576**
3.9s (DS39B)	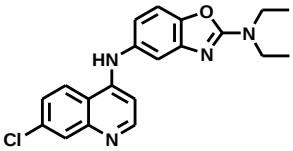	**1379**	**198.5389**	**512**	**13.4929**
3.9l (DS41B)	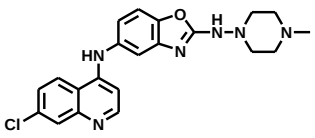	**240**	**12.1056**	**144**	**21.3212**
3.9m (DS42B)	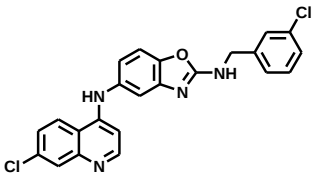	**223**	**9.7465**	**124**	**25.3047**
3.9c (DS46B)	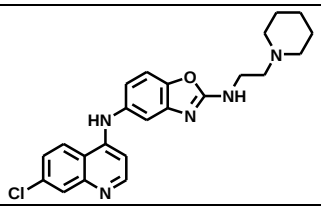	**23.7**	**7.3218**	**9.7**	**0.2370**
3.9q (DS47B)	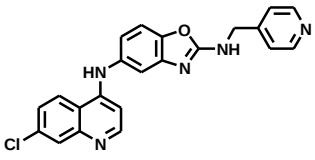	**1553**	**12.3174**	**630**	**0.2649**

Code	Structure	Antiplasmodial IC_{50} (nM)			
		K1	sd*	NF54	sd*
3.9j (DS48B)	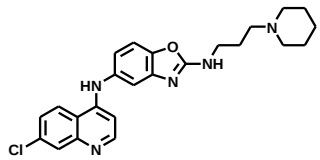	**39.0**	**2.6487**	**9.6**	**0.2649**
3.9r (DS49B)	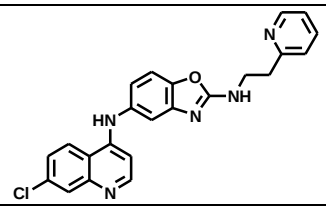	**851**	**8.5015**	**402**	**23.8043**
3.9f (DS50B)	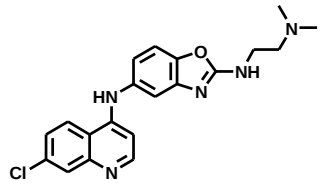	**41.9**	**1.5119**	**11.5**	**0.5451**
3.9t (DS51B)	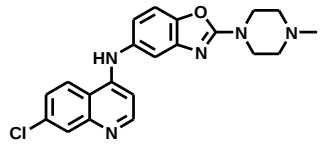	**99.0**	**5.8634**	**50.8**	**1.4658**
3.9u (DS52B)	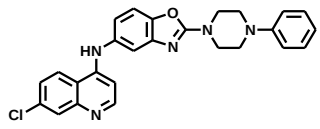	**875**	**13.9579**	**274**	**107.7236**
3.9v (DS53B)	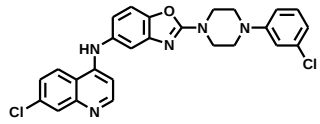	**412**	**1.4420**	**202**	**2.8839**
3.9n (DS54B)	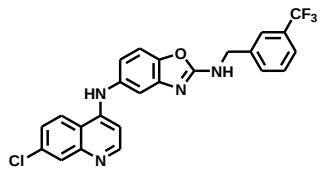	**282**	**57.3093**	**107**	**16.0081**
3.9k (DS56B)	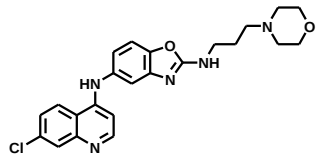	**79.9**	**6.9763**	**38.8**	**1.3184**

Code	Structure	Antiplasmodial IC_{50} (nM)			
		K1	sd*	NF54	sd*
3.9x (DS58B)	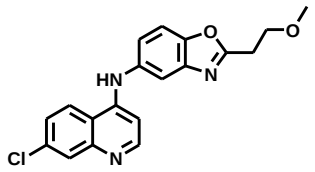	**2111**	**45.9679**	**1094**	**9.9930**
ADQ	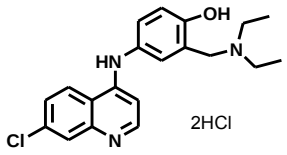	**9.6**	**0.6170**	**4.2**	**0.1649**
2.9b (DS23)	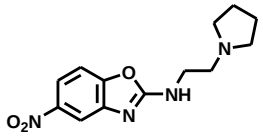	**2928**	**104.7331**	**1640**	**330.1454**
2.9o (DS32)	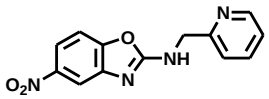	**>37004**	**-**	**35028**	**-**
2.9i (DS37)	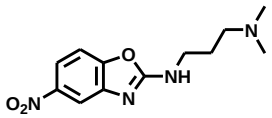	**10992**	**2659.5434**	**>37839**	**-**
2.9s (DS39)	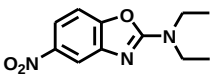	**30888**	**1382.7118**	**39691**	**-**
2.9r (DS49)	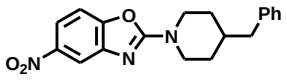	**21632**	**999.7627**	**>29641**	**-**
2.9t (DS51)	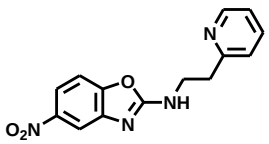	**30752**	**97.0105**	**>35178**	**-**

Code	Structure	Antiplasmodial IC_{50} (nM)			
		K1	sd*	NF54	sd*
2.9u (DS52)	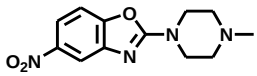	>38130	-	>38130	-
2.12b (DS62)	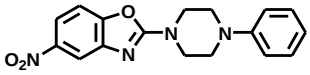	>30838	-	>30838	-
2.9b (DS23)	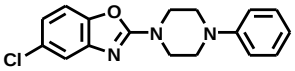	>31869	-	>31869	-
CQ	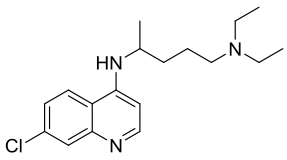	275	37.7101	9.7	1.6483
ARTS	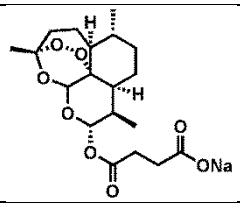	2.3	0.9461	3.4	1.2709

***sd=standard deviation; ADQ=Amodiaquine; CQ=Chloroquine; ARTS = Sodium artesunate**

W2 STRAIN

Code	Structure	Antiplasmodial IC_{50} (nM)	
		W2	sd*
3.2a (DS1F)	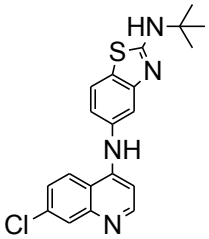	1158	125.86501
3.9a (DS4F)	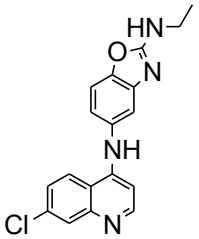	490.85	92.84312

3.6a (DS5G)	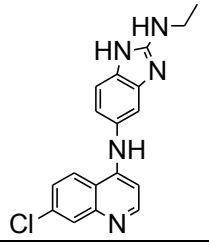	**500.78**	**580.28011**
3.2c (DS11B)	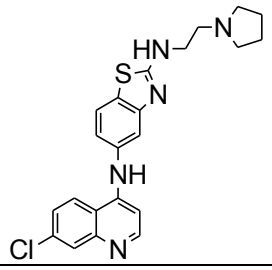	**12.185**	**0.2899138**
3.2d (DS12B)	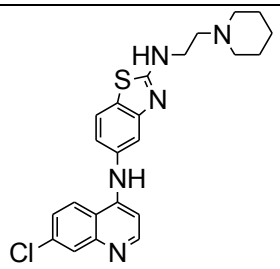	**12.955**	**0.2474874**
3.2e (DS13B)	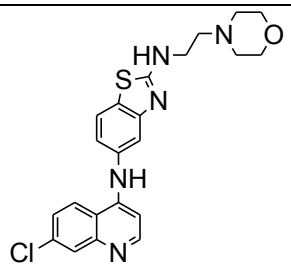	**39.625**	**1.9445436**
3.2f (DS18B)	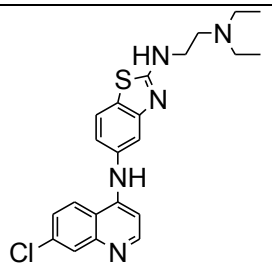	**10.565**	**0.1909188**
3.6b (DS21B)	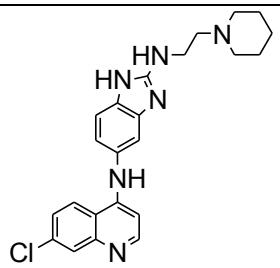	**4579.65**	**6305.059**
3.6c (DS22B)	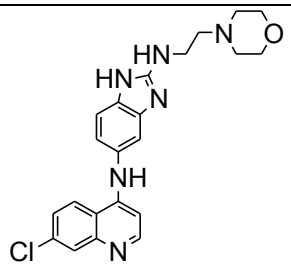	**188.6**	**4.5254834**

3.9b (DS23B)	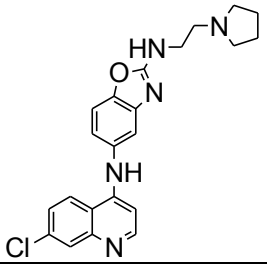	**8.3145**	**1.4163349**
3.6d (DS24B)	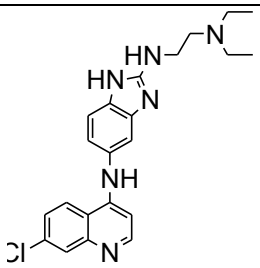	**199.65**	**5.4447222**
3.4a (DS26B)	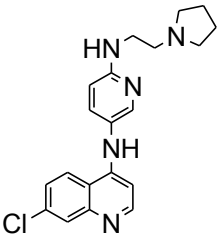	**20.68**	**2.2344574**
3.4b (DS27B)	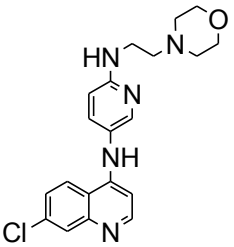	**40.79**	**4.7376154**
ADQ		**4.903**	**0.205061**
CQ		**49.49**	**1.2727922**
ARTS		**11.71**	**0.8768124**

***sd=standard deviation; ADQ=Amodiaquine; CQ=Chloroquine; ARTS = Sodium artesunate**